# Gold Nanoparticles-Based Tablet (AuNPs-Tablet) Sensor For Point-of-Use Applications

Zubi Sadiq

A Thesis
In the Department
of
Chemical and Materials Engineering

Presented in Partial Fulfillment of the
Requirements For the Degree of
Doctor of Philosophy (Chemical and Materials Engineering)
at Concordia University
Montreal, Quebec, Canada

September 2025

CONCORDIA UNIVERSITY SCHOOL

OF GRADUATE STUDIES

This is to certify that the thesis prepared

By: Zubi Sadiq

Entitled: Gold nanoparticles-based tablet (AuNPs-tablet) sensor for point-of-use applications

and submitted in partial fulfillment of the requirements for the degree of

DOCTOR OF PHILOSOPHY (Chemical and Materials Engineering)

complies with the regulations of the University and meets the accepted standards with respect to originality and quality.

Signed by the final examining committee:

_____ Chair

Chadi Assi

_____ External Examiner

Saji George

_____ Arm's Length Examiner

Chunjiang An

_____ Examiner

Catherine Mulligan

_____ Examiner

Nhat Truong Nguyen

_____ Thesis Supervisor

Sana Jahanshahi-Anbuhi

Approved by _____

Graduate Program Director

Defence date _____

Dean

## Abstract

Gold Nanoparticles-Based Tablet (AuNPs-Tablet) Sensor for Point-of-Use Applications

Zubi Sadiq, PhD

Concordia University, 2025

Point-of-use sensors are essential for environmental monitoring, food quality assessment, and disease diagnostics, particularly in remote and in-field settings. However, sensitivity, user-friendliness, and portability challenges limit their commercial availability, highlighting the need for improved sensing platforms. Gold nanoparticles (AuNPs) are promising for assay development due to their rapid synthesis, functionalization, and naked-eye colorimetric response, making them ideal for point-of-use applications. The central objective of this research is to develop a novel sensing platform called "lab-on-a-tablet" device as a potential point-of-use detection system.

This thesis introduces a low-cost, portable, and user-friendly detection platform using dextran-gold nanoparticles (dAuNPs), selected for their enhanced stability and simple synthesis. The dAuNPs-based tablet platform was developed using a pipette-out technique, ensuring solid, stable tablet formation (dAuNPs-Tablet). The pH-responsive behaviour of the tablet was assessed in various ionic solutions; the concentration of dextran was optimized; and different solid supports (e.g., composite, powder) were tested for optimal performance. The tablet-based approach offers superior portability, storage, and transportation compared to solution-phase dAuNPs (dAuNPs-Solution), quick production, easy handling, long-term stability (over four years), and low-cost (~1.22 CAD/100 tablets). Spectroscopic and microscopic analyses confirmed that dAuNPs retain their morphology during tablet formation, making dAuNPs-Tablet a robust and user-friendly alternative. A plasmonic tablet sensor was developed using dAuNPs-Solution, prepared under reflux conditions with post-synthetic dextran addition to facilitate tablet formation. This sensor detected reactive small species like hypochlorite and hydrogen peroxide. Hypochlorite was tested in swimming pool water, while hydrogen peroxide as an oxidative stress biomarker, was analyzed in urine sample using Fenton chemistry. Additionally, the antioxidant effect of green tea in reducing oxidative stress was explored.

Next, the tablet platform was advanced by developing a dual-functional system. We directly transformed dAuNPs-Solution into a tablet form, eliminating reflux conditions and post-synthetic dextran addition, resulting in the formation of a "direct tablet". This dual-functional tablet detected uric acid *via* its plasmonic response and glucose through its nanozyme activity, producing colorimetric signals within biologically relevant range. Thus, this thesis presents a transformative tablet-based detection platform with multiplexed capabilities, advancing point-of-use assays. The biocompatibility of dextran in dAuNPs-Tablets further highlights their potential for biomedical applications.

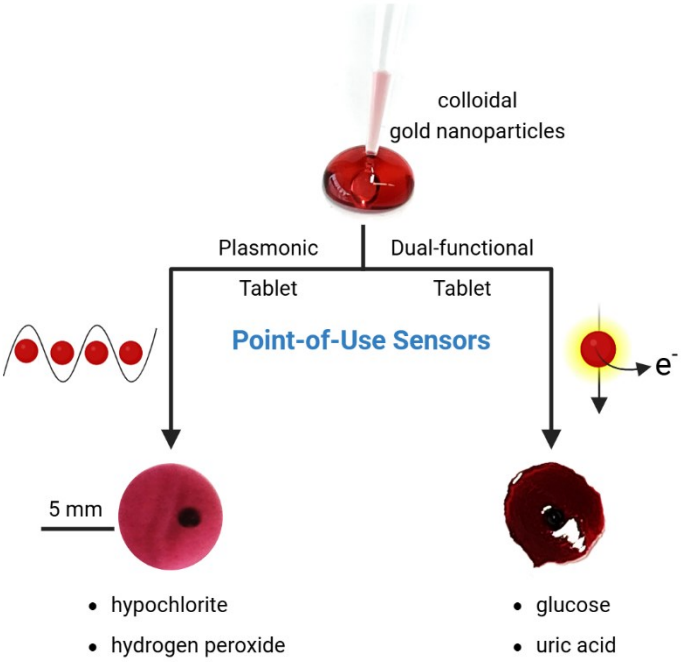

## Acknowledgements

All praise to the creator of the universe, who has bestowed upon us the wisdom to explore the opportunities and contribute to humanity. Firstly, sincere gratitude to my PhD supervisor, Dr. Sana Jahanshahi-Anbuhi, for her invaluable guidance, constructive feedback, and mentorship throughout this journey. Her considerate nature, inspiring personality, and trust in my abilities always motivate me to show my full potential. I also thank to my dissertation committee members: Dr. Catherine Mulligan, Dr. Deniz Erol, and Dr. Nhat Truong for their helpful comments and suggestions. Many thanks to the department Chair, Dr. Alex De Visscher, for fostering a productive research environment. I thank my mentor, Dr. Erum Akbar, for assisting me in understanding key concepts.

Special thanks to Dr. Nooshin Movahed, manager at Centre for NanoScience Research for providing microscopic analysis. Many thanks to Dr. Marc Antoni Goulet for useful discussions on research opportunities. I cannot forget my thoughtful sessions with Ms. Harriet Laryea, technical supervisor at CME department. Her encouraging behaviour always pushes me to focus on the priorities and built interpersonal skills. Thanks to Ms. Kerri Warbanski, chemical laboratory technician for her friendly nature and assisting me in characterization of nanoparticles. I acknowledge the guidance of GradProSkills team, who made my graduate experience memorable with their trainings, especially at 3MT competition (2023) and PhD Career Connect Program (2025). Thanks to Dr. Ann-Louise Davidson, director Innovation Lab for providing me an opportunity to participate in Fall 2024 Innovation Challenge.

I consider myself fortunate to have unforgettable memories with my amazing lab fellows; Hamid, Muna, Hasti, Maryam, Chinonso, and Abdolali. Brainstorming sessions with Hamid always boost my confidence and enhances my critical thinking. I would extend my appreciation to my mentor and guiding figure, Syed Mohi-ud-din M. Bukhari, for nurturing me and providing countless supports in Canada. I am grateful to my friends, Nageena and Tayyaba, for their moral support.

Words simply cannot express my gratitude and love to my husband, Asif Raheem, and my son Taha Asif for sharing my responsibilities, and being patience with me in stressful days. Thanks to my parents and siblings, especially my elder brother, Dr. Nadeem Sadiq, who is always available whenever I need his guidance. Finally, I acknowledge Concordia University for granting multiple awards and Graduate Doctoral Incentive Fellowship, and Govt. of Quebec for providing the FRQNT scholarship.

*To my Parents,*

*whose love and support are*

*the foundation of my achievements.*

# Table of Contents

## List of Figures

## List of Tables

## List of Abbreviations, Acronyms, and Notation

| | |
|---|---|
| ABTS | 2,2′-Azino-bis(3-ethylbenzothiazoline-6-sulphonic acid |
| AFM | Atomic force microscopy |
| ASSURED | Affordable, Sensitive, Specific, User-friendly, Rapid, Equipment-Free, Delivered |
| AuNPs | Gold nanoparticles |
| AuNPs-Cit | Citrate-gold nanoparticles |
| AgNPs | Silver nanoparticles |
| dAuNPs, dAuNPs-Sol, AuNPs-dSol, dAuNPs-Solution | Dextran-gold nanoparticles in solution form |
| dAuNPs-Tablet, AuNPs-dTablet, AuNPs-dTab | Dextran-gold nanoparticles in tablet form |
| dAuNPs-Swab | Dextran-gold nanoparticles embedded into the fibres of swab |
| dAuNPs-Comp | Dextran-gold nanoparticles in composite form |
| dAuNPs-Powder | Dextran-gold nanoparticles in powder form |
| DLS | Dynamic light scattering |
| DSC | Differential scanning calorimetry |
| EDS | Energy dispersive X-ray spectroscopy |
| FTIR | Fourier transform infrared |
| $H_2O_2$ | Hydrogen peroxide |
| LFIAs | Lateral flow immunoassays |
| LSPR | Localized surface plasmon resonance |
| LoD | Limit of detection |
| LLoD | Lower limit of detection |
| NaCl | Sodium chloride |
| $OCl^-$ | Hypochlorite |
| •OH | Hydroxyl radical |
| OP | Organophosphate pesticides |
| OPD | *o*-Phenylenediamine |
| POC | Point-of-care |

| | |
|---|---|
| Pox | Peroxidase |
| REASSURED | Real-time connectivity, Ease of specimen collection, Affordable, Sensitive, Specific, User-friendly, Rapid and Robust, Equipment-free or Environment friendly, Deliverable to user |
| REST-ASSURED | Real-time connectivity, Ease of specimen collection, Scalable, Transferability, Affordable, Sensitive, Specific, User-friendly, Rapid and Robust, Equipment-free, Deliverable to user |
| ROS | Reactive oxygen species |
| R% | Recovery% |
| RSD% | Relative standard deviation% |
| SD | Standard deviation |
| SEM | Scanning electron microscopy |
| SPR | Surface plasmon resonance |
| TEM | Transmission electron microscopy |
| TMB | 3,3′,5,5′-Tetramethylbenzidine |
| ULoD | Upper limit of detection |
| UV–vis | Ultraviolet–visible |
| WHO | World Health Organization |
| XRD | X-ray diffraction |
| ζ-potential | Zeta potential |
| $\pi$-$\pi$ | pi-pi |
| E | Molar extinction coefficient |
| λ | Wavelength |
| mM | Milli molar |
| μM | Micro molar |
| nM | Nano molar |
| 20X | 20 times |

# CHAPTER 1 Introduction

A sensor is a device that detects a specific stimulus and responds through a sensing element, transduction system, and output interface. The global sensor market, valued at USD 216.76 billion in 2023, is expected to expand at a compound annual growth rate of 8.7%, reaching USD 388.69 billion by 2030 [1]. Remote settings and in-field applications widely use point-of-use sensors to identify and quantify toxic analytes. These sensors are essential for environmental monitoring, facilitating pollution control, and contributing to improved quality of water, soil, and air, thereby promoting a sustainable environment [2,3]. Similarly, the healthcare field extensively uses these sensors for prompt disease detection and patient management [4]. The need for point-of-use sensors becomes indispensable at the time of sudden outbreaks of pathogens caused by contaminated food or sudden disease transmission. Also, the food industry utilises these sensors to track food quality through intelligent packaging or smart sensors [5,6]. As a result, the demand for point-of-use detection systems has significantly increased. In recent years, the focus of research is to design new low-cost smart sensing platforms with enhanced functional features that facilitates portability and user-friendliness. Conclusively, the point-of-use sensors are commonly employed in environmental monitoring, food quality assessment, and disease diagnostics.

This study aims to develop an innovative, user-friendly, robust, and low-cost point-of-use sensing platform for the detection of analytes useful for environmental monitoring and disease diagnosis. The proposed sensing methodology has the potential to improve existing detection assays through encapsulation strategy, well-suited for on-the-spot detection and in-field evaluations, particularly in low-resource settings and developing countries. The proposed sensing device can be utilized in other demanding applications like food quality assessment and forensics.

## 1.1 Point-of-Use Sensors

Detection with point-of-use sensors is demanding because it can be performed at the time and place of need with simple-to-use methods. More precisely, when a point-of-use sensor is used to detect a disease biomarker, the sensor is called a “point-of-care” (POC) sensor. The POC sensors can be used at any level of the diagnosis system, such as at home, in the emergency room of a hospital, in clinics, in laboratories, and testing at resource-limited regions. In 2003, the World

Health Organization announced the ASSURED (Affordable, Sensitive, Specific, User-friendly, Rapid, Equipment-Free, Delivered) framework for POC diagnostics, which became a benchmark in 2006 [7]. Since the advances in mobile technology, a modified REASSURED (Real-time connectivity, Ease of specimen collection, Affordable, Sensitive, Specific, User-friendly, Rapid and Robust, Equipment-free or Environment-friendly, Deliverable to user) criteria were the benchmark until recently. In the post-COVID era, the new REST-ASSURED (Real-time connectivity, Ease of specimen collection, Scalable, Transferability, Affordable, Sensitive, Specific, User-friendly, Rapid and Robust, Equipment-free or Environment-friendly, Deliverable to user) criteria are considered for the selection of POC diagnostics [8]. Ideally, these criteria can be followed for the development of point-of-use sensors. In point-of-use sensors, detection methodology should be straightforward and preferably rely on sample-to-answer methods. The main element of a sensor is the sensing probe, which is responsible for the selective and sensitive detection of an analyte. The sensing material interacts with a targeted analyte, resulting in molecular recognition through covalent bonding or noncovalent attractions (i.e., hydrophobic interactions, hydrogen bonds, electrostatic forces, van der Waals forces, and $\pi$-$\pi$ interactions) [9]. Advanced functional materials like nanoparticles are suitable candidates for molecular recognition. The recognition event resulting from the analyte-sensing probe interactions is translated into a measurable signal through the transducer. A transducer is the detector element that translates a concentration signal into color intensity (colorimetric sensor), enabling the quantitative or qualitative analysis of an analyte. Sometimes a sensing probe itself acts as a transducer (i.e., gold nanoparticles) or requires chromogenic substances (i.e., 3,3',5,5'-tetramethylbenzidine) to show the color output of a colorimetric detection [10]. Different platforms have been well-explored for point-of-use sensors, including microfluidic and lab-on-a-chip devices [11]. Commonly reported substrates are paper and polydimethylsiloxane (PDMS) chips [12]. Other examples include threads, swabs, face masks, tape, polymeric surfaces, and fabrics [13,14]. None of these platforms are fully established to comply with the REASSURED criteria or have been explored for selected analytes. In this context, the exploration of innovative sensing platforms for point-of-use sensors remains necessary.

### 1.1.1 Why Tablet-Based Assay is Needed?

The tablet-based assay offers a portable and user-friendly platform for the detection of analytes for in-field applications. Tablet as a detection platform was first introduced in early 1940s [15] but it became popular after Jahanshahi-Anbuhi *et al.* research in 2014 [16]. Tablets are cost-effective and pre-measured quantities of reagents can be encapsulated into the tablet that possess long shelf life. Tablets can be developed from liquid reagents or powdered chemicals by casting or pressing techniques, respectively. Jahanshahi-Anbuhi *et al.* proposed a tablet system from liquid reagent for the detection of a malathion pesticide in water. A known concentration of acetylcholinesterase enzyme and indoxyl acetate chromogenic substrate were encapsulated in two separate tablets by casting their liquid solutions in molds [16]. The encapsulation of reagents by pullulan has increased their shelf-life from weeks to months, which is an important criterion for developing ready-to-use assay kits. Tablet-based assays by direct compression of reagent powders were reported by Udugama and co-workers [17]. Initially, tableting reagents were lyophilized into powder using trehalose sugar due to their stabilizing property. Then, a pre-measured amount of the lyophilized reagent powder was mixed with mannitol sugar due to its bulk-forming property, followed by the compression of powder into ready-to-use tablets. These color-coded tablets stabilized heat-sensitive reagents and showed a broad range of applicability in detection (i.e., enzyme-based immunoassays and microbead diagnostics) [17]. Since then, tablet-based assays have been reported for different applications such as glucose and hepatitis B detection [17,18]. Also, multi-step assays have been reported using multi-layered tablets that enabled the sequential release of reagents [19].

In short, the tablet-based platform has great potential to produce user-friendly kits for in-field applications. However, a key challenge of tablet-based assays is their ability to encapsulate only selected reagents/chemicals, which limit the development of new assays. Also, only selected methodologies have been tested using the tablet platform, thus, innovative approaches are needed that can significantly expand the applicability of tablet-based detection in point-of-use devices.

### 1.1.2 Why Gold Nanoparticles (AuNPs) is Selected?

Gold nanoparticles (AuNPs) have been successfully applied in various applications worldwide from food and water monitoring to disease diagnostics and forensics [20,21]. Their role in sensor fabrication is appreciated due to their simple preparation, diversified surface functionalization,

high extinction coefficient, unique optical and catalytic properties, high surface-to-volume ratio, and visual observation without using any advanced instruments [20,22,23]. Mostly, AuNPs act as a complete nanoprobe as they provide a platform for molecular recognition and a signal output. They act as a transducing element and responsible for converting the molecular recognition process into a measurable optical signal in the form of a color change. A change in color from pink to purple happens upon aggregating, making them ideal components of colorimetric sensors.

The AuNPs-based plasmonic sensors work based on their optical property where the morphology of nanoparticles is highly important. In contrast to plasmonic sensors, AuNPs themselves did not contribute to visual read-out in nanozyme sensors so a chromogenic substance such as 3,3′,5,5′-tetramethylbenzidine (TMB), 2,2′-azino-bis(3-ethylbenzothiazoline-6-sulphonic acid (ABTS), or *o*-phenylenediamine (OPD) is required to generate a color signal [24]. The choice of chromogenic agent in a sensing system depends on different parameters such as pH, temperature, choice of analyte, and surface functionality of AuNPs. The operational concept of AuNPs-based plasmonic and nanozyme sensors is illustrated in Figure 1.1.

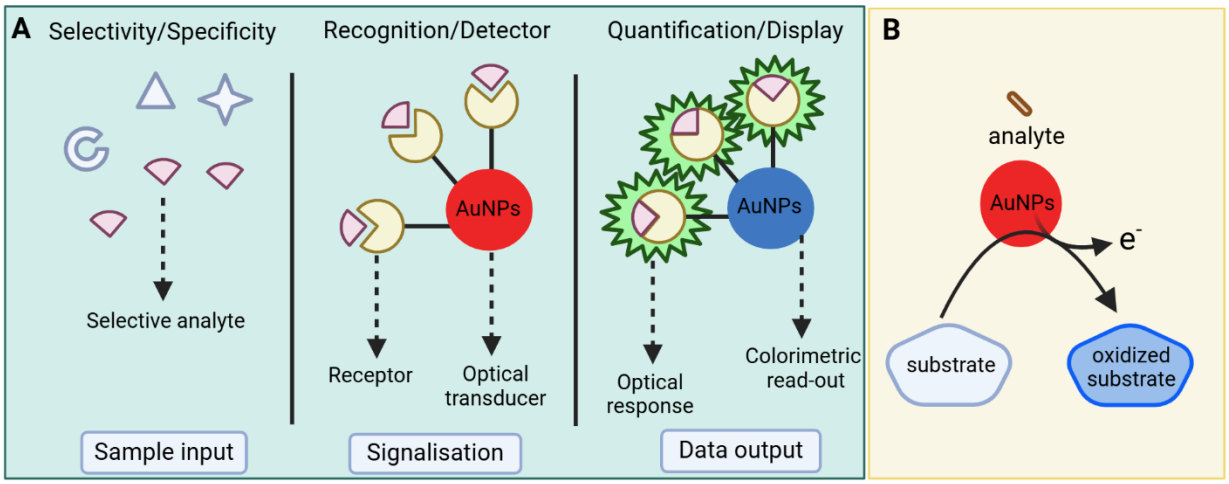


Figure 1.1 Functional overview of gold nanoparticles-based detection system.
A) Basic components of a plasmonic sensor; B) Illustration of AuNPs-based nanozyme sensor

Among a broad range of stabilizers, polysaccharides such as dextran, pullulan, alginate, cellulose, guar gum, and chitosan are famous capping agents to stabilize AuNPs due to their abundant oxygen-rich functional moieties in their structure [25,26]. These carbohydrates tightly bind with nanogold clusters *via* electrostatic interactions and offer steric and electrostatic

stabilization. Additionally, polysaccharides act as a reducer to facilitate the reduction of $Au^{3+}$ to $Au^{0}$ making its synthesis eco-friendly, facile, one pot, and inexpensive [27]. The synthesized AuNPs get embedded and stabilized within the polymer matrix. Such AuNPs are biocompatible due to their non-toxicity nature and are suitable for biomedical applications. Although polysaccharide-AuNPs present enormous potential in scientific research, their instability under physiological conditions (e.g., variations in pH, ionic strength, and temperature) prevents further uses [28]. Colloidal solution of AuNPs (AuNPs-Solution) surrounded by polysaccharides suffers unwanted aggregation because of fungus attack and/or deposition of particles at the bottom if stays at room temperature for a longer duration [29]. Such challenges have been overcome by presenting alternate platforms of solution phase AuNPs where polysaccharides act as a nano-template. Solid phase AuNPs (i.e., powder, hydrogel, and nanocomposite) require special treatment of AuNPs-Solution such as centrifugation, spray drying, labor-intensive experimental steps etc [29,30]. Also, these solid AuNPs require multiple weighing and careful optimization of experimental conditions. To overcome these limitations associated with AuNPs, there is a need to introduce new user-friendly platforms with enhanced stability, simple fabrication, easy storage, and transportation at room temperature.

### 1.2 Motivation of this Research Work

The AuNPs-Solution has been successfully applied in various applications worldwide, from food and water monitoring to disease diagnostics and forensics [20,21]. There are several challenges associated with AuNPs and point-of-use detection platforms that limit their applicability and reliability. I) the AuNPs dispersion in solution is highly prone to environmental changes (i.e., temperature, salt), and AuNPs quickly aggregate; thus, there is a need to improve the stability profile of AuNPs, II) transportation of AuNPs-Solution is challenging due to their low stability and difficult handling, III) the distribution of AuNPs varies from batch-to-batch synthesis and raising reproducibility issues that reduce the reliability of colorimetric assays, hence hindering their progression towards commercialization. On the other hand, solid format AuNPs, such as lateral flow immunoassays (LFIAs), are user-friendly due to their simplicity and low cost. However, they lack sufficient accuracy and exhibit relatively low sensitivity [31,32]. To overcome these challenges, there is a need to introduce a new stable platform that is easy to handle and transport and produces accurate, reproducible, and sensitive outcomes in the detection of targeted analytes.

Despite the increasing scientific research, only a few devices meet all REASSURED criteria with varying levels of complexity, cost, and other factors. The main drawbacks of the existing devices include a lack of portability and sensitivity. Hence, the whole motivation was to introduce a new sensing platform that is portable, user-friendly, ultra-sensitive, and has the capability of multiplex detection. We developed the device by encapsulating dextran-gold nanoparticles (dAuNPs) and named it a tablet sensor (dAuNPs-Tablet). The encapsulated dAuNPs in a tablet can be released at the time of use, showing a sensitivity comparable to the dAuNPs solution. Hence, the dAuNPs-Tablet is a promising approach to solve stability, handling, and transportation issues. The tablet sensor facilitates immediate testing for field applications and at-home testing for health monitoring and disease diagnostics.

## 1.3 Thesis Aim and Objectives

This PhD research is motivated by the growing demand for rapid, reliable, and user-friendly point-of-need detection platforms with real-world applicability. Drawing on the transformative potential of sensor technologies to bridge the gap between laboratory research and market-ready solutions, this work contributes to the broader vision of developing cost-effective and accessible tools for environmental monitoring and disease diagnostics.

The central objective of this research is to develop a novel sensing platform called "lab-on-a-tablet" device as a potential point-of-use detection system. Utilizing a unique encapsulation strategy, the aim is to produce a portable, robust, and easy-to-use tablet-based sensor suitable for in-field applications. In this thesis, the fabrication of a plasmonic tablet and a dual-functional tablet for in-field detection is presented.

### 1.3.1 Methodology

The methodology of this research work can be outlined as follows:

- Preparation of AuNPs-Solution using conventional and eco-friendly synthetic methods.
- Encapsulation of colloidal nanogold solution into a solid format, making it an easy-to-handle nanoscale material.
- Characterization of a tablet using various techniques, such as ultraviolet-visible spectroscopy (UV-vis), Fourier transform infrared spectroscopy (FTIR-ATR), transmission electron microscopy (TEM), dynamic light scattering (DLS), X-ray

diffraction spectroscopy (XRD), differential scanning calorimetry (DSC), and atomic force microscopy (AFM).

- Optimization of assays for point-of-use detection.
- Exploring the plasmonic behaviour of the tablet sensor for detecting an environmental analyte, hypochlorite ($OCl^-$), and a disease biomarker, hydrogen peroxide ($H_2O_2$).
- Development of a dual-functional tablet as an advancement in tablet technology.
- Exploring the dual-detection capabilities of a dual-functional tablet as both a plasmonic and nanozyme sensor, considering uric acid and glucose as biomarkers.

## 1.4 Organization of the Thesis

This thesis has been organized into following 7 chapters.

**Chapter 1 – Introduction:** This chapter highlights the significance of point-of-use detection system, the importance of gold nanoparticles (AuNPs), and the challenges associated with their applications in sensor technology. I describe the motivation and objectives of the research, then move on to the organisation of the thesis. Finally, I report the research outcomes in the form of publications and participation in conferences.

**Chapter 2 – An Overview of Gold Nanoparticles-Based Colorimetric Assays: From Fundamentals to Advanced Applications:** The research journey starts with a comprehensive overview of the literature that frames the thesis research area. This chapter emphasises the exponential growth in research on AuNPs-based colorimetric sensors for point-of-use applications. It examines recent advancements in their design and performance, starting with AuNPs characteristics, synthesis, and functionalization. Mechanisms are categorized into two types: surface plasmon resonance (SPR)-based sensors and nanozyme-based sensors. Detection of inorganic, organic, and biological pollutants in environmental and food samples is thoroughly reviewed. The study concludes by emphasizing the need for improved sensitivity, reproducibility, multiplexing, and cost-effectiveness to enhance rapid testing and mitigate environmental pollution and food contamination. This work has led to a publication in *Critical Reviews in Analytical Chemistry* journal [10].

**Chapter 3 – Development of a Plasmonic Tablet using Dextran-Gold Nanoparticles (dAuNPs) and its pH-Sensitive Behaviour:** The next goal of my project was to fabricate a solid, sensitive detection platform in a ready-to-use format for point-of-use applications. This

study presented a portable, cost-effective tablet platform (1.22 CAD per 100 tablets) using dextran-gold nanoparticles (dAuNPs-Tablet), fabricated through a ligand exchange reaction between citrate-gold nanoparticles solution and dextran powder. The tablet's pH-responsive behavior was studied, which showed stable dispersion in neutral and alkaline conditions and controlled concentration-dependent aggregation in acidic environments, suitable for the detection of acid labile analytes. This work has led to a publication in the *ACS Omega* journal [33].

**Chapter 4 – Optimization of the Plasmonic Response of a Tablet for Point-of-use Detection of Environmental Analyte:** In this chapter, a tunable plasmonic sensor was developed by varying dextran content in the dAuNPs-Solution. The dAuNPs-Solution was synthesized using one-pot wet chemical reduction method using dextran and gold salt in alkaline media. Liquid and solid formats, including tablet, powder, and composite, were prepared and characterized using UV–vis spectroscopy, TEM, DLS, and zeta potential analysis. Dextran content significantly influenced surface charge and hydrodynamic size, with low dextran content (0.01%) achieving the highest sensitivity, detecting hypochlorite ($OCl^-$) concentrations as low as 50 µM. The sensor demonstrated selectivity and real-world applicability through interference analysis and swimming water sample testing. Furthermore, a 20X concentration of dAuNPs was achieved without centrifugation or morphological changes, highlighting the method's simplicity, scalability, and cost-effectiveness. This work has led to a publication in the *Microchimica Acta* journal [34].

**Chapter 5 – Fabrication of Plasmonic Tablet and Swab Sensors for Point-of-care Detection of an Oxidative Stress:** This chapter focuses on the detection of a disease biomarker using tablet and swab sensors. We utilized a nanoscale, reagent-free approach for colorimetric detection of urinary hydrogen peroxide ($H_2O_2$), a key oxidative stress biomarker. Initially, the colloidal dAuNPs-Solution was transformed into tablet (dAuNPs-Tablet) and cotton swab (dAuNPs-Swab) formats, leveraging their plasmonic properties for sensitive detection. The $H_2O_2$ detection follows Fenton chemistry, triggering dextran degradation, which induces nanoparticle aggregation and results in a color change visible to the naked eye. This phenomenon is enhanced by sodium chloride. Detection limits were 50 µM (tablet) and 100 µM (swab) in artificial urine. We also explored the effect of antioxidant therapy in reducing oxidative stress. Green tea antioxidants reduced urinary $H_2O_2$ levels in volunteers, highlighting potential health benefits.

These portable sensors advance oxidative stress diagnostics and point-of-care platforms. This work has led to a publication in the *ACS Applied Nano Materials* journal [35].

**Chapter 6 – Development of a Dual-Functional Nanogold Tablet for Biomedical Sensing of Glucose and Uric acid:** This chapter advances tablet technology to dual functionality, transforming the plasmonic tablet into a dual-functional tablet. We describe a colorimetric tablet sensor with two functions that uses dAuNPs-Solution to detect uric acid and glucose in urine. Uric acid detection is achieved utilizing the plasmonic behaviors while glucose detection is performed considering the nanozyme properties of dAuNPs. This customizable, cost-effective, dual-functional platform advances POC testing, enabling rapid, accurate diagnostics. This work has led to a publication in the *Nanoscale Advances* journal [36].

**Chapter 7 – Conclusion and Future Directions:** This chapter summarizes the key findings of the research on developing the plasmonic tablet platform and its advancement into a dual-functional tablet for point-of-use environmental monitoring and disease diagnosis. Additionally, it outlines future research directions and provides recommendations for further improvements.

To comply with the Concordia thesis regulations, figures and tables may have been modified from the published article.

## 1.5 Research Contribution

The majority of the research presented in this thesis was conducted by the author of this thesis. Amongst the co-authors in the journals, Dr. Sana Jahanshahi-Anbuhi has conceived and supervised all the study and investigations presented in the thesis. Seyed Hamid Safiabadi Tali did brainstorming session in organizing thoughts and did review and give useful comments to enhance the clarity of the manuscripts. Muna Al-Kassawneh and Maryam Mansuri assisted me in formal analysis, resources, and optimization of the methodology developed for hypochlorite and glucose detection respectively. Hasti Hajimiri helped in drawing of graphics related to the colorimetric assays published in *Critical Reviews in Analytical Chemistry*.

### 1.5.1 Publications

**First author work**

• **Zubi Sadiq**, Seyed Hamid Safiabadi Tali, Maryam Mansouri, and Sana Jahanshahi-Anbuhi, Dual functional nanogold tablet as a plasmonic and nanozyme sensor for point-of-care applications, *Nanoscale Advances* (**2025**).

https://pubs.rsc.org/os/content/articlepdf/2025/na/d5na00082c

[#]*This research is presented in chapter 6.*

• **Zubi Sadiq**, Muna Al-Kassawneh, Seyed Hamid Safiabadi Tali, and Sana Jahanshahi-Anbuhi, Dextran-gold nanoparticle-based tablets and swabs for colorimetric detection of urinary $H_2O_2$, *ACS Applied Nano Materials*, 8, 1008-1020 (**2025**).

https://pubs.acs.org/doi/10.1021/acsanm.4c05691

[#]*This research is presented in chapter 5.*

• **Zubi Sadiq**, Muna Al-Kassawneh, Syed Hamid Safiabadi Tali, and Sana Jahanshahi-Anbuhi, Tailoring plasmonic sensing strategies for the rapid and sensitive detection of hypochlorite in swimming water samples, *Microchimica Acta*, 191, 183 (**2024**).

https://link.springer.com/article/10.1007/s00604-024-06246-y

[#]*This research is presented in chapter 4.*

• **Zubi Sadiq**, Seyed Hamid Safiabadi Tali, and Sana Jahanshahi-Anbuhi, Gold tablets: Gold nanoparticles encapsulated into dextran tablets and their pH-responsive behavior as an easy-to-use platform for multipurpose applications, *ACS Omega*, 7, 11177–11189 (**2022**).
https://doi.org/10.1021/acsomega.1c07393

[#]*This research is presented in chapter 3.*

• **Zubi Sadiq**, Seyed Hamid Safiabadi Tali, Hasti Hajimiri, Muna Al-Kassawneh, and Sana Jahanshahi-Anbuhi, Gold nanoparticles-based colorimetric assays for environmental monitoring and food safety evaluation, *Critical Reviews in Analytical Chemistry,* 1-36 (**2022**).

https://doi.org/10.1080/10408347.2022.2162331

[#]*This research is presented in chapter 2.*

• AmirReza R. Esfahani[†], **Zubi Sadiq**[†], Oyejide Damilola Oyewunmi, Seyed Hamid Safiabadi Tali, Ndifreke Usen, Daria Camilla Boffito, and Sana Jahanshahi-Anbuhi, Portable, stable, and sensitive assay to detect phosphate in water with gold nanoparticles (AuNPs) and dextran tablet, *Analyst,* 146, 3697-3708 (**2021**). https://pubs.rsc.org/en/content/articlehtml/2021/an/d0an02063j

*†These authors contributed equally to this work. Selected for highlight on the covers of Analyst Journal. [#]My contribution to this research includes conceptualization, methodology, review and editing, visualization, and addressing the reviewers' queries.*

**Co-author work**

• Seyed Hamid Safiabadi Tali, Rozhin Saebi, Abdolali Mehrjou, Farzad Mirzaie, **Zubi Sadiq,** Marc-Antoni Goulet, Sana Jahanshahi-Anbuhi, Do-it-yourself screen printing with sandwiched electrodes for sensitive electrochemical paper-based analytical devices (ePADs), *Lab-on-a-Chip* (submitted **2025**).

*[#]My contribution to this research includes reviewing, visualizing, and drawing the reaction scheme to enhance the clarity of the manuscript.*

• Seyed Hamid Safiabadi Tali, Muna Al-Kassawneh, Maryam Mansouri, **Zubi Sadiq**, and Sana Jahanshahi-Anbuhi, All-in-one reagent tablet with rapid auto-mixing for point-of-care diagnostics, *ACS Sensors*, 10 (5), 3493-3503 (**2025**).

https://pubs.acs.org/doi/10.1021/acssensors.4c03726

*[#]My contribution to this research includes reviewing, visualizing, drawing the reaction scheme, and providing thorough feedback to improve the clarity of the manuscript.*

• Maryam Mansouri, Seyed Hamid Safiabadi Tali, **Zubi Sadiq**, and Sana Jahanshahi-Anbuhi, User-friendly detection of nitrite in soil samples with tablet-based sensor, *Microchemical Journal,* 216, 114584 (**2025**).

https://www.sciencedirect.com/science/article/abs/pii/S0026265X25019381

*[#]My contribution to this research includes participating in brainstorming sessions, reviewing and editing, visualizing, and providing thorough feedback to improve the clarity of the manuscript.*

• Muna Al-Kassawneh, **Zubi Sadiq**, and Sana Jahanshahi-Anbuhi, User-friendly and ultra-stable all-inclusive gold tablets for cysteamine detection, *RSC Advances*, 13, 19638-19650 (**2023**). https://doi.org/10.1039/D3RA03073C

[#]*My contribution to this research includes project administration, review and editing, visualization, and providing feedback to enhance the readability of the manuscript.*

• Seyed Hamid Safiabadi Tali, Hasti Hajimiri, **Zubi Sadiq**, and Sana Jahanshahi-Anbuhi, Engineered detection zone to enhance color uniformity on paper microfluidics fabricated *via* Parafilm®-heating-laser-cutting, *Sensors and Actuators B: Chemical,* 380, 133324 (**2023**).

https://doi.org/10.1016/j.snb.2023.133324

[#]*My contribution to this research includes review and editing, drawing chemical reactions, visualization, and providing feedback to the manuscript.*

• Hasti Hajimiri, Syed Hamid Safiabadi Tali, Muna Al-Kassawneh, **Zubi Sadiq**, and Sana Jahanshahi-Anbuhi, Tablet-based sensor: a stable and user-friendly tool for point-of-care detection of glucose in urine, *Biosensors* 13 (9): 893 (**2023**).

https://doi.org/10.3390/bios13090893

[#]*My contribution to this research includes participating in brainstorming sessions, data curation, review and editing, visualization, and give feedback throughout the project.*

• Muna Al-Kassawneh, **Zubi Sadiq**, and Sana Jahanshahi-Anbuhi, Pullulan-stabilized gold nanoparticles tablet as a nanozyme sensor for point-of-care applications, *Sensing and Bio-Sensing Research*, 38, 100526 (**2022**).

https://doi.org/10.1016/j.sbsr.2022.100526

[#]*My contribution to this research includes conceptualization, project administration, drawing graphics, review and editing, visualization, and providing feedback throughout the project.*

• Seyed Hamid Safiabadi-Tali, Jason J. LeBlanc, **Zubi Sadiq**, Oyejide Damilola Oyewunmi, Carolina Camargo, Narges Armanfard, Selena Sagan, and Sana Jahanshahi-Anbuhi, Tools and techniques for severe acute respiratory syndrome coronavirus 2 (SARS-CoV-2)/COVID-19 detection, *Clinical Microbiology Reviews*, 34 (3): 1-63 (**2021**).
https://journals.asm.org/doi/10.1128/CMR.00228-20

[#]*My contribution to this research includes browsing relevant literature, organizing ideas into well-structured categories, and visualizing the manuscript.*

### 1.5.2 Conferences

• **Zubi Sadiq** and Sana Jahanshahi-Anbuhi, "An advancement in tablet technology: From plasmonic to nanozyme-based detection", CIC Montreal Annual Symposium 2025, Montreal, Canada, 26th May **2025** (Poster).

• **Zubi Sadiq** and Sana Jahanshahi-Anbuhi, "Plasmonic tablet sensor: A user-friendly tool for uric acid monitoring", Chemical Engineering Research Day, Montreal, Canada, 31st March **2025** (Oral).

#*This participation was recognized with the Presentation Award, 2nd place.*

• **Zubi Sadiq** and Sana Jahanshahi-Anbuhi, "Fabrication of a plasmonic swab sensor for the detection of oxidative stress biomarker", Chemical Engineering Research Day, Montreal, Canada, 27th March **2024** (Oral).

• **Zubi Sadiq** and Sana Jahanshahi-Anbuhi, "Plasmon-based sensing platforms for colorimetric detection of hypochlorite ($OCl^-$) in environment", PEOPLE 2023 conference, Montreal, Canada, 7-11th August **2023** (Poster).

[#]*This participation was recognized with the first prize, the "Student Poster Presentation Award".*

• **Zubi Sadiq** and Sana Jahanshahi-Anbuhi, "Plasmonic dextran-gold nanoparticles (dAuNPs) probe as a user-friendly sensor for point-of-care detection of the oxidative stress biomarker", Canadian Chemical Engineering Conference, Calgary, Canada, 29th October-01st November **2023** (Oral).

[#]*This participation was recognized through financial support from various sources, including the Conference and Exposition Allowance (CAD 750), the GCS Conference Travel Support (CAD 500), and the GSA's Conference Funding (CAD 125.27) for the CSChE 2023 International Conference.*

• **Zubi Sadiq** and Sana Jahanshahi-Anbuhi, "A tunable plasmonic nanosensor; Fabrication approach and its application to detect hypochlorite ($OCl^-$)", Chemical Engineering Research Day, Montreal, Canada, 17th March **2023** (Oral).

• **Zubi Sadiq** and Sana Jahanshahi-Anbuhi, "Portable AuNPs tablet as a colorimetric sensor", Chemical Engineering Research Day, Montreal, Canada, 17-18th March **2022** (Oral).

#*This participation was recognized with the "Outstanding Presentation Award" valued CAD 200.*

• **Zubi Sadiq** and Sana Jahanshahi-Anbuhi, "Encapsulated nanoparticles into biopolymer tablet as next-generation material for point-of-use applications", 6th Virtual Edition of Polymers, Plastics, and Composites, 08-09th December **2022** (Oral).

#*This participation was recognized through financial support under the Concordia University Conference and Exposition Award (CAD 218).*

• **Zubi Sadiq** and Sana Jahanshahi-Anbuhi, "AuNPs-dextran as next generation nanoprobes", CCEC 2021 – 71st Canadian Chemical Engineering Conference, Montreal, Canada, 24-27th October **2021** (Oral).

#*This participation was recognized through financial support under the Concordia University Conference and Exposition Award (CAD 368).*

• **Zubi Sadiq** and Sana Jahanshahi-Anbuhi, "Colorimetric sensor for phosphate detection", Chemical Engineering Research Day, Montreal, Canada, 30-31st March **2021** (Oral).

• **Zubi Sadiq** and Sana Jahanshahi-Anbuhi, "Sensing applications of AuNPs in environmental monitoring and diagnostic assessment", Chemical Engineering Research Day, Montreal, Canada, 16-17th March **2020** (Oral).

### 1.6 Awards and Recognition

- *Fonds de recherche du Québec – Nature et Technologies* (FRQNT) B2X scholarship (CAD 70,000), Govt. of Quebec, Canada (Summer 2022 – Summer 2025).
- *Concordia International Tuition Award of Excellence* (CAD 35,435), Concordia University, Montreal, Canada (Winter 2021 – Summer 2023).
- *Concordia University Graduate Doctoral Incentive Fellowship* (CAD 56,000), Concordia University, Montreal, Canada (Fall 2020 – Summer 2024).
- *Steven Goldberg Entrance Bursary* (CAD 5,000), Concordia University, Montreal, Canada (Fall 2019).

### 1.6.1 Student Leadership and Social Mobilization

I actively participated in Girls Summer Engineering and Technology Program for 4 years.

- Chemo/biosensors in modern life, GirlSET 2025
- Chemo/biosensors from lab to everyday life, GirlSET 2024
- Chemo and biosensors, GirlSET 2021
- Smart paper to detect water contamination, GirlSET 2020

I am the part of the selected cohort of students to be part of an innovation lab challenge "Innovations for Concordia Classrooms, Learning Spaces and Technologies: A Special Look at the Loyola Campus" with Centre for Teaching and Learning (CTL) and Lab for Innovation in Teaching & Learning (LITL).

I presented in the 2023 Concordia *3-Minute Thesis* (3MT) competition. The 3MT is a competition challenges students to distill complex research into a clear, jargon-free presentation that engages a non-specialist audience — all in just under three minutes and using a single, static PowerPoint slide.

I am responsible for maintaining the lab's chemical inventory and managing waste disposal. Also, I am a member of the volunteer committee responsible for organizing Chemical Engineering Research Day, where I chaired technical sessions, coordinated schedules, and managed registered presenters.

# CHAPTER 2 An Overview of Gold Nanoparticles-Based Colorimetric Assays: From Fundamentals to Advanced Applications

***This chapter is reproduced from the article published in Critical Reviews in Analytical Chemistry, 1-36 (2022). Additionally, recent publication from 2022 to 2025 have been included to provide updated and detailed information.***

In this chapter, a comprehensive viewpoint is discussed regarding an exponential increase in the research on gold nanoparticles (AuNPs)-based colorimetric sensors to revolutionize the point-of-use sensing devices. The chapter begins with the characteristics of AuNPs, followed by a brief explanation of synthesis and functionalization methods. Then, the mechanisms of AuNPs-based sensors are comprehensively explained in two broad categories based on surface plasmon resonance characteristics of AuNPs and their peroxidase-like catalytic properties (nanozyme). Surface plasmon resonance-based colorimetric sensors further categorize into aggregation, anti-aggregation, etching, growth-mediated, and accumulation-based methods depend on their sensing mechanisms. On the other hand, peroxidase activity-based colorimetric sensors are divided into two methods based on expression or inhibition of peroxidase-like activity. Next, the analytes in environmental and food samples are classified as inorganic, organic, and biological pollutants, and recent progress in detection of these analytes are reviewed in detail. Finally, conclusions are provided, and future directions are highlighted.

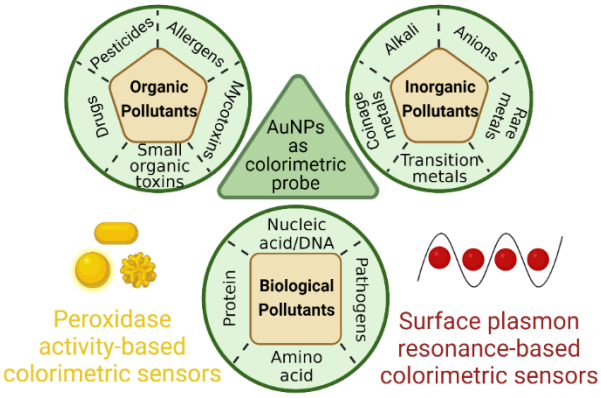

## 2.1 Introduction

Gold nanoparticles (AuNPs) have gained much interest during the past decades, and their applications and characteristics have been investigated in many disciplines, from physics and chemistry to biology and medicine. Historically, the use of AuNPs dates back to the 4$^{th}$ century A.D. when the Romans used them for producing gold ruby glasses, with the Lycurgus cup as a famous example [37,38]. Nonetheless, the modern scientific evaluation of the AuNPs began from 1850s, when Michael Faraday investigated the change in the color of Au particles with respect to their size [39]. Then, through the 20$^{th}$ century, reliable and efficient methods for the synthesis of AuNPs with different characteristics were developed, followed by the upsurge of publications and applications since the beginning of the 21$^{st}$ century [40–44]. AuNPs are usually used in the size range of 2-100 nm and have been developed in several shapes [45]. It is due to their outstanding characteristics such as high surface-to-volume ratio, straightforward synthesis, high stability, unique optical, catalytic and electrical properties, controllable size, biocompatibility, and versatile surface chemistry amenable to functionalization that they have been used in various applications, including therapeutics, forensics, imaging, and particularly detection [46–51]. Figure 2.1 displays the timeline of advancements in AuNPs research and applications since Romans times.

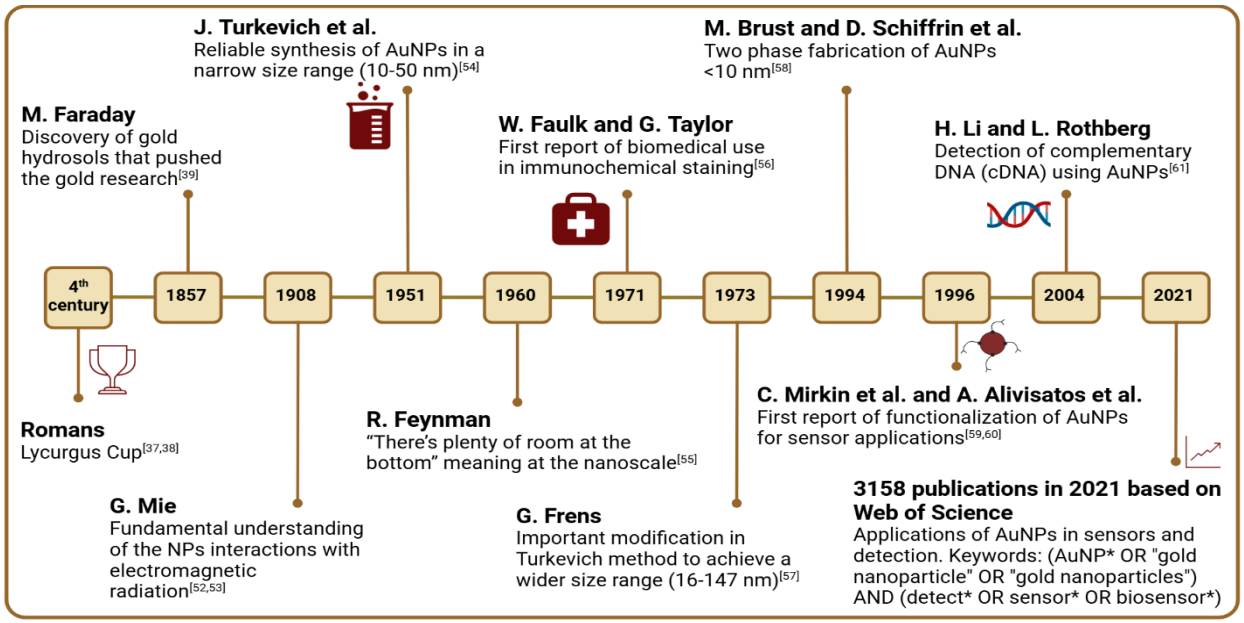


Figure 2.1 Timeline of advancements showing important developments and applications of AuNPs.

From left to right, a Lycurgus cup of Roman heritage was created holding Au-Ag NPs to obtain a dichroic effect [37,38]. Then, Michael Faraday made the discovery of gold hydrosols that pushed the gold research first time in 1857 [39]. In 1908, Mie theory was discovered as fundamental understanding of the NPs interactions with electromagnetic radiation [52,53]. Afterwards, Turkevich method of AuNPs synthesis in the range of 10-50 nm [54]. In 1960, Feynman mentioned in a famous lecture that "There's plenty of room at the bottom" meaning at the nanoscale[55]. In 1971, Faulk and Taylor used AuNPs in biomedical field for immunochemical staining [56] Frens reported an important modification in Turkevich method to achieve wide range 16–147 nm of AuNPs [57] Then, Brust and Schiffrin had fabricated AuNPs in less than 10 nm in two phases [58]. First report of functionalization of AuNPs as a sensor[59,60]. In 2004, Li and Rothberg reported the detection of complementary DNA (cDNA) using AuNPs [61]. Total 3158 publications had been reported in the detection and sensor field based on Web of Science.

Accurate and convenient detection of chemical and biological agents is of high importance for various applications such as food and environmental monitoring, disease diagnostics, and forensics [62–66]. Chemical and biochemical sensors have two main components: 1) target molecule recognition which is the specific binding of the sensor reagents to the target analytes and 2) transduction, which is the act of reporting the binding between the sensor reagent and the analyte. Both components are essential in order to have a sensor with high sensitivity and specificity [67,68]. Among various detection techniques, colorimetric sensors have attracted much attention due to their ease-of-use, relative simplicity in design, and allowing for equipment-free readout with naked eyes that makes them especially useful for on-site detection [69]. The incorporation of AuNPs in colorimetric sensors further accelerated this area, with AuNPs greatly enhanced signal transducing and opened new gateways for exploration [70]. So far, AuNP-based colorimetric assays have been utilized to detect various types of analytes, e.g., small molecules [71,72], nucleic acids [73,74], proteins [75,76], and metal ions [77–79]. Also, these assays have been coupled with convenient device formats such as lateral flow assay, paper-based, and microfluidic devices to enable rapid, portable, and low-cost detection tools [80–82].

Compared to other metals (e.g., cerium, zinc, and palladium) and polymer nanoparticles (e.g., silica and latex), AuNPs have been the preferred choice for colorimetric applications mainly due their excellent surface plasmon resonance, resulting in a characteristic color formation. Also, among other plasmonic materials such as silver and platinum, AuNPs are favored due to various reasons. For example, silver nanoparticles (AgNPs) have high toxicity profile and impart adverse health effects compared to AuNPs [83]. Moreso, AgNPs are light sensitive and special treatment

is required to improve their photostability [84]. Platinum nanoparticles (PtNPs) are usually used as a nanozyme and require a chromogenic agent to produce visible color change [85,86]. Hence, AuNPs have become limelight of research for scientists, researchers, and nanotechnologists. Recent years have witnessed a significant increase in the number of publications related to AuNPs, and many informative reviews have been published discussing colorimetric AuNPs-based sensors.[87,88] A few of them have addressed the use of paper-based microfluidic devices for environmental analysis.[89,90] Nonetheless, rapid progress in this area justifies the need for an updated compilation of information. This state-of-the-art review provides a comprehensive viewpoint on the AuNPs related surface plasmon resonance-based colorimetric sensors and peroxidase activity-based colorimetric sensors in environmental monitoring and food assessment with focus on recent publications. Of course, not all publications can be covered in a single paper, but this review provides an overview of the significant advances in these areas. First, synthetic methods, properties of AuNPs, and mechanisms of colorimetric detection with AuNPs are discussed briefly, followed by in-depth review of the significant publications in environmental and food monitoring. Furthermore, key findings of the references used are summarized in tables S2.1-S2.3 for better comparison of recent colorimetric approaches. Finally, current challenges and future directions are highlighted to point-out less-explored domains of AuNPs-based colorimetric sensors and pave the way for future advancements in this area.

## 2.2 Synthesis and Functionalization of AuNPs

### 2.2.1 Synthesis

Significant efforts have been dedicated over the past half century to develop and understand synthesis strategies for AuNPs. These strategies are divided into two broad categories of top-down and bottom-up, with the latter being the more effective and common one [91,92]. The top-down methods create nanoparticles by removal from bulk golds using techniques such as photolithography [93], laser ablation [94], ion sputtering [95], and aerosol technology [87,96]. Conversely, the bottom-up approaches create AuNPs by reducing the Au ions into Au atoms and subsequently clustering the atoms into nanoparticles, followed by a stabilization step done by capping agents which hinder the agglomeration of the nanoparticles [87,96]. The bottom-up approaches mainly divide into the two categories of chemical and green methods [87].

Of note, special focus has been on understanding the relations between different strategies and their parameters such as temperature, concentrations, and pH with the characteristics of the resultant AuNPs including size, shape, stability, absorption maximum, and applications to enable controllable synthesis of AuNPs [87,88]. So far, AuNPs in the size range of ~1.8 to 190 nm can be readily synthesized, and the shapes include nanosphere, nanorod, nanostar, nanoshell, and nanocage [45,87]. Figure 2.2A-E represents various shapes, sizes, colors, functional ligands, stabilization forces, synthetic approaches, and sensor types of AuNPs. For colorimetric detection, the mostly used AuNPs are nanospheres, with the chemical methods being the mostly used ones for the synthesis [45].

*2.2.1.1. Chemical synthesis of AuNPs*

In chemical synthesis, reactions occur in an aqueous or organic medium in the presence of a chemical reducing agent. The most common chemical synthesis method is the Turkevich-Frens method owing to its relative simplicity, controllable size, stability of the prepared colloidal AuNPs, as well as the relatively loose coating of citrates on AuNPs that can be easily replaced by other ligands with desired functionality [87]. Other common methods include the Brust-Schiffrin method and seed-mediated growth. These methods are reviewed in detail elsewhere [45] and are briefly discussed here.

The Turkevich-Frens method, also called sodium citrate reduction method or classical citrate method, was originally developed by Turkevich in 1951 based on many reported studies [88,97]. The basic principle of this method involves reduction of Au ions ($Au^{3+}$) in chloroauric acid into Au atoms ($Au^{0}$) by a reducing and capping agent, such as citrate, in reactions that undergo a series of color change from light yellow to ruby red [88,98]. However, the spherical AuNPs prepared by this method had a narrow size range of 10-50 nm, which limited their applications [99]. To solve this issue, in 1973, Frens changed the ratio of sodium citrate and gold chloride and achieved a size range of 16-147 nm by different ratios, after which the Turkevich-Frens method was established and used extensively in various applications [100]. Since then, variations of the method have been reported, including changes in the pH, reducing agents, and stabilizing agents to get varying sizes and stabilities [45,88]. While the Turkevich-Frens method is fairly reproducible and is commonly used, it has its own limitations, including the fact that the size range of stable spherical AuNPs is 10-50 nm beyond which the nanoparticles will aggregate and

become less spherical, the susceptibility to environmental conditions such as pH, ionic strength, and salt concentration depending on the stabilizing agent used, and relatively low yield [88].

The Brust-Schiffrin method was first introduced in 1994 and involves a two-phase liquid-liquid reaction inspired by the Faraday's two-phase system [101]. In this procedure, the $AuCl_4$ is transferred to the organic phase (i.e., toluene) by a phase-transfer reagent such as tetraoctylammonium bromide (TOAB) from its aqueous solution, followed by reduction using sodium borohydride ($NaBH_4$) in the presence of alkanethiol as the stabilizing agent [102]. The reaction mixture goes from orange to deep brown upon the addition of $NaBH_4$, and the synthesized AuNPs are spherical in the size range of 1.5-5.2 nm [88]. The size of the prepared AuNPs can be controlled by reaction conditions such as temperature, thiol/gold ratio, and reaction rate [88]. Also, several modifications of the Brust-Shiffrin method have been introduced using different thiol containing molecules [103–106]. Of note, one of the main advantages of this method is the direct synthesis of thiol-functionalized AuNPs, which have many applications in sensors area. Other advantages include thermal and air-stability as well as dispersibility in organic solvents without irreversible aggregation [88,107]. Nonetheless, the Brust-Schiffrin method is prone to limitations such as less dispersibility of the prepared AuNPs and the use of organic solvents in the process which may limit the use of AuNPs in some biological applications.

Another common method for the synthesis of AuNPs is the seed-mediated growth which became more common after reported by Wiesner *et al.* in 1989 in a procedure similar to the Faraday's original colloidal synthesis method [108]. While the seed-mediated growth is the most common method for the synthesis of rod-shaped AuNPs, spherical AuNPs are also reported, with a size range of 1.5-86 nm [45]. In this procedure, first, gold salts are reduced by a strong reducing agent such as citrate or $NaBH_4$, resulting in small size AuNPs that act as seeds for the fabrication of larger AuNPs. Then, a solution of AuNPs is added to the mixture in the presence of a weak reducing agent such as ascorbic acid, followed by addition of a structure directing agent that prevents further nucleation and enhances the growth of the AuNPs. Overall, since this method uses step-by-step increase of the size, it allows for the controllable synthesis of AuNPs with desired shape and size. Nonetheless, the relatively large number of influential parameters makes

the process difficult to control and optimize, including temperature, reducing agent and precursor concentrations, seed concentration, and the rate of the addition of the reducing agent [88].

Altogether, chemical methods are the most common methods for the synthesis of AuNPs due to their simplicity, ease-of-operation, and allowing for various shapes and sizes of AuNPs. Of note, in addition to the methods mentioned above, many other approaches have been reported in the literature using precursors other than chloroauric acid, various stabilizing reagents and techniques, and different synthesis procedures [45].

*2.2.1.2. Green synthesis of AuNPs*

In order to produce biocompatible AuNPs in eco-friendly processes, green synthesis methods have emerged which aim to reduce or eliminate the harsh chemicals used and produced in the synthesis of AuNPs. These procedures are divided into the two broad categories of physical and biological methods.

Physical techniques utilize the energy of electromagnetic or acoustic waves as well as particle-like radiation to induce chemical reactions in the solution, leading to the reduction of Au ions without the need for chemical reducing agents [88]. These techniques include gamma and X-ray radiations techniques [109–114], microwave-assisted methods [115–120], ultraviolet (UV) [121], laser ablation [122], ultrasonic [123,124], and electron beam irradiation [125], and encompass methodologies such as photochemical, thermolytic, and sonochemical procedures. The gamma irradiation allows for controllable synthesis of AuNPs, with spherical and nanorod AuNPs in the size range of 2-22 nm been reported. Photochemistry is a relatively simple method that uses a light source like sun or UV light to produce radicals in the system that act as the reducing agent to form AuNPs, while the whole reaction can occur within seconds to few minutes [126,127]. Microwave-assisted methods produce heat in the system that leads to reduction, and the procedure is rapid [128–130]. Overall, the physical methods allow for synthesis of AuNPs with controllable size and structure with reduced time and the possibility of simultaneous synthesis and sterilization of the products. Nonetheless, they have limitations such as low availability of some of the technologies such as X-rays and gamma irradiators, as well as susceptibility of some of the materials to the radiations, especially capping and stabilizing reagents.

Biosynthesis of AuNPs have gained much interest as a cost-effective green method that applies plant-based compounds and extracts (e.g., leaf, flower, and root) [87,131,132], microorganisms

(e.g., bacteria, fungi, and algae) [87], and biomolecules (e.g., proteins, amino acids, carbohydrates) [133–135] in the production of AuNPs. Using plant-based compounds is a facile method for producing various sizes of AuNPs (2-300 nm) that requires no additional stabilizers and capping agents [87]. Synthesis with microorganisms can be carried out via intracellular and extracellular methods, but the latter one is favored as it requires less purification steps and hence takes less time and effort. Also, the AuNPs produced with microorganisms showed less cytotoxicity on human cells compared to those of the typical synthesis methods [136]. In addition, studies have shown that AuNPs can be synthesized with biomolecules, including proteins (e.g., sulfite reductase) [137], amino acids (e.g., histidine) [138], and carbohydrates (e.g., dextrose) [139]. Of note, one possible issue that may occur when using microorganisms is the improper mixing of the solution that can lead to heterogenous results and products, thus should be carefully controlled [88]. Also, the mechanisms of biological synthesis are not fully understood, possibly due to the large number of interacting molecules, and more research is required to enable more efficient controllable synthesis by biological means.

In conclusion, both chemical and green synthesis methods have their own pros and cons that need to be considered with respect to the required application [140]. The chemical methods offer more flexibility in AuNPs surface chemistry and are simple, fast, and high yielded. Also, the AuNPs produced by chemical methods have reduced dispersity and high thermal stability. Nonetheless, the toxicity of the chemicals used in the chemical synthesis processes, or the by-products of the reactions may have detrimental effects on the environment and living organisms, raising concerns for their large-scale production and limiting their use in biological applications, respectively [88]. On the other hand, green route is beneficial due to being cost-effective, sustainable, non-toxic, and eco-friendly which produces less pollution and is considered safer for human health, making them suitable for biomedical applications. However, regarding the biosynthesis of AuNPs, plant extracts have little diversity in functional groups resulting in restricted choice of surface functionalities around AuNPs. Moreover, the procedure is often time-consuming due to issues related to the extraction of raw materials, often low yielded and produces less uniform particle size due to complexity of natural reducing agents [141]. Of note, green methods related to physical techniques produce uniform morphology of AuNPs with high-speed preparation processes and purity, but such procedures may require bulky equipment that are expensive.

### 2.2.2 Functionalization

While there is no precise definition of the term "functionalization" in the literature, functionalization in the case of AuNPs is usually referred to anchoring molecules to the AuNPs with specific properties and functions in addition to simple stabilization [142]. Regarding sensors and biosensors, this specific function is typically the facilitation of a specific response to the target analytes in order to provide high selectivity and sensitivity. Historically, the functionalization of AuNPs for sensor applications was first reported in 1996, when two research groups functionalized AuNPs with thiolated oligonucleotides and used them for the detection of DNAs [143,144]. So far, various categorizations have been proposed to classify functionalization of AuNPs based on the type of the binding between the functionalization agents and AuNPs, the procedure of functionalization, and the arrangement of functionalization agents on the surface of AuNPs as shown in Figure 2.2B.

Functionalizing agents can bind to the surface of AuNPs *via* physical adsorption or covalent binding. Physical adsorption is based on the forces such as electrostatic interaction between the oppositely charged molecules and van der Waals effects, and it is also referred to as physisorption or electrostatic adsorption [145]. For example, unfolded single-stranded DNAs (ssDNAs) [146,147] and streptavidin [148] were bound to the citrate-capped AuNPs *via* electrostatic forces and used for the detection of different analytes. Both, neutral ligands (e.g., Tween 80, Tween 20 and poly (ethylene glycol)) and charged ligands (e.g., citrate, phosphine, and borohydride) can be used with this technique [149–152]. While physical adsorption process is rapid and relatively simple, physical bindings suffer from limitations such as susceptibility to the environmental conditions (e.g., pH and ionic strength) as well as lack of proper orientation of ligands onto AuNPs which makes biological processes difficult to handle. Covalent binding, on the other hand, is the most widely used approach and provides high stability for AuNPs against different salt concentrations, thermal treatment, and attacks by other ligands. Covalent coupling is mainly based on the strong bonding between the S and Au atoms, and thus, many thiol and sulfur containing/modified molecules have been studied for binding onto AuNPs, including alkane thiolates [153], glutathione [154], thioethers [155], disulfide [156], xanthates [157], and DNAs and aptamers [158,159]. Amino acids, peptides, and proteins can also bind to the AuNPs via the thiol group on the cysteine amino acid or *N*-terminal primary amine [149,160]. In case of amino acid functionalized AuNPs, the presence of amino and carboxylic functionalities in their

structure makes them good cross-linkers for the aggregation purposes [161]. Hence, the amino acid modified AuNPs act as a recognition probe for a variety of analytes detection due to the presence of electrostatic interactions between analyte and carboxylate group of amino acid [162]. Additionally, these probes or small peptide modified AuNPs have been used for the detection of some amino acids for instance arginine, histidine, lysine, aspartic acid, and cysteine [163].

Regarding the procedure of functionalization, functionalization can either be performed simultaneously with the synthesis process or as another step after the synthesis. For the former one, various approaches can be adopted, including using only functionalization agents in the solution as well as a mixture of functionalization agents and stabilization agents [164,165]. Post-synthesis functionalization can be realized by the two approaches of ligand replacement of the stabilization agent with the functionalization agent or reaction onto the surface of AuNPs. Ligand exchange of the citrate-capped AuNPs with amine or thiol groups is relatively easy due to the weak binding of citrate to the AuNPs and can be done under the ambient conditions [166]. Nonetheless, the ligand replacement of thiol bound AuNPs with other thiol-containing molecules is more challenging and is typically done in a solvent such as toluene in ambient condition over several days [149,167]. Also, various techniques have been used to functionalize AuNPs by reaction on the surface of AuNPs as a platform. These techniques include ‘click’ chemistry, which typically refers to Husigen 1,3-dipolar cycloaddition of azides and terminal amides [149,168], and polymerization procedures such as living radical polymerization (LRP) [169] and surface-initiated atom-transfer radical polymerization (SI-ATRP) [170,171].

For certain applications, AuNPs may need to be co-functionalized with several ligands each with different functionality. For example, AuNPs co-functionalized with poly (ethylene glycol) (PEG) and peptides [172], and PEG and fluorescent dyes [173] have been reported for *in vivo* applications, showing high stability and circulation time inside the body. There are three types of co-functionalization according to the arrangement of the ligands on the surface of AuNPs, including mixed monolayers, co-functionalization by means of a linker molecule, and the combination of both, with the mixed monolayers being the most common one [149,167], Mixed monolayer coatings can be created by first replacement of the citrate on the citrate-capped AuNPs with a certain amount of thiolated PEG to produce partially coated AuNPs, and then reacting the prepared AuNPs with another ligand. In the co-functionalization by using a linker,

the AuNPs are first fully coated with a polymer such as PEG and the other ligand is bound to the other end of the polymer chain.

Of note, among various functionalizing agents, intensive research has been done on DNA or aptamer functionalization on AuNPs due to their high binding affinity towards analytes (low detection limit) and high specificity [174]. Also, as DNAs and aptamers are programable entities, they allow AuNPs to be organized uniformly into one-, two- or three-dimensional arrays and superstructures [175]. Different strategies have been opted to conjugate DNAs onto AuNPs following either physical adsorption or covalent binding [176]. Physical adsorption takes place either directly or through biomolecule promoted non-covalent binding. Direct physical adsorption is influenced by the natural affinity between nucleobases and AuNPs irrespective of the presence of thiol group. The binding strength of DNA bases to AuNPs *via* keto and imino groups are in the order of adenine > cytosine ≅ guanine > thymine [177]. This binding affinity helps to regulate/tune DNA density on AuNPs surface by controlling the amount of a specific nucleobase in an engineered DNA structure [178]. Of note, adsorption affinity of adenine base is weaker as compared to thiol moiety. Also, highly specific biomolecular interactions are involved in non-covalent binding of biotinylated DNA and protein-capped AuNPs (e.g., streptavidin or avidin). The streptavidin or avidin has four biotin-binding sites resulting attachment of more than one DNA per protein. On the other side, covalent binding takes place either by chemisorption or ligand-mediated covalent bonding. Commonly used thiolated DNAs have disulfide bond which is reduced to two thiol groups before conjugation [179]. Ligand-mediated covalent bonding is a post-synthesis functionalization and reaction takes place on the surface of AuNPs by cross-linking between two compatible functional groups of AuNPs and DNA. For example, EDC coupling has been used between an amine and carboxylic groups to form an amide bond as well as click chemistry-based on azide and alkyne groups to form triazole linkage [180]. In short, a wide range of engineered DNAs have been adsorbed onto AuNPs which have significantly advanced the biosensing technology.

Since the DNA functionalization onto AuNPs dramatically affects the colloidal stability, it is highly important to strategically control the density of DNA onto Au surface for various applications. In this regard, many researchers have presented landmark works to solve many issues such as time-consuming preparation process, adsorption of DNAs in a quantitative

manner, low density, and limited stability. Mixing of AuNPs with excessive thiolated DNAs cannot yield highly dense DNA surrounded AuNPs as electrostatic repulsion due to DNA phosphate backbones hinder this simple procedure. This challenge is solved by “salt-aging” method which utilizes slow addition of concentrated salt to effectively screen the charge of phosphate backbones in adsorbed thiolated DNAs on AuNPs [181]. However, the salt-aging process for getting highly dense DNA onto Au surface is tedious and time-taking which is replaced with other methods that involve addition of stabilizing surfactants or polymers, providing acidic environment, or freezing approach. Also, as hybridization between DNA-AuNPs and complementary DNA-AuNPs results in uncontrollable nanoparticles network structure, a precise control of DNA strands on Au surface is required which is achieved by getting low density of DNA onto AuNPs. Low density can be achieved by synthesizing discrete dimeric, trimeric, or multimeric AuNPs by controlling stoichiometric ratio [180]. Nonetheless, low grafting density of DNA onto Au surface is challenging with bigger size of AuNPs due to their less colloidal stability. Hence, efficient passivation with other ligands is used on AuNPs surface for low density of DNA strands. In short, conjugation of thiolated DNAs onto AuNPs can be achieved instantaneously (a few minutes) and controllably when considering DNA parameters (e.g., length, sequence, and functional groups) and AuNPs features (e.g., size, shape) in addition to immobilization strategy. Modified DNA bases or backbone with random DNA libraries adsorbed onto AuNPs can be a promising candidate for the detection of new analytes.

Overall, a plethora of methods and ligands have been proposed for the functionalization of AuNPs. Whether which one to use depends on the target analytes, detection mechanism, and the media/matrix and conditions that the sensor is intended to be applied. Of note, functionalization agents should provide sufficient stability for the modified AuNPs against agglomeration as often the stabilization agent is replaced with the functionalization agents. Also, a proper functionalization strategy should be adopted such that it does not alter the shape and size of the prepared AuNPs [165].

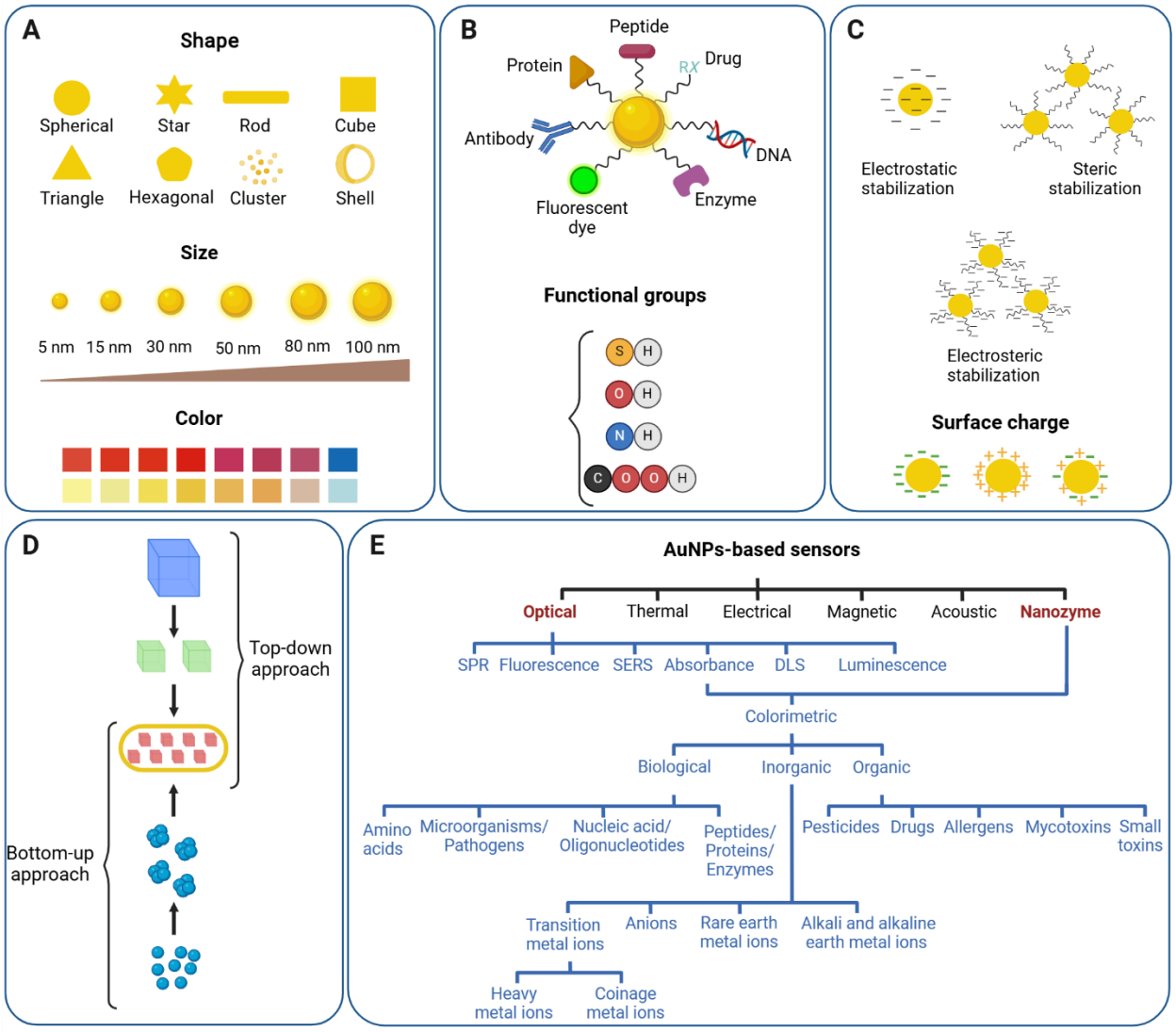


Figure 2.2 An overview of the AuNPs profile highlighting their main characteristics.
A) Representation of different shapes, size, and color of AuNPs; B) Surface functionalization of AuNPs with a variety of ligands having different chemical groups; C) Different types of stabilizing forces and surface charge around AuNPs; D) Synthetic approaches into top-down and bottom-up categories for the formation of AuNPs; E) The main categories of AuNPs-based sensors.

## 2.3 Characterization of AuNPs

After synthesis and functionalization, AuNPs need to be characterized from different aspects to understand whether the synthesis and functionalization have been conducted correctly, or the procedures need to be modified and optimized according to the desired properties. The common characteristics of AuNPs include size, size distribution, shape and morphology, surface charge, crystallinity, and surface chemistry. There are various tools and techniques to characterize

AuNPs each with their own applications, and often a combination of these techniques is required to comprehensively understand the properties of the AuNPs [182].

One of the most common methods to get basic understanding of the nanoparticles is transmission electron microscopy (TEM), which provides images of AuNPs and information about the size, and shape, size distribution and morphology of the particles [183]. Scanning electron microscopy (SEM) [184] and atomic force microscopy (AFM) [185,186] are other imagery techniques used. Dynamic light scattering can also be used to determine the size distribution of AuNPs [187]. Another conventional method is ultraviolet-visible (UV-Vis) spectrophotometry, which is usually used to investigate the formation and aggregation of the AuNPs [188]. Near-infrared (NIR) spectroscopy is also reported to investigate AuNP aggregates and different shapes of AuNPs [189]. To understand the surface chemistry of the prepared AuNPs, Fourier-transform infrared spectroscopy (FT-IR) is an effective method that provides information about the functional groups present on the AuNPs [188]. Gel electrophoresis is another technique that is mainly used to confirm the successful attachment of the oligonucleotides/polymers onto the surface of AuNPs through separating nano-conjugates based on their size and charge [190,191]. Other applications such as monitoring the surface density of the attached polymers has also been reported [192]. Another useful technique is measuring zeta potential of the colloidal solution that is the amount of the electric charge on the surface of AuNPs and is used for the estimation of the stability of the particles [193,194]. Higher level of stability of colloidal suspension of nanoparticle depends on the value of zeta potential ranging from −25 mV to +25 mV. Other methods used include X-ray diffraction (XRD),[195] energy-dispersive X ray (EDX),[196] surface-enhanced Raman spectroscopy (SERS),[197] single particle inductively coupled plasma mass spectrometry (SP-ICP-MS),[198] proton nuclear magnetic resonance (H-NMR) spectroscopy,[199] and laser desorption/ionization time-of-flight (LDI-TOF) mass spectrometry [200].

### 2.4 Mechanisms of AuNPs-based Colorimetric Sensors

In colorimetric devices, AuNPs can be used in two different ways. These particles are used as the transducer to produce the detectable signal in surface plasmon resonance-based colorimetric sensors while a capping agent is used as the sensing element. However, AuNPs act as a catalyst to facilitate the reaction between chromogenic substance (transducer) and targeted analyte in

peroxidase activity-based colorimetric sensors. The chemistry of molecular recognition step in colorimetric sensors determines the category of detection mechanism.

### 2.4.1 Mechanisms of AuNPs-related Surface Plasmon Resonance-based Colorimetric Sensors

In nano-optics community, AuNPs are recognized as noble nanoplasmon due to free electron gas density around the particle which offers limited motion because of their small size as compared to adequate motion of free electrons in case of bulk material. That is why, optical properties are significant in nanoscale material while electrical properties are considerate in bulk metals. The optical properties arise from their size confinement effect produce new electronic properties resulting a distinct feature of vibrant color of their colloidal solution [201]. The principle behind color change of AuNPs is based on surface plasmon resonance (SPR) phenomena as shown in Figure 2.3. Strong optical absorption in the visible range happened by the collective excitation of free electron cloud when Au nanoparticles are exposed to the light irradiation. The oscillation of the electron gas relative to the Au nuclei take place because of two opposite events; i) the displacement of the electron cloud relative to the Au nuclear framework due to the electric field of light ii) a reinstating force arises from Coulomb attraction between electrons and nuclei. For a typical spherical AuNP with a size of 13 nm, the maximum light absorption occurs at the wavelength of 520 nm, which is also responsible for the wine-red color of the solution. Nonetheless, the absorption spectrum is dependent on the size, shape, solvent, coating, temperature, and the proximity of other nanoparticles [165,171]. For example, increasing the diameter of spherical AuNPs resulted in the shift towards longer wavelengths (red shift) [202]. Also, forming anisotropic forms of AuNPs such as nanorods, stars, and shells resulted in additional peaks in the NIR region, which makes them useful for *in vivo* imaging and analysis [203,204]. Of note, aggregation of AuNPs result in a strong red shift (i.e., from ~520 nm to ~650 nm) and a significant color change from red to blue,[171,188] which has been the foundation of various AuNP-based colorimetric assays.

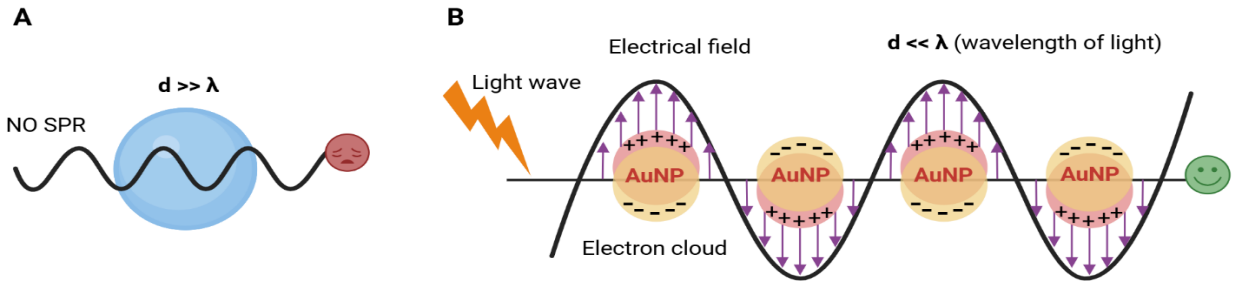


Figure 2.3 Principle of surface plasmon resonance-based colorimetric sensor.
This is due to surface plasmon resonance (SPR) phenomena which is the collective oscillation of the Au electrons in resonance with the electromagnetic field in the presence of light irradiation. A) No SPR happens when particle size is greater than the wavelength of light; B) SPR phenomena takes place successfully when wavelength of light is greater than AuNPs size to get a colorimetric response.

The surface plasmon resonance characteristic of AuNPs used in colorimetric sensing is categorized into five approaches based on the nature of mechanisms involved behind detection. These mechanisms include aggregation, anti-aggregation, etching, growth and accumulation of AuNPs [205]. Aggregation-based colorimetric detection is the most popular method where aggregation of nanoparticles leads to surface plasmon band towards a longer wavelength, resulting in the color change from red to blue. Mainly, two kinds of aggregation behavior exist: non-crosslinking aggregation and cross-linking aggregation. Non-crosslinking aggregation is a widely used mechanism due to its operational simplicity, well-defined sensing guidelines and no need of interparticle bond formation which can be explained by the Derjaguin–Landau–Verwey–Overbeck (DLVO) theory [206,207]. In this case, van der Waals attractive forces between particles become greater than electrostatic repulsive interactions, and hence, aggregation is promoted as shown in Figure 2.4A(i-iii). This interparticle aggregation can be induced either using salt or analyte that has higher affinity towards the stabilizer as compared to the stabilizer and AuNPs interactions. However, in some cases, especially with aptamers as the stabilizer, the analyte cannot release the stabilizer from AuNPs and thus modified procedures and conditions are required for biosensing applications [208,209]. The degree of aggregation can be determined according to the absorbance ratio between aggregated and dispersed nanoparticles or blue/red ratio.

Cross-linking aggregation can happen through direct interactions or requires a cross-linker. In the case of a cross-linker, aggregation is promoted when the analyte possesses at least two binding

sites, so interparticle attractive forces dominate over interparticle repulsive forces, resulting in a bond formation either through hydrogen bonding, metal-ligand coordination, electrostatic attraction or hydrophobic interactions as shown in Figure 2.4A(iv-v). Common examples of interactions are streptavidin–biotin, aptamer–target, lectin–sugar, antibody–antigen, and DNA hybridization. However, mostly an anti-receptor or a complementary unit is already attached to AuNPs which favors chemical binding between compatible groups adsorbed on AuNPs to promote aggregation when no crosslinker is involved as shown in Figure 2.4A(vi) [210]. A representative example of cross-linking aggregation is azide-AuNPs and alkyne-AuNPs based click chemistry that leads to triazole formation in the presence of copper ions [211].

Of note, higher degree of stabilization is achieved when functionality is anchored to AuNPs through covalent linkages. In this case, dispersion/aggregation behavior is flexible to control as compared to the system where functionality is immobilized on AuNPs via electrostatic interactions [212]. The color of the colloidal particle changes from red to purple/blue when the inter-particle spacing between the AuNPs is 2.5 times shorter than the average particle diameter [213]. As a result, the aggregated signal is recognized in the detection zone of a sensor as an "on" output in terms of blue color. This color shift is remarkable due to the extinction coefficients which are three to five orders of magnitude larger than normal organic dyes [214]. Sometimes, the addition of salt (e.g., chloride, sulfate, thiosulphate, and carbonate) becomes essential to improve the sensitivity of the sensor through enhanced aggregation by minimizing the interparticle electrostatic repulsion force [215,216]. Of note, non-crosslinking aggregation occurs quickly in a few minutes as compared to cross-linking aggregation that might require hours. In fact, relatively slow Brownian motion and strict temperature control required for reactions on colloidal surface make cross-linking aggregation based colorimetric detection less common.

AuNPs-based colorimetric sensors employing anti-aggregation mechanism utilize either crosslinker-based method or nano-affinity assisted assay. When a crosslinker is used as a main component of the detection system, linker molecules such as DNA, buffer, or any small unit build pre-existing interactions with AuNPs so the probe is aggregated without the presence of an analyte as shown in Figure 2.4B(i,ii) [217]. However, the active site of the crosslinker is suppressed in the presence of an analyte which stimulates the dispersion of AuNPs, resulting in a characteristic red color as a signal output. The key point of this mechanism is based on analyte

prompted shift of crosslinker from a functional state to a suppressed one. On the other hand, nano-affinity assisted assay utilizes target-aptamer binding-inhibited AuNPs aggregation (anti-aggregation) instead of binding-promoted AuNPs aggregation. Initially, positively charged, or neutral target protein is mixed with either a non-binding DNA sequence or a protein-specific aptamer. The AuNPs rapidly aggregate with proteins in the presence of non-binding DNA sequences due to negative charge of nanoparticles and positive charge of protein leading to a color change from red to blue. However, protein incubation with protein-specific aptamers generates aptamer-protein complexes which have a more negative charge leading to strong electrostatic repulsion between aptamer-protein complex and AuNPs resulting in inhibition of AuNPs aggregation (anti-aggregation) and retaining dispersed state of AuNPs as shown in Figure 2.4B(iii) [218]. The key point of this assay is to maintain the pH of a detection system at less or near to the isoelectric point of protein because charge on protein in AuNPs solution is pH-dependant. A variety of metal ions,[219,220] non-metal ions,[188,221,222] and amino acid [223] have been detected using anti-aggregation mechanism of modified AuNPs. Conclusively, anti-aggregation based detection is more selective compared to the aggregation based detection system due to utilizing specific interactions between AuNPs probe and analytes of interest. Moreover, anti-aggregation based detection system involves a multi-step procedure, whereas aggregation-based assay is a single step detection.

Besides stability of AuNPs, morphology changes also play an important role to develop colorimetric sensors. Certain chemical reactions happen on the surface of AuNPs that induce morphology alterations which result in a colorimetric signal generation for analyte detection [224]. Different shapes of AuNPs such as nanospheres, nanorods (AuNRs), nanotriangles (AuNTs), nanostars (AuNSs) and nanourchins have shown etching-based mechanism for colorimetric sensing, but AuNRs are the representative example in this category due to their high surface energy. The etching reaction involves the use of etchants such as $H_2O_2$, $I^-$, $Cu^{2+}$ ions that reduce the aspect ratio by etching the terminal ends of AuNRs resulting in a change in shape and size of the nanoparticles as shown in Figure 2.4C(i) [225]. These morphological changes shift LSPR peak with a visible color change read-out. Sometimes, ligand molecules or analytes facilitate etching process due to their high redox potential. For example, the electron injection from the ligand to the AuNPs is the mechanism of ligand-induced etching of gold nanoparticles [226]. Sometimes, ligand-induced etching is referred as target-mediated direct etching because

analyte behaves as ligand to decrease the redox potential of nanoparticles which promotes etching. Bimetallic core-shell AuNPs is the suitable example of this mechanism where outer metallic shell is etched first by analyte and dissolved oxygen producing red color solution and finally Au core is etched giving colorless solution as shown in Figure 2.4C(ii). This detection method shows higher sensitivity due to emphasized SPR feature of bimetallic alloy. Other common approaches in etching-based sensing mode involve alloy-promoted etching, intermediate-mediated etching such as enzyme or inhibitor mediated etching which changes the morphology and color of AuNPs in the presence of analyte as shown in Figure 2.4C(iii-iv) [227].

In summary, etching is a non-aggregation based colorimetric method which does not require labelling protocols. This detection mode is favoured over aggregation-based sensors due to having no false positive results because of auto-aggregation of nanoparticles. However, the presence of oxidizing agent, acidic condition, longer detection time and relatively high temperature requirements limit the application of etching-based detection.

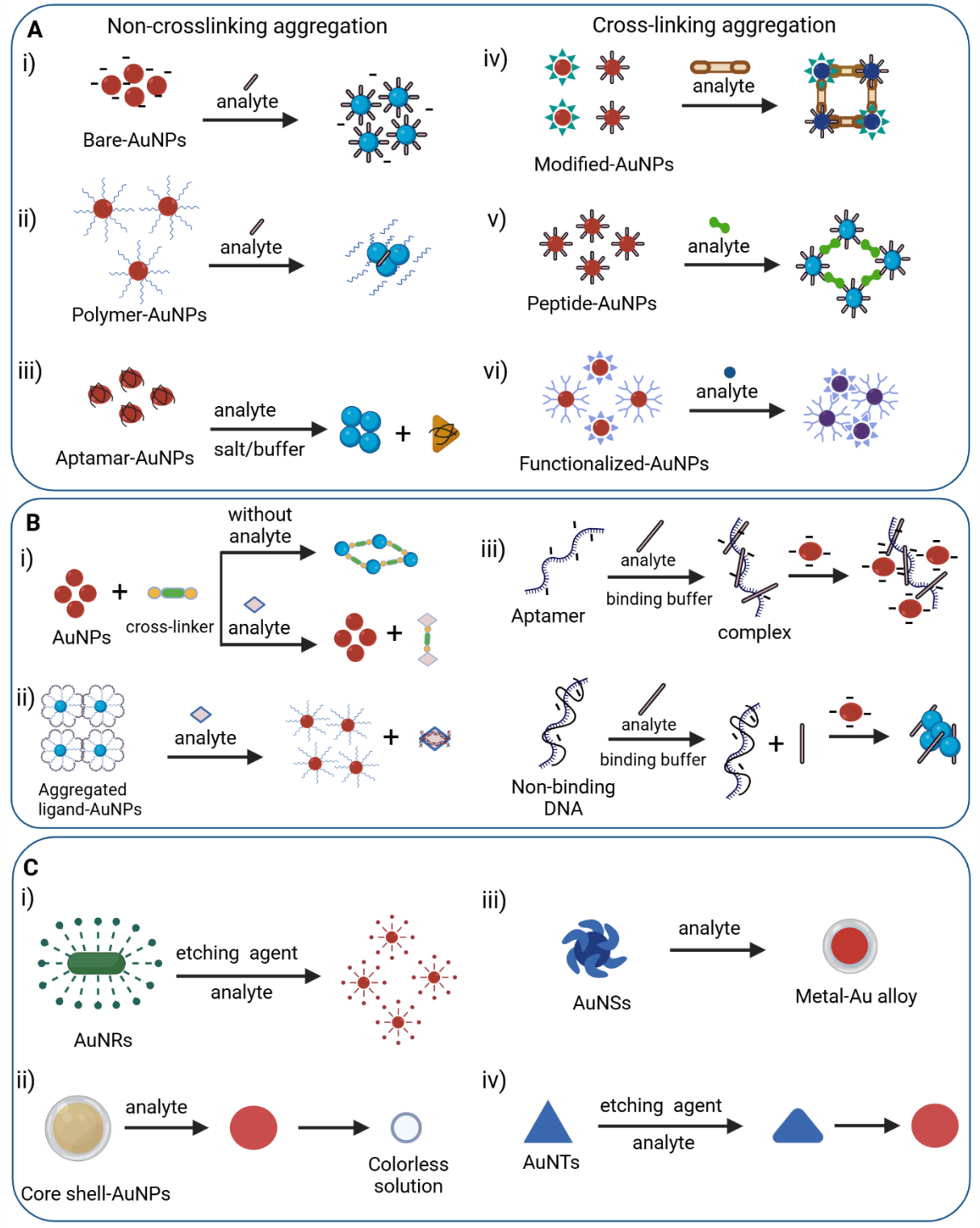


Figure 2.4 Representation of some common mechanisms in AuNPs-related surface plasmon resonance-based colorimetric sensors.

A(i–iii) Non-crosslinking aggregation mechanisms involving removal of surface stabilization around nanoparticles whereas A(iv–vi) cross-linking aggregation strategies promote intermolecular bond formation between ligand-functionalized AuNPs and analyte; B(i) Anti-aggregation method based on analyte triggered switch of linker molecule from active to suppressed state that promotes the dispersed state of AuNPs whereas B(ii) dispersion of AuNPs happen in the presence of analyte without participating any linker molecule; B(iii) nano-affinity assisted assay utilizing target-specific aptamer to form target-aptamer complex for anti-aggregation-based detection, whereas in the presence of non-binding DNA/aptamer sequence, the target analyte induces aggregation of AuNPs.; C(i–iv) Etching-based mechanisms in the presence of an analyte showing morphological changes in shape and/or size of AuNPs by the action of etchants to stimulate colorimetric plasmonic response.

Surface plasmon resonance-based colorimetric sensors also follow growth-based and accumulation-based mechanisms for colorimetric detection. The growth-based sensors are mainly divided into seed-mediated or target-mediated growth either by chemical transformation or enzymatic action. Seed-mediated growth assay is a direct reducing-target induced growth system where catalytic seeds of gold are involved to adsorb analyte on their surface, so growth of small sized AuNPs is promoted. As a result, cluster aggregation of AuNPs takes place by chemical transformation which triggers a wavelength shift and color change in the solution from grey-purple to red as demonstrated in Figure 2.5A(i) [228–230]. In target-mediated growth mechanism, ligand modified AuNPs act as a probe where ligand is detached from AuNPs in the presence of an analyte due to higher ligand analyte affinity whereas ligand-deprived AuNPs behave as an active substrate for AuNPs growth in the presence of $HAuCl_4/NH_2OH$. The grown AuNPs appear as a red solution as shown in Figure 2.5A(ii). In the absence of the target, the ligand modified AuNPs react with $HAuCl_4/NH_2OH$ and show morphological changes resulting in a blue color solution. Of note, an analyte accelerates the growth of AuNPs in growth-mediated assay but grown AuNPs size is varied and mainly depends on analyte concentration. The growth of bigger size AuNPs leads an aggregated state with blue color [231]. Other possible growth mechanisms are enzyme-promoted and enzyme passivated growth of AuNPs where an enzyme decomposes a non-reducing substrate into reducing agents to start AuNPs growth by redox chemistry or an enzyme produces inhibitor to block the growth of nanoparticles in the presence of an analyte [227]. Common application of growth-based assay is the plasmonic ELISA (enzyme-linked immunosorbent assay) that improves the sensitivity of an assay.

Accumulation-based mechanism of the surface plasmon resonance-based colorimetric sensors is common in lateral flow immunoassay (LFIA) devices which follow an immunological reaction for the detection of an analyte mainly in a qualitative manner. The test strip contains different zones and is equipped with a test line and a control line. Sample containing a target analyte is applied on the sample pad that transfers into the conjugate pad due to the capillary flow of the liquid. The conjugate pad contains specific AuNPs-antibodies which bind to the target analyte, resulting in AuNPs-antibody-analyte conjugates that flow further and reach to the detection zone. Instead of antibodies, aptamers can be used in the conjugate pad [232]. The detection zone comprises porous nitrocellulose membrane with immobilized lines of antibodies that cannot be washed away with liquid. In the test line, the target analyte is sandwiched between two antibodies, resulting in the accumulation of AuNPs and a visible red color. In the control line, AuNPs-antibodies, whether conjugated with the analyte or not, bind with another type of antibody to ensure the proper sample flow by capillary action as shown in Figure 2.5B. In LFIA, AuNPs has been used for signal amplification in addition to detection [233]. Various AuNPs have been evaluated for the test zone to achieve better detection brightness [234].

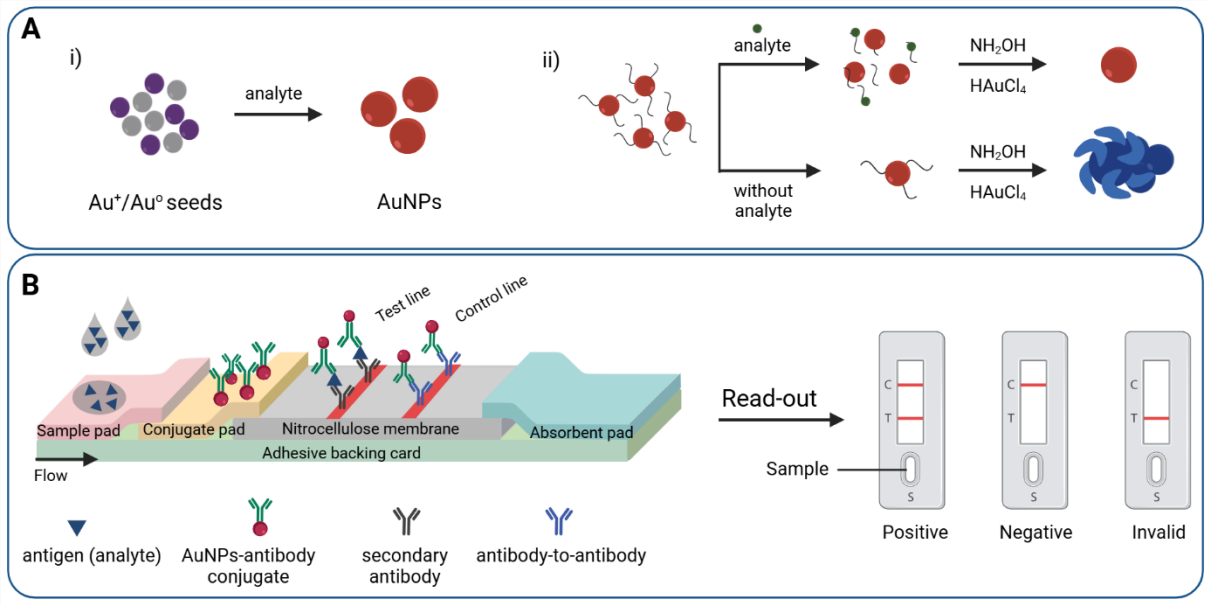


Figure 2.5 Representation of different mechanisms in AuNPs-related surface plasmon resonance-based colorimetric sensors.
A(i) Seed-mediated growth mechanism promotes growth of AuNPs from seeds of Au by chemicals or enzymatic action in the presence of an analyte to produce colorimetric read-out; A(ii) target-mediated growth mechanism involves the ligand modified AuNPs where ligand

detaches the Au surface due to strong affinity with analyte; hence ligand-deprived AuNPs start growing in the present of $HAuCl_4/NH_2OH$; B) Accumulation-based mechanism for lateral flow immunoassay (LFIA) devices where analyte is detected by the appearance of red line due to accumulation of AuNPs after immunological reaction.

### 2.4.2 Mechanisms of AuNPs-related Peroxidase-activity-based Colorimetric Sensors

Besides surface plasmon resonance characteristics of AuNPs, peroxidase-like catalytic behavior of colloidal gold has been explored to fabricate colorimetric sensors, also called nanozyme sensors. In the nanozyme mechanism, positive/negative charged AuNPs mimic the function of biological enzymes such as peroxidase, reductase, catalase, glucose oxidase, or superoxidase due to their enzyme-mimetic properties [235,236]. Being highly efficient and highly selective, these AuNPs accelerate chemical reactions like natural enzymes. However, their ease of preparation, cost-effectiveness, high stability due to lack of denaturation and inactivation, and intrinsic catalytic activity put AuNPs nanozyme in a superior position in catalysis which is fundamental to reactions. Among all, peroxidase activity of AuNPs is frequently used in environmental analysis and food safety while other enzymatic properties are beneficial for chemical, pharmaceutical, and clinical applications,[237] which is not the scope of this review. Surface chemistry and morphology of nanoparticles play important role in peroxidase activity-based colorimetric sensors similar to surface plasmon resonance-based colorimetric sensors. However, in contrast to surface plasmon resonance-based colorimetric sensors, AuNPs themselves do not contribute in visual read-out in nanozyme sensors, so chromogenic substances such as 3,3′,5,5′-tetramethylbenzidine (TMB), 2,2′-azino-bis(3-ethylbenzothiazoline-6-sulphonic acid (ABTS), and o-phenylenediamine (OPD) are required to generate color in the presence of analytes [238]. The choice of chromogenic agent depends on different detection parameters such as pH, temperature, and chemical moieties of the target analyte and functionalized-AuNPs. The nanozyme-based mechanism with TMB as a representative example of a chromogenic substance is demonstrated in Figure 2.6.

Peroxidase enzyme catalyses the oxidation of substrate in the presence of hydrogen peroxide which generates a signal being used to detect an analyte. Of note, smaller size of AuNPs shows better activity due to enhanced surface availability for catalytic reaction [239]. In case of peroxidase-like activity under acidic condition, $H_2O_2$ adsorbed on AuNPs surface generates ·OH radicals by breaking the O–O bond followed by partial electron exchange interaction between

·OH radicals and the AuNPs that would stabilize the radicals. Whereas under basic conditions, OH groups are adsorbed on AuNPs that trigger the decomposition of $H_2O_2$ into $H_2O$ and $O_2$ [239]. Many toxic substances and contaminants such as heavy metals, pesticides, antibiotics and micro-organisms have been detected utilizing AuNPs-nanozyme sensors [239].

Nanozyme sensors employing peroxidase behaviour of AuNPs detect analyte of interest either through expression or inhibition of peroxidase activity. Nanozyme sensors based on expression of peroxidase-like activity of AuNPs are common due to their ability to transform into $Au^0$ and $Au^{1+}$ oxidation state. In this method the target analyte can be detected by the expression or enhancement of peroxidase-like activity of AuNPs with respect to analyte concentration. AuNPs mimic the role of horseradish peroxidase to catalyze the oxidation of TMB/ABTS/OPD in the presence of $H_2O_2$ as the oxidizing agent to develop a blue/green/yellow color at absorbance 652/735/450 nm, respectively, in aqueous media which represents colorimetric assay. Bare-AuNPs show peroxidase-like activity which is tuned by ligand modification as well as in the presence of an analyte as shown in Figure 2.6A. Conclusively, the sensitivity of nanozyme-based assay can be controlled by modifying AuNPs surface which offers adjustable activity. Gold nanoclusters, nanostar, and nanotriangles show better activity due to having more interfaces as compared to nanosphere. In addition to shape, functional groups tailor the surface energy of AuNPs which plays an important role in catalyzing a substrate. Overall, expression or enhancement of peroxidase activity in the presence of analyte is a promising approach to detect and monitor environmental pollutants and food toxic substances.

Peroxidase activity-based chemosensors rely on the inhibition of peroxidase activity in the presence of an analyte is less prevalent due to natural peroxidase-like catalytic ability of AuNPs. Inhibition-based detection strategy is not as straightforward as other colorimetric approaches. In this assay, the surface of gold particles is blocked by an inhibitor, and hence, it is no longer available to express peroxidase-like catalytic role as shown in Figure 2.6B. For instance, sulfide ions ($S^{2-}$) inhibit the active sites of gold by forming $Au_2S$ species which provide coordination shielding on the surface of AuNPs [240]. Sometimes halide ions ($X^-$) work well to suppress the surface activity of protein-AuNPs by Au-X interactions [241]. In other situations, AuNPs might get aggregated due to the presence of the target analyte and lose their intrinsic-catalytic behavior. For instance, Zhao *et al*. reported sulfate ions detection through inhibition of peroxidase activity

of cysteamine-AuNPs because sulfate induced the aggregation of AuNPs via hydrogen bonding and electrostatic interaction, so relatively lighter blue color was observed as a reduced colorimetric signal [242]. Overall, inhibitor molecules attached to AuNPs surface are responsible to decrease the peroxidase activity, which is reflected in the color of the solution.

To this end, fundamental mechanisms involved in colorimetric detection of various analytes using AuNPs has been explained. The surface plasmon resonance-based or peroxidase activity-based catalytic sensing behavior of AuNPs mainly depends on surface modifications of nanoparticles which is suitably selected according to the nature of analyte to be detected. In some cases, reversible nature of aggregation and dispersion of AuNPs helps to develop a sensor which is repeatedly "on" and "off" and could be measured by visual read-out. In advance scenario “lab-on-a-nanoparticle” has been successfully developed for the detection of multiple analytes using a single sensing element [243]. Hence, AuNPs have used in several detection applications involving environmental and food monitoring.

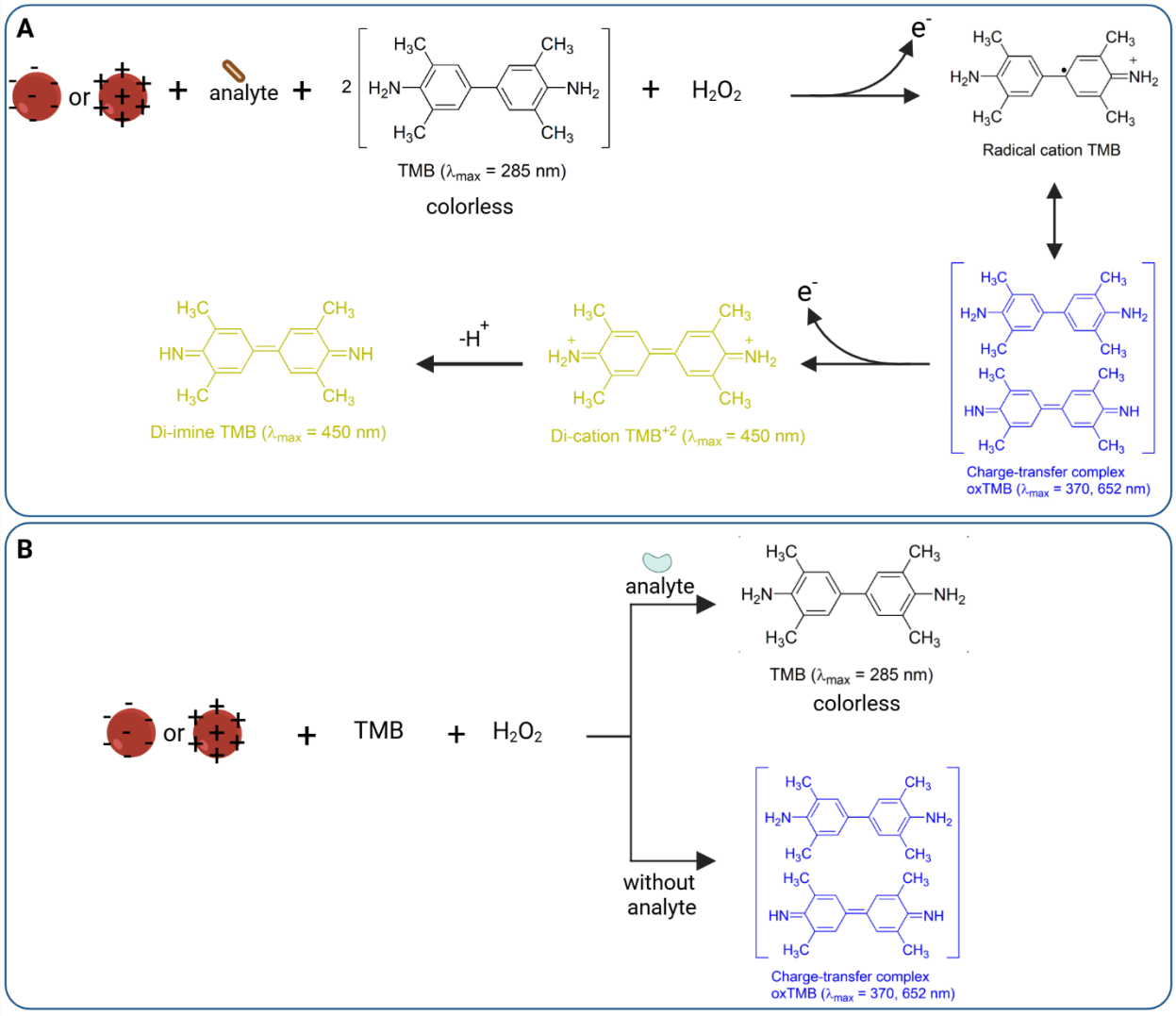


Figure 2.6 Principle of nanozyme sensors showing peroxidase-mimic role of AuNPs behind colorimetric detection.
A) Analyte detection based on expression of peroxidase-like activity of modified AuNPs that oxidize TMB substrate strongly in the presence of $H_2O_2$; B) Analyte detection based on inhibition of peroxidase-like activity of AuNPs where the surface of AuNPs is blocked due to analyte which suppress their peroxidase activity resulting no change in color of TMB.

## 2.5 Applications of AuNPs in Environmental and Food Monitoring

Gold nanoparticles have been used in environmental and food monitoring as a sensing tool to identify and prevent the potential hazards that could affect the quality of atmosphere and food. Many environmental pollutants are toxic chemicals produced from inorganic, organic, and biomolecules that are widely dispersed in ambient air, soil, and water [244]. These contaminants release into our environment through various natural and anthropogenic sources like industrial

wastes, agricultural fertilizers, and medical diagnostics [245]. These chemical pollutants present risks to humans, animals, plants, and ecosystems through many ways like direct ingestion, food chains, absorption by plants, and consumption of contaminated water. Also, when their amount crosses the threshold limit, these contaminants are considered poisonous and responsible for several ailments that cause serious health issues such as cardiac diseases, brain and nerve damage, pneumonia, liver and kidney failure, and infertility and miscarriages [246]. Hence, modified AuNPs have been used to rapidly detect and quantify various analytes of interest responsible for potential hazards to environment and humans. Additionally, the colorimetric assay has been used in combination with fluorometric, luminescent, electrochemical or capillary electrophoresis methods for better results [247]. Some researchers have shown luminescent-based G-quadruplex detection technique as a reliable method to monitor small molecules, heavy metals, and other analytes [248–250].

On the other hand, food inspection agencies are continuously reporting ever-increasing food frauds and adulterants. Food sectors are working hard to ensure food safety and food quality to avoid any possible contaminations such as pesticides, toxins, foodborne pathogens. Hence, food safety screening and regular monitoring is immensely important to guarantee the purity of food samples. Since decades, food microfluidics present improved solutions for food analysis,[251] and in this connection, AuNPs have been used in rapid detection protocols to build on-spot testing kits to inspect food quality.

Of note, AuNPs have also been used for the colorimetric detection of gaseous target molecules. In this case, the AuNPs probe can be solid as films or liquid as solution depends on the nature of targeted gas and detection mechanism. For example, $H_2S$ gas was detected using Au-$TiO_2$-NiO nanocomposite film in 2-10 ppm range by catalytic oxidation of $H_2S$ into SOx due to the oxide matrix [252]. The film porosity allowed gas molecules to reach the active sites on AuNPs surface where an interaction between sulphur and Au surface led to a reduction in oscillating free electrons resulting in broadening of plasmon peak [253]. On the other side, $H_2S$ gas in air was detected using Tween 80 functionalized AuNPs solution with an LoD of 0.5 ppm. The detection principle followed anti-aggregation mechanism [254]. Various other gas molecules such as nitrogen oxide (NO), phosgene ($COCl_2$), and formaldehyde ($CH_2O$) have been detected using SPR property of AuNPs [255–258]. However, detection of gas is a broad area of research that

falls out of the scope of this paper, so in the following sections only samples in solid and liquid phase will be considered.

### 2.5.1 Detection of Inorganic Ions in Environment and Food

Inorganic pollutants are non-carbon-based substances mainly of mineral origin that have released into the environment as by-product of mining, transportation, and industry and urban activities [259]. Their improper dumping and excessive accumulation in soil and water bodies are a matter of great concern. Their accumulation in living body damages immune system and attacks on different body organs [260]. In this concern, one of the major challenges is the precise on-site analysis of metal contamination in aqueous bodies. Literature contains many examples of alkaline earth metals, heavy metals, trace elements, and rare earth elements that have been detected using surface plasmon resonance and peroxidase-like catalytic properties of functionalized AuNPs [261,262]. Of note, after detecting a particular analyte, interference study with other anions like $NO_3^-$, $NO_2^-$, $F^-$, $Cl^-$, $Br^-$, $I^-$, $CO_3^{2-}$, $HCO_3^-$, $HSO_3^-$, $S^{2-}$, $SCN^-$, $HPO_4^{2-}$, $H_2PO_4^-$, $H_2PO_2^-$, $AsO_2^-$, $HAsO_4^{2-}$ as well as cations like $Li^+$, $K^+$, $Na^+$, $Ca^{2+}$, $Mg^{2+}$, $Ba^{2+}$, $Sr^{2+}$, $Pb^{2+}$, $Mn^{2+}$, $Hg^{2+}$, $Zn^{2+}$, $Cd^{2+}$, $Cu^{2+}$, $Ni^{2+}$, $Fe^{2+}$, $Co^{2+}$, $Al^{3+}$, $Cr^{3+}$, $Fe^{3+}$, $Cr^{6+}$ is necessary to report the outcomes of the sensor reliably in terms of the selectivity. In this review, we have categorized inorganic pollutants based on their position in the periodic table including alkaline earth metals, transition metals including heavy metals and coinage metals, rare earth elements, and anions. Figure 2.7 highlights the elements of periodic table that have been detected using AuNPs so far.

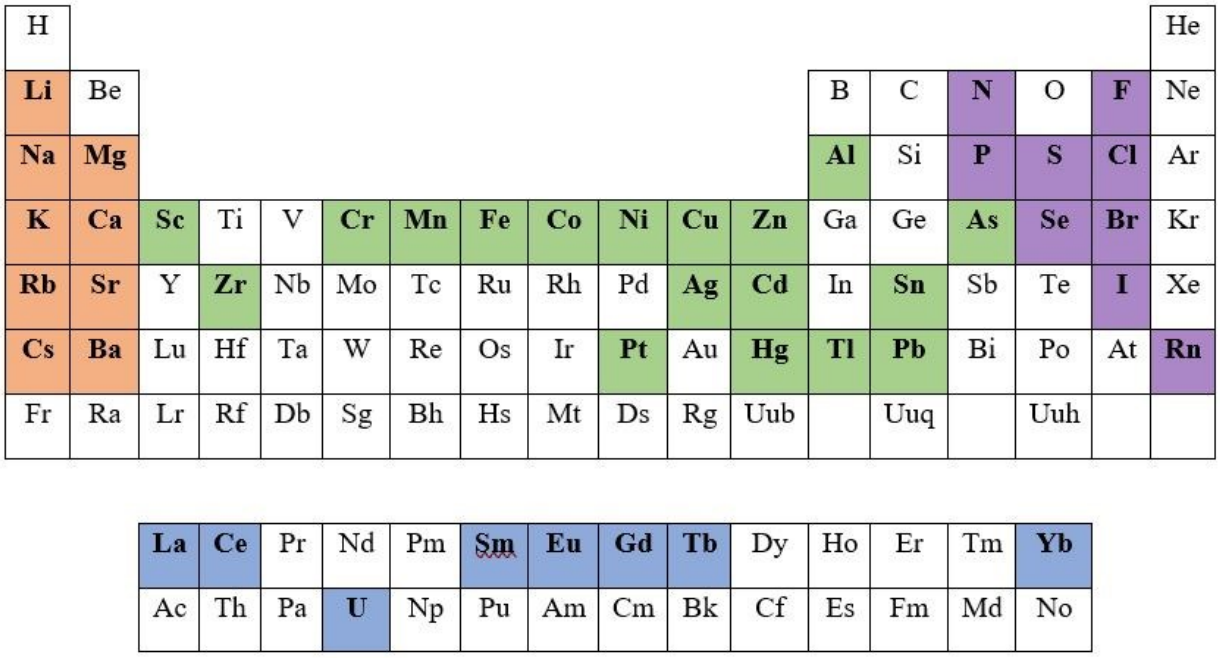


Figure 2.7 The elements of the periodic table that have been detected by using gold nanoparticles so far (the highlighted ones).

*2.5.1.1 Alkali and alkaline earth metal ions*

The alkali and alkaline earth metals occupy the first two columns in the periodic table and are referred to as Groups IA and IIA, respectively. Among all, $Na^+$, $K^+$, and $Ca^{2+}$ are the most important ions to be detected in water and food samples in addition to their detection as biomarkers in biological fluids including urine, serum, saliva and sweat samples. Mostly, group IA and IIA salts are utilized to aggregate the AuNPs probe used for the detection of DNA [263].

Naked eye visualization of $K^+$ ions was made by the interactions of cationic Yellow 5gl dye (Y5GL) with AuNPs that behaved as a new aggregator for colorimetric sensor.[264] In this case, potassium binding aptamers were dissociated from the surface of the AuNPs in the presence of $K^+$ and made a G-quadruplex structure; hence promoting the aggregation of free AuNPs due to balancing the surface charge with the cationic dye. This process is recognized by color change from blue/purple to green as shown in Figure 2.8A. The use of cationic dye as an aggregator instead of salt have improved the accuracy of the method by offering less interference with existing salts. To improve the sensor's sensitivity and selectivity towards $K^+$, the pH and incubation time was also important. This approach has also been investigated for paper-based microfluidic systems as a potential method to detect $K^+$ in biological fluids on-spot. Qiu *et al.*

have proposed a new strategy for the detection of $Cs^+$ ions with LoD of 30 μM using ferrocyanide-based Prussian blue precursor (PB-P) and citrate-AuNPs [265]. This colorimetric assay followed nonmorphological transition mechanism similar to anti-aggregation based detection. In the absence of $Cs^+$ ions, PB-P formed nanoshells on Au surface due to reduction of $Fe^{3+}$ to $Fe^{2+}$ by the citric acid resulting the color change from red to blue. However, a stable complex formed between $Cs^+$ and PB due to their strong affinity in the presence of targeted analyte which remained AuNPs wine red as shown in Figure 2.8B. Recently, a transparency sheet-based approach for the detection of $Ca^{2+}$ in water and artificial urine sample was reported by 4-amino-6-hydroxy-2-mercaptopyrimidine monohydrate capped gold nanoparticles with a LoD of 3.05 ppm at pH 6 [266]. The thiol moiety of the functional group was chemisorbed on AuNPs surface, whereas the hydroxyl and amine groups were available for easy binding with $Ca^{2+}$ ions. This real-time on-site detection method is helpful to develop point-of-use diagnostic systems for $Ca^{2+}$ ions detection based on aggregation mechanism of AuNPs.

Conclusively, aggregation and anti-aggregation mechanisms have been reported for alkali and alkaline metal ions detection utilizing aptamers binding and ligand's affinity approach. Aptamers have gained much interest due to their, high stability, and selectivity compared to antibodies with the same functionalities. Nonetheless, developing aptamers against special analytes is usually done through SELEX procedure which is time-consuming and labor-intensive. Importantly, cationic dye has been used as an efficient AuNPs aggregator instead of conventional inorganic salts. This replacement could be implemented in future to enhance the sensitivity of already established sensors. The affinity of Prussian blue towards $Cs^+$ has been explored using citric acid as a reducing agent which took 20 minutes of incubation. Other reducing agents could be tested to reduce the assay time.

*2.5.1.2 Transition metal ions*

Transition metals are the d-block elements that belong to groups 3 to 12 of the periodic table, where a few of them are popularly known as heavy metals, while others are called coinage metals that have had historical importance. The d-block elements of periodic table are the most common analytes detected in water and food matrices using AuNPs-based colorimetric approaches.

*2.5.1.2.1 Heavy metal ions.* Developing an efficient and sensitive AuNPs related surface plasmon resonance-based colorimetric sensors and peroxidase activity-based colorimetric sensor for heavy metals such as $Ni^{2+}$, $Hg^{2+}$, $Cd^{2+}$, $As^{3+}$, $Cr^{3+}$, $Cr^{6+}$, and $Pb^{2+}$ requires specific chemical or biological surface modifications of nanoparticles to prepare a colorimetric probe [267,268]. In a label free AuNPs-based biosensor, specific DNA sequence was used to build thymine-$Hg^{2+}$-thymine complex which is used to detect $Hg^{2+}$ on paper platform [269]. In such a system, conformational shift produced by interactions between DNA and heavy metal are important [270]. However, recently Hu *et al*. modified this approach by utilizing washed and unwashed AuNPs where interactions between $Hg^{2+}$ and AuNPs were considered instead of DNA/$Hg^{2+}$ binding. In this detection system, a blue-to-red color change was observed with increasing concentration of $Hg^{2+}$ while red-to-blue color produced for the washed AuNPs as shown in Figure 2.8C [271]. Another example of surface plasmon resonance-based colorimetric sensors is based on analyte aptamer affinity approach for the quantitative detection of $Cd^{2+}$ using AuNPs [272]. In general, aptamers provide the stability to gold nano-plasmon and keep them well dispersed in the solution. The availability of free aptamers around AuNPs become less in the presence of $Cd^{2+}$ ions due to $Cd^{2+}$ aptamer specific interactions which reduces the overall stability of AuNPs system. As a result, AuNPs aggregate in high-salt solutions, which leads to the color change of the solution. No salt-induced aggregation was applied in a colorimetric system in the absence of $Cd^{2+}$ due to the higher stability of aptamer-AuNPs. In a cross-linking aggregation approach, the quantification of $Cd^{2+}$ was achieved using guanidine thiocyanate (GT) modified AuNPs [273]. A stable complex was formed between $Cd^{2+}$ and GT-AuNPs because $Cd^{2+}$ stimulated the chelation crosslinking of GT-AuNPs through coordinate bonding resulting in a new peak at 682 nm of blue color agglomeration of AuNPs as shown in Figure 2.8D. This assay showed a linear range of 0.025-50 μM with a LoD of 10 nM.

Qi *et al*. has reported the nanozyme sensor using oxidase mimetic activity of unmodified AuNPs, where negative surface of AuNPs contributes towards oxidation of TMB in the presence of $Cr^{6+}$ resulting in a blue color solution [274]. The strong electrostatic interactions between AuNPs and TMB cations improved the sensitivity of the $Cr^{6+}$ detection at pH 3. The LoD for this sensor was 93 μg $L^{-1}$ for water samples which was improved to 0.1 μg $L^{-1}$ by Mohamed *et al*. in the same year using surface plasmon resonance-based colorimetric sensor relied on aggregation-induced color change of maleic acid-functionalized gold nanoparticles [275]. Recently, colorimetric

approach was coupled with electrochemical detection to fabricate a dual sensors system for $Cr^{3+}$ sensing using 3-mercaptopropionic acid ligand adsorbed on AuNPs [276]. This dual sensing system had LoD in uM which was improved to nM by replacing the ligand with L-glutamic acid [277].

In short, heavy metal ions are the most studied analytes among other metals due to their easy complexation with AuNPs and abundant existence as pollutants. It is common to build aggregation-based detection sensors because of fast chelation reactions between AuNPs and metal ions. Also, researchers have developed multiplex colorimetric systems for simultaneous detection of groups of ions, including $Fe^{3+}$, $Cr^{3+}$, $Co^{2+}$, $Mg^{2+}$, $Pb^{2+}$, $Ca^{2+}$, $Zn^{2+}$, $Ti^{4+}$, and $Sn^{4+}$,[278] $Hg^{2+}$, $Cd^{2+}$, $Pb^{2+}$ and $Cu^{2+}$,[279] $Ti^{4+}$, $Cr^{3+}$, $Mn^{2+}$, $Fe^{3+}$, $Pb^{2+}$, and $Sn^{4+}$,[280] $Pb^{2+}$ and $Cr^{3+}$,[281] $Hg^{2+}$ and $As^{3+}$[282]. As a principle, AuNPs were decorated with "suitable" multiple colorimetric chelators and used under optimized conditions to achieve the detection of the target analytes.

*2.5.1.2.2 Coinage metal ions.* Copper, silver, and gold are considered coinage metals in addition to being plasmonic nanomaterials, and hence, their nanoparticles can be used to develop analytical devices for the applications in environmental and food monitoring [283,284]. Lu *et al*. have reported an interesting approach for the detection of $Cu^{2+}$ ions in nM level using Ag coated AuNPs [285]. This non-aggregation method is based on catalytic leaching of silver around AuNPs by the action of $Cu^{2+}$ in the presence of thiosulfate; hence, the size of AuNPs decreased which affected the SPR properties of nanoparticles. Also, anti-aggregation/non-aggregation of AuNPs using polyvinylpyrrolidone/2-mercaptobenzimidazole, D-penicillamine [286], and catalytic etching approach *via* hexadecyltrimethylammonium bromide [287] have been reported for $Cu^{2+}$ detection previously. In another report, the addition of $Cu^{2+}$ to histidine modified AuNCs impaired peroxidase mimetic activity of AuNCs because the His/$Cu^{2+}$ complex was more stable due to the presence of the imidazole ring in histidine. However, this change was fully reversible by the addition of free histidine as ambidentate nature of amino acids was helpful for the selective recognition of $Cu^{2+}$ with LoD 0.1 nM. In this method, histidine as a ligand and TMB/$H_2O_2$ as substrate was used [288].

Utilizing the induced hybridization concept between two different ssDNAs adsorbed on AuNPs was employed for the colorimetric detection of $Ag^{+}$ in dark field microscopy [289,290]. This

imaging assay depended on the specific binding affinity between $Ag^+$ and cytosine-bases of ssDNAs that plays a dominant role in the production of C-$Ag^+$-C complex via aggregation of AuNPs. The color change of imaging happened at a single AuNP level from green to yellow and finally red which quantified the amount of silver ions. In a recent report, anti-aggregation mechanism of unmodified AuNPs made $Ag^+$ detection possible in the presence of thiamazole [291]. Anti-aggregation based detection of $Ag^+$ ions with LoD of 0.41 μM was reported employing tris(hydroxymethyl) aminomethane (tris) that inhibited AuNPs aggregation resulting in hypsochromic spectral shift with a color change from blue to red [292].

On the other hand, the aggregation-based mechanism was explored using peptide-AuNPs with high sensitivity as 7.4 nM [293]. The 4-coordinated complexes of $Ag^+$ with peptide were developed through the oxygen of carbonyl group and the nitrogen of α-amino group that induced folding in peptides leading to the aggregation of peptide-AuNPs. Metallization induced aggregation of chitosan-AuNPs also responsible for $Ag^+$ ions detection with LoD of 130 nM where $Ag^+$ interacted with the Au core and establish a metallic bond which was reduced by chitosan and deposited on AuNPs. This deposition produced Au-Ag core-shell NPs with a distinct color change from pink to orange [294]. Another sensitive $Ag^+$ ions detection in 2.05 nM was done with gallotannin-capped AuNPs that interacted with $Ag^+$ resulting a color change from pink to yellowish brown hence applicable for quantitative determination of $Ag^+$ ions in real water samples [295]. According to our best understanding, there is no method available for the detection of $Au^+$ using colorimetric approaches; however, this ion has been detected using absorption and fluorescence methods [296]. As AuNP itself act as a transducer for the detection of a wide range of analytes and must be present in the detection system, so its own colorimetric detection would be quite difficult.

In conclusion, AuNPs-based colorimetric approach for the detection of $Cu^{2+}$ is less explored in recent years due to its easy deposition on electrodes which favors the construction of electrochemical biosensors [297]. However, ligand modified AuNPs have been used for $Cu^{2+}$ detection employing anti-aggregation, etching, and nanozyme mechanisms. Anti-aggregation approach benefits from the chelation reaction, where $Cu^{2+}$ acts as a central metal towards ligands and hence keeps the AuNPs dispersed. Though etching process is efficient and quick, but it mainly depends on the presence of thiosulfate which could be a potential interference for another

matrix. Nanozyme-based approach is majorly pH-dependant which works well at pH 3 and hence limits $Cu^{2+}$ detection in neutral and alkaline medium. Colorimetric-based determination of $Ag^{+}$ has happened with aggregation and anti-aggregation mechanism. Aggregation-based detection is advantageous due to its superior simplicity, time-saving and high sensitivity in nM as compared to anti-aggregation mechanism which offers multistep detection with detection limit in μM. The aggregation-based assay should be investigated on solid portable system for an easy on-spot $Ag^{+}$ determination.

*2.5.1.3 Rare earth metal ions*

Rare earth elements belong to the f-block of the periodic table which include inner transition metals as lanthanide and actinide series. These metals have many applications in technological fields such as sustainable energy construction, electric automobiles, and microchip technology [298]. These metal ions may continually circulate and alter in the environment and accumulate in biological tissues, where their potential adverse effects to ecology and humans become obvious [299]. For example, lanthanide ($Ln^{3+}$) competes with calcium ions and keep depositing in bone tissue of human body,[300] while cerium ions ($Ce^{3+}$) accumulate in human tissues and liver,[301] causing cancer [302,303]. For these reasons, many efforts have been done to detect these metal ions using AuNPs [304].

Malonamide modified AuNPs have been used to detect $Ln^{3+}$ ions such as $Eu^{3+}$ and $Sm^{3+}$ with LoD of 50 nM using aggregation-based colorimetric assays [305]. In recent years, hydroxypyridinonate chelator was used as an indirect approach to sense a few lanthanides such as $La^{3+}$, $Gd^{3+}$, and $Tb^{3+}$ while quenching AuNPs [306]. This sensing principle involved the inhibition of particle growth due to lanthanides and offered a LoD of 3 μM to quantify a targeted analyte in industrial waste. Moreover, this assay offered a tunable dynamic range by varying $Au^{3+}$ concentrations and octadentate chelator. In another report, biogenic AuNPs were used to detect $Ce^{3+}$ through fast aggregation of particles due to the formation of coordinate complex between $Ce^{3+}$ and –COO/–NH surface functionalities of AuNPs [307]. This agglomeration was reversible by the addition of EDTA which leads to chelation with $Ce^{3+}$ ions, leading to the regeneration of the dispersed AuNPs in the solution as red color colloids. A dual colorimetric sensor was built for the simultaneous detection of $Eu^{3+}$ and $Cr^{3+}$ ions in aqueous media utilizing 1,2,3-triazole-4,5-dicarboxylic acid adsorbed on AuNPs at a fairly good pH range 4-10 [308].

This ligand offered high selectivity as a range of heavy metals and other lanthanide ions have been tested as potential interference. Free carboxylic groups around AuNPs shifted an SPR peak from 527 to 633 nm in case of $Cr^{3+}$ ions and from 527 to 671 nm for $Eu^{3+}$ ions resulting the color change from red to blue. To conclude, a few lanthanides such as $Eu^{3+}$, $Sm^{3+}$, $Ce^{3+}$, and $Gd^{3+}$ have been detected using instrument dependent colorimetric approach of AuNPs. There is no report for on-site detection methods of these trivalent metal ions except for $Eu^{3+}$ [309]. $Ce^{3+}$ has been detected using biogenic AuNPs which make a synthetic method environment friendly due to extracellular culture of fungus instead of harsh chemicals, but it requires careful handling so there is a need to explore $Ce^{3+}$ detection using chemical synthetic methods.

*2.5.1.4 Anions*

Anions are negatively charged ionic species that include halide ions ($F^-$, $Cl^-$, $Br^-$, $I^-$), oxoanions ($HSO_4^-$, $H_2PO_4^-$, $HPO_4^{2-}$, $CH_3COO^-$, $NO_3^-$), cyanide ($CN^-$ and $SCN^-$), sulfide ($SO_4^{2-}$, $SO_3^{2-}$, $S^{2-}$) and other anions ($N_3^-$). Anions have the affinity to bind with biological materials such as protein, DNA, and RNA causing chronic diseases,[310] and hence their timely detection is important. However, their colorimetric detection using AuNPs is more challenging as compared to cationic species due to their lower charge to radius ratio, wide range of geometries such as linear, spherical, trigonal, tetrahedral, pH sensitivity, and solvation dependent binding strength and selectivity [311]. Recently, Sepahvand *et al*. documented the role of nano-plasmonic materials for the detection of nitrate and nitrite ions through aggregation, anti-aggregation, and etching-based detection mechanisms [312]. Recently, nitrite ions were detected (LoD 0.012 mg $L^{-1}$) as a degradation product of ammonium dinitramide using AuNPs coupled with azo dye ingredients necessary for the Griess assay, which is a common method for nitrite detection [313]. In another study, nitrite ions were detected by iodide accelerated etching mechanism using 20 nm Au nanospheres, nanorods and nanotriangles which induced a plasmonic shift towards longer wavelength [314]. Nitrite being oxidant oxidizes iodide ion and facilitates the etching of AuNPs by iodide ions. The LoD for etching method was 4.5 μM [315] comparable to the LoD of nanozyme method which was 4.6 μM [316]. Nitrite ions besides being an analyte were used as an electrophilic oxidant to oxidize TMB substrate in the presence of AuNP-cerium oxide ($CeO_2$) NP-adsorbed on graphene oxide (GO) sheets. The oxidized TMB produced green color as signal read-out. This study reported a colorimetric recognition for nitrite in aqueous solution based on peroxidase-mimic role of hybrid AuNPs [317].

An important anion coexisting with nitrate is the phosphate ion which was detected using mercaptoacetic acid (MA) adsorbed on AuNPs with europium ($Eu^{3+}$) as an aggregating agent [318]. Underlaying detection principle is based on anti-aggregation phenomena of MA-AuNPs in the presence of Pi. The coordination of carboxylate groups of MA with $Eu^{3+}$ was significantly interrupted due to the higher binding affinity of $Eu^{3+}$ for Pi, and hence MA-AuNPs remain dispersed. The LoD for this method was 76 nM which was significantly improved by our research group to 3 nM utilizing the $Eu^{3+}$ encapsulated dextran tablets [188]. Similarly, anti-aggregation mechanism was explored for the detection of bromide ions $Br^-$ with and a LoD of 0.04 mM using citrate-AuNPs as a colorimetric probe and $Cr^{3+}$ as a cross-linking aggregating agent [319]. The coordination of $Cr^{3+}$ with carboxylate groups of citrate ions resulted in a color change from red to blue without $Br^-$, whereas the solution color remained red in the presence of $Br^-$ ions as shown in Figure 2.8E. In 2023, a plasmon-based colorimetric method was developed utilizing cysteamine-capped gold nanoparticles for the detection of cyanide ions ($CN^-$) in tap water, dam water, and drinking water. The detection mechanism was based on nanoparticle aggregation, achieving a detection limit of 159 nM [320].

Conclusively, anion detection is more difficult than cation recognition due to the different chemical nature of these ionic entities. Nitrite and nitrate ions have been detected with AuNPs via different mechanisms including aggregation, anti-aggregation, nanozyme and etching, but all of them have involved acidic environment because of underlaying chemistry. Griess reaction involved in nitrite detection is acid catalyzed; hence, no detection is recorded in alkaline media which needs exploration. Also, phosphate ions have been reported by colorimetric sensors which can be converted to in-field applications in the future.

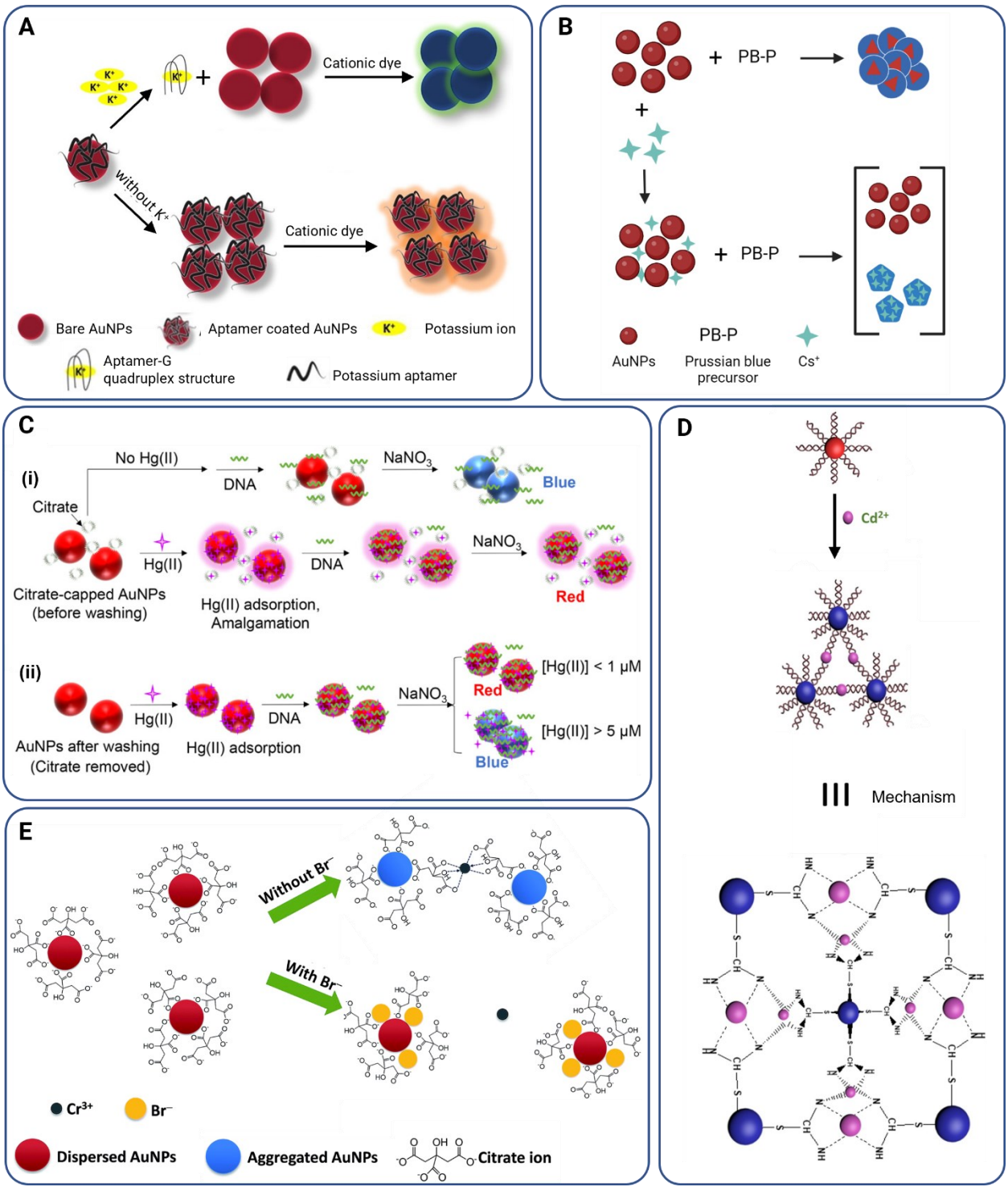


Figure 2.8 An overview of AuNPs-based colorimetric detection methods for various inorganic analytes.

(A) Selective aptasensor for the detection of potassium ions ions using aptamer modified AuNPs as nanoprobe and Cationic Yellow 5GL dye as an aggregating agent which showed green color in the presence of $K^+$ due to interactions between free AuNPs and cationic dye. Reproduced with

permission from Ref. [264] with modifications. Copyright 2018 Elsevier; B) Detection of cesium ions by nonmorphological transition mechanism where a stable complex between $Cs^+$ ions and Prussian blue precursor (PBP) is formed due to their strong affinity and AuNPs remained dispersed and red in color showing the presence of $Cs^+$ ions whereas the AuNPs color and morphology was changed in the absence of $Cs^+$ ions due to the formation of PB nanoshells on AuNPs surface by the reduction of $Fe^{3+}$ into $Fe^{2+}$ in acidic condition [265]; C) A label-free detection strategy for mercury ions based on $Hg^{2+}$ and DNA adsorption on AuNPs which affected their stability. The C(i) represents unwashed AuNPs having free citrate molecules which make an amalgam with $Hg^{2+}$ and promoted DNA adsorption on AuNPs which make the system stable against salt-induced aggregation hence, showing red in color whereas in C(ii) no free citrate molecules were present in a system so a low concentration of $Hg^{2+}$ was adsorb on AuNPs which promoted higher DNA adsorption, giving more stability to the particles. $Hg^{2+}$ adsorption was dominated when its concentration was >5 μM which favored less DNA adsorption hence producing blue color in the detection system. Reproduced with permission from Ref. [271] with minor modifications. Copyright 2021 American Chemical Society; D) Detection of cadmium ions using guanidine thiocyanate modified AuNPs by crosslinking aggregation mechanism due to coordinate bonding interaction between $Cd^{2+}$ and functionalized nanoparticles. Reproduced with permission from Ref. [273] with some modifications. Copyright 2021 Elsevier; E) Detection of inorganic bromide ions using anti-aggregation mechanism of citrate-AuNPs assisted by $Cr^{3+}$ ions. Reproduced with permission from Ref. [319] with minor modifications. Copyright 2018 Elsevier.

### 2.5.2 Detection of Organic Pollutants in Environment and Food

Organic pollutants refer to biodegradable contaminants in the environment, which can cause serious toxicological effects such as carcinogenicity and neurotoxicity [321,322]. Persistent organic pollutants in environment include polychlorinated biphenyls, polybrominated diphenyl ethers, and polycyclic aromatic hydrocarbons as a result of industrial and household waste [323–328]. Other well-documented pollutants are pesticides, drugs, allergens, mycotoxins, and a variety of small toxic substances such as melamine. The routine use of these organic substances in agricultural and livestock production leads to their heavy accumulation in atmosphere, soil, water, and eventually human body through the food chain, raising threats to the humans. That is why the detection of these contaminants at earliest is crucial, and efforts are ongoing to develop efficient AuNPs-related surface plasmon resonance-based sensors using colorimetric methods to detect and monitor the amounts of organic pollutants in environment and food matrices to prevent their devastating effects. In this connection, several recently published literature reviews have specifically covered the detection of organic pollutants from different aspects [329–331]. In

the following sections, we will focus on the recent advancements on the AuNPs-based colorimetric detection of such pollutants.

*2.5.2.1 Detection of pesticides*

Being widely used, pesticides have been detected in water, fruits, and vegetables samples using colorimetric probe of AuNPs. Most of the pesticides are rich in active functionalities such as amino, thio, cyano, hydroxyl, carbonyl, and sulphide groups which has binding attraction towards the negatively charged surface of gold particles, and hence distance-induced optical changes in nanoparticles can be seen by naked eye besides UV-vis spectroscopy measurements. Prothioconazole,[332] acephate, phenthoate, profenofos, acetamiprid, chlorothalonil, and cartap pesticides [333] have been detected in μM to nM range with citrate-capped AuNPs. Citrate ions were eliminated after pesticides adsorption on AuNPs, which reduced the electrostatic repulsion force among particles. Van der Waals attraction and hydrogen bonding formation between pesticide molecules facilitated the aggregation of AuNPs which turned solution from red to blue. On the other hand, ligand modified approach worked for some of the pesticides like pencycuron with 6-aza-2-thiothymine,[334] carbendazim with aptamer/poly-diallyldimethylammonium chloride,[335] paraquat, dipterex, cartap, dursban, and methyl thiophanate with tetrakis(*N*-methyl-4-pyridiniumyl) porphyrin,[336] paraquat with aptamer 77F [337] or sodium 3-mercapto-1-propanesulfonate [338]. In ligand functionalized AuNPs, not only the selectivity but also the sensitivity of the probe was improved. The quantity of pesticides controls an aggregated or dispersed state of AuNPs.

Acetylcholinesterase (AChE) enzyme-mediated detection of organophosphate pesticides (OP) is common and widely used in many applications of water and food safety because active site of the AChE is permanently blocked in the presence of pesticide, which can be used in pesticide detection with high selectivity. Using this principle, core-shell $MnO_2$-decorated AuNPs were used besides the enzyme to detect OP [339]. Enzyme AChE hydrolyzed acetylthiocholine iodide (ATCh) to thiocholine (TCh) which served as a reducing agent to decompose the $MnO_2$ shell, forming $Mn^{2+}$ around AuNPs in the absence of OP. This etching process induces a sharp decrease in the extinction coefficient and a blue shift in the SPR peak in the sensing system which could be seen in dark-field microscopy at a single particle level [340]. However, with OPs, AChE enzyme activity was inhibited, and no TCh was produced, and in turn, no etching process

occurred. As the whole detection mechanism worked at single particle level, a very low LoD of 0.006 pg $mL^{-1}$ was achieved.

Other than etching mechanism, AChE has also been used to indicate nanozyme behavior of AuNPs where peroxidase-like activity was explored for the detection of OP. Without OP, AChE was functional that catalysed the acetylcholine (ACh) into choline and acetate, but in the presence of OPs such as parathion ethyl pesticide, the AChE became inactive, and resultantly no choline was produced [341]. As choline was absent in the sensing solution, dispersed cysteamine-AuNPs behaved as nanozyme and oxidized TMB in the presence of $H_2O_2$ which generated intense blue color solution in the presence of the OP. However, cysteamine-AuNPs were aggregated in the presence of choline and lost their peroxidase-like catalytic activity, resulting in no oxidized TMB production indicated by the colorless solution. Similar peroxidase-mimicking activity of AuNPs has been investigated for the detection of OPs such as dimethoate without AChE assay [342]. In this approach, o-phenylenediamine was used as a substrate instead of TMB which was oxidized to yellow color 2,3-diaminophenazine product in the presence of $H_2O_2$. The peroxidase-like catalytic performance of AuNPs was inhibited in the presence of dimethoate pesticide resulting in colorless to light yellow solutions as shown in Figure 2.9A. This method offered an LoD of 4.7 μg $L^{-1}$.

In summary, a range of pesticides have been detected using bare as well as modified AuNPs employing different mechanistic approaches such as aggregation, etching, and nanozymes. Among all, aggregation-based detection method is frequently studied due to its operational simplicity, but this approach offers a high LoD as compared to ligand modified AuNPs probe. In case of etching-based detection system, AChE assay is frequently employed for the detection of OPs with instrument-dependent read-out like dark-field microscopy. However, AChE assay can also be used for in-field colorimetric detection of OPs when nanozyme role of AuNPs is considered, but in this case, the overall procedure becomes cumbersome which takes longer detection time. Moreover, peroxidase-like catalytic behavior of AuNPs is only functional under an acidic environment which limits its application in alkaline systems.

*2.5.2.2 Detection of drugs*

So far, various drugs such as neurotransmitters, anticancer, and polyionic drug molecules have been detected in pharmaceutical and biological fluids using AuNPs [343]. However, antibiotic

drugs are the main concern in case of environmental and food samples which is the scope of this review article. Different antibiotics such as oxytetracycline, tetracycline, kanamycin, ofloxacin, chloramphenicol, and ceftriaxone have been detected by colorimetric approach of AuNPs [344–348]. Their detection is quick and label-free that mainly involves the use of citrate stabilized AuNPs or specific aptamers according to antibiotic compatibility with the assistance of sodium chloride for the visual read-out due to the aggregation of AuNPs [349–351]. The aptasensors follow two kinds of mechanisms depending upon the reagent addition sequence. In the most common way, antibiotics cannot induce aggregation in AuNPs directly, but salts can do. That is why, free aptamers are introduced in the detection system as the initial step which are adsorbed onto the surface of AuNPs and provide resistance to aggregation against salt. Regarding the reasons behind aptamer adsorption onto AuNPs surface, there has been inconsistency in the literature. While some researchers have stated that the electrostatic interactions between positively charged nucleobases with negatively charged AuNPs is responsible for adsorption,[352] others have argued that all four nucleobases are charge neutral at neutral pH and the reason for adsorption is coordination [353]. Wu et al. detected multiplex antibiotics using aptamer functionalized AuNPs and smart phone read-out [352]. According to the authors, the recognition part of aptamer bounded with analyte such as chloramphenicol or tetracycline was dissociated from AuNPs as a folded rigid structure. Meanwhile, it was hard for non-recognition fragment of aptamer to maintain AuNPs in a stable dispersed state, so aggregation took place upon addition of salt [352]. This method offered LoDs of 32.9 and 7.0 nM for tetracycline and chloramphenicol, respectively. Instead of salt, poly dimethyl diallyl ammonium chloride can be used as cationic species which induce aggregation [354].

In the second mechanism, colorimetric detection was mainly dependant upon antibiotic adsorption on AuNPs instead of aptamer binding which was confirmed by the color change of solution when kanamycin was added to AuNPs as shown in Figure 2.9B [355]. Moreover, kanamycin did not induce specific desorption of aptamers from the AuNPs as mutated aptamers, and a random DNA sequence were used which were not bound to kanamycin. Comparative study concluded that the inhibited aptamer adsorption on AuNPs surface was due to kanamycin-AuNP interactions and not by the kanamycin-aptamer binding. This assay showed a LoD of 90 nM. The detection procedure takes a relatively longer time (10 min) when lateral flow assay was involved [356] but on a paper-based microfluidic device, it took only 2 min for the detection of

gentamicin [357]. To enhance the signal output, magnetic beads were used as a separator and TMB or OPD as chromogenic substances generated the color in the presence of antibiotic [358]. In short, a wide range of antibiotics have been detected using different aptasensors [352,355,359,360].

Another approach uses the polymer stabilized AuNPs for the colorimetric determination of antibiotics such as ceftriaxone and cephradine by aggregation mechanism [361–363]. In this scenario, antibiotic reacts with polymer functionalities present at the surface of nanogold. Polymers being rich in oxygen, nitrogen, or sulphur moieties can stabilize AuNPs as well as developing interactions with functional groups of antibiotics to induce aggregation. Specificity and sensitivity of chemical linkages play dominant role in the construction of a selective chemosensor. For example, poly (vinyl alcohol) stabilized AuNPs hydrogel were employed for colorimetric determination of ceftriaxone where borax molecules were used as cross-linker inside the main chain of polymer [364]. The absorbance peak at 517 nm due to AuNPs was decreased in the presence of ceftriaxone, resulting in the size increase of particles with a color change from red to colorless. This assay showed a linear range in 1-90 μg $mL^{-1}$ ceftriaxone concentration with a LoD of 0.33 μg $mL^{-1}$.

In summary, aptasensor and chemosensor-based colorimetric detection has been reported for a variety of antibiotics. In the case of aptasensors, citrate capped AuNPs without any ligand modification works well with high specificity and sensitivity. High-affinity aptamers can measure lower concentrations of antibiotics. For chemosensors, polymer was used as stabilizing agent and sodium borohydride was used as reducing agent, but this colorimetric probe was less sensitive than aptasensors. However, both approaches have strong potential to fabricate paper-based devices for in-field applications due to strong affinity of these sensors with cellulose matrix. These portable devices would have many applications in food industries and clinical settings.

*2.5.2.3 Detection of allergens*

An allergen is a sort of antigen proteins or genes that triggers an aggressive immune response that the immune system defends the body against a perceived danger [365]. Allergens significantly impact the quality of life and, hence, remain a big problem for susceptible people especially children [366]. Thus, rapid detection of food allergens utilizing colorimetric response

of AuNPs are extremely important to detect [367]. Cross-linking and non-crosslinking aggregation behaviors have been studied in detail to detect a range of allergens in a variety of food samples such as shrimp, fish, eggs, peanuts soybeans, barley, sesame seeds, walnuts, almonds, pistachios [368–370] as well as allergenic fungal spore [371].

In the case of cross-linker mediated aggregation, biotinylated antibody as a switchable linker is used to induce aggregation in a detection system. The device follows lateral flow assay where antigen-antibody interactions are the key detection reaction. For example, for the detection of Ara h 1 antigen, it specifically reacted with the biotinylated anti-Ara h1 antibody in the target recognition step which was visualized with the addition of streptavidin-AuNPs [372]. The concentration of cross-linker is important to quantitatively detect the target. On the other side, non-cross-linking mediated aggregation follows hybridization chain reaction between the complementary and target DNA without any enzymes and sophisticated read-out machine [373]. No target DNA was available for the reaction in the absence of allergen gene, so single-stranded portion of hairpin probe remained adsorbed on AuNPs as red dispersed colloids which were resistant to ionic strength. However, in the presence of the allergen as low as 0.5 nM, long double-stranded DNA was formed which could not stabilize the AuNPs and hence released from the gold surface making nanoparticles prone towards aggregation after adding NaCl. In a similar way, pollen allergen Cry j 2 was detected at 0.2 ng $mL^{-1}$ which was 130-times improved due to signal amplification based on catalytic DNA hairpin self-assembly [374]. The bare AuNPs showed purple aggregation after surface detachment of P1 and P2 (DNA probes) that have built two DNA three-way junctions in the presence of Cry j 2. However, in the absence of target Cry j 2, no color change happened in the colloidal solution because of adsorption of ssDNA which was responsible for interparticle electrostatic and steric repulsion among particles as shown in Figure 2.9C. Overall, allergen genes and proteins can be detected using biomolecules modified AuNPs probe which are highly specific and sensitive. Hybridization chain reaction happened between compatible DNA strands which would allow AuNPs accumulation under high salt concentration. This approach has successful standing in developing biosensors for a variety of different allergen detection [373,375].

*2.5.2.4 Detection of mycotoxins*

Mycotoxins are a broad range of toxic secondary fungal metabolites with low molecular weight (300-700 Da) that are harmful for humans and livestock [376]. Out of >300 different types, common examples of mycotoxins are aflatoxins, ochratoxins, zearalenone, deoxynivalenol, fumonisins, patulin, and T-2 toxin, which have been detected using colorimetric sensors. Among them AuNPs-based immunosensors have been used extensively to detect a variety of mycotoxins including fumonisin B1, aflatoxin B1, zearalenone, and ochratoxin A [377–380]. This approach shows multicolor response on lateral flow test strips based on the concentration and type of tested mycotoxin which serves as rapid diagnostic platform for in-field detection. Sample matrix interferences are avoided by simply dilution method [381].

A second widely used approach is AuNPs-based aptasensors that specifically bind to the targeted mycotoxin and detach from AuNPs surface making these particles prone to salt-induced aggregation. Through this approach, T-2 toxin in wheat and corn samples were detected at 57.8 pg $mL^{-1}$ using label-free T-2 specific aptamer [382]. Fumonisin B1 was also detected with aptamers as ssDNA using 40 nt and 96 nt sequence in the presence of Tris-HCl and $MgCl_2$, respectively [383]. Similarly, aflatoxin M1 was detected with LoD of 0.002 ng $mL^{-1}$ considering 72-mers ssDNA by Lerdsri and coworkers [384]. In another study, instead of salt, charged molecules like cationic perylene was used to detect aflatoxin B1 at 0.18 ng $mL^{-1}$ [385]. However, the detection sensitivity was improved to 35 pg $mL^{-1}$ by utilizing magnetic bead (MB) associated aptasensor, where hybridization reaction between aptamer and complementary DNA (cDNA) was the key to get higher sensitivity, and the catalytic reaction was responsible for colorimetric detection. In this study, aptamer surrounded $Fe_3O_4$@Au magnetic beads and cDNA-AuNPs made a bioconjugate which released the cDNA-AuNPs as signal probe in the presence of aflatoxin B1 due to higher affinity of cDNA with aflatoxin B1 as compared to its affinity with magnetic bead aptamer. The signal probe underwent colorimetric detection utilizing peroxidase-like behavior of AuNPs with TMB-$H_2O_2$ system to detect aflatoxin B1 [386]. Similar magnetic bead separation strategy has been used for ochratoxin A (OTA) detection with some modifications [387]. Here, alkaline phosphatase (ALP) was used as an external enzyme to facilitate colorimetric response by hydrolyzing ascorbic acid 2-phosphate to the ascorbic acid (AA) which reduced $MnO_2$ nanosheets to $Mn^{2+}$ that promoted AuNPs aggregation as shown in Figure 2.9D. The DNA-ALP-immobilized MBs contained OTA aptamer, biotinylated cDNA, and streptavidin–alkaline phosphatase (SA-ALP), where biotinylated cDNA hybridized with OTA aptamer to form an

aptamer–cDNA duplex. In the presence of an analyte OTA, an aptamer–cDNA duplex switched to an aptamer-OTA complex which liberated ALP-cDNA from DNA-ALP-immobilized MBs. This magnetic separation is followed by ALP-induced aggregation of AuNPs through $Mn^{2+}$ ions [388]. The enzyme ALP response was directly related to the OTA concentration through aptamer shape switching on MBs and could detect as low as 5 nM of ochratoxin A. Instead of $MnO_2$ nanosheet, Tian *et al*. have utilized AuNRs for the detection of OTA where $Ag^+$ ions were reduced to Ag shell around nanorods by AA to generate a blue-shift of the longitudinal SPR peak which showed visible multicolor change as shown in Figure 2.9E [389]. Another useful probe consists of $Fe_3O_4$@Au which has been used for the detection of ochratoxin A at 0.5-80 ng $mL^{-1}$ detection range by catalyzing TMB under acidic conditions [390].

Besides recognition abilities of AuNPs, these particles have been used as signal amplifier due to their higher surface area which favors the adsorption of larger number of ligands. For example, AuNPs enhanced horseradish peroxidase-linked aptamer assay that was used for the detection of zearalenone as low as 0.08 ng $mL^{-1}$ in spiked oil sample [391]. Also, three kinds of mycotoxins (i.e., aflatoxins, ochratoxins, and zearalenone) were detected in human food and animal products using three distinct reducing or capping agents on the paper platform [392]. The detection mechanism was based on the sort of bonds that each capping agent created with AuNPs such as hydrogen bonding, and capping agents like caffeic acid and glucose which shared the protons of their hydroxyl groups with analytes. Nevertheless, the interaction between sensor and analyte arose from the acid-base dissociation of these chemical compounds at appropriate pH which caused the aggregation and changing the color of AuNPs from red to blue [393].

Overall, different shapes of AuNPs such as nanospheres, nanocacti, nanoflowers, and hyperbranched blackbodies have been involved to build immunosensors for the detection of mycotoxins as the common colorimetric strategy, which is simple, portable and timesaving [394]. Selection of AuNPs shape is highly dependant on target of interest which would generate variable color response accordingly and would help to construct multiplex nanosensor. On the other hand, aptasensors for the detection of mycotoxins have been widely used due to its specificity and sensitivity. Aptasensor-based magnetic bead separation followed by enzyme-induced detection would enhance the method's sensitivity.

*2.5.2.5 Detection of small organic toxins*

Physical and chemical interactions of targeted analytes with AuNPs have been used for the detection of a range of small molecules including illegal food additives like melamine,[395] endocrine-disrupting compounds like bisphenol A (BPA),[396] iodinated X-ray contrast chemicals like iohexol,[397] toxic chemicals like nerve agent VX (*O*-ethyl-S-2-(*N*,*N*-diisopropylamino)ethyl methyl-phosphonothioate),[398] disinfectants such as 5-chloro-2-methylisothiazol-3(2*H*)-one/2-methyl-4-isothiazolin-3-one (CMIT/MIT), and many reducing sugars. Target-AuNPs interactions have been used to study competitive binding behavior of analyte either with AuNPs or aptamer which would help to build a sensor for a specific analyte. For example, dopamine detection was made possible due to its strong adsorption onto AuNPs, and hence, dopamine was specifically detected in this system [399]. On the other hand, aptasensor was used to detect BPA at pM level with truncated 63-mer BPA-specific aptamer which were 12-mer and 38-mer [400]. The use of truncated aptamer improved the sensitivity of sensor approximately 265-fold with 38-mer and 140-fold with 12-mer as compared to 63-mer aptamer.

Taking the advantages of aggregation mechanism, a AuNPs probe commonly utilizes specific molecular recognition approach to detect a wide range of compounds either with bare or modified AuNPs. For example, a fatal chemical compound VX was detected along with its hydrolyzed product 2-(diisopropylamino)ethanethiol (DAET) using citrate capped AuNPs through aggregation mechanism with LoD of 100 nM [401]. Their colorimetric system was highly pH-dependent which favored the VX detection under acidic environment and DAET detection in alkaline condition. On the other hand, 3-aminophenylboronic acid modified AuNPs have been used for colorimetric sensing of iohexol in environmental samples [402]. In 2025, Guo *et al*. reported a colorimetric sensor for perfluorooctanoic acid (PFOA) detection with a LoD of 170 nM. The sensor leveraged host–guest interactions between PFOA and cyclodextrin-modified gold nanoparticles, inducing nanoparticle aggregation and resulting in a visible color shift from red to blue-purple, enabling visual detection [403].

The growth-based detection mechanism of AuNPs was used for the detection of small sugar molecules. Reducing sugars were detected through synthetic approach where room temperature production of AuNPs was dependent on the concentration of reducing sugars involving cetyltrimethylammonium bromide as a surfactant [404]. The participation of sugar in oxidation-

reduction reactions of gold salt was responsible for the production of AuNPs and hence, these sugar molecules can be detected by estimating the rate of reaction as higher rate was observed with fructose and lowest with mannose due to their structural chemistry. The variable concentration of sugar leads to different reactions time and yield of nanoparticles. LoD values for monosaccharides such as fructose, glucose, and mannose were 0.067, 0.081, and 0.106 mM respectively while for disaccharide such as lactose was 0.087 mM.

Detection of melamine using surface plasmon resonanceproperties of AuNPs is a hot topic in colorimetric sensing due to easy aggregation of nanoparticles induced by exocyclic amino groups of melamine [405,406]. Moreover, AuNPs synthesized either by chemical reduction or plant extracts suit well in detection. The LoD of 8 nM was observed with 3-mercapto-1-propanesulfonate ligand which was improved to 1 nM when bare AuNPs were used [407,408]. Usually, electrostatic interactions between AuNPs and melamine trigger the aggregation responsible for color change, but recently, Xie *et al*. have explained the dehydrating condensation phenomena responsible to detect melamine [409].

In summary, a range of small organic toxic substances can be detected using modified or bare AuNPs. The detection based on target-AuNPs interactions are simple to follow but require case-by-case exploration because each analyte has different attractions with AuNPs, so this approach is case-specific. Reducing sugars can be detected with direct synthetic approach, but the detection time was as high as 60 min with a LoD in mM which needs an improvement. Moreover, this was a base-assisted synthesis which limits its applications under acidic conditions. In the case of melamine detection, many colorimetric sensors have been established but there is a need to make this assay portable due to high demand of melamine detection in food on-spot.

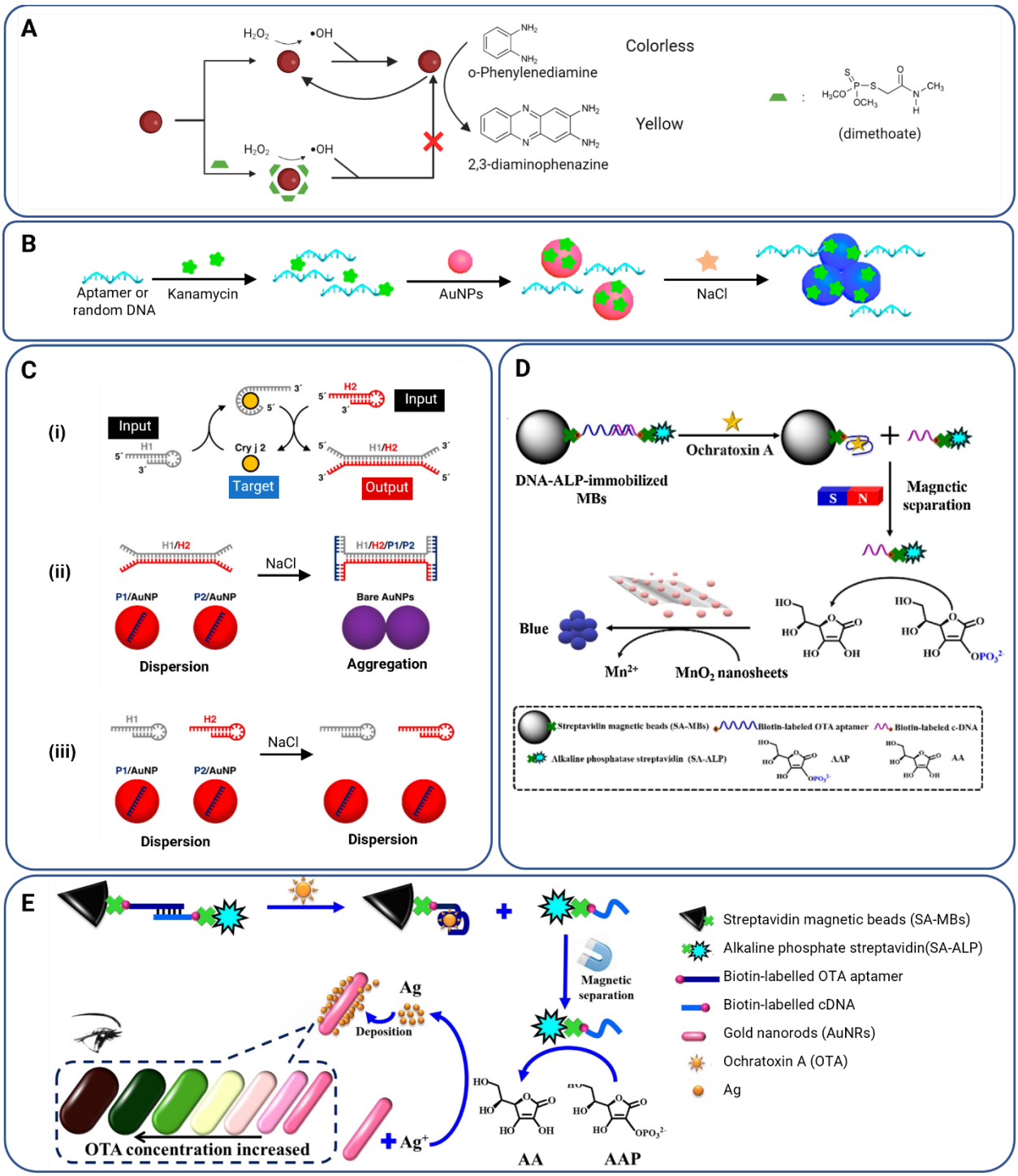


Figure 2.9 A representation of different detection strategies for a variety of organic pollutants using AuNPs-based colorimetric sensors.

A) Detection of dimethoate pesticides based on inhibitory effect of peroxidase-like catalytic activity of AuNPs using o-phenylenediamine as chromogenic agent which did not oxidize to a yellow 2,3-diaminophenazine product in the presence of analyte [342]; B) A label-free biosensor for the detection of Kanamycin antibiotic using AuNPs and arbitrary sequenced DNA where

kanamycin adsorbed on AuNPs and responsible for colorimetric signal instead of DNA adsorption on Au surface. Reproduced with permission from Ref. [355] with some modifications. Copyright 2020 American Chemical Society; C) (i) A pollen allergen Cry j 2 recycling, (ii) in the presence of Cry j 2 analyte, P1 and P2 DNA probes were detached from AuNPs constructing two DNA three-way junctions whereas the bare AuNPs showed salt-induced aggregation, (iii) in the absence of target Cry j 2, the P1 and P2 DNA probes were remained adsorbed on AuNPs surface and responsible for interparticle electrostatic and steric repulsion among particles leading no color change after salt addition. Reproduced with permission from Ref. [374] with some modifications. Copyright 2019 American Chemical Society; D) Detection of ochratoxin A by target-responsive aptasensor where ascorbic acid 2-phosphate was hydrolyzed by alkaline phosphatase (ALP) to produce ascorbic acid (AA) which reduced $MnO_2$ to $Mn^{2+}$ that caused aggregation of AuNPs. Reproduced with permission from Ref. [387] with some modifications. Copyright 2020 Elsevier; E) An aptasensor-based ochratoxin A (OTA) detection utilizing AuNRs where aptamer-OTA complex released ALP-labelled complementary DNA which catalyzed the ascorbic acid 2-phosphate to ascorbic acid (AA). AA reduced $Ag^{+}$ ions which deposited on AuNRs resulting multicolor read-out. Reproduced with permission from Ref. [389] with some modifications. Copyright 2020 Elsevier.

### 2.5.3 Detection of biological analytes in the environment and food

Biological pollutants are mainly living organisms that can pose serious health dangers to humans when present in aquatic and terrestrial environments [410]. These bio-pollutants include bacteria, viruses, molds, and animal dander that cause many diseases such as indoor allergies, foodborne diseases, bacterial and viral infections [411]. These bio-analytes can be detected as a whole microorganism or specific nucleic acid sequences of a pathogen [412,413]. Of note, detection of different amino acid, peptides, proteins/enzymes, nucleic acids/oligonucleotides fall into the category of biomarkers which are important regulator to know the health conditions. AuNPs-based biosensors and immunosensors for the detection of different disease biomarkers have achieved many important milestones which is not the concern of this document, and details can be found elsewhere [414,415]. Detection of different pathogens in water and food samples is important for environmental monitoring and food quality inspection.

Foodborne and waterborne pathogens have emerged as contagious species endangering human health from skin rash to life-threatening diseases including central nervous disorders, intestinal infections, pneumonia, endocarditis, osteomyelitis, sepsis, scalded skin syndrome, and toxic shock syndrome [416,417]. These pathogens found in contaminated poultry, meat, vegetables, fruits, eggs, dairy products etc [418]. AuNPs have been widely used for the detection of pathogens in water, food and environment [419]. Mostly oligonucleotide functionalized AuNPs

play a significant role in developing biosensors for microbial detection. Working principle of DNA-based nanosensors employing non-cross-linking mechanism of aggregation in modified AuNPs has been explained by He and coworkers [420]. Also, Marin *et al*. have compiled a comprehensive review on point-of-need bacterial and their toxins detection present in food matrices using AuNPs [421].

The common recognition units for microbial detection are ssDNA probes, oligonucleotide, peptides, antibodies, bacteriophages, and aptamers. In DNA-based recognition system, the ssDNA adsorbs onto AuNPs through non-covalent interactions which make these particles stable against salt-induced aggregation in the absence of the target. However, salt-mediated aggregation of AuNPs happens with the target due to the formation of dsDNA which has a little or no affinity towards AuNPs. Interestingly, Jiao *et al*. investigated an opposite behavior of DNA-based detection platform while assessing *L*-histidine [422]. In this assay without histidine, DNA1 and DNA2 as histidine aptamers were partially hybridized to form a swing-like unique structure which helped the DNA duplex absorption on AuNPs and make them dispersed. *L*-histidine was determined with a LoD of 3.6 nM when sessile phosphodiester of the DNA1 was cleaved into two parts via self-cleavage due to catalytic action of histidine which disturbed the swing structure of duplex and created ssDNA segments. These cleaved ssDNA parts did not provide sufficient stability to AuNPs in concentrated salt media, and hence, the particles were aggregated resulting in blue color development.

*2.5.3.1 Detection of microorganisms/pathogens*

Pathogen detection is important to control foodborne and waterborne intoxication, resulting in continual advancements in colorimetric detection technology which offers easy-to-perform devices that intend for rapid point-of-need testing. Different shapes of AuNPs such as sphere, cluster, triangle, and hexagonal are involved in microbial detection which work through either LSPR phenomena or peroxidase-like catalytic behavior of AuNPs. Mostly, different biorecognition elements are adsorbed on AuNPs such as ssDNA, aptamers, antibodies, peptides, and bacteriophages to improve the sensitivity and specificity of bacterial detection system [423]. Besides these biomolecular receptors, graphene oxide,[424] iron oxide,[425] citrate,[426] and antibiotic-modified AuNPs [427] have been employed for microorganism detection.

It is well known that the surface of bacteria is unique and considered negatively charged under physiological conditions [428]. The surface electronic properties of bacterial cells have different interactions with AuNPs at different pH. Electrostatic repulsion develops between negatively charged bacterial surface and negative surface of AuNPs which creates a steric hindrance on the surface of bacteria, and resultantly, AuNPs remain dispersed in neutral or alkaline medium. Conversely, in acidic conditions, the surface of bacteria becomes positively charged which attracts negative AuNPs quickly *via* electrostatic attractive forces, and aggregation of nanoparticles can be observed by naked-eye as blue color. These pH-dependent interactions generate trigger-based aggregation in colorimetric aptasensors and would be responsible for selective bacterial detection. For example, *Escherichia coli* O157:H7 has been detected with thiolated-aptasensor HS-Apt@AuNPs probe using acidic to alkaline pH range as shown in Figure 2.10A [429]. The detection limits of 40.46 cfu $mL^{-1}$ with HCl, 94.08 cfu $mL^{-1}$ with NaOH and 147.6 cfu $mL^{-1}$ with $MgCl_2$ were achieved in this assay. However, when simple citrate-AuNPs were used instead of aptamer bounded AuNPs, both the sensitivity and specificity were compromised. For example, seven different kinds of foodborne pathogens named *Staphylococcus aureus*, *Vibrio para*haemolyticus, *Shigella flexneri*, *Bacillus subtilis*, *Pseudomonas aeruginosa*, *Escherichia coli* O157:H7, and *Salmonella typhimurium* were detected with citrate capped AuNPs in LoDs of $2.8\times10^5$ to $4.4\times10^7$ cfu $mL^{-1}$ at a low pH ~3.2 within 5 min [428].

Instead of direct trigger-mediated response, detection of bacteria can also be achieved by indirect method which includes the enhancement of the peroxidase-like catalytic activity of nanogold in the presence of a target. For example, Chen *et al*. detected *S. typhimurium* recently through TMB-$H_2O_2$ system utilizing bovine serum albumin surrounded gold nanoclusters (BSA-AuNCs) as shown in Figure 2.10B [430]. Basically, it was the enhancement of peroxidase-like activity of AuNPs after the addition of targeted bacteria resulting deeper blue color due to the formation of diamine and diimine charged complex. The surface of BSA-AuNCs was modified with dual aptamers *via* Au–S bonds of thiolated aptamers which made this detection system as sensitive as 1 cfu $mL^{-1}$ which was comparable to an electrochemical sensor. This method was advantageous due to dual aptamer modified probe which occupied different binding sites on the surface of bacteria cell resulting higher sensitivity.

In another approach, aptamers were used in the detection system considering their high binding affinity towards a target. In this method, detection probe was consisted of aptamer-thiolated polystyrene-cysteamine conjugates that reacted with *S. typhimurium* target if present in the sample otherwise with complementary DNA-magnetic nanoparticle (cDNA-MNP) conjugates. AuNPs were introduced in the detection system after magnetic separation of nanoconjugates, where AuNPs were aggregated by reacting with sulfhydryl groups of cysteamine, giving a visible color change from red to blue in a positive sample with a LoD of $6.0\times10^{1}$ cfu $mL^{-1}$. However, in case of negative sample, complementary DNA-aptamer conjugate had already been separated from the detection platform, so there was no thiolated polystyrene nanoconjugates in the solution, and hence the red color of AuNPs remained red as shown in Figure 2.10C [431]. Complementary DNA approach without magnetic separation has also been used for *K. pneumoniae* detection with the help of thiolated oligonucleotide probes where DNA hybridization was the key principle of the detection [432]. In another study, simultaneous detection of nineteen different *Salmonella* species was achieved by single stranded oligonucleotides 30-mer modified AuNPs through sandwich hybridization with 192-bases of ttrRSBCA of *Salmonella* strains with and LoD of <10 cfu $mL^{-1}$ [433]. In 2024, Oliveira *et al.* developed a biosensor for *Salmonella* detection utilizing gold nanoparticles coated with anti-Salmonella polyclonal antibodies. This sandwich-type lateral flow immunoassay strip achieved detection within 15 minutes, with a LoD of $10^{3}$ cfu $mL^{-1}$. The device successfully identified *Salmonella* in contaminated samples of chicken, milk, black pepper, and eggs and chocolate [434].

As another AuNPs-based aptasensor strategy, the etching process is widely used to detect a specific analyte and to enhance the method sensitivity. In the case of detection, usually $MnO_2$ nanoparticles serve the purpose while iron oxide nanoparticles are used when signal amplification is required to enhance the activity via etching process. However, in both scenario, microorganism detection requires immunomagnetic separation technology, where the binding of recognition antibodies and target bacteria leads to sandwich-type immunocomplex. The $MnO_2$ nanoparticles on this immunocomplex is etched with a reducing agent to generate $Mn^{2+}$ ions that would cause aggregation in AuNPs. For example, detection of *V. parahemolyticus* was achieved by IgY-MBs and IgG-$MnO_2$ NPs that bind to different specific binding sites of bacteria through antigen−antibody interactions. After a magnetic separation, the bacteria-attached $MnO_2$ NPs

were etched by ascorbic acid to produce excess $Mn^{2+}$ ions which led to aggregation in AuNPs through metal-ligand interaction as shown in Figure 2.10D [435]. The amount of $Mn^{2+}$ ions generated was directly proportional to the bacterial concentration, which gave a LoD of 10 cfu $mL^{-1}$ for this method. In case of etching-enhanced peroxidase activity of aptamer-AuNPs, Staphylococcus aureus was detected with and LoD of 10 cfu $mL^{-1}$ [436]. In this system, IgY antibodies modified $Fe_3O_4$/Au nanocomposite were used to separate target bacteria, and thiol-aptamer-AuNPs showed peroxidase-like catalytic activity which was revealed by the TMB-$H_2O_2$ reporting agent. Deep yellow color changed to pale yellow with the increased concentrations of *S. aureus*. In short, the etching process can be used either to reveal or enhance the colorimetric detection of pathogens in AuNPs-based immunoseparation assay.

In addition to aptasensors, Gram-positive and Gram-negative bacteria can be detected with chemosensors utilizing the interactions of antibiotics with bacterial cell wall; hence antibiotic modified AuNPs probe has been synthesized. Recently, polypeptide and *β*-lactam structural features of antibiotics have been used to reduce gold salt to AuNPs in addition to their sensing properties for different bacterial species like *S. aureus, P. aeruginosa, and E. coli* [437]. Polymyxin, bacitracin, penicillin, and cephalexin antibiotics have produced spherical, hexagonal and triangle shaped AuNPs in different sizes and population. The detection was based on the interaction between specific binding sites of bacterial membrane and variable functional groups of antibiotics. The LoD was not determined for any bacterial species which needs further exploration. Similarly, vancomycin-AuNPs probe was used to detect *S. aureus, M. luteus*, and *B. subtilis* at $1\times10^9$ cells $mL^{-1}$ on a test strip which differentiated Gram-positive bacteria from Gram-negative strains [438]. Vancomycin-AuNPs and Gram-positive bacterial cell suspension showed the red color on a nitrocellulose strip which became deepened with increasing bacterial concentrations. Silver treatment for the signal enhancement was applied which changed red color to black due to reduction of silver ions on the Au surface. The bare eyes detection limit for *S. aureus* was $\sim2\times10^9$ without treatment and $\sim1\times10^9$ cells $mL^{-1}$ after Ag enhancement. No significant change in LoD was observed for *M. luteus*, and *B. subtilis*. Liu *et al.* reported the detection of a food born pathogen *S. aureus* with a LoD of 2.4 cfu $mL^{-1}$ using a click reaction between azides-AuNPs and alkyne-AuNPs [439]. The aptamer and ALP dual functionalized $Fe_3O_4$NPs were used as recognition as well as signal transduction agent. The ascorbate-2-phosphate (AP) was catalyzed by ALP to generate ascorbic acid (AA). The AA reduced $Cu^{2+}$

present in the solution to $Cu^{+}$ which triggered a click reaction for azide- and alkyne AuNPs, resulting in the aggregation of AuNPs with the development of blue color as shown in Figure 2.10E. In the presence of *S. aureus,* the binding of $Fe_3O_4$NPs to the bacterial surface inhibited the substrate to show the peroxidase-like catalytic performance, hence, stopping the colorimetric sensing of bacteria resulting in red color of the solution.

Conclusively, AuNPs-based biosensors have been used for the detection of pathogenic bacteria through target-stimulated approach, enhancement of peroxidase activity, thiolated polystyrene-analyte interactions, DNA hybridization and antibody-antigen interactions. Among all, target-mediated approach is simple and inexpensive but very sensitive to pH changes which requires a careful assay handling. Detection through enhancement of peroxidase-activity is a more sensitive approach as compared to all other methods due to involvement of peroxidase-like catalytic role of AuNPs which makes detection system highly sensitive and efficient. While in case of thiolated polystyrene-analyte interactions and antibody-antigen interactions, immunomagnetic separation is involved which is time consuming (~45-60 min) and makes detection protocols cumbersome. These AuNPs-based aptasensors are highly specific towards bacterial strains as compared to chemosensors based on antibiotic-AuNPs. AuNPs-based antibiotic assisted bacterial detection system is complex due to involvement of multiple amine, amide and carboxylic groups in structure which are acid and base sensitive moieties and require a good control over pH. However, this approach is equally suitable for a variety of Gram-positive and Gram-negative bacteria due to bacterial cell wall interactions with compatible antibiotics. Moreover, silver enhancement protocols in these chemosensors help to increase the color intensity of results which make this procedure favorable over other detection systems.

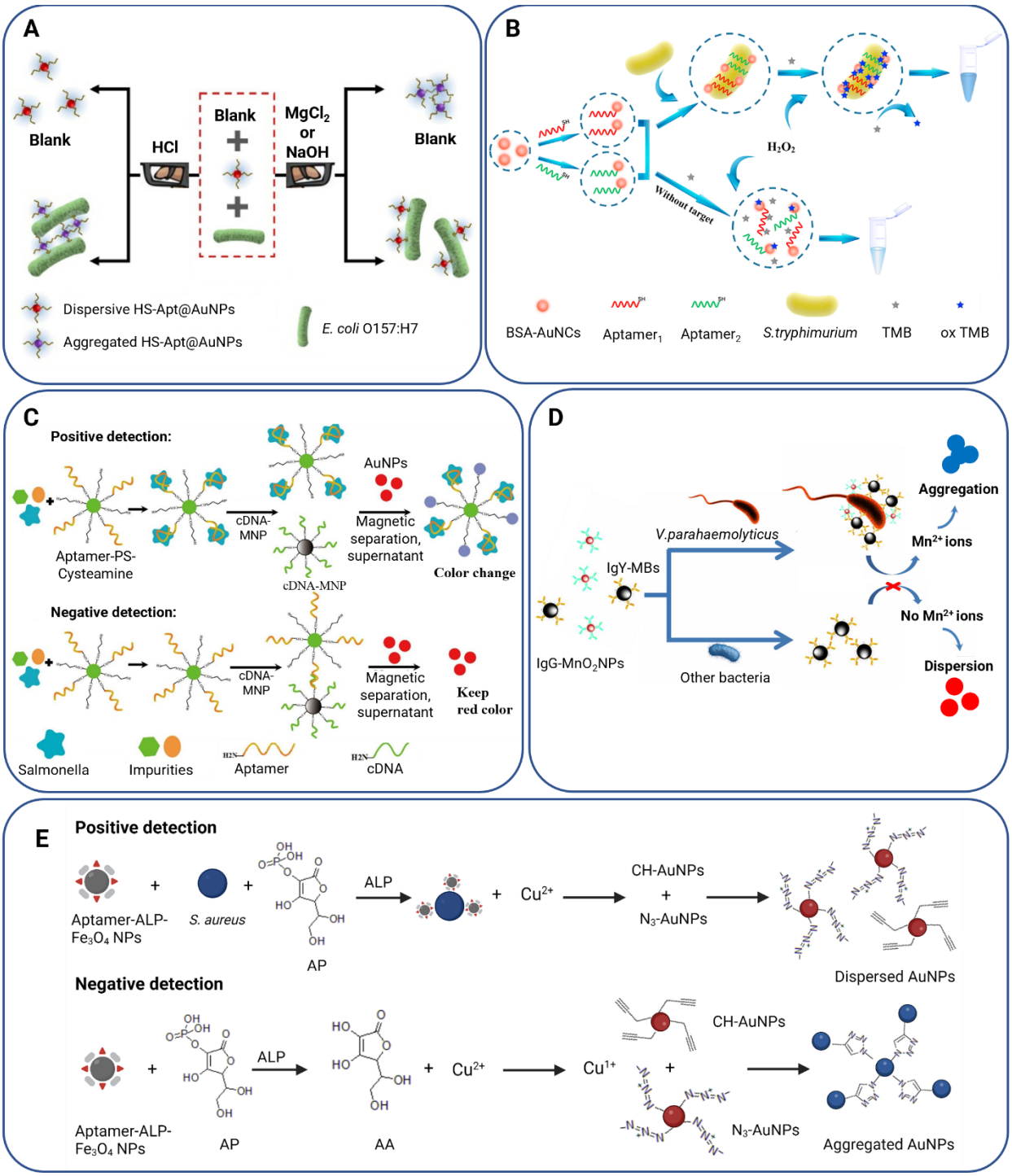


Figure 2.10 Detection of different biological pollutants using AuNPs-based colorimetric sensors. A) A pH-mediated detection of *E. coli* O157:H7 using thiol-aptamer functionalized AuNPs where acidic condition induced aggregation in AuNPs indicating the presence of bacteria whereas dispersion in AuNPs was observed in basic and neutral condition. Reproduced with permission from Ref. [429] with some modifications. Copyright 2021 Elsevier; B) Detection of *S. typhimurium* using aptamer-gold nanoclusters (Apt-AuNCs) which showed an enhanced

peroxidase-mimicking activity in the presence of bacteria as indicated by intense blue color. Reproduced with permission from Ref. [430] with some modifications. Copyright 2021 Elsevier; C) Detection of *S. typhimurium* using aptamer-thiolated polystyrene-cysteamine conjugates which reacted with *Salmonella* and aggregated AuNPs, resulting a colorimetric read-out whereas complementary DNA magnetic nanoparticle conjugates reacted with the free aptamer-PS-cysteamine conjugates in case of negative results. Reproduced with permission from Ref. [431] with slight modifications. Copyright 2021 Elsevier; D) Detection of *V. parahemolyticus* using magnetic bead assisted sandwich immunoassay where polyclonal IgG antibodies coated $MnO_2$ particles recognized the targeted bacteria liberating $Mn^{2+}$ in the presence of ascorbic acid followed by AuNPs aggregation. Reproduced with permission from Ref. [435] with slight modifications. Copyright 2018 American Chemical Society; E) Detection of S. aureus using AuNPs which were aggregated by $Cu^{+}$ mediated alkyne-azide cycloaddition reaction. The aptamer-ALP-$Fe_3O_4$NPs (IMB) were used to separate targeted analyte. Blue color was observed in the absence of analyte because ascorbate-2-phosphate (AP) was hydrolyzed to ascorbic acid (AA) by ALP followed by reduction of $Cu^{2+}$ to $Cu^{1+}$ which triggered click reaction [439].

## 2.6 Challenges of Matrix Effects and Cross-Reactivity in Analyte Detection

In the development of point-of-use sensing platforms, especially colorimetric assays based on AuNPs, matrix effects and cross-reactivity remain significant challenges that can compromise specificity and accuracy. Complex sample matrices such as environmental water samples, food extracts, and biological fluids contain various interfering substances (e.g., salts, proteins, organic matter) that can affect the sensor response by altering the physicochemical environment or directly interacting with the recognition elements.

Cross-reactivity, particularly in multi-component systems, poses a risk of non-specific detection, which may lead to false-positive or false-negative results [439]. For example, structurally similar compounds or ions may compete with the target analyte for binding sites, while some matrix components may trigger unwanted aggregation of nanoparticles, falsely mimicking the colorimetric response. It is important to emphasize that the success of the sensing system depends greatly on its ability to minimize or compensate for these matrix-induced interferences. Several strategies are considered in the design and development of the platform:

- *Optimization of assay conditions,* including pH, ionic strength, and buffer composition, to stabilize nanoparticle interactions and reduce background signals.
- *Surface modification of nanoparticles* with selective ligands (e.g., aptamers, antibodies, functional polymers) to enhance target specificity and reduce non-specific adsorption.
- *Sample pre-treatment or dilution protocols* to mitigate matrix effects without compromising detection sensitivity [381].

- *Incorporation of internal controls or reference zones* within the sensing system to account for matrix variability in real-time.

Addressing these challenges is essential for the deployment of the detection platform in complex real-world samples. Future efforts will focus on further enhancing selectivity and validating performance with real matrices to broaden the platform's applicability across different analyte types and sample sources.

## 2.7 Summary

The prevalence of AuNPs in scientific research and nanotechnology has been admitted without any debate. The unique surface plasmon resonance and peroxidase-like catalytic properties of AuNPs varies with particle size, geometric shape, and surface chemistry. This comprehensive review presents the main characteristics and synthetic approaches of AuNPs as well as a detailed comparative discussion on different sensing mechanisms of colorimetric detection. Analytes involved in environmental monitoring and food quality control have been broadly categorized into inorganic, organic and biological sections. Of note, physical properties of AuNPs are controlled by their method of preparation, while the detection method is dependent on the nature of functional groups adhered to AuNPs surface. It is noteworthy to mention that the focus of this review paper is on analytics, device performance and key findings of assay including the nature of functional groups around AuNPs, chemical forces involved, experimental conditions of method, assay time, and limit of detection for the real samples. This review paper is different from other published work on application to environmental and food analysis.

Among AuNPs-related surface plasmon resonance-based colorimetric sensors, the non-crosslinking aggregation method is sensitive, quick, and simple as analyte-triggered destabilization of AuNPs involves only a few steps. However, this method is prone to interference with non-targeted agents and thus has relatively low selectivity. In comparison, the cross-linking aggregation method is less sensitive, and more time-consuming due to the involvement of true chemical bonds by chemical reactions, but it has a higher selectivity. Moreover, salt-induced signal amplification is successful in case of non-crosslinking aggregation, whereas cross-linking aggregation requires additional chelating agents or enzymes to achieve lower limit of detection. Etching-based non-aggregation methods are more sensitive compared to aggregation methods but require harsh conditions such as the use of oxidizing

agents or corrosion chemicals. Moreover, etching being a slow process takes longer detection time.

AuNPs-related peroxidase activity-based colorimetric sensors are more sensitive as compared to surface plasmon resonance-based colorimetric sensors due to involvement of peroxidase-like catalytic properties of AuNPs which offers detection limits usually in nM and pM level. However, nanozyme sensors require lengthy detection protocols. In this regard, expression of peroxidase activity method is more efficient and is better studied than the method relying on inhibition of peroxidase activity given to less prevalence of inhibiting agents. Bimetallic nanocomposites offer higher peroxidase-like catalytic activity as compared to ligand modified AuNPs. Although ligand attachment on the surface of particles alters the enzyme mimicking activity of AuNPs, this modification usually detects single analyte, and hence multiplexed identification of analytes is highly challenging in nanozyme sensors as multiplexing capabilities of AuNPs is difficult to achieve. Nanoscale size <10 nm of AuNPs shows better peroxidase-like catalytic activity which is further improved when particle size drops below ~3 nm, while detection systems work well in terms of sensitivity when AuNPs >10 nm are used in surface plasmon resonance-based colorimetric sensors. Overall, AuNPs-colorimetric sensors are less explored as compared to electrochemical sensors in the area of inorganic ions detection. Chemosensors are widely used for the detection of organic analytes, whereas biosensors are frequently employed for the detection of bio-analytes.

## 2.8 Future Perspectives

Worldwide research on AuNPs to construct colorimetric sensors highlights a few points to consider in future. Besides distinct advancement in sensors and detection field, only a few commercial devices using AuNPs are available for a limited variety of analytes. With rapid increase in pollution crises and food frauds, it is crucial to develop colorimetric sensors for on-spot inexpensive testing having rapid results without the need of any instrument, especially in resource-limited areas. Thus, considerable efforts have been made to explore new strategies for the detection of pollutants and toxic substances, as well as to tackle the current challenges associated with existing sensing approaches. Of note, the prevalence of AuNPs in environmental monitoring and food safety has been admitted since decades but further exploration is required to implement signal amplification approaches to improve the sensitivity by naked eye readout. In

addition to this, it is necessary to identify more aptamers for designing new aptasensors as aptamers are highly specific to targeted analyte and have higher stability compared to antibodies.

Currently, nanozyme sensors work in a narrow pH range which needs to be broadened to enhance the versatility of nanozyme platform. The disadvantage of nanozyme sensors is the longer detection time because of slow enzyme kinetics which needs to be improved by introducing new functionalities on AuNPs surface. Moreover, it is important to work on less-explored corner of catalytic properties of AuNPs such as catalase, oxidase, and reductase. Besides, analytes in complex food matrix are challenging for on-spot colorimetric detection which require the establishment of in-field sample separation techniques. Moreover, colorimetric reactions usually happen in the solution phase which are susceptible to external environment, and hence, reagent encapsulation or lyophilization strategies should be emphasized for portable detection systems.

Sample matrix interference on the performance of AuNPs-based assays should be considered since AuNPs are vulnerable to aggregation in the presence of sample matrix. In some cases, sample digestion is required to eliminate the effect of a complex sample matrix, but this step increases the acidity or alkalinity of the media which may cause unwanted aggregation of unprotected AuNPs. In another approach, pre-separation of the target analyte from sample via column-based pre-concentration or solvent extraction can alleviate matrix interferences, but such steps are tedious and add complexity in the operation. Alternatively, simple dilution can be used to limit the matrix effect. However, dilution can be applied to selected samples and will decrease the concentration of the analyte in the sample, making it difficult to detect the analyte in low concentrations. Till today, the common approach to avoid interferences is to prepare AuNPs probe with appropriate functionalization which is being used by many researchers.

Overall, colorimetric detection is sensitive to colloidal stability which needs to be improved for better quantification purposes. Morphology of particles govern the analyte sensing capacity, so reproducible synthetic approaches for AuNPs are encouraged as homogeneity and stability of large batch of AuNPs is difficult to achieve. Single AuNP can be functionalized with multiple ligands to fabricate multiplex detection devices. Altogether, AuNPs are considered smart materials in sensors technology due to strong potential applications in environmental monitoring and food applications. AuNPs-based colorimetric sensors could lead to tackle upcoming

challenges regarding pollution removal, wastewater treatment, and food safety. The development of state-of-the-art microfluidic devices such as paper-based microfluidic devices using AuNPs, and gold nanocomposites may improve the applicability and sensitivity of established sensors. Active collaboration among researchers is encouraged in the field of sensors, detection, nanomaterials and computational to advance the AuNPs research. Moreover, improving the stability and reproducibility profile of AuNPs will maximize its utilities in food quality monitoring and pollution detection towards commercialization.

# CHAPTER 3 Development of a Plasmonic Tablet using Dextran-Gold Nanoparticles (dAuNPs) and its pH-Sensitive Behaviour

***This chapter is reproduced from the article published in ACS Omega, 7, 11177–11189 (2022).***

This chapter presents the fabrication of a plasmonic tablet as a low-cost, user-friendly, portable, and sensitive detection platform. Dextran-gold nanoparticles were synthesized via a two-steps process involving conventional reflux and ligand exchange. Additionally, the pH-responsive behavior of the tablet was investigated under various ionic conditions.

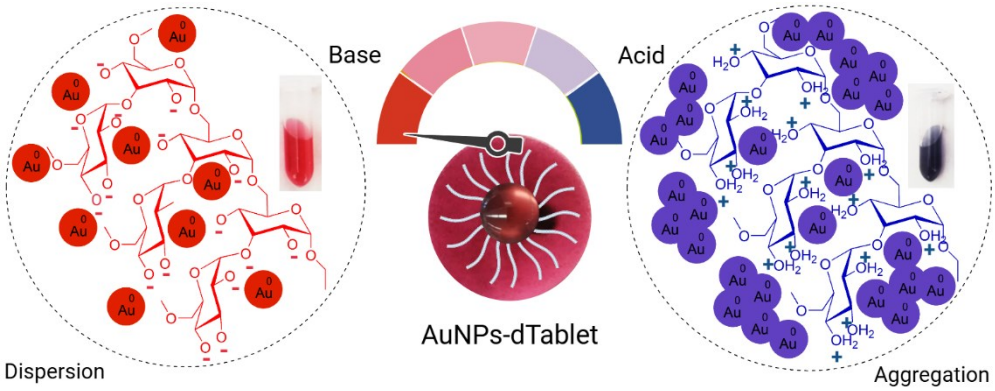

## 3.1 Introduction

Gold nanoparticles (AuNPs) have diverse applications in the area of heterogeneous catalysis [440], food sciences [441], biomedical engineering [442–444], drug delivery [445,446], biosensing [447–450] bioimaging [451] and many more. These nanoparticles have shown remarkable chemical, biological, optical, thermal, and electronic characteristics. Several chemical, biological, and physical approaches have been reported for the synthesis of these nanometallic particles under mild conditions [98,452,453]. Their ease of preparation, variable surface chemistry, and nano size variation make AuNPs suitable candidates for a range of applications such as food packaging, water purification, batteries, nanoceramics, and electronics [454–457]. One of the aspects is surface plasmon resonance phenomena which is a fundamental principle of many colorimetric sensing applications. This unique feature can be tuned sharply based on surrounding functionality and stabilization forces around nanogold as well as their interparticle distance and morphology. Usually citrate capped gold nanoparticles are electrostatically stabilized which is very sensitive to ionic strength. Alternatively, if particles are sterically stable instead of electrostatic forces, e.g., in the case of polymer bound gold nanoparticles, these particles are less prone towards aggregation and offer extra stability in high salt concentration [206]. That is why these particles have been engineered with different capping agents depending upon the required properties according to the target of interest.

In this connection, extensive research has been conducted over many decades to investigate the potential applications of AuNPs. Various studies have been performed to explore the colorimetric role of AuNPs in the detection of toxins in food [458], hazardous substances in environment [459], as well as in forensics and diverse biomedical applications. For example, aptamer wrapped AuNPs have been reported for the detection of T2-toxin in wheat and corn [460], aflatoxins in milk [461,462], and antibiotics in many food and environmental samples [463]. Recently, Zha *et al.* reported a dual-modal immunosensor based on biotin-labeled IgG-modified AuNPs for the detection of chloroacetamide herbicides [464]. Also, sodium malonate capped AuNPs were reported for the detection of barium ions in gunshot residue as a potential application in forensic sciences [465].

AuNPs are also famous due to their distinct position in disease diagnostics and nanomedicine due to their compatibility with biomolecules [466,467]. Under controlled conditions, these

nanoparticles are well dispersed, stable in the media, and red in color. However, a fluctuation in temperature and pH dramatically changes the electrostatic stabilization of gold nanoparticles and favour the aggregation of particles corresponding to a blue color. That is why their thermo-responsive and pH-responsive behaviour is important to mention whenever their role in sensing and biomedical applications has been investigated [468]. Most of the chemical linkages are sensitive to acidic environment such as hydrolysis of acetal, ketal, ester, amide, imine, hydrazone and oxime [469,470]. Gold nanoparticles as drug-loaded acid-degradable nanocarriers can be administered to the body through intravenous injection, and hence, this acid induced degradation is important in living systems because it allows the release of encapsulated therapeutics in a controlled/enhanced fashion [470]. In this connection, dextran stabilized AuNPs are of particular interest because these particles utilize the functional properties of both entities to maximize their benefits.

Dextran is a natural biocompatible and biodegradable homopolysaccharide of glucose that has historical significance in pharmaceutical and medical applications [471]. This polymer also has a strong ability to surround AuNPs due to the –OH and –COR groups in its chains which stabilize nanoparticles through steric as well as electrostatic forces [206]. These hydroxyl groups in polymeric chain have been oxidized to carbonyl functionality when dextran is primarily used as a reducing agent during the synthesis of AuNPs. Utilizing this concept, Wang *et al.* reported the colorimetric detection of dihydralazine sulfate in uric samples based on hydrazone chemistry between aldehydic group of dextran and hydrazine moiety of analyte [472]. In another report, Davidovi *et al.* detected cysteine colorimetrically by replacing dextran from the nanoparticle as thiol group interacts more strongly with metallic particles compared to ketone and aldehyde groups of dextran [473]. On the other hand, when dextran is used exclusively as a surface coating material around AuNPs, it may require harsh reaction conditions to break its polymeric steric stabilization. It is important to point out that the long-term stability is a prerequisite for any application of colloids.

Due to these outstanding characteristics, various formats of dextran-encapsulated AuNPs have been developed including colloidal solutions, gold nanocomposites/hydrogels [474] as well as powder [475] with applications in drug delivery [466], cell imaging [476], wound healing [477] and microbial susceptibility [478]. Nonetheless, dextran capped AuNPs solutions gradually

aggregate to form bigger size particles due to the sedimentation phenomenon of AuNPs in colloidal systems after some time. On the other hand, storage and transportation of AuNPs solution are not always convenient. In fact, it was observed that several samples of the synthesized dextran functionalized AuNPs solution stored at normal condition were randomly attacked by fungi [475]. In case of powdered/gel samples, there is a serious issue of quantitative measurement of AuNPs-dSol powder/gels for a specific test every time, and hence, these samples are not suitable for direct applications and require extensive calibration procedures.

Keeping these issues in mind and in addition to our ongoing efforts to fabricate portable sensors for environmental monitoring and providing easy to use platforms [64,479,480], we have developed a dextran based AuNPs tablet (AuNPs-dTab) as a simple and ultrastable platform for multipurpose applications. These tablets can be prepared in different concentrations of colloidal gold with a variable amount of dextran, hence a pre-measured and calibrated/optimized amount of dextran capped AuNPs can be stored in the form of solid tablets. These pre-loaded tablets with the right mass of reagent will lower the user interventions and eliminate the need to weighing balance, pipettes and other equipment. Our approach is an easy substitute of solution phase of AuNPs-dSol without compromising on the stability and efficiency of nanoparticles.

The tablets were obtained in three easy steps without involving any laborious work-up as mentioned in Figure 3.1. In this study, after optimization of the fabrication technique with various concentrations of dextran, we spectroscopically characterized the tablets using UV-vis, FTIR, DLS, TEM, XRD, DSC and AFM techniques. Next, we have demonstrated the outstanding stability of AuNPs-dTab under ambient conditions as well as at high salt concentration. These tablets show pH tolerance in alkaline condition, while the tablets were highly responsive at lower pH as aggregation of nano gold in acidic pH range is an important feature of colorimetric sensors. Being oxygen impermeable, these tablets are highly stable against oxidative stress in addition to their thermal stability. Our proposed fabricated AuNPs-dTabs are stable for nine months and even longer as no stability issue is recorded till the preparation of this manuscript. Morphology of these tablets was also analyzed in terms of thickness, diameter, density and opacity. In short, this simple, easy to store and easy to carry tablet opens new avenues in biosensing and biotechnology research due to being user-friendly and low cost.

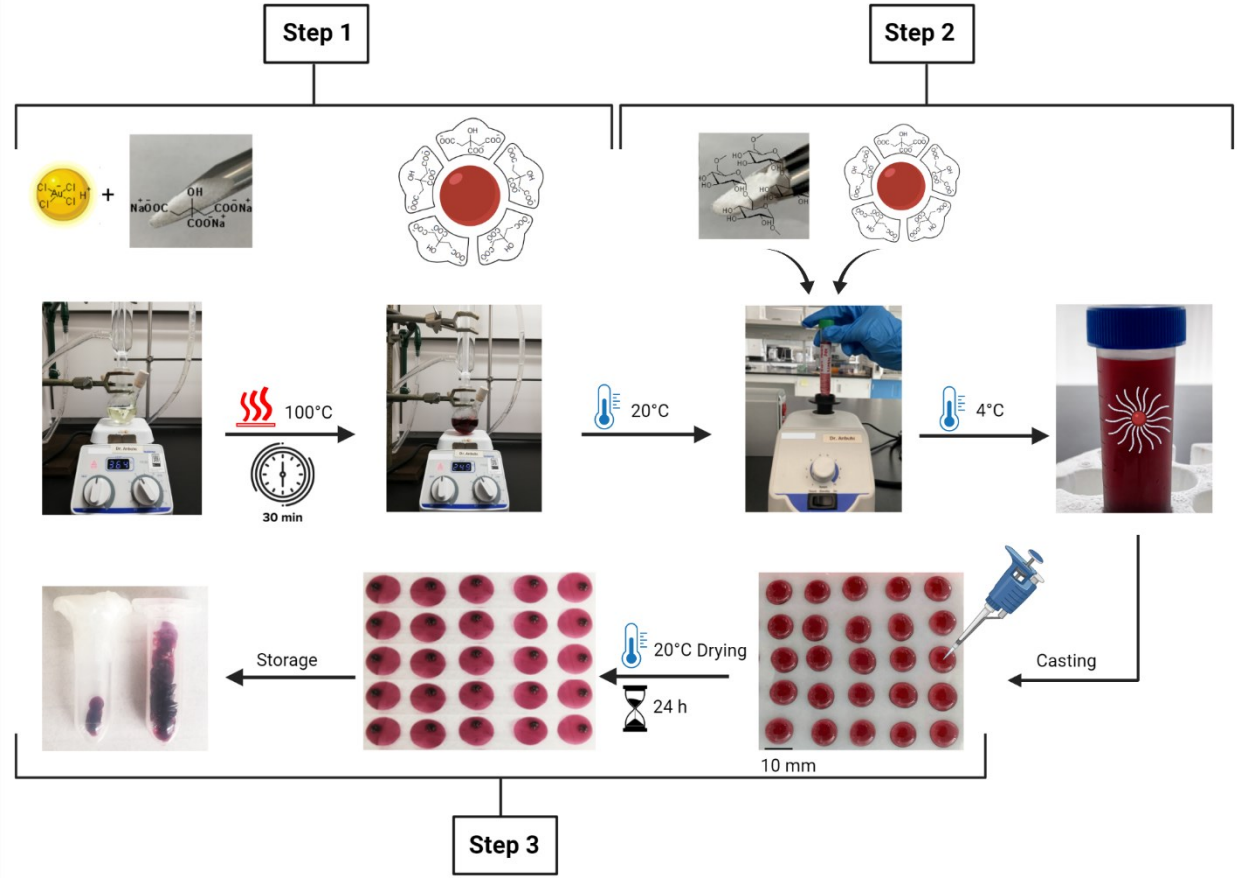


Figure 3.1 Representation of AuNPs-dTabs formation stepwise.
In step 1, citrate capped gold nanoparticles (AuNPs-Cit) were synthesized by boiling chloroauric acid with sodium citrate for 30 minutes. In step 2, dextran powder was added to the cooled solution of AuNPs-Cit and mixed well using vortex to get homogenized dextran capped gold nanoparticles (AuNPs-dSol) solution and stored in fridge. In step 3, AuNPs-dTabs were casted by pipetting technique followed by air drying for 24 h at room temperature and finally stored in airtight plastic vials. The tablets were portable and low-cost approx. 1.22 CAD per 100 tablets of 100 µL.

## 3.2 Experimental Section

### 3.2.1 Materials and Methods

All reagents and solvents were used as received without further purification. Gold (III) chloride solution 99.99% (trace metals basis, 30 wt. % in dilute HCl) and trisodium citrate dihydrate were purchased from Sigma Aldrich, USA. HPLC grade water, hydrochloric acid 37%, and nitric acid 65% were purchased from Sigma Aldrich. Dextran (*Leuconostoc spp.* M ~100 kDa) were purchased from Sigma Aldrich, China. Sodium hydroxide was purchased from Sigma Aldrich, Switzerland. Sodium chloride was purchased from central chemical store, Concordia University. Plastic sheet of polypropylene was purchased from local stationary shop.

pH measurements were recorded using plastic pH indicator strips made from Fisher Scientific, USA, and AB200 pH/mV/conductivity made from Fisher Scientific accumet, Singapore. *ImageJ* software was used from National Institutes of Health, Bethesda, MD, USA. Vortex, model # 9454FIALUS, 50/60 Hz Fisherbrand was used to get homogenized AuNPs-dTab solution. Particle size analyzer (PSA), model Litesizer 500 (Anton-Paar, Austria) was used for nanoparticles size distribution and polydispersity index. Particle size range for the machine is 0.3 nm – 10 μm. All samples were also run for Zeta potential *via* electrophoretic light scattering using cmPALS technique (European Patent 2 735 870) for high sensitivity. PSA has a particle size range from 3.8 nm to 100 μm for zeta potential measurements. The colloidal concentration of nanoparticles was taken in Ω-shaped polystyrene cuvettes at 25 °C and the data were taken in triplicate.

The extinction spectra of AuNPs were recorded on UV-vis spectrophotometer (BioTek, Cytation 5, imaging reader) at room temperature. Infrared spectra of samples were obtained from Nicolet™ iS20 FTIR spectrometer (Thermo Scientific Instrument Co., Madison, Wisconsin, USA) using the single reflection horizontal ATR accessory Smart Orbit, and a diamond crystal with ZnSe lens at an incident angle of 42°. The FTIR spectra were acquired in the range of 4200 to 650 $cm^{-1}$ with 0.25 $cm^{-1}$ spectral resolution to identify potential chemical interactions between dextran and gold nanoparticles. Each sample was scanned twice to ensure good reproducibility. Transmission electron microscopy (TEM) was performed using a Talos™ L120C (20-120 kV) for structural examinations and investigation of particle shape and size. We used copper grid with a coating of formvar, FCF-300-CU, 300 mesh purchased from electron microscopy sciences. AuNPs solutions (2 μL) were deposited on a grid and dried for 24 h before performing the run.

The surface morphology measurement and data acquisition of AuNPs-dTab sample were carried out by the atomic force microscopy (AFM) system (Anton Paar Tosca 400, Austria) with the tapping-mode in air. The aluminum reflex coated cantilever (thick: 30 nm, resonance frequency: 285 kHz, spring constants: 42 $Nm^{-1}$, curvature radius: <10 nm, height 10 – 15 μm) were used for the experiment, and the 500 × 500 pixels images were collected at the line rate of 1 lines/s. Image analysis was done using *Gwyddion* (free, open-source software, version 2.59).

### 3.2.2 Formation of Dextran Capped Gold Nanoparticle Solution

In a first step, citrate-capped gold nanoparticles (AuNPs-Cit) were prepared following the direct method of Turkevich approach [479] with slight modifications. The concentration of this colloidal solution was estimated to be 8.01 nM, according to Beer's law while using extinction coefficient ($\varepsilon$) of 13 nm AuNPs due to their surface plasmon resonance (SPR) wavelength at 520 nm [479]. In the second step, dextran-capped gold nanoparticles (AuNPs-dSol) were achieved by replacing citrate ions with dextran being strong stabilizer as well as capping agent. This is called "post-modification of pre-formed AuNPs". For this purpose, concentration of polysaccharide solution in weight by volume (w/v) was used to cast the tablets where 10 g of dextran powder was mixed using vortex with required volume of AuNPs-Cit suspension to get 10% (w/v) solution of AuNPs-dSol. From this stock solution, a serial dilution of 1-9% (w/v) AuNPs-dSol were prepared for further experiments. FTIR spectra of AuNPs-Cit and AuNPs-dSol samples were recorded to identify the functional groups around gold nanoparticles and their surface chemistry.

### 3.2.3 Formation of Dextran Capped Gold Nanoparticles Tablets (AuNPs-dTabs) and Their Morphological Studies

AuNPs-dTablets were casted by squeeze dropping of 100 µL of AuNPs-dSol solution of variable % concentrations (w/v) on clean plastic sheet of polypropylene. The drops were air-dried overnight at 20 °C, 48% RH and atmospheric pressure. In another batch, tablets were dried in oven at 80 °C to compare the effect of heat on tablet formation. Tablet formation was considered not fully completed if the tablet could not be removed from the sheet. Uniformity and color of all tablets 1-10% (w/v) were recorded. These tablets were dissolved in a fixed volume of water to observe the dispersion of colloidal nanoparticles in the solution by recording absorbance at 520 and 650 nm UV-vis spectrophotometrically.

Once optimum ratio of dextran and AuNPs-Cit solution was obtained depending upon the stability of particles, tablets of variable sizes such as 50, 100, 200, 300, 400 and 500 µL were casted to see the effect of volume on tablet's diameter. To study further, 100 µL of different concentration of AuNPs (8, 4, 2 nM) were mixed with different amount of dextran separately to get 6 and 10 % (w/v) tablets. These tablets were considered for measuring hydrodynamic diameter (ø, mm), thickness (e, mm), density (ρ, g/cm$^3$) and opacity (Op, A/mm).

Particle size and shape were recorded through TEM analysis and AuNPs-dTab was compared with AuNPs-Cit solution. Topological network of gold nanoparticles embedded in dextran matrix has been successfully imaged by AFM in the tapping-mode. This nano-imaging with high spatial resolution and exceptionally low invasiveness is useful to explain particle height. The line profiles are used to determine the height and length for each particle. Moreover, for the crystallinity and thermal analysis of the AuNPs-dTab material, XRD and DSC studies were carried out.

### 3.2.4 Stability of AuNPs-dTabs

The stability of AuNPs-dTabs placed in different conditions was determined by measuring the absorbance at 520 nm on different days. These tablets were kept at 20 °C and 4 °C for different lengths of time such as 1, 7, 14, 21, 28, 90, 180 and 270 days before being tested. These tablets were also stored in open air and air-tight packing to study the effect of humidity on the performance of AuNPs-dTabs. To test the dispersion state of nanoparticles, 200 µL of HPLC water was used to dissolve two AuNPs-dTabs (100 µL, 5.79 mm diameter × 0.313 mm thickness) to obtain homogenous solution and then transferred to a 96-well plate to measure the absorbance of red color. Observation was recorded in triplicate at A520 nm on a UV-vis spectrophotometer plate reader and compared with the AuNPs-dSol solution. To ensure the stability of rest of the tablets/solution over the period of time, only aliquot was taken out for the measurement each time. A comparative stability study was also conducted between AuNPs-dTab and AuNPs-Cit solution under working environmental conditions where both the samples were exposed to ambient temperature and light continuously. Zeta potential and dynamic light scattering studies were also conducted to see the stability of different colloidal solutions such as AuNPs-Cit, AuNPs-dSol and AuNPs-dTab solution.

### 3.2.5 Screening of AuNPs-dTabs under Variable Ionic Strength and pH

Effect of different concentrations of sodium chloride (100-1000 mM) on the aggregation behavior of AuNPs was studied using 6% AuNPs-dTab. Different strength of acidic and alkaline media was also provided to the AuNPs-dTab to check their pH-responsive behavior as well as sensitivity of the tablet material. For this purpose, these tablets were dissolved in a required amount of HPLC grade water using vortex to get a homogenized colloidal dispersion. Subsequently 0.1 M NaCl, 0.1 M HCl and 0.1 M NaOH solution were added in separate vials in

1:1 ratio with AuNPs-dTab solution. Absorbance of the solution at 520 and 650 nm were recorded using UV-vis spectrophotometer. Based on this initial screening, the dextran stabilized AuNPs aggregation assay was optimized at variable pH in the acidic range. Kinetic study of AuNPs-dTab 6% (w/v) was performed with 0.1M NaCl concentration till 3 hours. Finally, a comparative analysis of acid-induced aggregation of AuNPs-dTab solution was conducted in the presence and absence of 100 mM sodium chloride solution.

**Statistical Analysis**

All statistical analysis was performed by Microsoft Excel 2019. Unpaired t-student test was used to identify the statistically significant differences between the results, with $p$-values < 0.05 were interpreted as significant.

### 3.3 Results and Discussion

We prepared the dextran encapsulated gold nanoparticles-based tablets (AuNPs-dTabs) by mixing the colloidal suspension of citrate stabilized AuNP with dextran powder. These tablets were fully characterized by UV-vis, FTIR, TEM, DLS, XRD, DSC, and AFM technique. Their pH-responsive behavior towards neutral, acidic, and basic environment was investigated to show the effect of a range of pH towards stabilization of AuNPs. Moreover, AuNPs-dTab morphology has been explained in terms of its diameter, thickness, opacity, and density.

AuNPs-Cit was achieved by conventional Turkevich protocols using direct method where bottom-up approach is followed to reduce the $Au^{+3}$ ions with a reducing agent as mentioned in Figure 3.2A. In this method, non-toxic citrate ions electrostatically stabilize spherical gold colloids. Different $Au^{+3}$ complexes with citrates exhibit in a solution at a given time [481] In a typical direct procedure, solution of sodium citrate is added to a refluxed and stirred solution of hydrogen tetrachloroaurate solution at a fixed ratio. Here, citrate acts as a surfactant as well as reducing agent and pH of reaction solution gradually changes from acidic to neutral. The color of the gold colloidal suspension depends on the size and shape of AuNPs, which will affect the wavelength of light that is scattered and absorbed; thus, evolution of color with time is a qualitative measure of the rate of particle formation [481]. This approach is considerably reproducible as Kettemann *et al.* have presented monodispersed particles with reproducibility of ± 0.1 nm [481].

In a simplified bioconjugation procedure, AuNPs-Cit was turned into AuNPs-dSol by ligand exchange reaction under mild reaction conditions. The proposed chemical structure of AuNPs embedded in dextran matrix is presented in Figure 3.2B. Dextran being strong ligand as compared to citrate ions, can easily surround gold nanoparticles without any adjustment of solution pH and hence acts as an efficient capping agent as shown in Figure 3.2C. However direct one-pot synthesis of AuNPs-dSol is time consuming and required harsh reaction conditions such as extremely basic pH (12) and prolonged reaction time of 12 h [445]. Similarly, Tang et al. reported hydroxide assisted synthesis of AuNPs-dSol utilizing 1 M sodium hydroxide solution which is strongly basic [482]. It is also well known that, upon variation of pH, the hydrophilic–hydrophobic balance of some polymers can be disturbed by the change in ionization state of the weak acid or base groups. In this context, special attention has been given to explore the pH-responsive behavior of AuNPs-dTab.

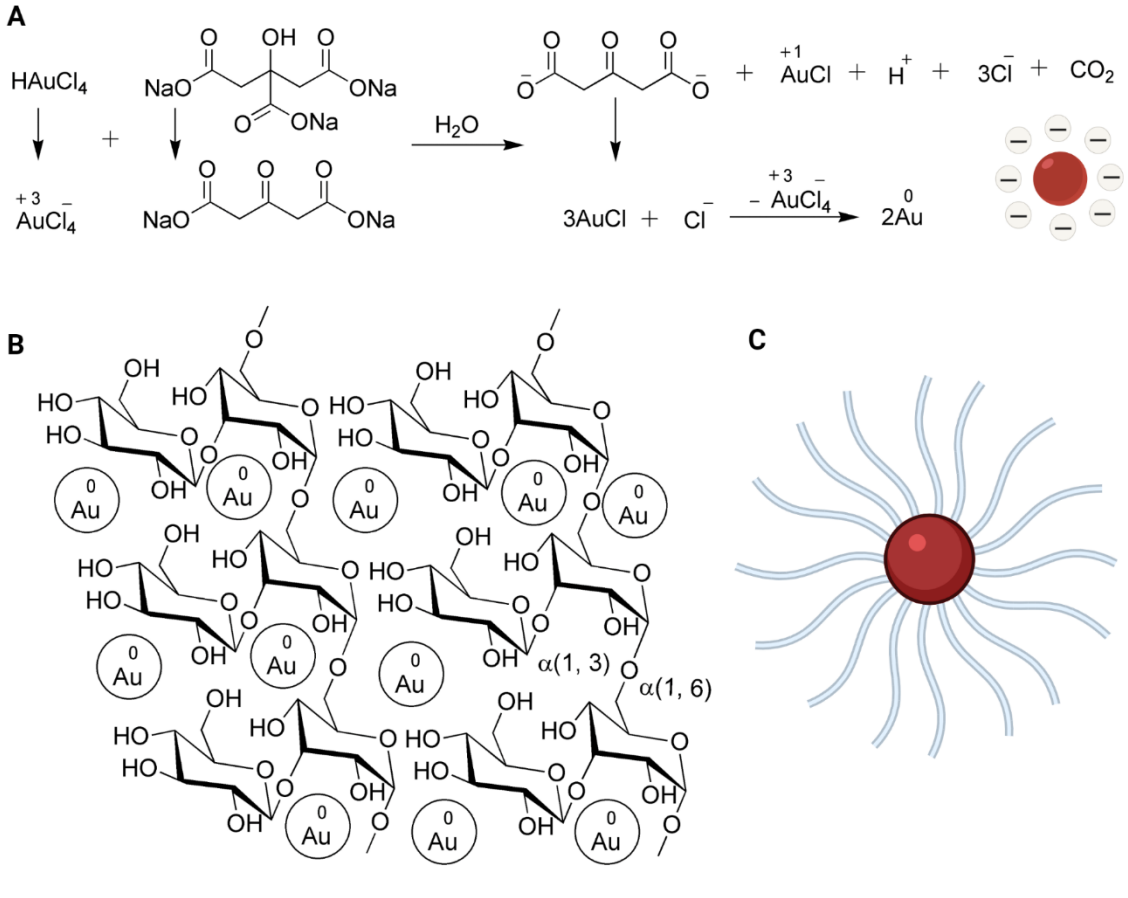


Figure 3.2 Chemical outline of the synthesized gold nanoparticles.

A) Stepwise chemical reactions involved in Turkevich protocols for the synthesis of AuNPs-Cit which are electrostatically stabilized as shown by charged red circle in the right corner; B) Proposed structural representation of AuNPs-dSol where nanoparticles are embedded in the dextran biopolymer; C) Electrosteric stabilization of dextran around nanoparticle in AuNPs-dSol.

### 3.3.1 Optimization of Dextran Concentration

The easiest approach to coat plasmonic AuNPs with dextran is to homogeneously mix the dextran powder with appropriate volume of colloidal citrated capped AuNPs. Over time, dextran being strong stabilizing and capping agent removes the citrate ligands around AuNPs by ligand exchange reaction and surrounds the nanoparticles very tightly. For this purpose, concentration of the polysaccharide solution in weight by volume was used to cast the tablets where 10% (w/v) dextran in AuNPs solution (AuNPs-dSol) was prepared as a stock which was subsequently used in the preparation of dilution series ranging from 1-9%. From this study, it was found that 6% (w/v) AuNPs-dTab was the optimum concentration that have maintained all the nanoparticles in fully dispersed stage as shown in Figure 3.3A. So, this concentration was selected for further investigations as lower amount of dextran in 1-3% (w/v) solution was not sufficient to stabilize AuNPs till 24 h. That is why blue tablets were formed which has shown the aggregated phase of AuNPs and guided us to enhance the stabilizing agent. Whereas AuNPs-dTabs from 4 and 5% solution were dark purple and purple red, respectively, which indicated the need of a little more dextran to completely stabilize the AuNPs as shown in Figure 3.3B. Finally, 6% AuNPs-dSol solution produced red tablets in which AuNPs remained completely dispersed and stable for an extended period of time (see section stability) because in general, polysaccharides such as dextran, chitosan, hyaluronan, and alginate with oxygen rich structures in hydroxyl and ether groups lead to tightly binding to nanoparticles via steric and electrostatic interaction [475]. Results from 7-10% AuNPs-dTabs were similar to 6%; however, higher concentration of dextran was avoided to enable breaking the stabilization under mild conditions.

AuNPs-dTab was characterized using spectroscopic and microscopic techniques as well as DLS measurements and the results were compared with AuNPs-Cit and AuNPs-dSol solution wherever was required. In case of optical analysis under UV-vis, maximum absorption spectra appeared at 520 nm as mentioned in Figure 3.3C, where the inset displays an image of deep red suspensions of AuNPs-Cit and AuNPs-dSol solution along with AuNPs-dTab. The surface plasmon resonance (SPR) band is produced through collective oscillations of free conduction

electrons of AuNPs. Essentially, the extinction spectra of all three nanomaterial samples were the same. The maximum absorption band appeared at a wavelength of 520 nm for all three samples which is a characteristic of 13 nm AuNPs. The concentration of AuNP-dSol colloidal solution was 8.1 nmol $L^{-1}$ by means of Lambert–Beer's law, wherein the value of ε used is 2.7 x $10^8$ $Lmol^{-1}cm^{-1}$ [479]. This result demonstrated that the particles were fully dispersed, and their size was almost in the same range with AuNPs-Cit and AuNPs-dSol without any contamination as a change in size or dispersibility would change the place of the absorption maxima [483]. It is a proven fact that by increasing the particle size of nano gold, the absorption maxima move towards a higher wavelength resulting in a bathochromic (red) shift. Moreover, the peak intensity of all samples was similar showing that encapsulation of gold nanoparticles in the form of tablet did not interfere with the performance of the particles, and these particles were equally effective and stable as in case of solution. Thus, our tablet platform is suitable for all those applications where solution phase of AuNP-dextran is used, while eliminating any complexity in handling and transportation.

Interactions of dextran with AuNPs was identified by measuring the Fourier-Transform Infrared spectroscopy (FTIR) spectra with an Attenuated Total Reflectance (ATR) detector. Figure 3.3D demonstrates the results for the four samples of pure dextran, AuNPs-dTab, AuNPs-dSol, and AuNPs-Cit pure dextran powder were compared with AuNPs-dTab and AuNPs-dSol spectra. The spectrum plotted in green represents the spectrum of dextran, whereas the curve plotted in red, black and yellow represents the spectrum of AuNPs-dTab, AuNPs-dSol solution and AuNPs-Cit solution respectively. Apparently, AuNPs-dTab spectrum is similar to the AuNPs-dSol spectra with a major difference of peak intensity at 3293 $cm^{-1}$ which is due to the symmetric stretching vibration mode of OH group of water [482]. This peak is less widening in a tablet as compared to the similar broad peak in AuNPs-dSol solution. Moreover, the intensity of this peak is comparable to the intensity of the similar peak for powder dextran, so it also confirms the dehydrated state of our tablet due to the evaporation of solvent molecules. The peak at 2875 $cm^{-1}$ is assigned to –CH group stretching vibrations of dextran while it has shifted to 2915 $cm^{-1}$ in AuNPs-dTab. The bands at 1102 $cm^{-1}$, 1061 $cm^{-1}$, and 985 $cm^{-1}$ correspond to the stretching vibrations of C-O bonds, the alcoholic hydroxyl (C-OH), and $\alpha$-glycosidic bonds (C-O-C), in dextran, respectively [482] Similar bands but with less intensity was observed in AuNPs-Tab spectrum, so these changes indicated the strong interactions of dextran with AuNPs. An

absorption band appeared at 1639 $cm^{-1}$ due to the C=O stretching vibration mode present in the spectrum of AuNPs-dSol and AuNPs-Cit, which suggested the involvement of C=O group in the formation of AuNPs [445]. The peak intensity was similar for both liquid samples, while it was less intense in case of solid samples; AuNPs-Tab and dextran powder. This fact might be due to the strong H-bonding of C=O group with water in a solution phase. Also, common pattern was observed near 2160 $cm^{-1}$ and 1977 $cm^{-1}$ for all the samples except pure dextran, which indicated the similar nature of a material. Hence, FTIR measurements showed that dextran molecules were involved in the fabrication of AuNPs-dTab.

In conclusion, AuNPs-dTabs were fabricated with 6% (w/v) solution of AuNPs-dSol for further investigations as this concentration was the optimum amount of dextran that kept the nanoparticles stable for an extended period. It was also clear that particle size remained unchanged when we transformed AuNPs-dSol liquid phase to the solid AuNPs-dTab.

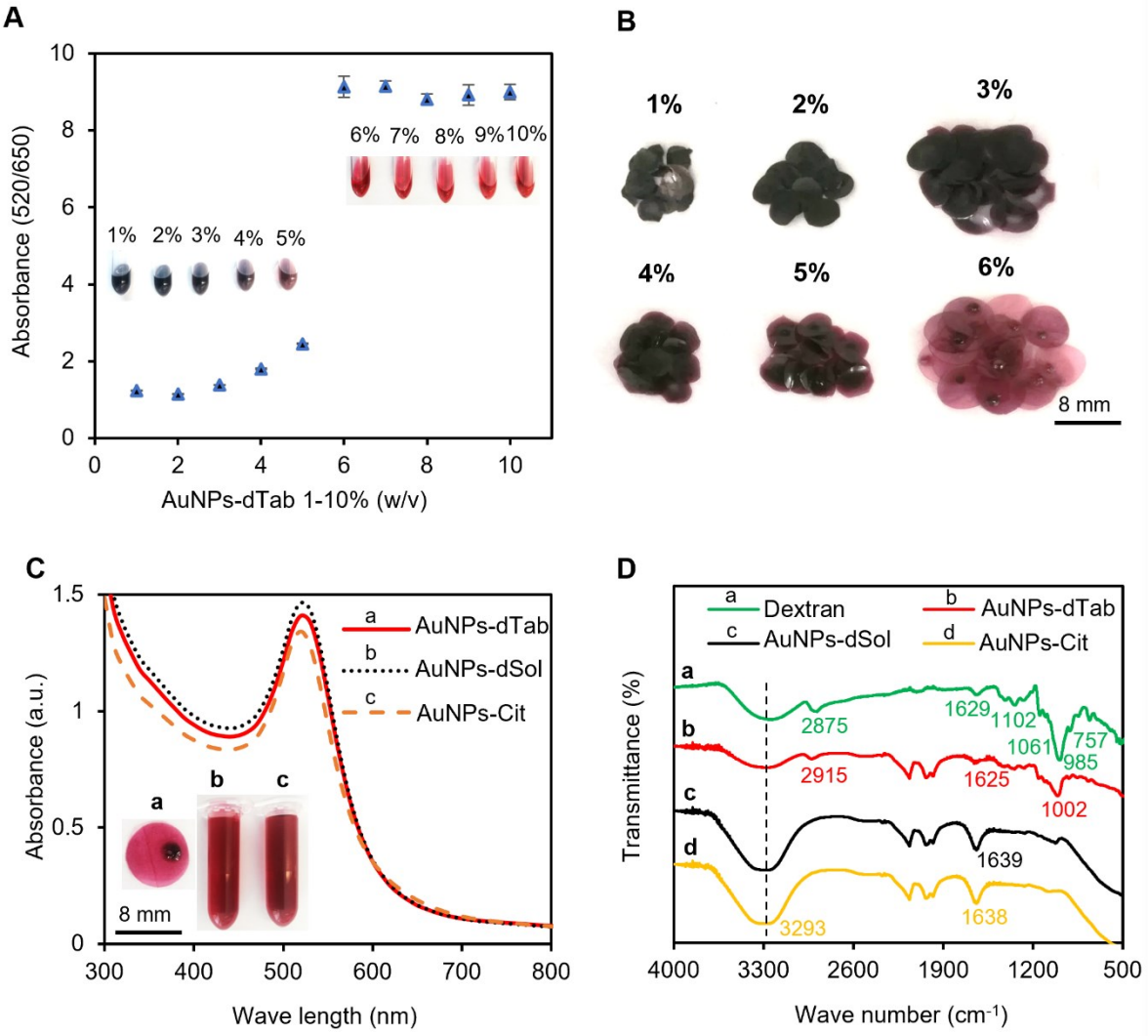


Figure 3.3 A pictorial and spectroscopic characterization of AuNPs-dTab.
A) Screening at A520/650 of different concentrations 1-10% (w/v) of AuNPs-dTab dissolved in 200 µL of water using UV-vis spectrophotometer; B) Different concentration of AuNPs-dTab 1-6% (w/v); C) UV-vis spectra of AuNPs-dTab, AuNPs-dSol, and AuNPs-Cit; D) FTIR spectra of pure dextran, AuNPs-dTab, AuNPs-dSol and AuNPs-Cit.

### 3.3.2 Dextran Encapsulated AuNPs-Tablets (AuNPs-dTabs)

Tablets from AuNPs-dSol solution 6% (w/v) were casted to measure surface characterization and record the stability test. Tablet formation is considered complete only if the tablet leaves the hydrophobic surface of plastic sheet freely and have a constant weight. Tablets were casted by pipetting out a fixed volume of solution instead of drop squeezing method to maintain the amount of captured nanoparticles similar in each tablet. Mostly wine-red round shaped tablets

were produced but quasi-spherical shape was also observed due to difference in drying environment as shown in Figure 3S1. We dispensed out a variety of droplets ranging 100-500 μL of solution and collected small and big tablets depending upon the volume. By this strategy, pre-measured quantities of reagents can be easily stored inside the tablets. Our tablet-based encapsulation approach is beneficial over powdered AuNPs-dSol [475] due to storing of a known amount of substances, which is ready-to-use.

The amount of dextran has a direct influence on the size of nanoparticles as by increasing the dextran quantity, size of the AuNPs decreased with a few exceptions [475,482]. In our study, dextran was used in the ligand exchange reaction to replace the citrate ions and did not involve in the reduction of hydrogen tetrachloroaurate, so the size of the nano gold might remain the same in any concentration of dextran above 5%. The particle size and shape of AuNPs-dTab and AuNPs-Cit were estimated through their TEM images as shown in Figure 3.4A and 3.4B respectively. The average particle size for AuNPs-dTab and AuNPs-Cit was found to be 11.74 ± 1.39 nm and 11.53 ± 1.48 nm, respectively. Gold nanoparticles remained spherical in shape and uniform irrespective of the nature of the capping agent.

DLS measurement was also recorded for AuNPs-dTab, AuNPs-dSol, and AuNPs-Cit solutions in triplicate. Hydrodynamic diameter for AuNPs-Cit solution was found to be 14.38 ± 1.39 nm with polydispersity index (PDI) 37.80% whereas this diameter was changed to much higher value of 127.17 ± 5.81 nm with PDI 24.43% for AuNPs-dSol solution which indicated the successful surface modification of particles from citrate to dextran by ligand exchange method. However, when particles were embedded into dextran matrix as tablet platform, these particles became much bigger as shown by average hydrodynamic diameter of AuNPs-dTab by DLS 304.12 ± 16.43 nm with PDI 17.33% although the particle's diameter was 11.70 nm by TEM analysis which confirmed that particle diameter in a tablet did not change because diameter of particle along with surrounded capping agent is considered in case of DLS measurement whereas TEM analysis record the diameter of nano particle alone. Blue tablets indicated the presence of aggregation between particles which make them bigger as confirmed by their hydrodynamic diameter 686.5 ± 136.13 nm with PDI 17.3% by DLS studies.

Additionally, we have investigated various physical characteristics such as thickness, diameter, weight, density, and opacity of the tablets using 6 and 10% dextran with 2, 4 and 8 nM AuNPs

concentrations to better understand the effects of these parameters on the tablets. The maximum thickness was 0.71 ± 0.10 mm for the 10% dextran tablets with 4 nM AuNPs. The maximum diameter recorded for the tablets was 7.64 ± 0.17 mm for the 6% dextran tablets with 2 nM AuNPs. The maximum weight observed was 4.3 ± 0.3 mg for 10% tablets with 8 nM AuNPs. The maximum density was 0.247 ± 0.0.039 g/cm$^3$ for the 6% dextran tablets with 8 nM AuNPs. The maximum opacity was 4.009 ± 0.107 for the 6% dextran tablets with 8 nM AuNPs. For the detailed procedure and results, refer to Figure 3S2A and 3S2B. Overall, the increase in the concentration of dextran significantly increased the thickness, diameter, and weight of the tablets, while it decreased the opacity and had no significant effect on the density.

In order to analyze the AuNPs with their surrounding environment in the solid state of the tablets, high resolution surface images of AuNPs-dTab were taken using AFM scanning probe microscopy. AuNPs were embedded into dextran matrix as dispersed particles when tablet is red in color and as aggregated particles in case of a blue tablet as shown in Figure 3.4C and 3.4D respectively. Phase trace image in Figure 3.4C shows that the mean height of the AuNPs was 10-30 nm, indicating that the AuNPs are well dispersed throughout the exopolysaccharide substance. The biggest gold particle in the given image has the diameter 90.60 nm. For 2D and 3D height profile of AuNPs-dTab as surface roughness and texture description, see Figure 3S3. These particles have round shape as also supported by the TEM image. It could be explained on the fact that free alcoholic hydroxyl groups of dextran are able to stabilize AuNPs by the interaction between the surface Au atoms of AuNPs and oxygen atoms of dextran. Importantly, high density of hydroxyl functionality in dextran could lead to extensive inter and intramolecular hydrogen bonding, favors the stability and dispersion of AuNPs [484]. Hence, AFM results showed that AuNPs were distributed mainly on the surface of polysaccharide and offer strong interaction in a tablet when particles are dispersed. In case of blue tablet, particles were aggregated and considered as “non-responsive” towards SPR phenomena. Crystallinity and thermal stability of AuNPs-dTab were recorded using XRD and DSC analysis, and results were reported in Figure 3S4.

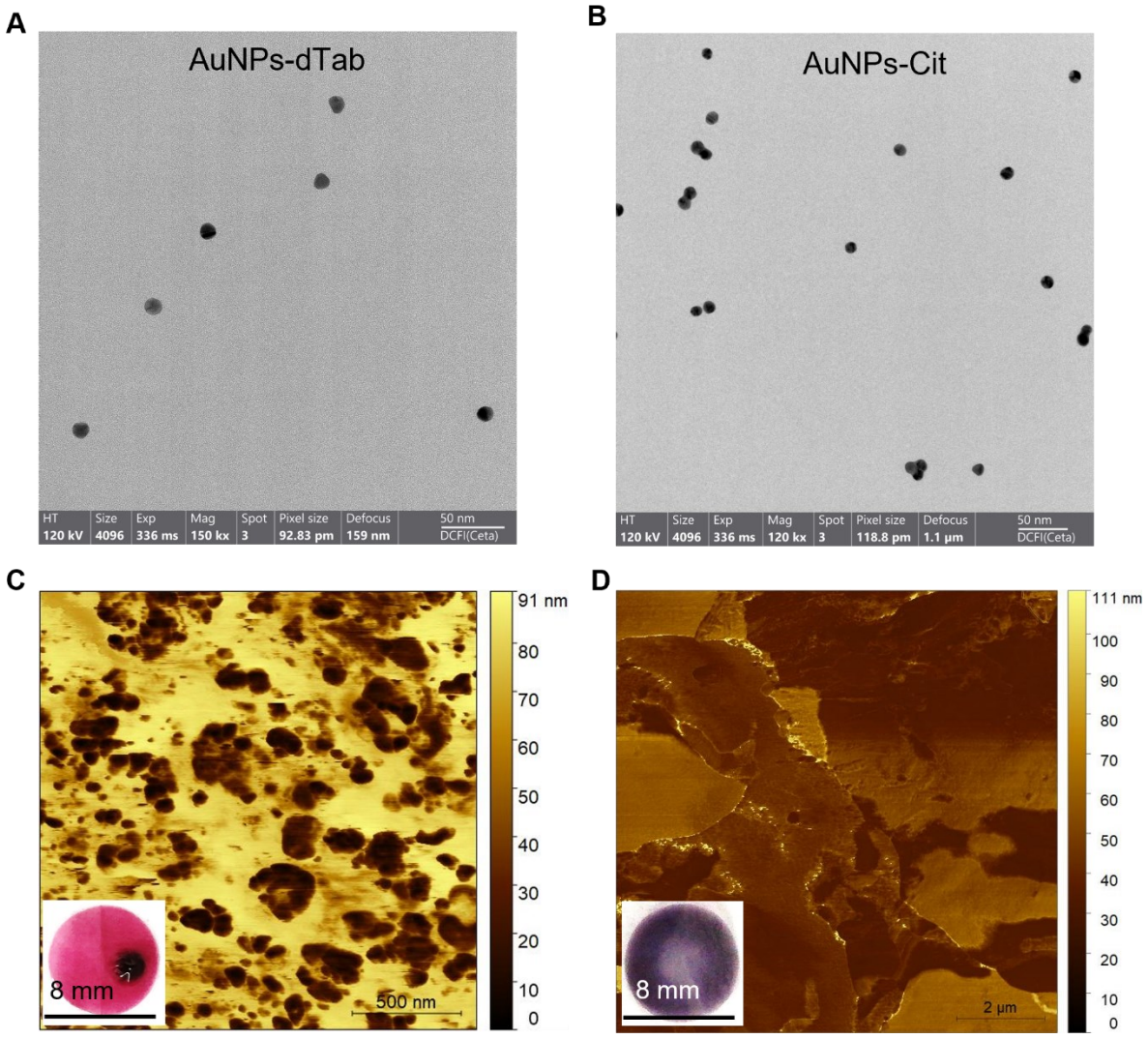


Figure 3.4 Images representing morphological analysis of AuNPs-dTab in terms of particle and tablet material.
A) TEM image of AuNPs-dTab showing the size and spherical shape of particles; B) TEM image of AuNPs-Cit indicating the size and shape of particles; C) The phase trace AFM image of AuNPs-dTab showing the dispersed state of nanoparticles in an "active" red tablet; D) Phase trace of AuNPs-dTab showing the aggregated state of nanoparticles in a "dead" purple tablet.

### 3.3.3 Stability and Storage of AuNPs-dTabs

AuNPs-dTabs were kept at room temperature and in the fridge in an open and air-tight sealed packing for different durations before being tested for their stability. Generally, AuNPs are very stable when surrounded by a stabilizing agent under controlled conditions. Stabilizers are either charged species like citrate ions that offer ionic stabilization or neutral surface bound matrix like dextran that offers steric and electrostatic stabilization. Dextran has hyperbranched structure that

has oxygen-rich functionalities like hydroxyl and ether groups, which lead to a tightly bind with nano gold clusters via electrosteric interactions [485]. Electrostatic particles are kinetically stabilized while steric force generates thermodynamic stabilization [486].

AuNPs-dTabs were dried for 24 h and then stored at different conditions. AuNPs-dSol solution was used as the control to compare and measure the stability of nanoparticles encapsulated in the tablets. UV-vis absorption at 520 nm for the four samples AuNPs-dTab and AuNPs-dSol solution at 20 °C (referred as room temperature or RT) and AuNPs-dTab and AuNPs-dSol solution at 4 °C (referred as fridge or FR) showed almost the similar intensity up to three weeks as depicted in Figure 3S5. However, there was a gradual decrease in stability for the AuNPs-dSol solution placed at room temperature. It might be due to the contamination of solution as many synthesized samples of AuNPs-dSol solution stored in normal conditions are randomly attacked by fungi [475]. To avoid this problem, we have transformed solution phase of AuNPs-dSol into solid tablets. Also, we observed that random temperature fluctuations, humidity and direct light interactions with AuNPs-dSol solution might produce a purplish colour with solid particles at the bottom in vial which indicated the loss of stabilization around gold nanoparticles. This condition sharply reduced absorbance values at 520 nm which indicated the lose of dispersed state of AuNPs. Slightly greater decrease in the stability of the AuNPs-dSol particles as compared to AuNPs-dTab stored at room temperature was shown in Figure 3.5A. AuNPs-dTab remained stable under working conditions of continuous light and humidity exposure as shown in Figure 3.5B while AuNPs-Cit solution could maintain stability only for 3 h followed by a sudden decrease in stability which was approximately 30 and 65% in 4 and 5 h, respectively. Comparatively, tablets in a fridge were a little more stable than those at room temperature. It is also concluded that our fabricated tablets have shown long term stability in room temperature under continuous working environment till to-date.

Stability of particles was also measured by recording zeta potential as particles with values greater than 20 mV or less than -20 mV have enough electrostatic repulsion to remain stable in the solution. However, it is important to note that when particles are surrounded by biopolymers, their electrostatic repulsion due to citrate ions is decreased as shown by high ζ potential values. At this point, primarily, stabilization force is steric in nature. Zeta potential was measured for AuNPs-Cit, AuNPs-dSol, and AuNPs-dTab solutions at pH 5.86, and values for all the samples

were negative. The ζ potential obtained for the AuNPs-Cit particles was -45.4 ± 6.0 mV, while it was -6.6 ± 0.3 mV and -3.5 ± 0.2 mV in the case of AuNPs-dSol and AuNPs-dTab solutions, respectively. These results indicated that citrate capped particles are more negatively charged as compared to dextran capped particles at this pH as supported by the literature [445]. However, surface charge will remain identical in case of AuNPs-dSol solution and AuNPs-dTab. It also confirms that AuNPs-dTab is a good alternative to AuNPs-dSol solution without any change in the stability of particles. Our fabricated tablets are free from contamination and stable for more than a year if carefully stored at a constant temperature and light.

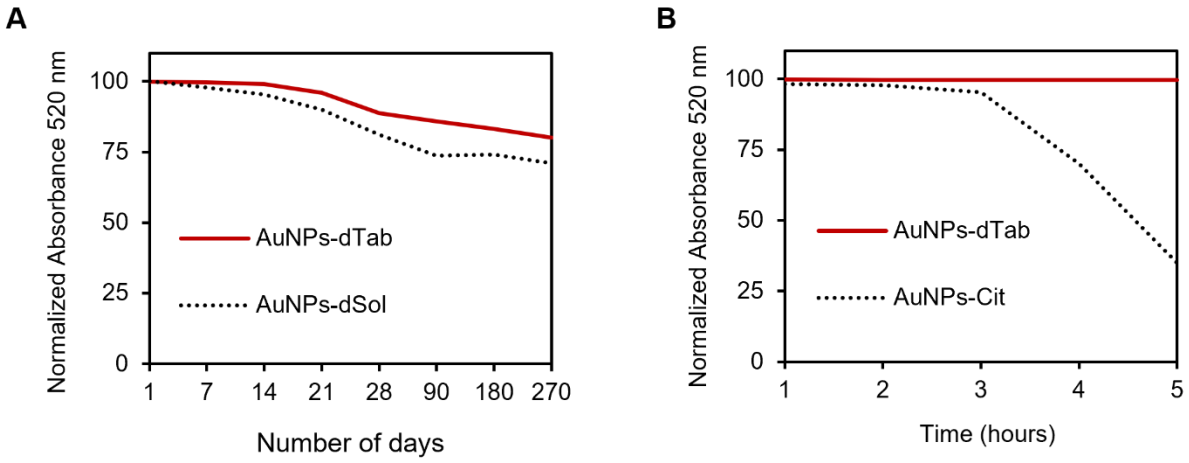


Figure 3.5 A comparative study of stability profile for AuNPs-dTab with AuNPs-dSol and AuNPs-Cit.
A) AuNPs-dTab showing higher stability as compared to AuNPs-dSol at room temperature 20 °C till 9 months.; B) AuNPs-dTab stability remains unaffected till 5 h while AuNPs-Cit solution was stable only for 3 h followed by a sudden decrease in stability which was approximately 30 and 65% in 4 and 5 h, respectively under operating environmental conditions of continuous light exposure and humidity at room temperature.

### 3.3.4 Effect of Salt on AuNPs-dTabs

Besides morphological properties of gold nanoparticles, surface functionality is another important aspect to be studied because functional groups attached to nano gold are directly controlling the SPR phenomena which is a fundamental principle of colorimetric sensors. Primary results indicated that 100 mM NaCl solution has induced aggregation in AuNPs-dTab solution (8.01 nM), but this aggregation is not visible by naked eye and solution remains red as supported by Wang et al [472]. However, UV-vis spectra showed a decrease in A520/650 value

from 9.13 to 5.64 that confirms the aggregated state of particles. To enhance this aggregation, higher concentrations of salt up to 1 M were tested, but there was no significant change in the visual observations as well as by UV-vis machine. The effect of 100 mM salt solution was comparable to 1000 mM with no significant changes in the absorbance ($\lambda_{max}$) values as shown in Figure 3.6A. Increasing the ionic strength of the solution did not induce further destabilization in case of AuNPs-dSol as the polysaccharide surface binding to the AuNPs provides extra stability against higher ionic strength. However, in case of AuNPs-Cit, as the ionic strength of the solution increased by the addition of sodium chloride, the additional ions would protect the electrostatic repulsive interactions, causing van der Waals attractive interactions to dominate and the particles to aggregate [487]. Further, kinetic study of AuNPs-dTab in the presence of 100 mM sodium chloride was explored till 3 h as shown in Figure 3.6B. A slight decrease in A520/650 value was observed in inset of Figure 3.6B which concluded that maximum aggregation due to salt solution has happened at once and there was a negligible increase in aggregation over time.

A control experiment was carried out to check the difference between salt concentration required to destabilize AuNPs-Cit and AuNPs-dSol solution. Considering 8.01 nM AuNPs, the optimum concentration of NaCl was 170 mM that induced a good aggregation and a visible colour change from red to blue. However, in case of AuNPs-dSol solution, stabilization forces were much stronger, and AuNPs remained dispersed/stabilized at super saturated concentration (10 M) of NaCl. Furthermore, upon heating this solution, there was no effect in colour change at all which concluded the thermal stability of particles at high salt concentration. This observation is also supported by literature as Wang and co-workers [472] monitored the stability of the AuNPs-dSol under physiological conditions (0.157 M, NaCl) by UV-vis spectroscopy observing that the colloidal stability is not affected at all upon the addition of a very high salt content. Further, aggregation kinetics of dextran capped gold nanoconjugates in the presence of 100 mM NaCl was studied to find the effect of time on the rate of aggregation. There was a negligible increase in aggregation of particles over 3 h resulting the spontaneous response of salt on AuNPs-dTab to promote aggregation as a quick reaction. A slight decrease in A520/650 value was observed (results are not shown here). This concludes the higher stability of dextran capped gold nanoparticles and their higher resistance even in high ionic strength solutions. This is an important aspect which confirms the outstanding stability of dextran capped AuNPs in

physiological saline solution so particles can be used in analytical applications without further surface modifications [472].

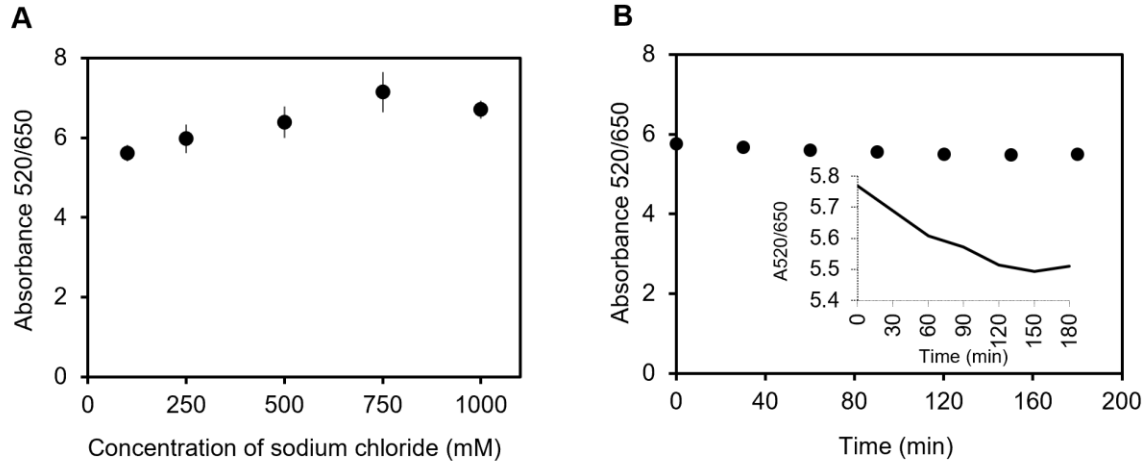


Figure 3.6 Effect of ionic solution on AuNPs-dTab 6% (w/v).
A) Screening of different concentrations of sodium chloride with AuNPs-dTab in 1:1 ratio; B) Kinetic study of AuNPs-dTab with 100 mM NaCl solution till 3 h where inset highlights the change during this period for the 520/650 absorbance ratio value in the range of 5.4 to 5.8. This figure indicated the rate of aggregation in AuNPs-dTab solution with 100 mM NaCl solution was almost comparable to 10 times concentrated salt solution that remains unchanged till 3 h.

### 3.3.5 pH-Responsive Behaviour of AuNPs-dTabs

Undoubtedly, pH responsive sensitivity of ligands attached to the gold surface has a direct influence on the optical characteristics of AuNPs. Lv *et al.* have reported that behaviour of dextran derivatives towards AuNPs is strongly pH dependant [468]. Stabilization around AuNPs is greatly affected by acidic or basic solutions because it can increase the dissolution rate of the nanoparticles into an ionic form that can re-deposit onto existing nanoparticles changing the average diameter and size distribution.

Initially, AuNPs-dTabs 6% (w/v) were tested against 0.1 M hydrochloric acid, 0.1 M sodium hydroxide, and 0.1 M sodium chloride solutions to see the effect of highly acidic (pH = 1.31), highly basic (pH = 13.03), and neutral (pH = 5.53) environment on the stability of nanoparticles. Basic and ionic solutions did not induce any naked eye colour change; however, acidic condition changed the solution from red to purple color which indicated the aggregation as shown in Figure 3.7A. Absorption maxima at 520 and 650 nm were recorded for all solutions using a UV-

vis spectrophotometer. Absorbance values at A520/650 nm were reduced slightly in a basic solution whereas these values were much lower in case of acidic conditions. This is the indication of breaking of steric stabilization due to dextran around AuNPs which lead to the aggregation of particles. Hence, we can conclude that destabilization was prominent at lower pH, whereas higher pH (basic) did not cause a significant change in stabilization due to the presence of the biopolymer. Upon variation of pH, the hydrophilic–hydrophobic balance of a few polymers is disturbed by the change in ionization state of the weak acid or base groups [468]. As the steric stabilization is the major force in this system due to dextran macromolecular configuration which is difficult to break and required harsh conditions as compared to electrostatic stabilization of AuNPs-Cit solution which is highly sensitive to ionic strength. In case of AuNPs-dTab, molecular weight of the macromolecule and surface graft density are dominant factors. In general, thicker polymer layers and higher graft densities lead to more effective steric stabilization [206].

The substantial acid catalyzed deterioration of polysaccharide molecules was investigated using AuNPs-dTab 6% (w/v) with different concentrations of hydrochloric acid ranging 0.0001-12 M. Due to the abundance of hydroxyl groups in dextran, acidic pH strongly influenced the aggregation of AuNPs by protonation of -OH to $OH_2^+$ on dextran chain [473] In the acidic condition, cations are present in the solution, and negatively charged stabilizing species around AuNPs are no longer maintained in the solution, which is why nanoparticles become destabilized and hence aggregated. This aggregation was observed by naked eye at pH 1.31 and lower than this. A rapid colour change happened from red to purple when 0.1 M HCl was added to the nanoparticles solution in 1:1 ratio. However maximum aggregation was recorded at pH 0.26 below which pH did not have any influence on colour. We observed that pH $\leq$ 1 induced prominent aggregation without salt due to protonation of dextran's functional groups. Full spectra scan 300-800 nm of AuNPs-dTab 6% (w/v) with variable hydrochloric acid concentration in 1:1 ratio can be seen in Figure 3S6. However, to improve the sensitivity of the signal, salt solution was used in an equal ratio. As discussed previously, effectiveness of 100 mM NaCl solution was comparable to 1000 mM in this system, so the lower concentration of salt was selected. Black dots in Figure 3.7B represent the destabilization of the particles in the presence of salt. It was clear that the effect of salt was predominant up to pH 1.31, and ionic solution contributes to break the stabilization strongly in the presence of acid above pH 0.53. However

lower than pH 0.53, salt effect became negligible as maximum aggregation has already been happened due to acid aggregation of dextran.

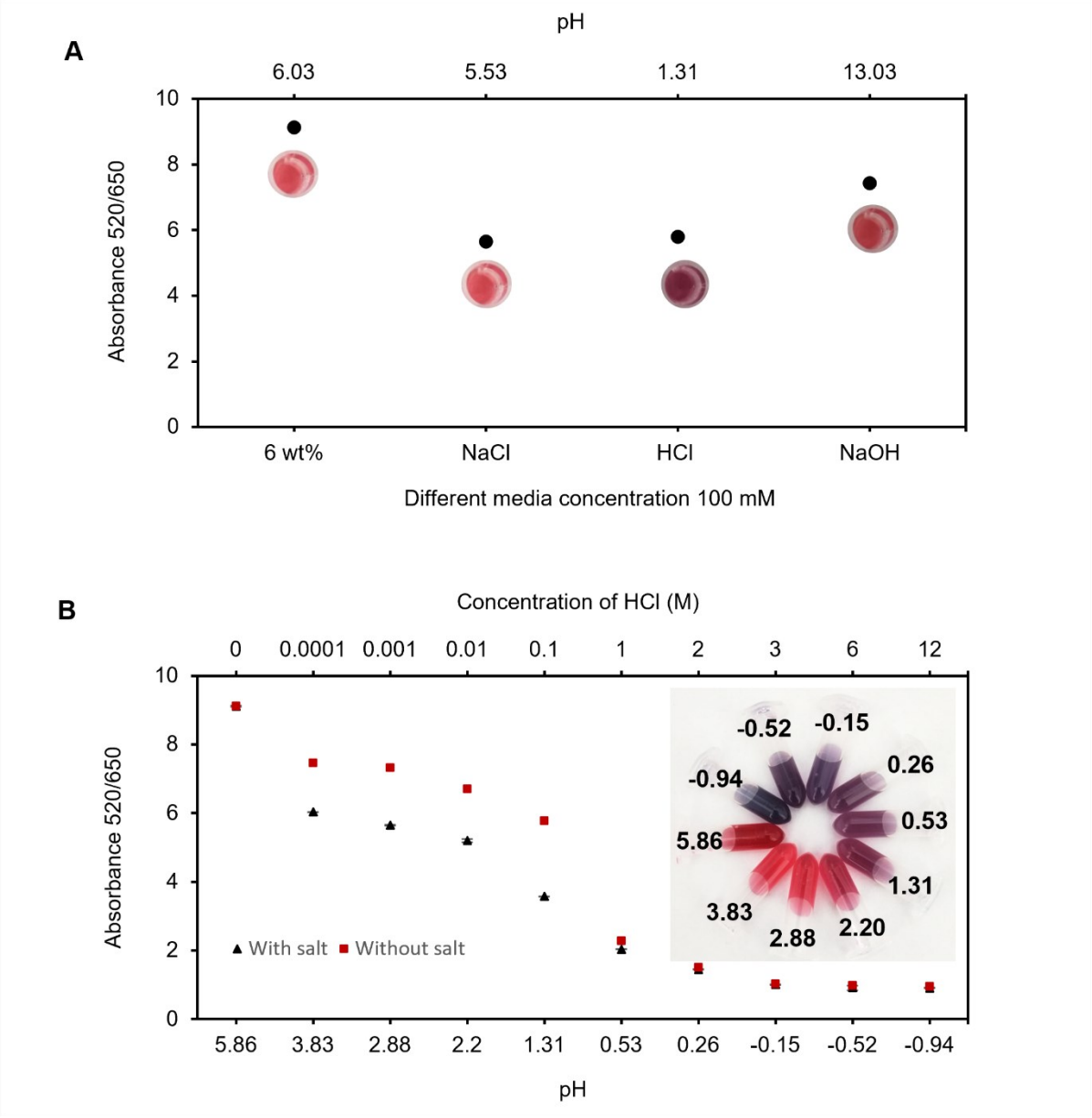


Figure 3.7 pH responsive behavior of AuNPs-dTab 6% (w/v).
A) Initial screening of AuNPs-dTab using 100 mM solution of sodium chloride, hydrochloric acid and sodium hydroxide; B) Concentration dependent acid-promoted aggregation behavior of AuNPs-dTab with and without sodium chloride solution (100 mM) indicates the aggregation profile of AuNPs-dTab suitable for a range of applications where acid sensitive linkages are involved. The experiment data are the mean of the three replications (n = 3) ± SD where some error bars were hidden behind the data points.

It is well known that dextran offers sterically stable non-covalent coating around gold nanoparticles [206,488]. The proposed chemical reaction along with UV-vis spectra of dispersed and aggregated dextran capped gold nanoparticles were shown in Figure 3.8. Reaction media's pH greatly influences the oxygen-hydrogen bond of dextran and leave the oxygen-carbon bond intact. At pH 13.03 the electrostatic repulsive interaction between negatively charged AuNPs and negatively charged –CO⁻ of dextran chain make AuNPs stable resulting red color of colloidal solution as shown in Figure 3.8A. However, at pH 1.31 negatively charged –CO⁻ of dextran change into –COH, which formed strong hydrogen bonds with each other and led to the aggregation and precipitation of AuNPs resulting blue solution as shown in Figure 3.8B.[485] This investigation also confirms the suitability of basic media for the synthesis of AuNPs-dSol. Our AuNPs-dTabs have potential applications in acid sensitive linkages such as hydrolysis of acetal, ketal, ester, amide, imine, hydrazone and oxime [469]. Our research is an open invitation to the researchers who are exploring the properties of nanomaterials under acidic environment such as drug delivery, tumor imaging, and diagnostic applications. For instance, at pH ~4 glutathione detection in human blood serum has been reported [489] whereas 30 nm AuNPs-Cit have been used as an efficient pH sensor to measure the acidity [490].

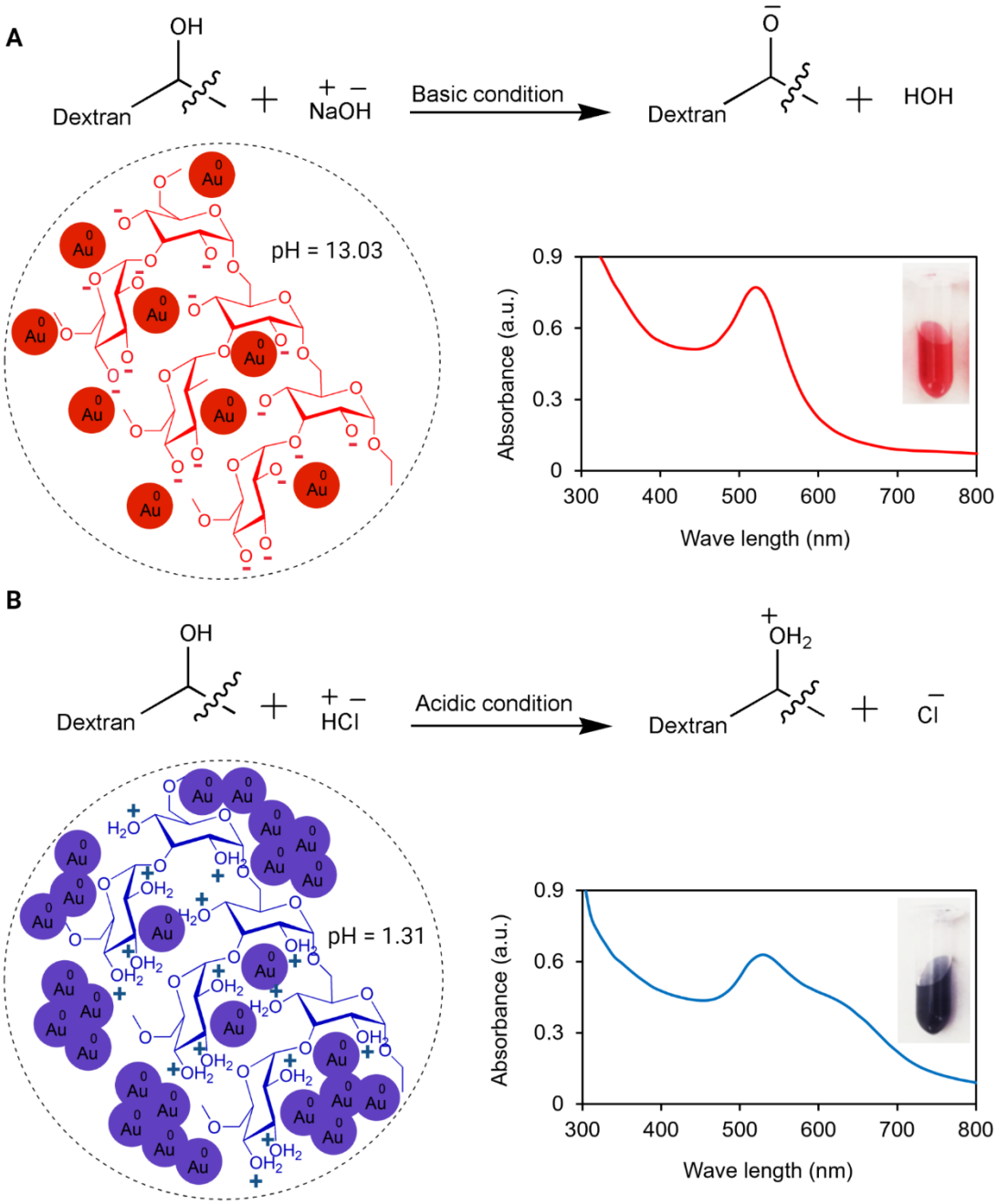


Figure 3.8 Influence of the acidic and basic environment on AuNPs-dTab along with plausible structural drawings.
A) Particles in AuNPs-dTab solution were stable in alkaline condition; B) Spontaneous acid-promoted aggregation of particles in AuNPs-dTab solution indicating the use of AuNPs-dTab as potential smart sensing material.

## 3.4 Conclusions

In this research, we presented the successful formation of dextran encapsulated AuNPs tablets (AuNPs-dTabs) by a simple and straightforward approach utilizing post-modification of AuNPs-Cit with dextran powder. These tablets provide an easy-to-use platform to have pre-measured quantities of reagents for a long duration as AuNPs-dTabs were stable for at least nine months (tablets were still stable at the time of this manuscript preparation) at room temperature and in the fridge as proved by stability test. Once the amount inside the tablet was calibrated, there is no need of weighing and labor extensive optimization of reagents every time. Additionally, these tablets are low-cost approx. 1.22 CAD per 100 tablets of 100 µL and an easy-going substitute to AuNPs-dextran solution (AuNPs-dSol) without compromising on particles stability as proved by various characterization results. We have measured the tablet morphology in terms of thickness, diameter, density and opacity using 6 and 10% dextran with 2, 4 and 8 nM AuNPs-Cit. We also reported the concentration dependant acid promoted aggregation of tablets at variable pH that can be seen by naked eye due to the strong colorimetric response of nanoparticles from red to blue. However, neutral and basic conditions favor the stability of tablets and render the particles well-dispersed in colloidal solution. We believe that the AuNPs-dTabs presented in this study have a great potential to be used in colorimetric detection applications where acid sensitive aggregation is the primary concern. This smart material shows promising potential for future applications in nanosensing and diagnostics. Hence, researchers could pay attention to explore these tablets to prepare ready-to-use kits for the detection of hazardous analytes of interest for environmental monitoring and food assessment. Moreover, further investigation is required to apply encapsulation strategy towards functionalized AuNPs and to understand the variable factors affecting the steric stabilization of polymer around AuNPs in a tablet platform.

# CHAPTER 4 Optimization of the Plasmonic Response of a Tablet for Point-of-use Detection of Environmental Analyte

***This chapter is reproduced from the article published in Microchimica Acta, 191, 183 (2024).***

This chapter explores the tunability of the plasmonic tablet by varying dextran content (0.01–30.01%) and employs a wet-chemical reduction method to synthesize colloidal nanogold solution. Advantages of the tablet format over powder and composites are discussed. The plasmonic probes detected hypochlorite ($OCl^-$) in water across mM to µM ranges, and a method for achieving 20X colloidal concentration without altering particle morphology is demonstrated.

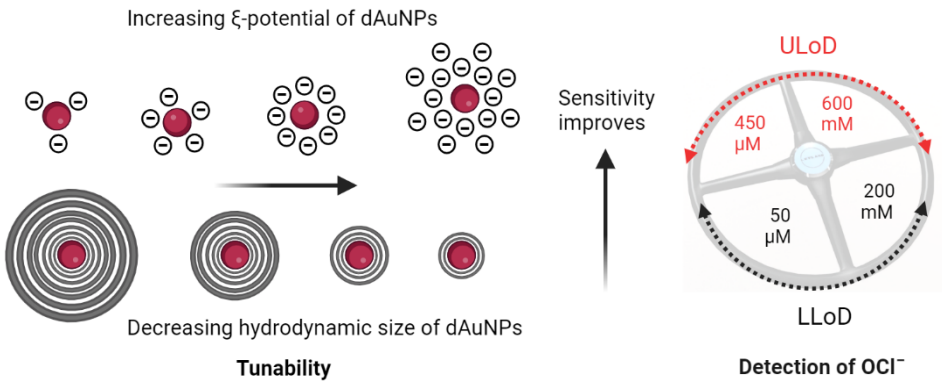

## 4.1 Introduction

Disinfectants used for indoor and outdoor settings are a part of routine life. Among these, sodium hypochlorite (NaOCl) is one of the recommended disinfectants according to the Environmental Protection Agency (EPA) [491]. While implementing sanitization practices, it is highly important to follow quality control measures. The excessive use of hypochlorite ($OCl^-$) as a disinfectant can led to serious health issues, including severe respiratory problems, hypoxemia, pneumonia, bronchitis, pulmonary edema, and acute respiratory distress syndrome as well as skin irritations [492–494]. Reports indicate that the American Association of Poison Control Centers receives approximately 44,000 inquiries per year related to hypochlorite-related injuries [495]. Similarly, liquefaction necrosis or tissue damage [496], atherosclerosis [497], neurodegeneration [498], and periodontal disease [499] may occur due to excessive amounts of $OCl^-$ in swimming pool water. According to the World Health Organization (WHO), the maximum recommended level of free chlorine in public swimming pools and hot tubs is 3-5 ppm [500], which is similar to the drinking water guidelines (5 ppm) [501]. Likewise, varying concentrations of $OCl^-$ are required in other media such as bleach, mouthwash, and root canal irrigant to disinfect and sterilize objects as well as maintain hygiene standards in daily life [502]. Traditional methods to detect and quantify $OCl^-$ in water samples include spectrometry [503], potentiometric [504], and iodometric titration [505], which are prone to limitations such as being expensive, bulky, location-restricted, time-consuming, and requiring multiple reagents and formal training. In contrast, colorimetric sensors offer a promising alternative, providing cost-effective, rapid, and straightforward on-the-spot detection of $OCl^-$ in water [506–508]. A variety of sensing materials, including gold-silver alloy nanoparticles, carbon dots, and tetraphenylethylene-centered tetraaniline, have been used to construct a sensitive recognition probe for the colorimetric detection of $OCl^-$[509–512]. Among different functional materials, gold nanoparticles (AuNPs) are favored for the fabrication of colorimetric sensors due to clear naked-eye readout, ease-of-preparation, and diversified functionalization rendering sensitive and selective affinity towards target analytes [513–517].

The colorimetric response of AuNPs-based sensors is primarily plasmonic, driven by the localized surface plasmon resonance (LSPR) phenomena, resulting in a strong absorption band within the visible range [518,519]. The shift in the LSPR band due to the strong oxidizing ability of $OCl^-$ has been explored by numerous studies [520,521]. For instance, oxidative leaching of

gold nanorods [522] and etching of gold/silver alloy nanoparticles [523] in the presence of $OCl^-$ produced LSPR shift with a visible color change from red to yellow and from yellow to purple, respectively. Zhang *et al.* utilized the oxidizing power of $OCl^-$ to convert alkanethiol-AuNPs into a sulfonate derivative which aggregated AuNPs and demonstrated a limit of detection (LoD) of 1.5-2.0 μM [509]. Similarly, in another study, an anti-aggregation mechanism was employed utilizing citrate-AuNPs and dithiothreitol (DTT) which has the cross-linking capability with $OCl^-$. The DTT caused aggregation of citrate-AuNPs in the absence of $OCl^-$. However, the thiol groups of DTT were readily oxidized in the presence of $OCl^-$ and, consequently, were unable to be chemisorbed on the AuNP surface; hence, colloidal dispersion remained red which was responsible for $OCl^-$ detection with LoD of 2 μM [506]. However, these methodologies often operated either in extremely acidic conditions (pH ~2) or required specifically functionalized AuNPs for selective detection of $OCl^-$ which made the detection procedure laborious, cost-intensive, and time-consuming. Overcoming such challenges calls for the utilization of AuNPs-based $OCl^-$ detection methods capable of operating under mild conditions, without the need for specific labels or additional aggregating agents.

Label-free sensing probes can be achieved by stabilizing AuNPs with functional materials such as polymers. Dextran is frequently used in AuNPs synthesis due to its intrinsic chemical properties as dextran chains are rich with –OH and –COR groups giving steric and electrostatic stability to dextran-coated gold nanoparticles (dAuNPs) [524,525]. The encapsulation of dAuNPs into forms such as dextran tablet (dAuNPs-Tab), composite (dAuNPs-Comp), and powder (dAuNPs-Powder) provides a solid platform that is superior to the liquid phase due to being more thermally stable, user-friendly, easy-to-transport, and resistant to oxidation compared to the liquid phase dAuNPs [526–528]. Previous attempts at obtaining solid or concentrated AuNPs involved evaporation, but this method caused AuNPs aggregation due to the increased salt concentration after water evaporation [34]. Diem *et al.* utilized a gamma Co-60 irradiator along with spray drying, coagulation, or centrifugation to produce powdered dextran-gold nanoparticles [525]. Other attempts to synthesize highly concentrated metallic nanoparticle solutions resulted in large polydisperse particles [39]. Considering this, the anti-solvent precipitation approach appears to be a preferable choice for obtaining concentrated AuNPs. Liu *et al.* employed poly(vinyl alcohol) surrounded AuNPs to achieve 10-times concentrated colloidal solution using isopropyl alcohol to assist the precipitation process [40].

Herein, we develop a tunable plasmonic sensor using dextran-gold nanoparticles (dAuNPs) for the quantitative detection of $OCl^-$ in swimming water as illustrates in Figure 4.1. Various formats of dAuNPs including solution (dAuNPs-Sol), tablet (dAuNPs-Tab), composite (dAuNPs-Comp), and powder (dAuNPs-Powder), were prepared through quick and straightforward procedures and subsequently characterized. We investigate the role of the dextran layer surrounding dAuNPs on zeta potential (ζ-potential) and hydrodynamic size, influencing the sensor's overall performance. Our investigation includes testing a wide range of $OCl^-$ concentrations (µM-mM) with different dAuNPs probes. Interference study shows good selectivity of dAuNPs probe towards $OCl^-$ detection. Furthermore, we evaluated the practical application of the dAuNPs sensor by measuring $OCl^-$ levels in various swimming water samples. In addition to successful $OCl^-$ detection, we achieve a 20-fold (20X) concentrated dAuNPs without the use of a centrifuge machine, without altering particle morphology in concentrated dAuNPs. Our findings are expected to inspire material scientists and nanotechnologists involved in the development of multiplex plasmonic sensors for in-field applications.

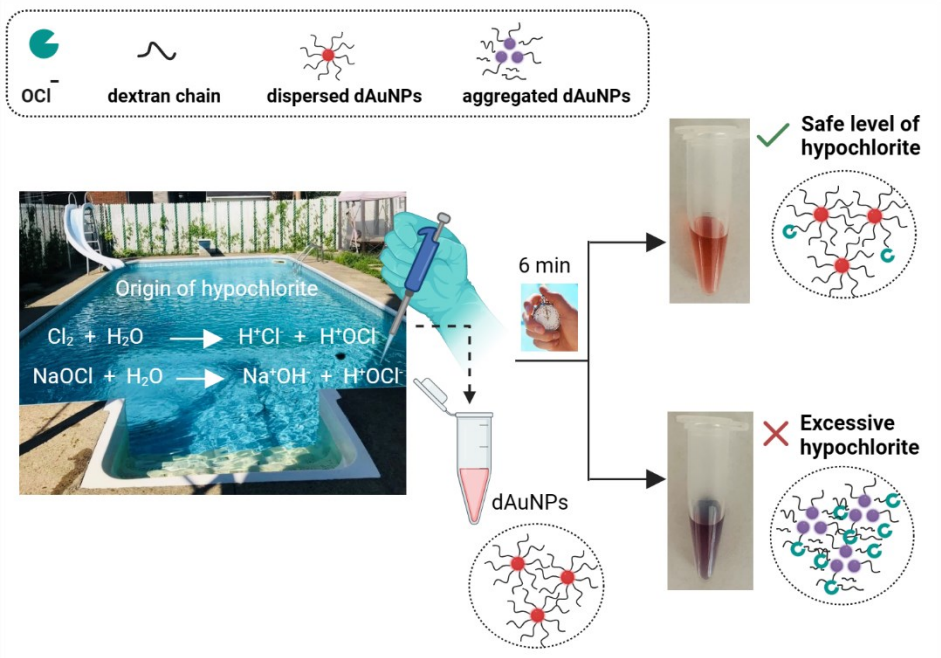


Figure 4.1 Dextran-gold nanoparticles (dAuNPs) as a tunable plasmonic sensor for the detection of hypochlorite ($OCl^-$) in swimming pool water.
Red colloidal dAuNP solution does not show any color change indicating the safe level of $OCl^-$ whereas the purple-blue solution shows an excess amount of $OCl^-$ warning of the $OCl^-$ poisoning in the swimming pool.

## 4.2 Experimental

### 4.2.1 Materials and Reagents

All reagents and chemicals were analytical grade and used as received. Gold (III) chloride solution (30 wt.% in dilute HCl), trisodium citrate dihydrate ($C_6H_9Na_3O_9$), dextran from *Leuconostoc spp.* (av. Mw. ~100 kDa), sodium hydroxide (NaOH), sodium hypochlorite (NaOCl) (4-4.99% w/v), sodium chloride (NaCl), ammonium chloride ($NH_4Cl$), acetone ($C_3H_6O$), reagent alcohol (mixture of methanol (4.0-5.0% v/v), ethanol (88-91%) and isopropyl alcohol (4.5-5.5%), ethanol ($C_2H_6O$) (95%), methanol ($CH_4O$) (≥99.9%), hydrogen peroxide ($H_2O_2$) (30%), sulphuric acid ($H_2SO_4$), nitric acid (65%), hydrochloric acid (37%), magnesium sulfate heptahydrate ($MgSO_4 \cdot 7H_2O$) (≥97%), calcium chloride dihydrate ($CaCl_2 \cdot 2H_2O$), sodium bicarbonate ($NaHCO_3$), copper sulphate pentahydrate ($CuSO_4 \cdot 5H_2O$), aluminium oxide ($Al_2O_3$, insoluble in water) and ferric chloride ($FeCl_3$) were purchased from Sigma-Aldrich, USA. Deionized water from Sigma Aldrich, USA was used to prepare all solutions. A carbon steel tray (Betty Crocker) was purchased to cast tablets from a local store, in Canada.

### 4.2.2 Synthesis of Dextran-Gold Nanoparticles (dAuNPs) by Wet Chemical Reduction Method

To ensure the elimination of trace amounts of organic compounds, all glassware was washed three times with deionized water after being cleaned with fresh aqua regia solution. Dextran-gold nanoparticles solution (dAuNPs-Sol) was synthesized according to the literature procedure with some modifications [41]. The solution of $HAuCl_4$ (1 mM, 25 mL) was magnetically stirred at 90 °C for 5 min followed by the addition of dextran solution (5%, 50 µL) and NaOH solution (1 M, 50 µL). The reaction mixture turned to light pink from a colorless solution that was stirred for 1 hr until stable wine-red dAuNPs were synthesized. The dAuNPs colloidal absorbance was measured at $\lambda_{520}$ nm using a UV-vis spectrophotometer (BioTek, Cytation 5, imaging reader). The molar extinction coefficient (ε) is a measure of how strongly a chemical substance absorbs light at a particular wavelength and was determined according to the formula as $ln\,\varepsilon = 3.32\,ln\,d + 10.8$ where ε is the molar extinction coefficient and d is the diameter of dAuNPs which was calculated as 13 nm by *ImageJ* software [42]. The dAuNPs concentration was calculated by Beer's-Lambert law using an extinction coefficient of $2.4 \times 10^8$ $M^{-1}$ $cm^{-1}$ [42].

### 4.2.3 Preparation of Composite, Tablet, and Powder

A one-pot anti-solvent extraction technique was employed to obtain gold nanocomposite (dAuNPs-Comp) from the dAuNP s-Sol solution. Different solvents including acetone, reagent alcohol, methanol, and ethanol (5 mL) were used separately to extract the nanocomposite from dAuNPs-Sol solution (2000 µL) pre-mixed with different amounts of dextran powder (0.51, 1.01, 2.01, 3.01% w/v). The mixture was shaken vigorously to get a solid mass of dAuNPs-Comp which was separated and dried in air. The dAuNPs-Comp was redissolved in water (100 µL) to obtain 20X concentrated colloidal dAuNP solution as compared to the dAuNPs Sol. The concentrated dAuNP solution was diluted threefold with distilled water to record UV-vis extinction spectra.

From dAuNP solution, tablets (dAuNPs-Tab) were fabricated according to our previously established protocols [38]. Briefly, dAuNPs-Sol was mixed with dextran powder to obtain 2.01% (w/v) colloidal solution which was used to cast tablets by pipetting technique. Tablets were air dried at room temperature for 24 h and stored in airtight glass vial. Powder (dAuNPs-Powder) was prepared through coagulation method as described by Diem *et al.* [35] with a few modifications. In short, 4 volumes of ethanol were mixed with 1 volume of dAuNP solution which was premixed with dextran (2.01%, w/v). The resulting coagulate was filtered, washed with ethanol, and dried in laboratory oven at 60 °C for 2 hr followed by grinding in mortar pestle to obtain homogenous powder. Particle size and surface charge (ζ-potential) of all the synthesized dAuNPs were measured on a Litesizer 500 particle size analyzer using dynamic light scattering (DLS) on a zeta universal dip cell and polystyrene cuvettes in a Malvern Zetasizer Nano ZS equipment (Malvern, England) at 25 °C. The morphology of Au particles was analyzed using transmission electron microscopy (TEM) on an FEI Titan Krios Cryo-STEM system (200 kV).

### 4.2.4 Colorimetric Detection of Hypochlorite ($OCl^-$) using Different dAuNPs Probes

A wide range of $OCl^-$ concentrations was freshly prepared in deionized water using a stock solution of sodium hypochlorite (970 mM of $OCl^-$). Variable concentrations of ammonium chloride ($NH_4Cl$) solution were tested to see the effect of salt in dissociating the hydrodynamic layer of dextran around dAuNPs. The 210 mM of $NH_4Cl$ was used as a signal amplifier. Initially, dAuNPs-Sol was mixed with a variable amount of dextran (0.01 – 30.01%) and subsequently

used for $OCl^-$ detection. For this, 200 µL of given dAuNP solution was mixed with 200 µL of different concentrations of $OCl^-$ followed by the addition of 50 µL of $NH_4Cl$ solution. The extent of aggregation in the dAuNPs probe due to $OCl^-$ was determined by measuring the absorbance ratio (650/520). Furthermore, various plasmonic platforms such as dAuNPs-Tab, dAuNPs-Comp, and dAuNPs-Powder were used for the quantitative detection of $OCl^-$. Of note, a similar gold concentration in all different probes was used throughout the experiments. The intensity-based ratiometric absorbance method was used to draw a calibration curve.

### 4.2.5 Interference Study for Colorimetric Detection of Hypochlorite ($OCl^-$)

Potential interferants in swimming pool water can be anions (e.g., $Cl^-$, $HCO_3^-$, $SO_4^{2-}$), cations (e.g., $Mg^{2+}$, $Ca^{2+}$, $Cu^{2+,}$ $Fe^{3+,}$ $Al^{3+}$), and/or oxidizing agents (e.g., $H_2O_2$). These ions were tested to check the selectivity of the dAuNPs probe towards $OCl^-$ detection. The same experimental procedure was followed as mentioned in section 4.2.4 using dAuNPs-Sol and 0.1 mM $OCl^-$ in the presence of 1 mM anions and $H_2O_2$ as well as 0.1 mM cations separately. The absorbance was recorded after 6 min of incubation using UV–vis spectrophotometer.

### 4.2.6 Application of dAuNPs sensor for $OCl^-$ Detection in Real Swimming Pool Samples

To verify the applicability of our proposed detection method in real samples, different swimming pool samples were collected from different locations in downtown Montreal including Plaza Tower in Atwater street, Le Chatel building on Maisonneuves street, Cedar Plaza in Avenue Cedar, and La Citadelle in Saint Marc street, Canada. Real samples were spiked with different concentrations of $OCl^-$, then treated with dAuNPs-Sol probe in 1:1 (v/v) ratio, and the resultant solution was studied with UV-vis spectroscopy and verified against the calibration curve. These results were recorded in triplicate. Finally, the $OCl^-$ concentration in spiked real samples were also determined by UV-vis spectroscopy method and results were compared with our dAuNPs probe. The UV-vis spectroscopy method is based on its characteristic absorbance in the UV region. The $OCl^-$ exhibits a strong absorption band at 292 nm due to electronic transitions associated with the Cl–O bond. A calibration curve was prepared using standard sodium hypochlorite solutions of known concentrations, and the absorbance at the selected wavelength was recorded. The concentration of unknown samples was then quantified using Beer–Lambert's law, ensuring that measurements were performed within the linear range of detection.

## 4.3 Results and Discussion

### 4.3.1 Synthesis and Characterization of Dextran-Gold nanoparticles (dAuNPs) Probe

A colloidal dispersion of dextran-gold nanoparticles as the solution (dAuNPs-Sol), tablet (dAuNPs-Tab), composite (dAuNPs-Comp), and powder (dAuNPs-Powder) was synthesized and characterized using ultraviolet-visible spectrophotometer (UV-vis), transmission electron microscopy (TEM), and dynamic light scattering (DLS), and ζ-potential measurements. A green approach opted for the synthesis of dAuNPs-Sol in alkaline media utilizing the gold chloric acid solution and dextran as a sole reducing and capping/stabilizing agent. The 1 mM $HAuCl_4$ solution was used to produce dAuNPs-Sol, giving a concentration of ~8.42 nM of dAuNPs according to the Beer-Lambert Law [42]. The dAuNPs were synthesized through multiple reactions in alkaline conditions (pH ~13) *via* disproportionation or dehydration-based growth mechanism [41]. In the disproportionation pathway, NaOH is used as an initiator and/or accelerator to change the standard oxidation-reduction potentials of $Au^{3+}$ and $Au^0$ species to $Au^{3+}$. On the other hand, the dehydration mechanism involves aggregations between dextran and Au complexes following the dehydration reaction to fabricate well-dispersed spherical dAuNPs [41]. Generally, the oxidation of dextran is followed by the reduction of $HAuCl_4$ to produce the aurous salt (AuCl). Alkaline media not only promotes the formation of gold complexes as $[AuCl_{4-x}(OH)_x]^-$ (x = 0-4) but also facilitates these complexes to easily approach abundant alcoholic hydroxyl groups of the dextran chain. The disproportionation reaction of AuCl produces gold atoms, which act as the monomers for the formation of nanoparticles [41]. The color of reaction media changes from colorless ($Au^{3+}$) to bright red followed by reddish pink and eventually burgundy/wine red ($Au^0$) as clear colloidal dispersion. The reaction was kept stirring for 60 min at 90 °C to ensure that there was no appreciable increase in absorption intensity of dAuNPs-Sol which indicated the completion of the reaction. The single narrow symmetrical absorption peak reveals that the colloidal dAuNPs-Sol is primarily made up of spherical shape nanoparticles (i.e., aspect ratio = 1).

Next, the dAuNPs-Sol was mixed with variable amounts of pristine dextran to produce different solid platforms such as tablet, composite, and powder (Figure 4.2). The dAuNPs-Tabs were cast from dAuNPs-Sol pre-mixed with 2% dextran using our previously reported method [38]. The nanogold composite was prepared by anti-solvent precipitation method using dAuNPs-Sol pre-mixed with variable amounts of dextran (0.51, 1.01, 2.01, and 3.01%). It was noted that a higher

amount of dextran facilitated the extraction process, and dAuNPs-Comp was separated efficiently as depicts in the optical image of dAuNPs-Comp with variable dextran amounts (Figure 4S1A). Of note, the dAuNPs solution was condensed by the anti-solvent precipitation method and precipitates were collected without a centrifuge machine as shown in the step-by-step extraction procedure (Figure 4.2D). To obtain the maximum precipitation of dAuNPs, the role of different organic solvents such as acetone, reagent alcohol, methanol, and ethanol was also studied. Extraction of dAuNPs solution with alcohol is successful due to getting dispersed particles, whereas acetone causes aggregation of particles as shown by the purple color solution in Figure 4S1B. Ethanol was selected as anti-solvent in this work due to its environment-friendly or less toxic nature as compared to methanol and reagent alcohol [43]. Of note, after anti-solvent precipitation, the supernatant was completely colorless indicating no traces of dAuNPs. Furthermore, the UV-vis spectra of supernatant showed no absorption peak which confirmed a complete separation of solid dAuNPs from solution dAuNPs. The dAuNPs-Comp was redissolved in 100 μL deionized water to get 20X concentrated dAuNPs colloidal suspension without altering particle morphology. It is noteworthy to mention that 20X is the maximum concentration was achieved through this method. Since the maximum gold salt used in this study was 1 mM, the maximum concentration of dAuNPs obtained after the synthesis was 0.019% (wt%). Compared to other studies in the literature, poly (vinyl alcohol) surrounded gold nanoparticles have been concentrated up to 10X using isopropyl alcohol [40].

It is important to mention that dAuNPs-Comp and dAuNPs-Powder with 0.51% dextran are stable, whereas dAuNPs-Tab with a similar amount of dextran is unstable as shown by the broad absorption peak in Figure 4S1C. The dAuNPs-Tab with 1% dextran is also not fully dispersed and shows a red shift of maximum absorption from 520 to 540 nm. The plasmon bandwidth is decreased from 57 to 45 nm as the dextran concentration is increased from 1.01 to 2.01% (spectra did not show here). Thus, dextran concentration ≥ 2.01% produces stable Au tablets of red color which can be stored at room temperature.

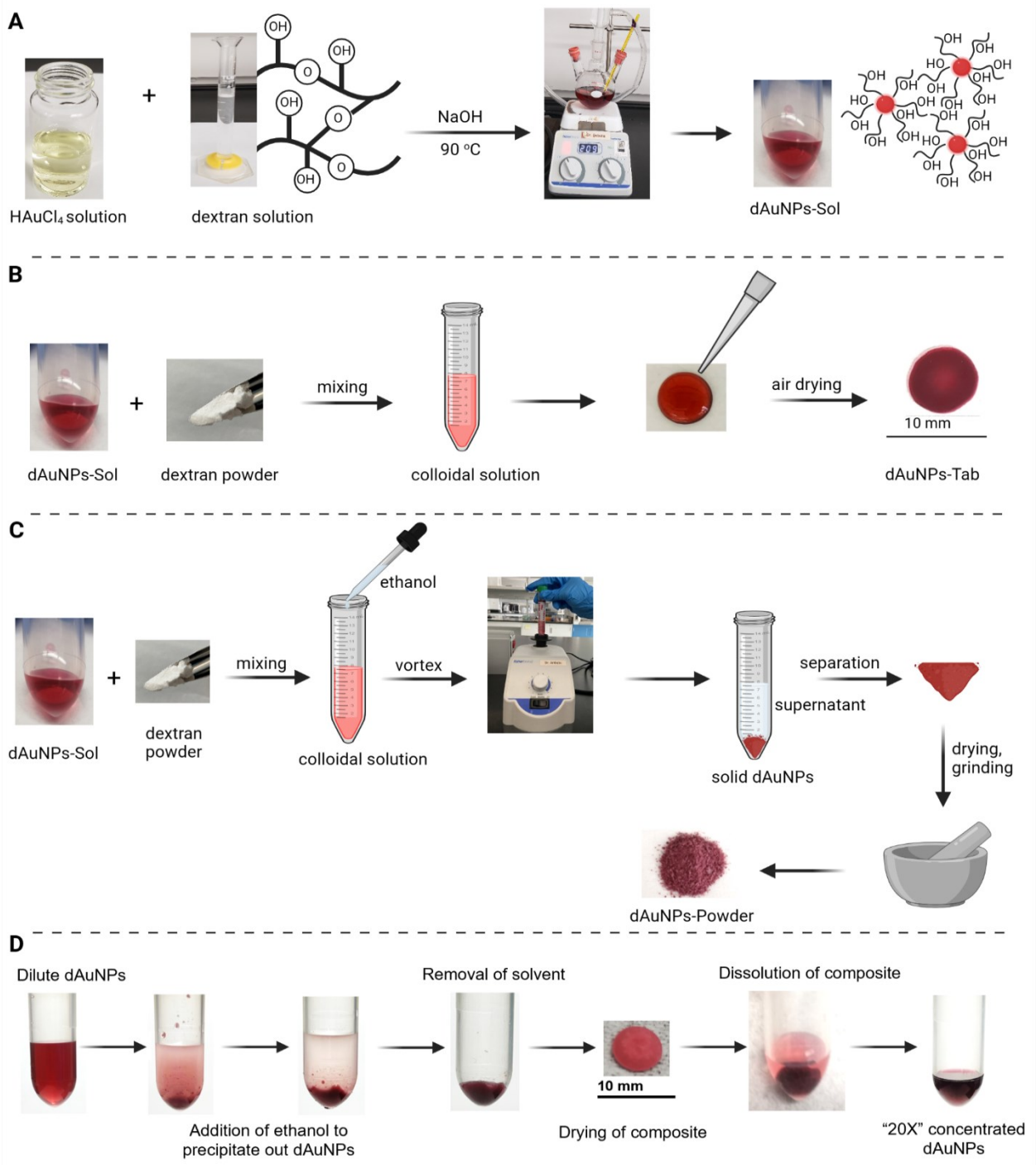


Figure 4.2 Preparation methods for different forms of dAuNPs.
A) The dAuNPs-Sol synthesis by a wet chemical reduction method using $HAuCl_4$ solution and dextran in alkaline media; B) Tablet formation by pipetting out method; C) Powder formation by coagulation method; D) Composite formation by anti-solvent precipitation method followed by obtaining highly concentrated nanogold solution. The addition of ethanol (extracting solvent) in dilute dAuNP solution (2000 µL) were precipitated out all the dAuNPs as a composite which was dried and redissolved in water (100 µL) to get 20X concentrated dAuNPs solution.

Extinction spectra of nanoparticles provide information about particle size, shape, and concentrations of AuNPs [44]. It is well known that size variations in nanoparticles can be easily controlled by altering the ratio of gold salt and reducing agent [41]. Smaller size dAuNPs can be achieved with concentrated dextran solution because dextran being a capping agent stabilizes the nanoparticles quickly and prevents their agglomeration which otherwise leads to bigger size dAuNPs [41]. UV-vis spectra of different formats of dAuNPs showed $\lambda_{max}$ at 520 nm as depicts in Figure 4.3A. It is worth mentioning that the absorption spectra of dAuNPs-Comp could not be recorded when it was 20X concentrated solution. As such, 3 times diluted solution was used for the UV-vis reading (Figure 4.3A (c)).

There is a significant variation in ζ-potential and hydrodynamic size of different dAuNPs dispersions besides all of them appearing at $\lambda_{520}$ nm (Fig 3B). The highest surface charge is observed for dAuNPs-Sol (-40 mV) which is greatly reduced in the case of solid formats such as dAuNPs-Tab (-10 mV), dAuNPs-Comp (-9 mV), and dAuNPs-Powder (-10 mV). As the dextran amount is kept constant in all solid forms, the variation in hydrodynamic size and ζ-potential of dAuNPs is due to the significant difference in their preparation steps and final solid state. This indicates that colloidal dispersion of dAuNPs-Sol is stable, and no agglomeration is observed when stored at 4 °C for at least 6 months which is in accordance with the literature [45]. The surface charge on particles is greatly decreased during the steps taken to get a solid format. Similarly, there is a difference in their hydrodynamic size such as dAuNPs-Sol is the lowest (40.71 nm), then dAuNPs-Comp (138.11 nm) and dAuNPs-Tab (212.99 nm), and finally the highest size is observed for dAuNPs-Powder (486.48 nm). The reason behind the larger hydrodynamic size of solid dAuNPs could be the thicker layer of polymer around dAuNPs as compared to dAuNPs-Sol because an additional amount of dextran powder was added to make particles stable in the dried solid phase [46]. TEM images of all different dAuNPs are provided in Figure 4.3C which show an average diameter of Au particles around 12 nm; much smaller than the hydrodynamic size. It is worth noting that solid dAuNPs are convenient for storage and transportation, but ensuring the preservation of their original morphology becomes crucial upon re-dissolving in aqueous media. The UV-vis spectrum and TEM image of solid dAuNPs (when dissolved in water) reveals a uniform re-suspension without aggregation affirming the retention of the dAuNPs' shape and size.

Overall, both the anti-solvent precipitation method and tablet casting approach are simple and effective in obtaining solid dAuNPs without altering particle morphology. The precipitation method is advantageous in terms of utilizing the minimum amount of polymer to give stable dAuNPs and is capable of achieving 20X concentrated dAuNPs colloidal suspension. However, the surface charge on nanoparticles is greatly reduced during the extraction process as indicates by the low ζ-potential value. On the other side, tablet formation is easy, quick, and encapsulates a pre-measured volume of dAuNPs solution which reduces the user intervention. Similarly, the powder phase of dAuNPs has a higher surface area and dissolves in the aqueous phase quickly. In short, all solid dAuNPs can serve the purpose of detection for many applications (e.g., detection of acid-labile analytes). A brief comparison of the characteristic properties of dAuNPs in different formats is given in Table 4.1.

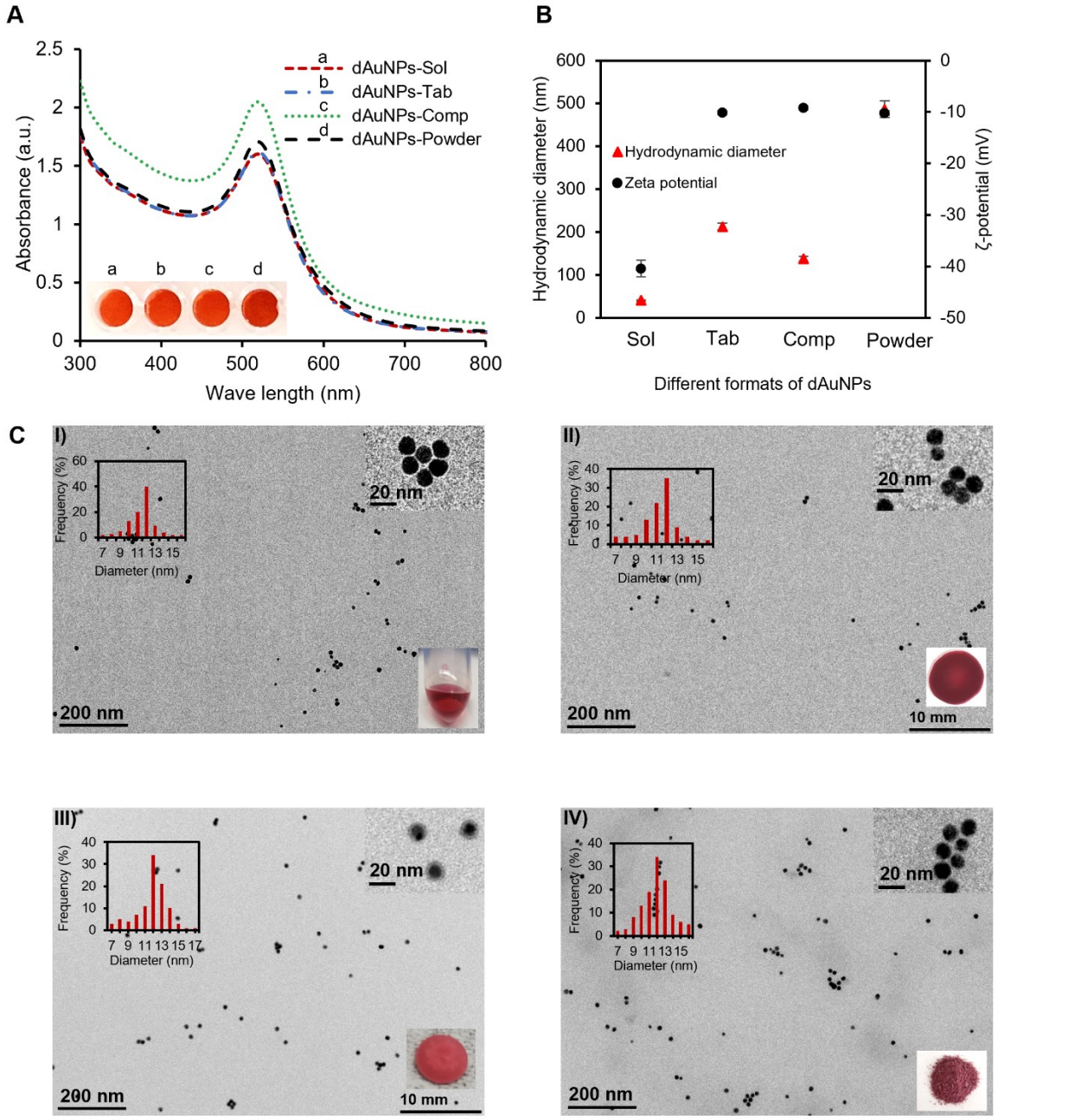


Figure 4.3 Characterization of different formats of dAuNPs.

A) The UV-vis spectra of solution (dAuNPs-Sol), tablet (dAuNPs-Tab), composite (dAuNPs-Comp), and powder (dAuNPs-Powder) have $\lambda_{max}$ at 520 nm showing the similar size of Au particles; B) The ζ-potential and hydrodynamic size of different dAuNPs probes reveal the highest negative surface charge for dAuNPs-Sol and highest hydrodynamic size for dAuNPs-Powder; C) The TEM images showing well-dispersed spherical shape of dAuNPs in all four formats with an average particle size for (I) dAuNPs-Sol as 12.1±0.94 nm, (II) dAuNPs-Tab as 12.3±1.96 nm, (III) dAuNPs-Comp as 12.3±2.2 nm, and (IV) dAuNPs-Powder as 12.6±2.2 nm.

Table 4.1 Comparison of dAuNPs sensor in different format

| # | *Characteristics* | *Solution* | *Tablet* | *Powder* | *Composite* |
|---|---|---|---|---|---|
| 1 | Simplicity of method | ✓✓✓ | ✓✓✓ | ✓ | ✓✓ |
| 2 | Easy to handle | ✓ | ✓✓✓ | ✓ | ✓✓ |
| 3 | Surface area | - | ✓✓ | ✓✓✓ | ✓ |
| 4 | Dissolution speed | ✓✓✓ | ✓✓ | ✓✓✓ | ✓ |
| 5 | Sensitivity | ✓✓✓ | ✓✓ | ✓✓ | ✓ |
| 6 | Wide working range | ✓✓✓ | ✓✓ | ✓ | ✓✓ |
| 7 | Stability | ✓ | ✓✓✓ | ✓✓✓ | ✓✓✓ |

✓✓✓ = most efficient; ✓✓ = efficient; ✓= less efficient

*4.3.1.1 Post-synthetic addition of pristine dextran into dAuNPs-Sol*

So far, we have studied the difference in surface charge and hydrodynamic size of solution and solid dAuNPs where an additional 2% dextran was added to the dAuNPs-Sol to create tablet, powder, and composite. In this case, the variation in surface charge and hydrodynamic size is due to the variation in their operational procedures. Next, to better understand the influence of dextran contents, we post-synthetically mixed variable amounts of dextran up to a total of 30.01% in dAuNPs-Sol. It is noteworthy to mention that different amounts of dextran in dAuNPs-Sol have a negligible effect on the absorption spectrum of dAuNPs and does not alter the peak position. Further, ζ-potential and hydrodynamic size were recorded for different dAuNPs probes pre-mixed with dextran. Dextran contains many neutral OH-groups that build an attraction with the surfaces of dAuNPs providing stability to dAuNPs in colloidal solution. The hydrodynamic size is increased, and ζ-potential values became less negative with increasing dextran concentration (Figure 4.4). Table 4S1 shows ζ-potential and hydrodynamic size values against variable dextran amount in dAuNPs solution. The reduction of negative charge at the surface of dAuNPs is due to extraneous neutral dextran that slowly forms a diffuse layer near the dAuNPs surface partially neutralizing their negative charge. The bigger hydrodynamic size is due to the thickening of the dextran layer around Au particles as shown in Figure 4.4C. Reduction in ζ-potential with the thickening of the hydrodynamic layer can be explained in terms of decreased dynamic mobility due to the strong interactions of the hydrodynamic and electrical

field disturbance around each Au particle [47, 48]. In short, there is a very slow, gradual weakening of the negative ζ-potential of AuNPs upon the addition of dextran, and overall ζ-potential remains negative.

Manipulation of the hydrodynamic layer around nanoparticles helps to configure the plasmonic response of dAuNPs and in turn, fabricates a tunable sensor with a variable working range. Also, the surface charge/ζ-potential of dAuNPs varies because changes in the thickness of the capping ligand influence the colloidal characteristics [49]. Therefore, the hydrodynamic size and surface charge of dAuNPs are critical parameters to determine the dispersity, stability, and sensitivity of dAuNPs [50]. Furthermore, the change in the hydrodynamic size and ζ-potential of dAuNPs can be utilized to identify and predict the susceptibility of aggregate formation of nanoparticles upon interaction with an analyte [51]. Such measurements are important to build plasmonic sensors that show the different working ranges and tunable limit of detection (LoD).

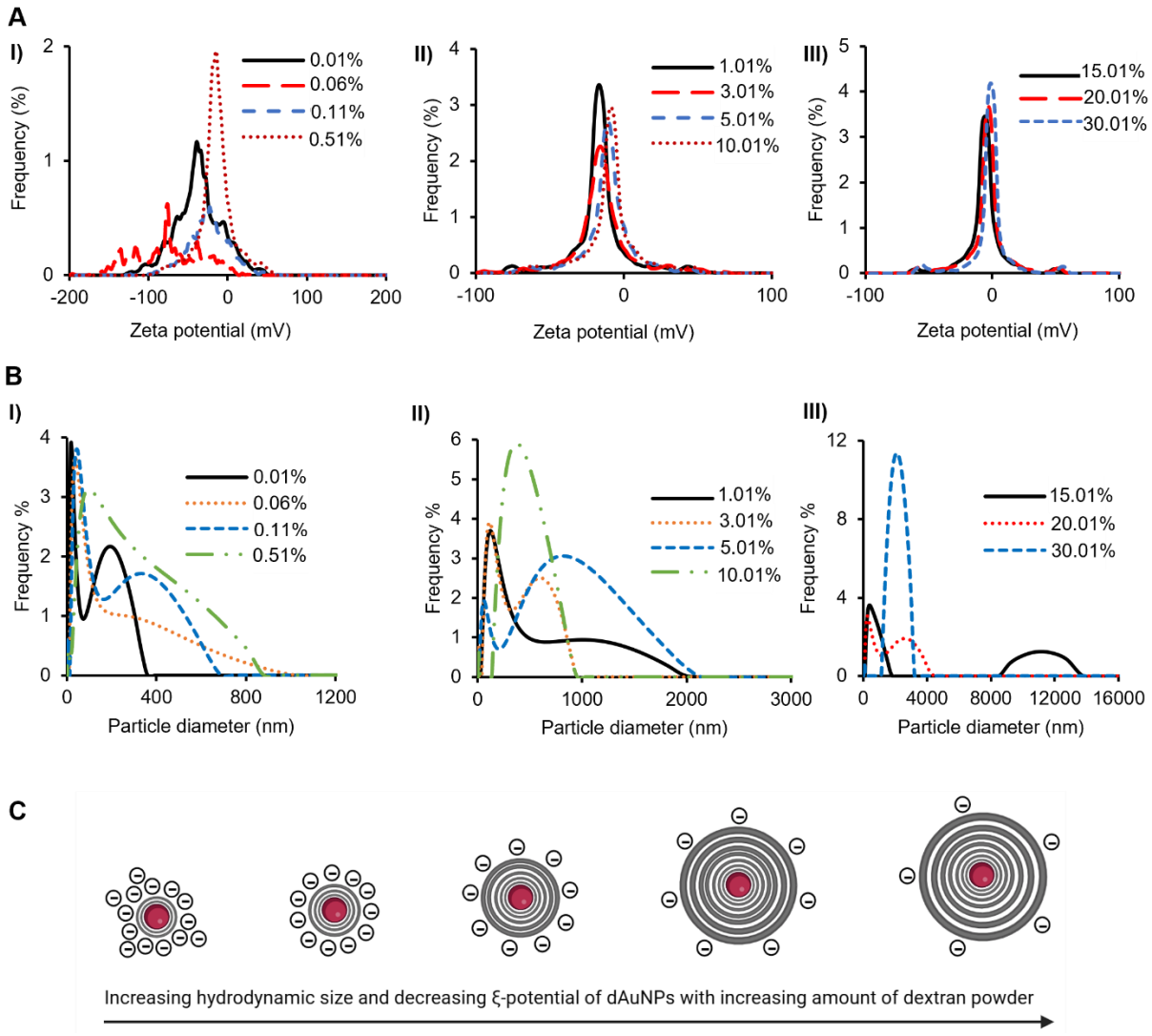


Figure 4.4 The surface charge and hydrodynamic size of dAuNP solution as a function of post-synthetic dextran addition (0.01-30.01%).
A) The ζ-potential plots where I) covers a range of 0.01-0.51%, II) 1.01-10.01%, and III) 15.01-30.01% dextran in nanogold solution; B) The hydrodynamic size plots where I) covers a range of 0.01-0.51%, II) 1.01-10.01%, and III) 15.01-30.01% dextran in nanogold solution; C) An imaginary diagram showing a gradual increase in hydrodynamic size and decrease in surface charge of dAuNPs with increasing dextran content.

### 4.3.2 Sensing Principle of Hypochlorite ($OCl^-$) Detection

Strong oxidizing behavior of $OCl^-$ would generate oxidized dextran derivatives that cannot protect dAuNPs in the same way as unoxidized dextran chains, and through the degree of dAuNPs aggregation, the concentration of $OCl^-$ could be determined. The detection strategy for $OCl^-$ involves the oxidation of dextran polymer generating poly aldehyde [52] and carboxyl

groups with ring opening structure [53] which are not able to sufficiently stabilize dAuNPs dispersion by electrostatic repulsion, and hence aggregation of Au particles is promoted. Oxidized dextran was supposed to depolymerize in the presence of $OCl^-$ resulting in small fragments of oxidized dextran around dAuNPs which greatly reduced steric stabilization. Consequently, the dextran layer around dAuNPs is assumed to become thinner which cannot shield Au particles effectively resulting in susceptibility to external stimuli as illustrated in Figure 4.5A. At this point, the presence of an electrolyte such as NaCl or $NH_4Cl$ further enhances the aggregation by depressing electric double layer around dAuNPs [54, 55]. This phenomenon is evidenced by reporting $\lambda_{max}$ at 650 nm due to aggregated dAuNPs, a lower ζ-potential value (-13 mV), higher hydrodynamic size (875 nm), and presence of dAuNPs aggregates in TEM image due to the presence of $OCl^-$ and $NH_4Cl$ (Figure 4.5B).

Of note, the role of $H_2O_2$ as an intrusive entity in $OCl^-$ sensing was explored and no change in dAuNPs probe was observed even when $H_2O_2$ was 10X higher in concentration than $OCl^-$. The $OCl^-$ has a greater oxidation effect compared to $H_2O_2$. This observation is supported by the fact that NaClO/NaBr had a stronger ability to oxidize dextran and produced more carboxyl groups than $H_2O_2$ at the same concentration [53]. The oxidation degree of $H_2O_2$ is affected by reaction time, temperature and pH. Hence, dAuNPs probe is aggregated in the presence of $OCl^-$ exclusively.

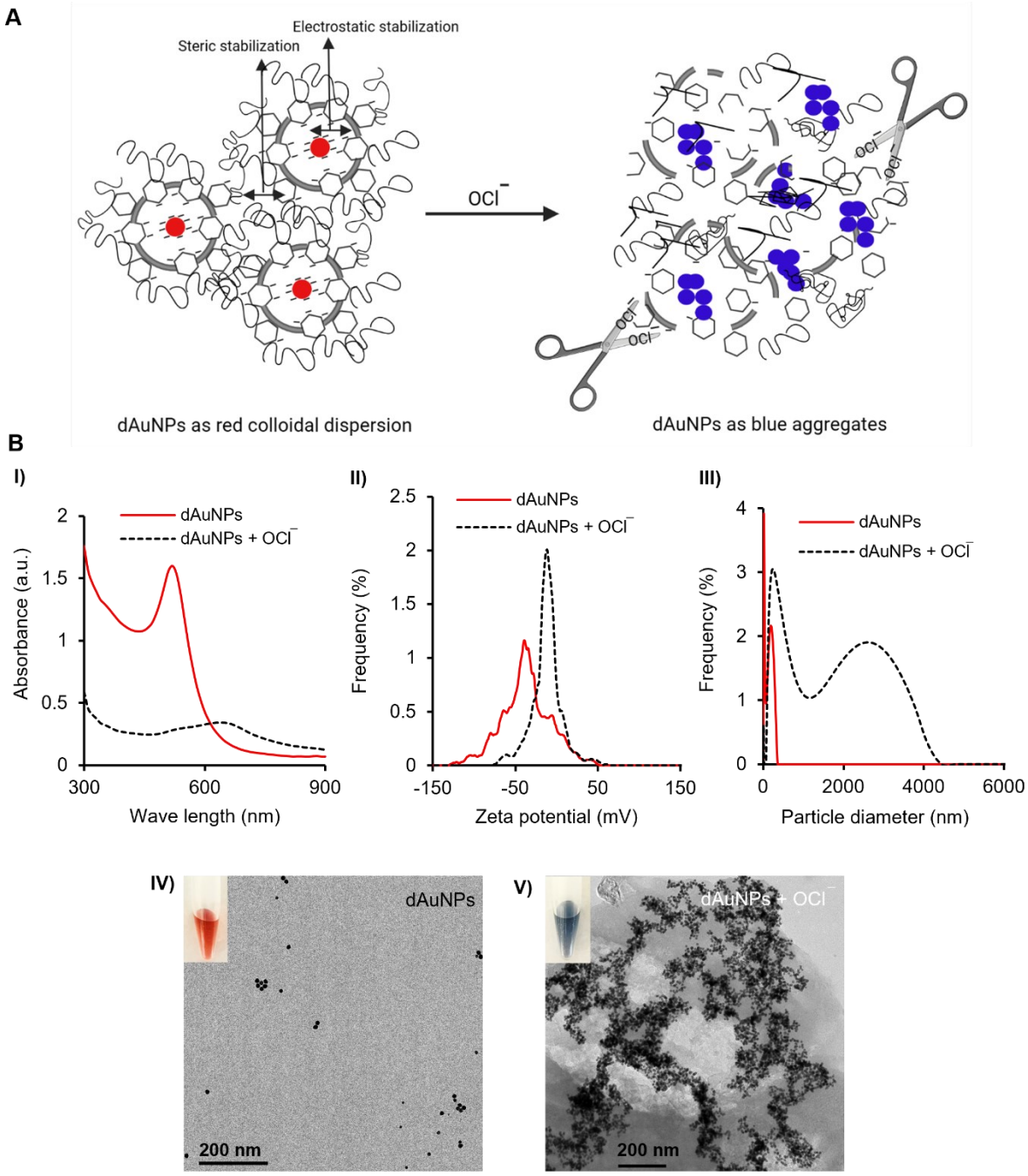


Figure 4.5 The dAuNPs probe in the absence and presence of $OCl^-$.
A) An illustration showing the role of $OCl^-$ in breaking dextran shielding around dAuNPs resulting in blue aggregates of dAuNPs. B) Spectroscopic plots and microscopic images of dAuNPs probe with and without $OCl^-$ where I) is absorbance spectra, II) zeta potential graph, III) a plot of hydrodynamic size, and IV) TEM images.

### 4.3.3 Reaction Kinetics for Quantitative Detection of Hypochlorite ($OCl^-$)

The dAuNPs plasmonic probe was used without modifications for quantitative detection of $OCl^-$ in water. Thes swimming pool water has a very narrow pH range (7.0 – 7.6) due to the health concerns of the swimmers, hence we did not explore the possible effect of pH on $OCl^-$ detection. The oxidizing ability of $OCl^-$ destabilizes the dAuNPs causing their aggregation which is depicted by red to blue color change. The characteristic absorption of the $OCl^-$ solution occurs at $\lambda_{292}$, dispersed dAuNPs at $\lambda_{520}$, and aggregated dAuNPs at $\lambda_{650}$. The ratio of 650/520 is used to measure the extent of aggregation in the presence of $OCl^-$. The dAuNPs-Sol can tolerate >100 mM sodium chloride (NaCl) concentration while citrate-capped AuNPs aggregates quickly at 20 mM NaCl [45] indicating the suitability of the dAuNPs probe without intricate surface modifications for $OCl^-$ detection. The effect of different concentrations of ammonium chloride ($NH_4Cl$) and NaCl is explored to dissociate the hydrodynamic layer around dAuNPs. Rather than selecting a gradient concentration scale, our choice of different concentrations of salt is based on experimental results. Aggregation in dAuNPs-Sol is not noticeable up to 210 mM of NaCl and $NH_4Cl$ whereas a minor change in color intensity is observed at 250 mM as shown in Figure 4.6A. Further, an effective aggregation is observed with $NH_4Cl$ as compared to NaCl due to the strongest dehydration behavior of $NH_4Cl$ which reduces the hydrodynamic layer of polyanions (dextran) around dAuNPs and improvs the sensitivity of the dAuNPs sensor [56, 57]. Hence, 210 mM of $NH_4Cl$ salt was used in all experiments as a signal amplifier. Aggregation of nanoparticles is a kinetic process and detection response in colorimetric assays varies with time [58]. Herein, a kinetic study was conducted in the presence and absence of salts using 200 µM $OCl^-$. The rate of aggregation is negligible without salt and took a longer time (12 min) to reach maximum whereas NaCl and $NH_4Cl$ required 9 and 6 min respectively to show maximum aggregation, as displays in Figure 4.6B. Hence, absorbance readings were recorded after 6 min in our proposed $OCl^-$ assay. Of note, there is a slight change in the pH of the dAuNP solution when $NH_4Cl$ (pH 6.2) or NaCl (pH 6.8) is used in the proposed $OCl^-$ assay. Therefore, the difference in the reaction kinetics of both salts is purely due to the presence of $OCl^-$. It is important to mention that aggregation took place without $OCl^-$ when dAuNPs-Sol was incubation with 210 mM of $NH_4Cl$ for 30 min.

So far, we observe that $NH_4Cl$ presence greatly influences the colorimetric signal resulting in improving the limit of detection (LoD). Salt acts as a signal amplifier by facilitating the

aggregation of nanoparticles as reported in the literature [59]. An increased amount of salt improves LoD due to the generation of a noticeable signal with a lower concentration of $OCl^-$. For example, 0, 200, and 210 mM of $NH_4Cl$ with dAuNPs-Sol sensor give 0.6, 0.1, and 0.05 mM LoD for $OCl^-$ detection. Further, we obtain a sharp slope with 210 mM $NH_4Cl$ as compared to the flat slope with 0 mM $NH_4Cl$ as displays in Figure 4S2. The higher slope of a calibration curve represents the higher sensitivity of a sensor [60]. These observations confirm the signal amplification role of $NH_4Cl$ in the colorimetric assay of $OCl^-$ detection.

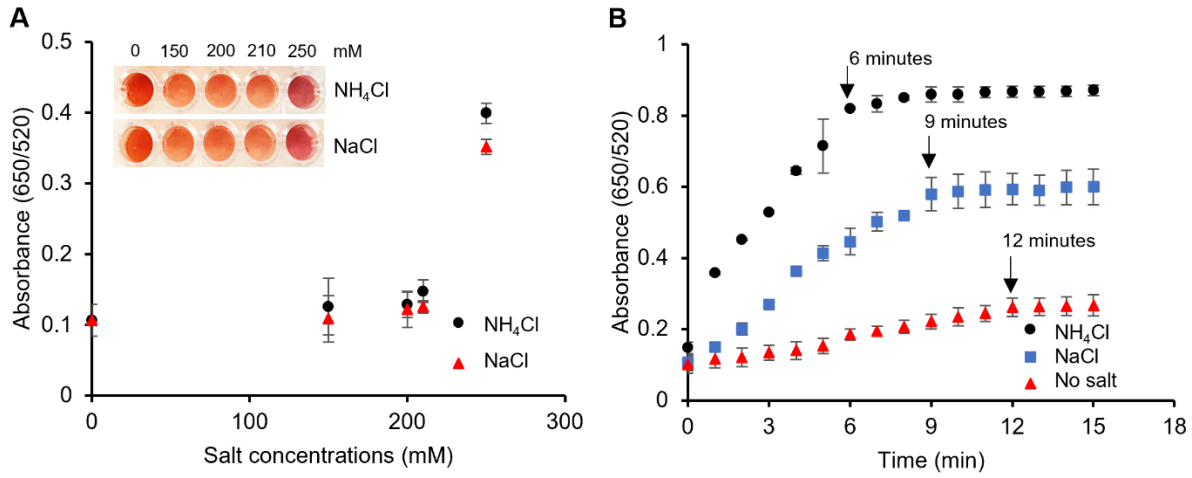


Figure 4.6 The effect of salts in $OCl^-$ detection assay and their corresponding kinetic study using dAuNPs-Sol.
A) Ammonium chloride ($NH_4Cl$) is more efficient than sodium chloride (NaCl) to aggregate dAuNPs-Sol as indicated by its higher absorbance ratio (650/520). Since 250 mM salts produces a visible color change in dAuNPs, 210 mM $NH_4Cl$ is selected as a signal amplifier; B) The kinetic studies using 210 mM $NH_4Cl$, 210 mM NaCl, and no salt in the presence of 200 µM $OCl^-$ solution. The use of $NH_4Cl$ greatly reduces the detection time from 12 to 6 min.

### 4.3.4 Colorimetric Detection of Hypochlorite ($OCl^-$) using Plasmonic dAuNPs Sensors

A wide concentration range of $OCl^-$ (µM to mM) was tested quantitatively using solution and solid formats of dAuNPs sensors followed by calculating their lower and upper limit of detection. The lower limit of detection (LLoD) is determined as the minimum amount of analyte that the sensor can detect and can be calculated using the formula: 3 times the standard deviation (SD) of the blank plus the mean value of the blank signal. The upper limit of detection (ULoD) represents the highest concentration of analyte that can be analyzed using the proposed approach and can be calculated using the formula: 3 times the SD of the highest signal minus the mean value of the highest signal [23]. First, different amounts of pristine dextran (up to 30.01%) were

added into dAuNPs-Sol to prepare nanogold probes having variable dextran shielding. These plasmonic probes were tested against different concentrations of $OCl^-$ to see the influence of dextran thickness in tuning the nanogold probe toward the detection limit. As expected, we observe a great variation in the working range of different dAuNPs probes (Figure 4.7). For example, the most sensitive detection is achieved with a nanogold probe having 0.01% dextran showing 0.06 mM LLoD and 0.45 mM ULoD. An increased dextran amount from 0.06 to 15.01% dramatically changes the LLoD and ULoD as shown in Figure 4.7B. The images showing a variation in color change of nanogold probe against a broad range of $OCl^-$ concentrations are provided in Figure 4S3. Higher amounts of dextran produce a thicker layer around dAuNPs which indicates a strong shielding of nanoparticles. Hence, a high concentration of $OCl^-$ is required to break this shielding resulting in higher LoD.

Of note, 0.01% dextran is the minimum amount of the ligand that produces 13 nm AuNPs [41] while < 0.01% dextran produces bigger AuNPs (~40 nm) which is not useful for our study. Similarly, we achieve a gradual colorimetric response till 15.01% dextran addition whereas 20.01 and 30.01% dextran in dAuNPs-Sol produce a signal with ≥500 mM $OCl^-$ as shown in Figure 4S4. In conclusion, our proposed detection system is highly versatile because the LoD and the $OCl^-$ concentration ranges could be modified by simply changing the concentration of the dextran in the nanogold plasmonic probe. A tunable plasmonic sensor is important in the detection area because of changes in the LoD as per requirements.

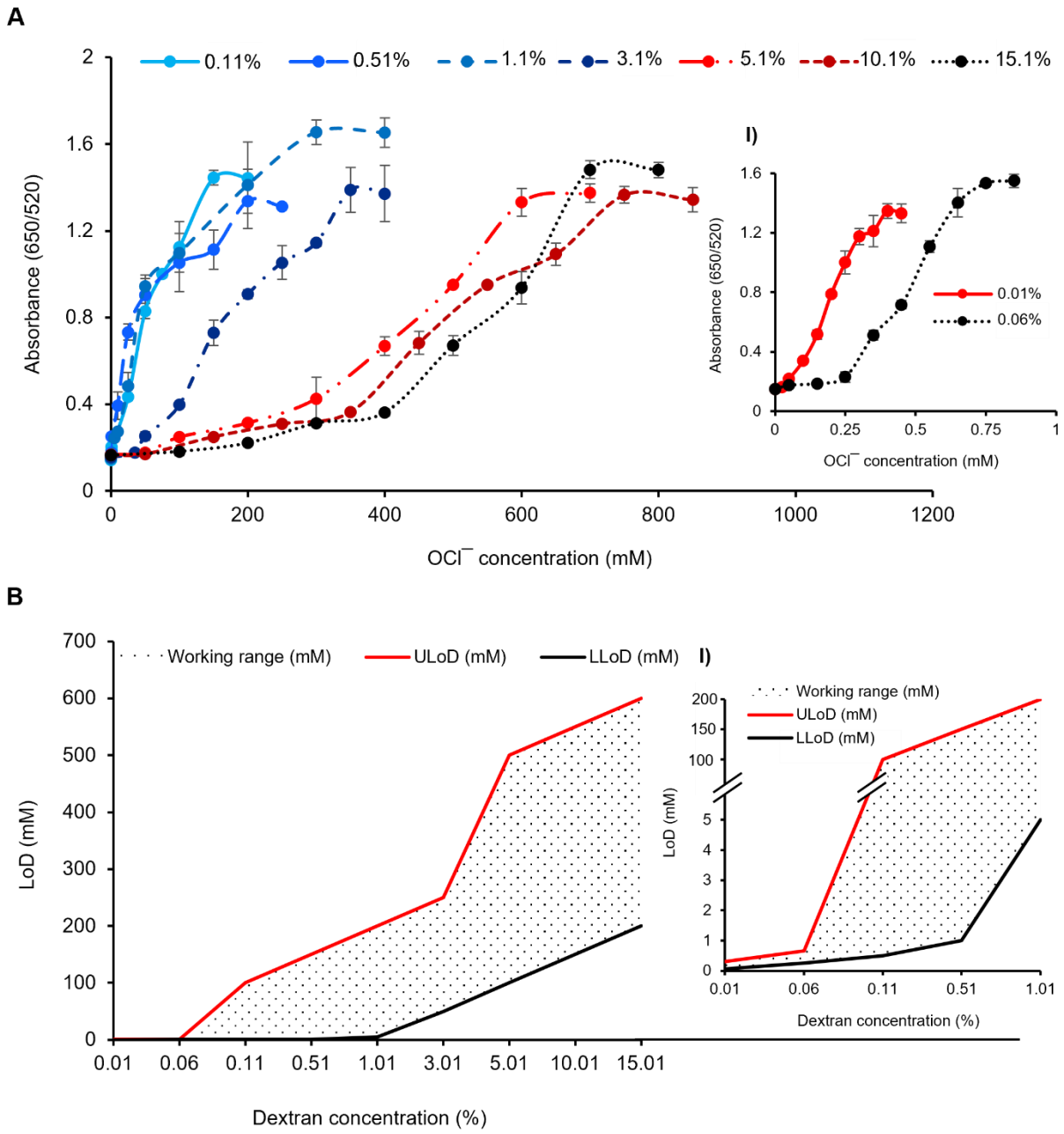


Figure 4.7 Hypochlorite ($OCl^-$) detection in water using solution phase dAuNPs probe having variable dextran content (0.01-15.01%).
A) Calibration curves (0.11-15.01%) where I) indicates the most sensitive detection due to less dextran contents (0.01 and 0.06%) in nanogold solution; B) A plot showing ULoD and LLoD with different dAuNP solutions. The I) indicates 0.06 mM LLoD with 0.01% dextran which increases with higher dextran contents. Also, the wider working range is observed with higher dextran contents.

Furthermore, solid dAuNPs probes including tablet, composite, and powder were tested for $OCl^-$ detection because nanoparticles in solid format are easy to transport and user-friendly promoting the formation of portable sensors for on-spot detection. It is noteworthy to mention that we produced all different solid platforms from dAuNPs-Sol mixed with 2% dextran. A standard S-shaped curve shows a dose-response function when a plot between $OCl^-$ concentrations and corresponding absorbance values is sketched. A clear colorimetric response is observed in different dAuNPs probes with rising concentrations of $OCl^-$ as shown in Figure 4.8. The LLoD for all solid forms is 10 mM of $OCl^-$ by 3 times the standard deviation of the blank signal. This observation highlights the importance of dextran amount in nanogold probes. All solid probes have shown excellent stability to date (~ two years) hence, highly suitable for fabricating ready-to-use commercial kits. In short, dextran quantity is the main factor in tuning a plasmonic probe which is slightly dependent of operational procedures adopted to achieve a solid platform. All solid plasmonic probes were used for the quantitative detection of $OCl^-$ with a higher sensitivity. Solid nanogold platforms can be used to fabricate portable sensors that show promising potential in nano-sensing and biomedical applications in the future.

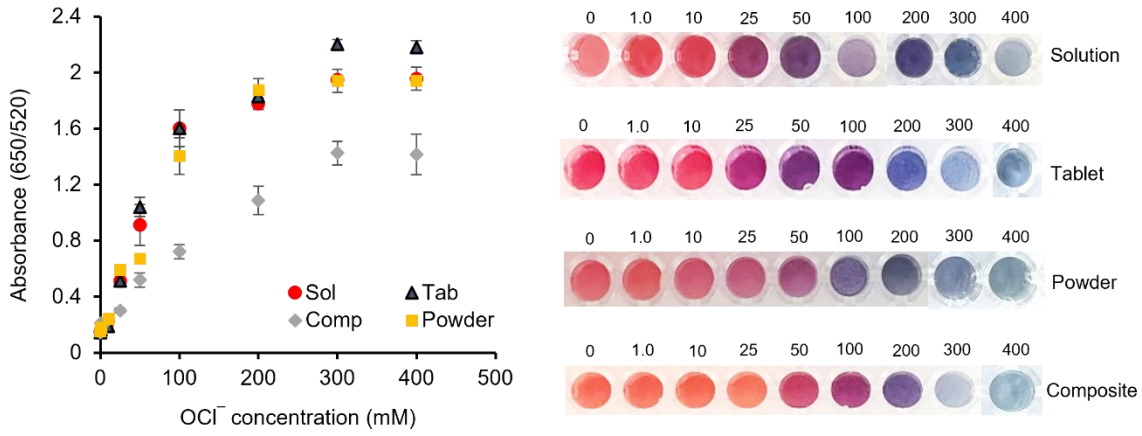


Figure 4.8 Calibration curve for colorimetric detection of $OCl^-$ in water with different dAuNPs formats (2.01% dextran) showing a variation in ULoD (100 mM with powder; 200 mM with solution, tablet, and composite) while LLoD remains 10 mM for all plasmonic probes (i.e., solution, tablet, powder, and composite). Each data in the graph is the mean value of three replications ± standard deviation.

### 4.3.5 Selectivity Analysis for the Detection of Hypochlorite ($OCl^-$)

The selectivity of the dAuNPs-Sol probe was tested in the presence of potential interferants, including anions (e.g., $Cl^-$, $HCO_3^-$, $SO_4^{2-}$) and cations (e.g., $Mg^{2+}$, $Ca^{2+}$, $Cu^{2+}$, $Fe^{3+}$, $Al^{3+}$) that

might coexist with $OCl^-$ in swimming pool water. None of the tested interfering ions even at higher orders of magnitude concentration than $OCl^-$ cause any noticeable change in the dAuNPs-Sol. It is important to mention that some $OCl^-$ sensors are known to be susceptible to other oxidizing agents such as hydrogen peroxide ($H_2O_2$) interference [61]. Our proposed assay indicates that there is only a minimal impact of $H_2O_2$ even at a concentration of 1 M, possibly owing to its weaker oxidation capacity than that of $OCl^-$ under tested conditions as displays in Figure 4.9A.

### 4.3.6 Determination of Hypochlorite ($OCl^-$) in Real Swimming Water Samples

To gauge the viability of our plasmonic sensor in real-world situations, different swimming water samples were analyzed using dAuNPs-Sol probe. Four samples were collected from different public indoor swimming pools one day before testing and stored at 4 °C. The $OCl^-$ detection assay was conducted using a routine spiking procedure through standard addition method to assess the method's accuracy. The standard addition method is a quantitative technique employed to study the matrix effect that may interfere with analyte signal. Importantly, the collected swimming pool samples did not exhibit any quantifiable traces of $OCl^-$. The chosen spiked concentrations fall within the working range of our dAuNPs-Sol sensor (50 – 450 μM) which also complies the WHO standard for the maximum recommended level of free chlorine in public swimming pools (58.32 – 97.18 μM) [10]. In brief, real pool water samples were spiked with varying concentrations of $OCl^-$ (0.05-0.25 mM, Table 4.2) and subsequently detected using the dAuNPs sensing probe. The color change and the corresponding absorption response of the plasmonic probe for $OCl^-$ in pool water were then observed. The spiked samples are compared with a calibration curve obtained from deionized water as displays in Figure 4.7A (0.01% dextran). The experimental data follows the trend of the calibration curve and are near the regression line after spiking. Finally, %R and %RSD were calculated using their relevant formulas [62] and data is presented in table 2. The %R values are in the range of 80–113% indicating the validity of our proposed method and %RSD values (0.57-3.89%) show a precision of dAuNPs-Sol sensor towards the quantitative detection of $OCl^-$ in real swimming water samples. Our proposed dAuNPs-Sol probe meets the detection requirements of $OCl^-$ in real swimming water sample as permitted by the WHO [10]. Additionally, we conducted a comparative analysis by evaluating the performance of our proposed assay against conventional UV-vis spectroscopy method (Figure 4S5). The results are comprehensively presented in Table

4.2, demonstrating comparable recovery outcomes for both methods and affirming the authenticity of our proposed assay. Finally, a comparison of the current assay with previously reported methods is outlined in Table 4S2. The analytical performances of the present method surpass those of reported approaches. Also, our assay stands out for its quite simplicity, tunability, rapidity, and suitability for $OCl^-$ sensing in swimming pool water samples compared to other fluorophores and various nanomaterials.

Table 4.2 The spiking recovery analysis results of proposed colorimetric assay in comparison with conventional method

| Samples | Amount added (mM) | Proposed dAuNPs colorimetric assay | | | Conventional spectroscopy method | | |
|---|---|---|---|---|---|---|---|
| | | Amount found (mM) | %R | %RSD | Amount found (mM) | %R | %RSD |
| Plaza tower, Atwater | 0.099-0.170 | 0.103-0.191 | 85-112 | 0.574-2.885 | 0.091-0.144 | 84-111 | 0.733-3.571 |
| Le Chatel building, Maisonneuve | 0.100-0.250 | 0.0932-0.255 | 93-113 | 2.144-3.826 | 0.115-0.242 | 96-115 | 0.701-2.168 |
| Plaza Cedar, Cedar | 0.050-0.150 | 0.048-0.131 | 80-97 | 2.259-3.896 | 0.058-0.127 | 84-116 | 2.777-3.646 |
| La Citadelle, Saint Marc | 0.170-0.220 | 0.151-0.216 | 89-105 | 1.931-3.322 | 0.150-241 | 88-109 | 0.705-1.811 |

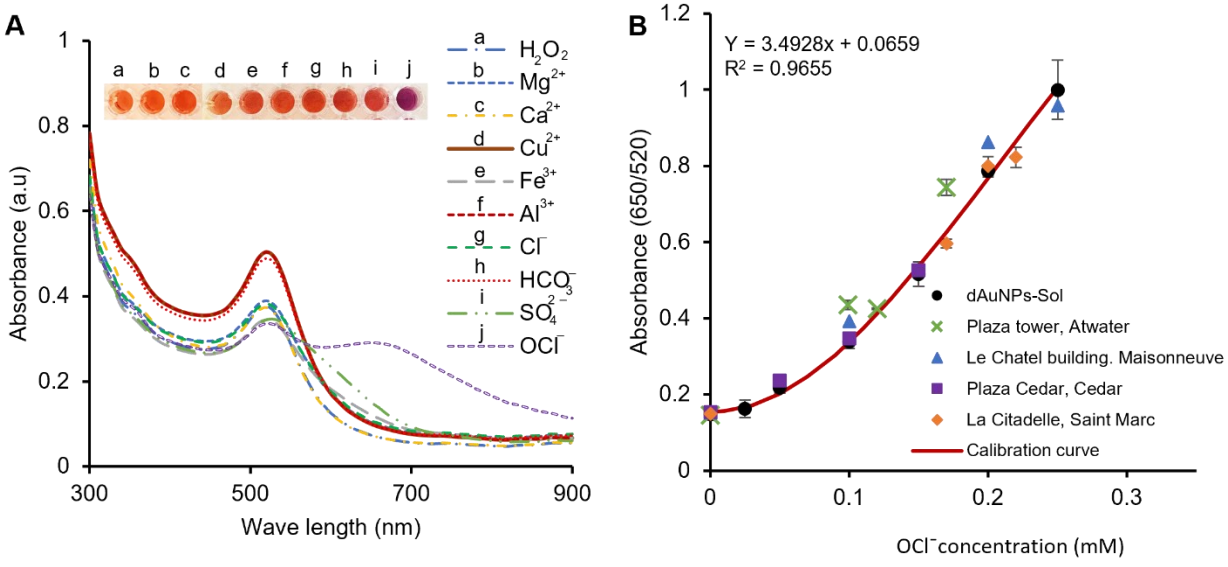


Figure 4.9 The interference study for the detection of $OCl^-$ using dAuNPs-Sol sensor

and its application for real swimming pool water samples. A) The absorption spectra of common interfering cations (1 mM of $Mg^{2+}$, $Fe^{3+}$, and $Al^{3+}$, $Cu^{2+}$, $Ca^{2+}$), anions (1 mM of $Cl^-$, $HCO_3^-$ and $SO_4^{2-}$), and an oxidizing agent (1 mM $H_2O_2$) display the specificity of dAuNPs sensor towards $OCl^-$ detection. The dAuNPs-Sol is aggregated in the presence of 100 µM $OCl^-$ ions causing a peak shift from 520 to 650 nm; B) The $OCl^-$ detection in spiked real swimming pool water collected from Plaza tower Atwater, Le Chatel building, Maisonneuves Street, Plaza Cedar, Cedar and La Citadelle, Saint-Marc, Montreal, Canada. The data points for unspiked samples are lied above each other. Calibration curve is drawn only in the range of spiking concentrations (0-0.25 mM) for better clarity.

### 4.4 Conclusions

In this study, we developed a tunable plasmonic sensor from dextran-gold nanoparticles solution (dAuNPs-Sol) and successfully detected hypochlorite ($OCl^-$) in water. The preparation of dAuNPs-Sol involves a chemical reduction method followed by the post-synthetic addition of different amounts of dextran (ranging from 0.01 to 30.01%) to create tunable nanogold probes with different shielding capabilities. Subsequently, we transformed the dAuNPs-Sol to different solid platforms, including tablet, composite, and powder by pipette-out, anti-solvent precipitation, and coagulation techniques, respectively. All liquid and solid dAuNPs probes were utilized to detect a broad range of $OCl^-$ concentration, offering a customizable limit of detection (LoD). Our analysis of the impact of dextran in dAuNPs-Sol included the investigation of surface charge, hydrodynamic size, and LoD. We observe that an increase in the dextran amount leads to a corresponding increase in the hydrodynamic size of dAuNPs, while the magnitude of surface charge on Au particles is decreased from -43.89 to -0.52 mV due to the charge-neutral nature of pristine dextran. We notice that the dAuNPs probe exhibits more sensitivity with less dextran, resulting in a lower LoD for the sensor. The oxidizing potential of $OCl^-$ disrupts the dextran shell around dAuNPs, leading to a colorimetric response from the sensor. A higher concentration of $OCl^-$ is required to dissociate the thicker dextran layer caused by a greater dextran concentration, in contrast to the thinner layer with less dextran. The dAuNPs-Sol sensor was used to detect $OCl^-$ in swimming pool water samples by spiking method to demonstrate its applicability for real-world applications. This plasmonic probe shows a robust selectivity for $OCl^-$ detection, as validating by interference analysis. In addition to this, we achieve highly concentrated dAuNPs (up to 20X) without compromising particle morphology, using a simple method that eliminates the need for a centrifuge machine. This research holds promise for the

scientific and researcher communities engaged in the development of user-friendly plasmonic sensors for on-site detection of hazardous substances.

# CHAPTER 5 Fabrication of Plasmonic Tablet and Swab Sensors for Point-of-care Detection of an Oxidative Stress

***This chapter is reproduced from the article published in ACS Applied Nano Materials, 8, 1008-1020 (2025).***

This chapter investigates the plasmonic tablet and swab sensors for colorimetric detection of urinary hydrogen peroxide ($H_2O_2$), as an oxidative stress biomarker, via Fenton chemistry. The tablet showed superior stability, while the swab degraded by ~40% over three months. A decrease in urinary $H_2O_2$ levels in healthy volunteers after green tea consumption suggests a potential antioxidant effect in mitigating oxidative stress.

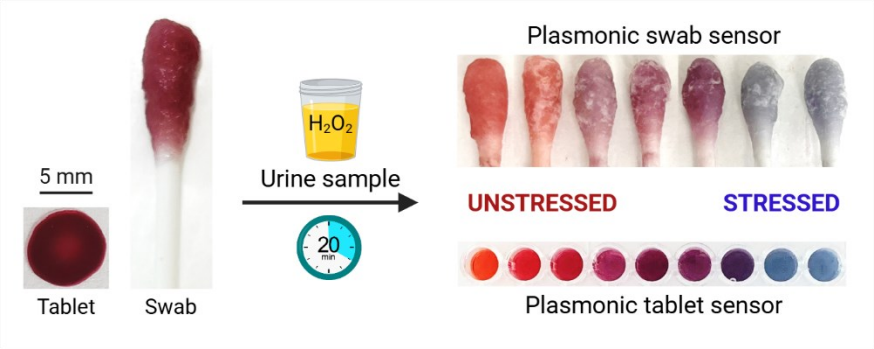

## 5.1 Introduction

Oxidative stress is an imbalance between the production or accumulation of reactive oxygen species (ROS) and the detoxification ability of antioxidants or biological systems because of poor dietary habits or the body's own metabolic functions [557]. Increased level of oxidative stress is associated with several metabolic disorders (e.g., diabetes, kidney damage) [558], neurodegenerative illnesses (e.g., Alzheimer's disease, Parkinson's disease) [559], cardiovascular conditions (e.g., heart failure) [560], and cancer [561]. Therefore, timely monitoring of oxidative stress is highly important to avoid life-threatening conditions. Various biomarkers for oxidative stress include end-products of oxidative damage to different biomolecules such as 8-hydroxy-2-deoxyguanosine (8-OHdG) [562], malondialdehyde (MDA) [563], 3-nitrotyrosine [564], or explicit determination of oxygen radicle production such as aromatic hydroxylation [565] or spin trapping [566]. As oxidative stress is not routinely tested in the clinical laboratory, the majority of these biomarkers rely on mass spectrometry, electron spin resonance spectroscopy, or use HPLC-based determination [567]. Considering these limitations, hydrogen peroxide ($H_2O_2$) as a whole-body oxidative stress biomarker has been highlighted in the literature [568,569]. Various biological samples such as exhaled breath, sweat, blood, and urine release different levels of $H_2O_2$. Among these, urine is an attractive medium for point-of-care applications due to its easy and non-invasive collection. Urinary $H_2O_2$ level varies drastically in healthy individuals with an average value of 100±60 μM [570]. However, this level is increased up to 3-fold in different patients (e.g., cancer, diabetes) [571]. Similarly, a raised level of urinary $H_2O_2$ is associated with oxidative stress which can be lower using antioxidant therapy [572].

Fenton chemistry has a well-known standing for $H_2O_2$ detection in the presence of low-valency transition metal ions (i.e. $Cu^{+1}$, $Fe^{+2}$, $Cr^{+3}$) [573]. Fenton reagents (i.e., $H_2O_2$ and $Fe^{2+}$) generate hydroxyl radicle (•OH) which is a strong oxidizer with +2.80 V oxidation potential; slightly inferior to fluorine oxidation potential (+2.87 V) [574]. This •OH can react with a variety of organic compounds leading to either degradation of these compounds or their conversion into less toxic products [575]. Moreover, the •OH initiates macromolecular damage in proteins, DNAs, and lipids causing cell damage [557]. Further, the •OH species is related to the detection of $H_2O_2$ because $H_2O_2$ is the precursor of •OH. Thus, the detection of $H_2O_2$ through the Fenton reaction is the center of attraction for scientific research. Fenton-mediated detection of $H_2O_2$ such as ferrous ion–o-dianisidine complex (TOS-dianisidine) assay, ferric-xylenol orange (FOX)

assay, and reactive oxygen metabolites derived compounds (d-ROMs) assay either use the carcinogenic substance, require longer incubation periods and centrifugation steps or has a high tendency of false results [576]. Hence, there is a need for new methodologies as well as improvement in the existing approaches for $H_2O_2$ detection.

The $H_2O_2$ detection assays utilizing Fenton reagents and nanomaterials are both straightforward and cost-effective, providing a colorimetric read-out and portability for enhanced convenience[577]. A variety of nanomaterials such as silver nanoparticles (AgNPs) [578], platinum nanoparticles (PtNPs) [579], copper oxide nanoparticles (CuONPs) [580], graphene composite [581] , and gold nanoparticles (AuNPs) [582] have been employed for $H_2O_2$ detection. Among these, AuNPs have been well-explored due to their superior optical, catalytic, and photothermal conversion properties besides their high surface-to-volume ratio, easy preparation and multifunctional surface modifications [583–589]. The $H_2O_2$ detection with AuNPs-based sensors has been reported with instrument-dependant techniques as well as portable methods. Instrument-dependant techniques include spectrophotometry, fluorometry, electroanalysis, chemiluminescence, resonance light scattering assays, and chromatography [590–592]. For portable methods, colorimetric readout receives considerable attention due to allowing for easy, low-cost, and user-friendly assay. The AuNPs-related portable detection platforms could be based on substrates such as paper, textile fabric, synthetic polymer, thread, tablet, or swab that require an ultra-low volume of the sample [583,593,594]. In such systems, quantification can be achieved through RGB color intensities using smartphone imaging [595]. Overall, the detection of $H_2O_2$ using AuNPs is important for the development of point-of-care sensors.

Lin *et al.* detected $H_2O_2$ using DNA-modified AuNPs where hydroxyl radicals were used to break the phosphodiester bonds in DNAs and decreased the quantity of DNAs on the surface of AuNPs causing their aggregation [596]. However, this assay required extensive pre-treatment of DNA before the detection step. For example, the reduction of thiol-modified oligo disulfide was time consuming and required −20 °C condition to prepare and store the reduced thiol-DNA followed by 16 hr stirring in the dark to adsorb the thiol-DNAs onto AuNPs. In another study, Wu *et al.* detected $H_2O_2$ through the aggregation of AuNPs because $H_2O_2$ treatment removed polyethylene glycol chains from the AuNPs surface that exposed inner hydrophobic ligands, causing AuNPs aggregation in water [597]. Again, this method required up to 28 h for the

detection of $H_2O_2$ in a dynamic μM range. Hence, there is a need to introduce a new detection strategy which is simple, portable, quick, user-friendly and cost-effective. Our group has a solid background in the tablet-based detection platform used for various applications [18,583,598–601]. We fabricated a tablet sensor by encapsulation of AuNPs used for the detection of acid-labile groups [583]. Additionally, our team has developed pullulan stabilized AuNPs-based tablet sensors for detecting glucose and cysteamine through the expression and inhibition of peroxidase-mimetic behavior, respectively [18,598].

Herein, we developed the plasmonic tablet and swab sensors for point-of-care detection of oxidative stress biomarker using urinary $H_2O_2$. Both, the tablet and swab sensors were prepared from dextran-gold nanoparticles solution (dAuNPs-Sol). The synthesis of dAuNPs-Sol, along with the preparation of tablet and swab sensors, is illustrated in Figure 5.1A, while their colorimetric responses are presented in Figure 5.1B. These sensors underwent comprehensive characterization using techniques such as ultraviolet-visible and Fourier transform infrared (FTIR) spectroscopy, transmission electron microscopy (TEM), scanning electron microscopy (SEM), energy dispersive X-ray spectroscopy (EDS), zeta potential and dynamic light scattering (DLS). The detection mechanism relies on the Fenton-assisted •OH radicle generation, leading to the degradation of the polymeric layer surrounding dAuNPs and subsequent loss of colloidal stability. Sodium chloride (NaCl) was then employed as an aggregating agent to induce a visual color transition from red to blue. The observed color change directly correlated with the concentration of $H_2O_2$, offering an estimation of whole-body oxidative stress. Calibration curves were generated by plotting $H_2O_2$ concentration against the aggregation/dispersion state of dAuNPs, utilizing *ImageJ* software for the tablet and swab sensors. Both sensors demonstrated high analytical performance in quantifying $H_2O_2$ levels. Unlike conventional chromogenic methods that are toxic and require specific buffer for preparation, our approach leverages the unique plasmonic properties of dAuNPs for a clear color change upon hydroxyl radical interaction. Moreover, the assay's adaptability into portable formats, such as tablets and swabs, coupled with its long-term stability and high selectivity, highlights its practical advantages over traditional methods.

To assess the sensors' real-world applicability, urinary $H_2O_2$ concentration was measured as an oxidative stress biomarker in real urine samples collected from healthy male and female

volunteers before and after a specific duration of consuming green tea. This evaluation not only showcased the performance of our plasmonic sensors in practical scenarios but also allowed us to observe the impact of diet on oxidative stress levels. Moreover, our sensors are promising for point-of-care applications such as diagnosing kidney inflammation through ROS detection in human urine.

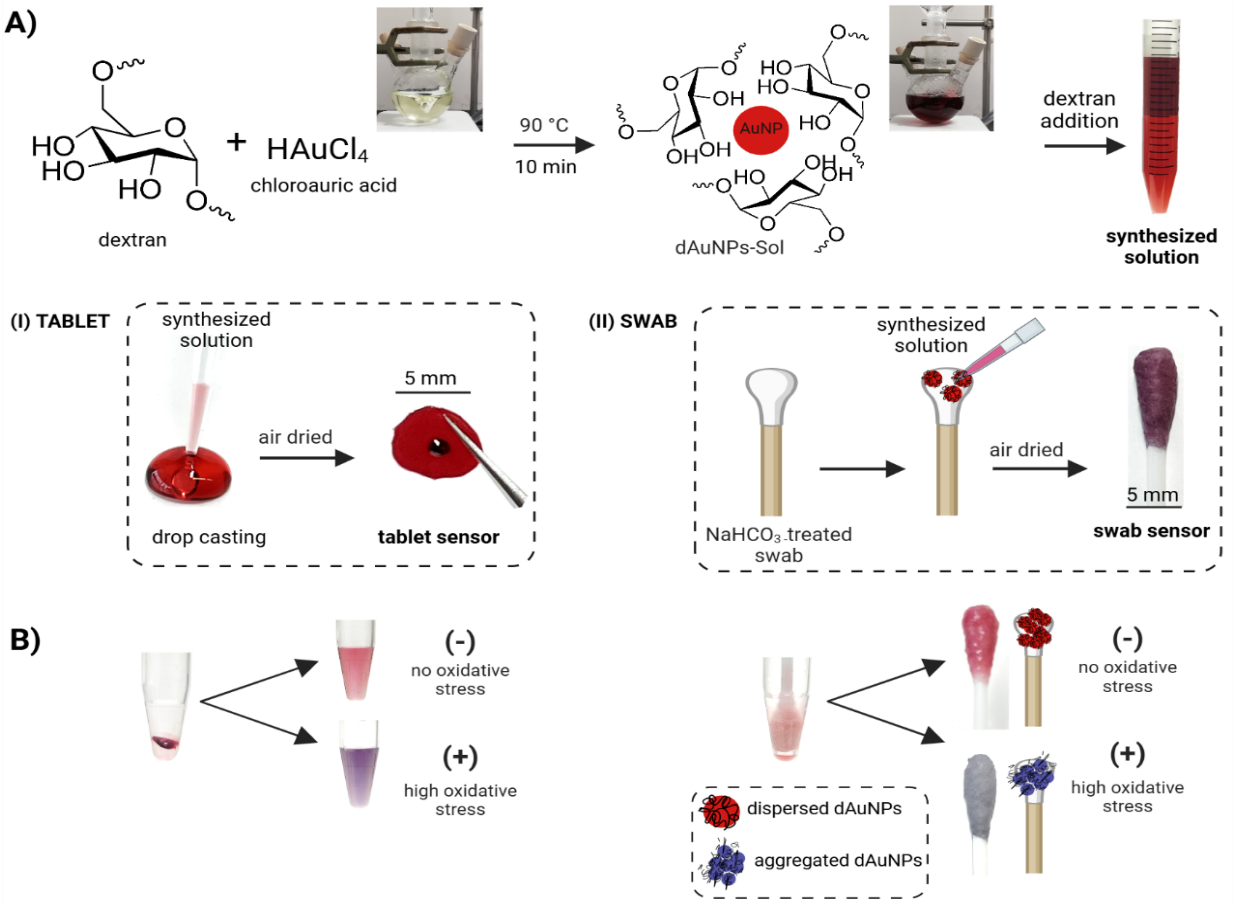


Figure 5.1 Synthesis of dextran-gold nanoparticles (dAuNPs) colloidal solution followed by a tablet and a swab sensor formation for the colorimetric detection of hydrogen peroxide ($H_2O_2$) as an oxidative stress biomarker. A) The dAuNPs solution was synthesized using chloroauric acid as a source of gold atoms and dextran as a reducing and stabilizing agent (yellow mixture in a flask). The dAuNPs-Sol (wine-red solution in a flask) was then mixed with dextran post-synthetically to get the plasmonic probe solution. This probe solution was used to cast the (I) tablet via drop casting technique and was also (II) poured onto the alkaline-treated swab; B) The plasmonic tablet and swab sensors were utilized to measure the concentration of urinary $H_2O_2$ based on the Fenton reaction, where a blue color readout indicates a high level of oxidative stress.

## 5.2 Experimental

### 5.2.1 Chemicals and Instrumentation

Tetrachloroauric acid ($HAuCl_4$, 30 wt.% in dilute HCl), hydrogen peroxide ($H_2O_2$, 30 wt.% or 9.8 M), ferrous sulfate heptahydrate ($FeSO_4 \cdot 7H_2O$), dextran (100 kDa), sodium phosphate monobasic monohydrate ($NaH_2PO_4 \cdot H_2O$), disodium hydrogen phosphate ($Na_2HPO_4$), sodium bicarbonate ($NaHCO_3$), sodium chloride (NaCl), citric acid ($C_6H_8O_7$), sodium hydroxide (NaOH), ascorbic acid ($C_6H_8O_6$), and sulfuric acid ($H_2SO_4$) were purchased from Sigma-Aldrich. Zinc chloride ($ZnCl_2$) and copper chloride ($CuCl_2$) were purchased from Thermo Scientific Chemicals. Deionized water was used to prepare all solutions. Citrate-phosphate buffer was prepared using 0.2M disodium hydrogen phosphate and 0.1M citric acid. The final pH was adjusted using citric acid. Ferrous sulphate solution was prepared in citrate-phosphate buffer. Artificial urine (99.99% purified) was obtained from Biochemazone, USA. The volunteers consumed Japanese green tea (sencha and matcha blend, Kirkland Signature brand) in the concentration of 1.5 g/200 mL water. Cotton swabs and a carbon steel tray (Betty Crocker) were purchased from a local Walmart store, Montreal, Canada. A vortex machine (model # 9454FIALUS, 50/60 Hz, Fisher) was used to dissolve a tablet into a Fenton reagent. The morphology and chemical nature of dAuNPs were studied by transmission electron microscopy (TEM, Talos L120C,20−120 kV). and scanning electron microscopy (SEM, Phenom ProX). SEM-EDS images were captured at 15 keV with solid samples cast on carbon grids. Absorption spectra of dAuNPs were recorded on a UV−vis spectrophotometer (BioTek, Cytation 5, imaging reader). The particle size analyzer (Litesizer 500, Anton-Paar, Austria) was used to record the hydrodynamic size of dAuNPs *via* the dynamic light scattering (DLS) technique. Surface charge on dAuNPs was measured in Ω-shaped polystyrene cuvettes, with zeta potential analyzed via electrophoretic light scattering using the cmPALS technique (European Patent 2735870). All samples were run in triplicate. The nanogold tablets were dried at room temperature or 50 °C in a laboratory oven without forced air convection (Thermo Scientific, Model# PR30525G, USA). The $NaHCO_3$ soured cotton swabs after nanogold adsorption were dried at room temperature and stored in an airtight box until use. Images of swab and tablet sensors were captured using an iPhone 13 and analyzed with *ImageJ* software (National Institute of Health, USA).

### 5.2.2 Fabrication of Plasmonic Tablet and Swab Sensors

The glassware was washed thrice with deionized water after being cleaned with fresh aqua regia solution. Colloidal solution of dextran-gold nanoparticles (dAuNPs-Sol) was synthesized as per the literature procedure with some modification[602]. In short, 25 mL of 1 mM $HAuCl_4$ solution was stirred with 50 µL of 5% dextran solution at 90 °C followed by the addition of 50 µL of 1 M NaOH solution. The flask contents were changed from light yellow to colorless, then light pink and finally into wine-red dispersion which confirmed the synthesis of dAuNPs. The concentration of dAuNPs solution was estimated to be ~4.6 nM by Beer's-Lambert law using UV–vis spectrophotometer based on a calculated extinction coefficient (ε) of $2.4 \times 10^8$ $M^{-1}cm^{-1}$ at 520 nm for 13 nm particles [601]. The nanogold solution after post-synthetic addition of 2% dextran powder was mixed for 1 min and transformed to tablets (dAuNPs-Tablets) according to our previously established protocols [583,601]. In short, a plasmonic tablet was created by pipetting 100 µL of the dAuNPs solution on a non-stick tray followed by airdrying overnight at ambient conditions of 20 °C and 45% indoor humidity. Fully dried tablets were collected from the tray and stored in a glass vial at room temperature.

Also, the dAuNPs-Swab sensor was prepared in two steps. Initially, commercial cotton swabs were boiled in $NaHCO_3$ solution (25 mM) for 5 min to remove any hydrophobic compounds including fats and waxes. The $NaHCO_3$ soured swabs were washed with deionized water five times or till to obtain a neutral pH (~7) using pH paper. These swabs were oven-dried at 60 °C for 1 hr followed by pouring a fixed volume (200 µL) of nanogold solution onto each swab. The plasmonic swabs were air-dried for ~8 hr and stored in an air-tight glass jar at room temperature till further use. Notably, a fixed concentration (~4.6 nM) and volume of dAuNPs were consistently used during tablet formation and swab preparation in each batch to prevent clumping and ensure consistency in the amount of dAuNPs across different tablets and swabs. A controlled drying environment, including regulated temperature and humidity, was also maintained to promote particle uniformity and prevent aggregation during solvent evaporation. However, even if non-uniform particle distribution occurs within a tablet or swab, it does not impact the results, as the entire tablet is dissolved in the Fenton reagent, giving the exact same concentration of dAuNPs and resulting in a consistent color change. Similarly, the entire swab is immersed in the Fenton reagent to generate the blue color for analysis.

### 5.2.3 Optimization Study and Reaction Kinetics of Hydrogen Peroxide ($H_2O_2$) Assay

Reaction conditions were optimized to establish the experimental protocols for the $H_2O_2$ assay. Major operational parameters such as the amount of dextran in dAuNPs, concentration and pH of ferrous sulfate solution, concentration and volume of sodium chlorite as well as temperature of reaction medium were investigated. Further, the Fenton-based •OH radicle generation was confirmed by using ascorbic acid as a radicle scavenger. For this, 1 mM ascorbic acid (10 µL) was incubated with Fenton's reagent for 10 min followed by the addition of a plasmonic tablet and NaCl solution. Finally, the reaction kinetics was studied using 1 mM $H_2O_2$ in the presence and absence of ascorbic acid.

### 5.2.4 Detection of $H_2O_2$ as a Potential Oxidative Stress Biomarker

*Fenton reaction-based colorimetric assay using a tablet sensor:* The colorimetric detection of $H_2O_2$ based on Fenton chemistry is comprised of two steps; generation of free hydroxyl radicle (•OH) and detection of $H_2O_2$ using dAuNPs probe. The first step involves the Fenton reagent where a reaction between ferrous ions and $H_2O_2$ takes place to produce •OH. For this, 50 µL of different concentrations of $H_2O_2$ in water (30, 50, 100, 125, 250, 500, 700, 1000 µM) were mixed with 10 µL of 3 mM ferrous sulfate (pH 3) followed by the addition of 200 µL deionized water. This solution was incubated for 10 min to ensure the generation of •OH which participated in the detection step. In the second step, a plasmonic tablet (100 µL of dAuNPs) was added to the previously formed Fenton solution and vortexed to get a homogenized mixture. Finally, 30 µL of 1M NaCl solution was added, and UV–vis spectra were collected after 10 min of incubation. Next, $H_2O_2$ assay was employed in artificial urine using the same experimental protocols where artificial urine was spiked with different concentrations of $H_2O_2$ ranging from 30 to 1000 µM. The color change of tablet solution was recorded as blue/red color intensity using *ImageJ* software in addition to measure their absorbance intensity at $\lambda_{520}$ and $\lambda_{650}$ nm using a UV-vis spectrophotometer. Notably, for the analysis, a full well of the 96-well plate was selected as the region of interest in *ImageJ* to eliminate any inconsistencies in color selection. Each experiment was conducted in triplicate to ensure reproducibility.

*Fenton reaction-based colorimetric assay using a swab sensor:* A plasmonic swab was used for the colorimetric detection of $H_2O_2$ facilitated by Fenton chemistry in aqueous media, and artificial urine samples. For this, 10 µL of 3 mM ferrous sulfate (pH 3), 200 µL of deionized-

distilled water, and 50 µL of different concentrations of $H_2O_2$ (30, 50, 100, 125, 250, 500, 700, 1000 µM) were incubated for 10 min followed by dipping of dAuNPs-Swab in Fenton solution. Afterward, 30 µL of 1M NaCl solution dropped onto the swab. After 10 min, optical images of swabs were collected and analyzed by *ImageJ* software for any change in their color intensity. The RGB color analysis was used to plot a calibration curve for quantitative analysis. Similarly, for the cotton swab analysis, the entire area of the swab was chosen as the region of interest, which minimized any discrepancies in color variation across the swab. This experiment was also performed in triplicate to confirm consistent and reliable results.

### 5.2.5 Interference Study using Plasmonic Tablet and Swab

Possible interferants that might exist in the urine sample are anions ($Cl^-$), cations ($Na^+$, $K^+$, $NH_4^+$, $Mg^{2+}$, $Ca^{2+}$, $Zn^{2+}$, $Cu^{2+}$), glucose, uric acid, and ascorbic acid. These potential interferants were tested to check the selectivity of a plasmonic tablet and swab sensors towards $H_2O_2$ detection. The same experimental procedure was followed as mentioned in section 5.2.4 using 0.1 mM $H_2O_2$ in the presence of 1 mM anions and 0.1 mM cations, and 0.1 mM glucose, uric acid, and ascorbic acid separately. The change in color intensity was estimated using *ImageJ* software for plasmonic tablet and swab sensors.

### 5.2.6 Determination of oxidative stress in male and female volunteers

The newly proposed $H_2O_2$ assay was utilized to measure oxidative stress level in healthy individuals (male and female) before and after consuming green tea 200 mL three times a day for a week. The volunteers did not take any drug, ergogenic aids, or antioxidant supplements for at least 10 weeks before the study. A standard literature method as reported by Halliwell *et al.* was followed to collect the urine samples [603]. These samples were spiked with known concentrations of $H_2O_2$ (160, 200, 250, and 500 µM) and quantitatively analyzed using a plasmonic tablet and a swab sensor following the same procedure as mentioned in section 5.2.4. We use a buffer to ensure that variations in the sample's pH do not affect the sensor's performance. The recovery% (R%) and relative standard deviation% (RSD%) were calculated using their standard formula to show the practical applicability and precision of both plasmonic sensors [598].

## 5.3 Results and Discussion

### 5.3.1 Characterization of Plasmonic Sensors

In this section, we thoroughly explore the characterization of our plasmonic sensors, crucial for understanding their performance and mechanisms. Through a comprehensive analysis employing various spectroscopic and microscopic techniques, we studied the structural and functional properties of these sensors. This detailed characterization lays the groundwork for subsequent discussions on their efficacy in detecting oxidative stress biomarkers. A colloidal solution of dextran-gold nanoparticles (dAuNPs-Sol) was prepared according to the literature method by reacting chloroauric acid with dextran in an alkaline medium [602]. Subsequently, dAuNPs-Sol was encapsulated as a tablet (dAuNPs-Tablet) or deposited on pre-treated cotton swabs (dAuNPs-Swab) to fabricate plasmonic sensors. The dAuNPs from both solid platforms (tablet and swab) were released into deionized water to analyze their morphology and surface charge employing UV-vis and FTIR spectroscopy, dynamic light scattering (DLS), transmission electron microscopy (TEM), and zeta potential analyzer. Apart from solution phase characterization of nanoparticles, scanning electron microscopy (SEM) with energy dispersive X-ray spectroscopy (EDS) analysis of solid plasmonic sample is reported herein, whereas we have already published atomic force microscopy (AFM) analysis of a solid tablet [583].

A classical bottom-up approach employing a wet chemical reduction method opted for one-pot NaOH-assisted synthesis of dAuNPs solution. The gold chloric acid solution was refluxed in alkaline media with dextran as a reducing, stabilizing, and capping agent [602]. Generally, dextran oxidation is followed by $HAuCl_4$ reduction to produce aurous salt (AuCl) which undergoes a disproportionation reaction producing monomers for the formation of nanoparticles [602]. Alkaline media facilitated the formation of different gold complexes during the synthesis. The AuNPs were readily stabilized by copious alcohol hydroxyl groups of the dextran chain. Within 5 min, the color of the reaction medium was shifted from colorless ($Au^{3+}$) to light pink, and finally burgundy/wine red ($Au^0$) transparent colloidal solution. The reaction was kept under the same conditions for an additional 30 min to ensure no further increase in absorption intensity of dAuNPs-Sol. A sharp, narrow, and symmetrical absorption band appeared at $\lambda_{520}$ nm demonstrating monodispersed dAuNPs of 13 nm. FTIR spectrum has characteristic functional peaks of dextran and AuNPs solution as supported by the literature [602]. The hydrodynamic

size was 35.02 nm (15% PDI) and the surface charge was -42.6 mV as shown by DLS and zeta potential analysis respectively (Figure 5S1).

The dAuNPs-Sol was mixed with pristine dextran (2%) to get the highly stabilized nanogold dispersion used to cast plasmonic tablets according to our previously established protocols[583]. The plasmonic swab was prepared by dropping the nanogold colloidal dispersion onto pre-treated cotton swabs. Of note, aggregation of nanogold was observed when $NaHCO_3$-soured swabs were directly soaked in dAuNPs dispersion and dried. The reason for aggregation may be the adsorption of maximum nanogold particles, hence, a pre-measured volume (200 µL) of dAuNPs dispersion was carefully pipetted out on alkaline treated swabs. However, if the same volume of dAuNPs solution was pipetted out on untreated swabs, again, nanoparticles were aggregated on the surface of the cotton swab at random places due to the presence of the existing wax layer on the swab (Figure 5S2A). It is also important to mention that cotton swab was preferred over different materials such as cotton ball, face-mask thread, cotton thread, and mouth floss because these materials did not adsorb nanogold efficiently and could not sustain them well-dispersed on the surface. All of these materials turned purplish-blue after drying, hence unsuitable to be used as a colorimetric probe (Figure 5S2B).

UV-vis extinction spectra of dAuNPs-Tablet, dAuNPs-Swab and dAuNPs-Sol are identical indicating the post-synthetic addition of dextran in dAuNPs solution did not change particle morphology in tablet and swab. However, the decreased intensity of the peak in swab as compared to the tablet was due to the partial release of dAuNPs into solution from dAuNPs-Swab (Figure 5.2A). Of note, the surface of $NaHCO_3$-scoured swab in neutral solutions is negatively charged due to dissociation of functional groups, such as hydroxyl and carboxyl groups as well as adsorption of dAuNPs from the solution, indicating the stability of gold particles on a swab [604]. Infrared analysis of dAuNPs in tablet and swab formats showed a peak at 1634 $cm^{-1}$ corresponding to the C=O stretching frequency present in aldehyde groups which indicated the conversion of some of the dextran's hydroxyl groups into aldehyde functionality after oxidation, a process coupled with the reduction of $Au^{3+}$ to $Au^0$ species [605]. Intense broadband at 3319 $cm^{-1}$ suggested the presence of symmetrical stretching vibrations of hydroxyl functional groups (O–H), which might have arisen from alcoholic groups of dextran. The bands at 1150, and 997 $cm^{-1}$ corresponded to the stretching vibrations of C–O bonds, and $\alpha$-glycosidic

bonds (C–O–C) in dextran, respectively[602]. The absorption peak at 2925 $cm^{-1}$ can be assigned to –CH group stretching vibrations of dextran which can be seen in dAuNPs-Tablet and dAuNPs-Swab. The FTIR analysis showed the involvement of dextran in fabricating dAuNPs as well as surface attachment on nanogold particles (Figure 5S3).

The ζ-potential of dAuNPs-Tablet was estimated as -28.54 mV and dAuNPs-Swab as -15.16 mV which supports that the nanoparticles boundaries are well separated from the adjacent particles of a similar charge in the dispersion. These phenomena resist aggregation and confer stability of dAuNPs as tablet and swab platforms. The decrease in surface charge of the swab as compared to tablet might be due to the partial release of nanogold particles in solution and most of the particles remained absorbed onto the swab surface. The hydrodynamic size of dAuNPs-Tablets and dAuNPs-Swab was 160.6 nm (20% PDI) and 102.0 nm (33% PDI), respectively, as depicted from DLS analysis (Figure 5S3). The increased hydrodynamic size in the tablet solution as compared to the swab solution might be due to the efficient surrounding of solvent molecules around nanogold particles [606]. The increased size in both solid formats as compared to dAuNPs-Sol was due to the additional amount of dextran polymer resulting in a thicker polymeric layer around dAuNPs leading to a bigger hydrodynamic size [539]. The surface morphology of a tablet and swab was characterized by TEM and SEM analysis, respectively as shown in Figure 5.2. The average particle diameter of the tablet was 12 ± 1 nm with a round shape morphology observed in the TEM images (Figure 5.2B). The SEM micrographs of low and high magnifications (Figure 5.2C), depict the uniform distribution of dAuNPs aggregates (size in the tens of nanometers) on the cellulose fibers of the swab. EDS quantitative analysis confirmed the elemental composition of the dAuNPs-Tablet as 13.09% gold, 80.79% carbon, and 6.12% oxygen, while the dAuNPs-Swab consisted of 9.21% gold, 82.55% carbon, and 8.23% oxygen, as presented in Figure 5S3D.

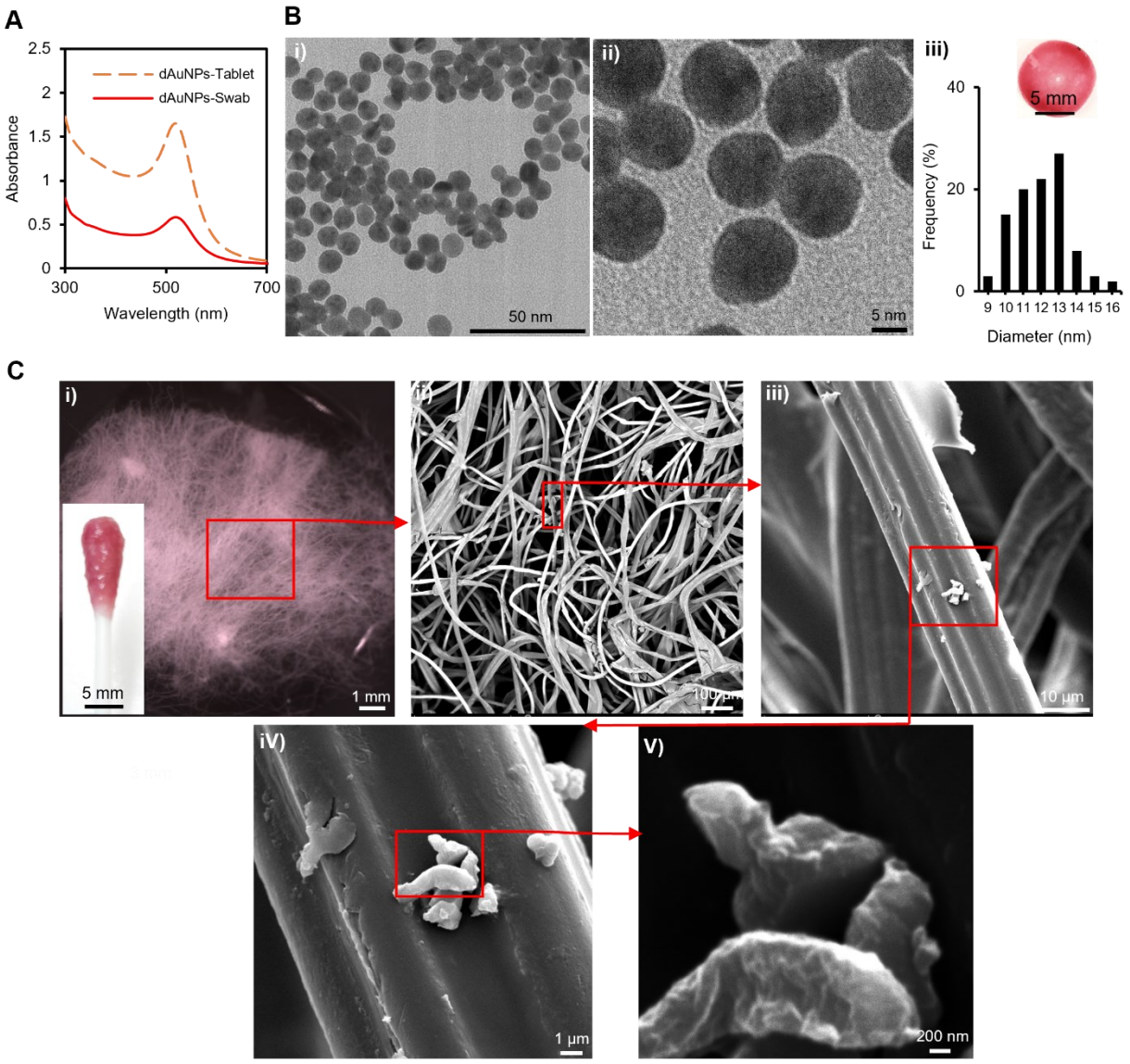


Figure 5.2 Characterization of gold nanoparticles in tablet and swab formats.
A) Absorption spectra showing peak maxima at 520 nm for both tablet and swab; B) The TEM image of dAuNPs-Tablet shows i) an average particle size of 12 ± 1 nm, ii) the round shape of nanoparticles, and iii) a particle distribution graph, with the optical image of a tablet shown as an inset; C) The SEM images of dAuNPs-Swab show clusters of Au particles distributed within the cellulose fibers of the cotton swab at different scale bars: i) 1 mm (with the optical image of dAuNPs-swab shown as an inset), ii) 100 µm, iii) 10 µm, iv) 1 µm, and v) 200 nm.

### 5.3.2 Optimization Study for $H_2O_2$ Assay

Next, we conducted an optimization study to refine the $H_2O_2$ assay methodology. By systematically investigating key parameters and experimental conditions, we aimed to enhance

the sensitivity, accuracy, and reliability of our detection approach. Several influencing parameters such as the concentration of dextran in dAuNPs suspension (0.01 or 2.01%), concentration of ferrous ion ($Fe^{2+}$) in Fenton reagent, amount of NaCl salt, pH and temperature of reaction medium were optimized in a univariate approach for $H_2O_2$ assay as shown in Figure 5S4. The dAuNPs-Tablet solution is more stable as compared to 'as-synthesized' dAuNPs-Sol because of having 2% additional dextran powder which stabilized nanoparticles more effectively. The addition of $Fe^{2+}$ or $H_2O_2$ alone caused no aggregation in dAuNPs-Tablet but a slight decrease in peak intensity in the case of $H_2O_2$ (Figure 5S4A, curves b and e). Next, different concentrations of ferrous sulfate (1, 2, 3, and 6 mM) were tested with dAuNPs-Tablet to choose the best concentration that could not induce aggregation in dAuNPs-Tablet. Highly concentrated ferrous sulfate solution (6 mM) induced aggregation in dAuNPs-Tablet, hence, unsuitable for the assay.

The dAuNPs-Tablet withstands high ionic strength as previously reported by our group [583]. Different volume (10-50 µL) of 1 M NaCl solution was incubated with dAuNPs-Tablet solution for 10 min which showed no visible color change till 30 µL of NaCl. Thus, 30 µL of NaCl was chosen to enhance the signal read-out in $H_2O_2$ detection. Further, 100 µM of $H_2O_2$ in the presence of 1-3 mM ferrous sulfate was used to generate •OH radicle followed by the addition of 30 µL NaCl to see the visual color change in dAuNPs-Tablet solution. Results indicated that only 3 mM $Fe^{2+}$ produced aggregation while <3 mM salt was not enough to generate radicle from $H_2O_2$. As the radicle generation is highly dependent on reaction pH, an acidic pH range of ferrous solution was tested because at higher pH values (i.e., basic range) ferric ions precipitated as hydroxide, hence unsuitable for the Fenton reaction[607]. In our assay, the ferrous solution was prepared in the citrate-phosphate buffer. The high amount of •OH radicle was produced at pH 2.5-3.0 which was selected for $H_2O_2$ assay. Finally, a wide temperature range (till 50 °C) was studied for the Fenton reaction showing the optimal temperature was 20-30 °C because the •OH radicle generation was reduced at higher temperature.

### 5.3.3 Mechanism of Fenton-Assisted Oxidative Damage of Dextran layer around dAuNPs

In this section, we further explored the mechanism underlying the Fenton-assisted oxidative damage of the dextran layer surrounding dAuNPs. This is with the aim of gaining insight into the processes that drive the colorimetric response observed in our plasmonic sensors. Understanding

these intricate molecular interactions is essential for interpreting the sensor's performance and optimizing its sensitivity and specificity for detecting urinary $H_2O_2$ as an oxidative stress biomarker. Fenton-mediated colorimetric detection of $H_2O_2$ through •OH-assisted dextran degradation, resulting in dAuNPs aggregation, is shown in Figure 5.3A.

Dextran-gold nanoparticles (dAuNPs) are stable due to the electrostatic forces as well as steric hindrance caused by the long chains of polysaccharide around nanoparticles. Oxidative damage of polysaccharide chains generates small fragments of polymer that cannot stabilize the gold colloidal suspension, hence promoting aggregation of nanoparticles. Among different oxidative approaches, the Fenton reaction is well known. It is worth mentioning that the incubation of a plasmonic tablet with $H_2O_2$ did not cause aggregation even when the concentration of $H_2O_2$ exceeded 5M. Fenton's reagent produces highly reactive •OH radicle which initiates dextran degradation by abstracting hydrogen atom at any C–H bonds of the glucopyranose ring [608]. This hydrogen abstraction may generate a radical on the carbon atom which leads to the cleavage in either of the two directions as shown in Figure 5S5. If the radical is at carbon which forms glycosidic bonds, it undergoes a $\beta$-scission reaction resulting in depolymerization of dextran chains with and/or without ring opening[608]. However, if the radicle is on any carbon other than glycosidic bond-associated carbon, it promotes ring opening reaction leading to the formation of a carbonyl group [609]. The multiple oxidized species are produced which are relatively unspecific due to the availability of a large number of C–H bonds in the dextran chain which forms stabilized $\alpha$-hydroxyalkyl radicles (·C(OH)RR′)[610]. The oxidized dextran fragments are unable to stabilize the colloidal gold suspension, hence aggregation is induced as shown in Figure 5.3B. Overall, the $H_2O_2$ detection strategy relies on •OH-mediated oxidative damage of dAuNPs followed by the distance-dependent color transition with the assistance of salt due to its signal amplifying role.

The aggregation of dAuNPs in tablet solution and on swab is visually apparent and evidenced by SPR peak broadening (Figure 5.4A), reduced ζ-potential (-10 mV and -5.9 mV, respectively) (Figure 5.4B), and increased hydrodynamic sizes (911 nm and 558 nm, respectively) (Figure 5.4C). TEM/SEM imaging further confirms these aggregates, highlighting the role of $H_2O_2$ in nanoparticle aggregation (Figure 5.4D-E).

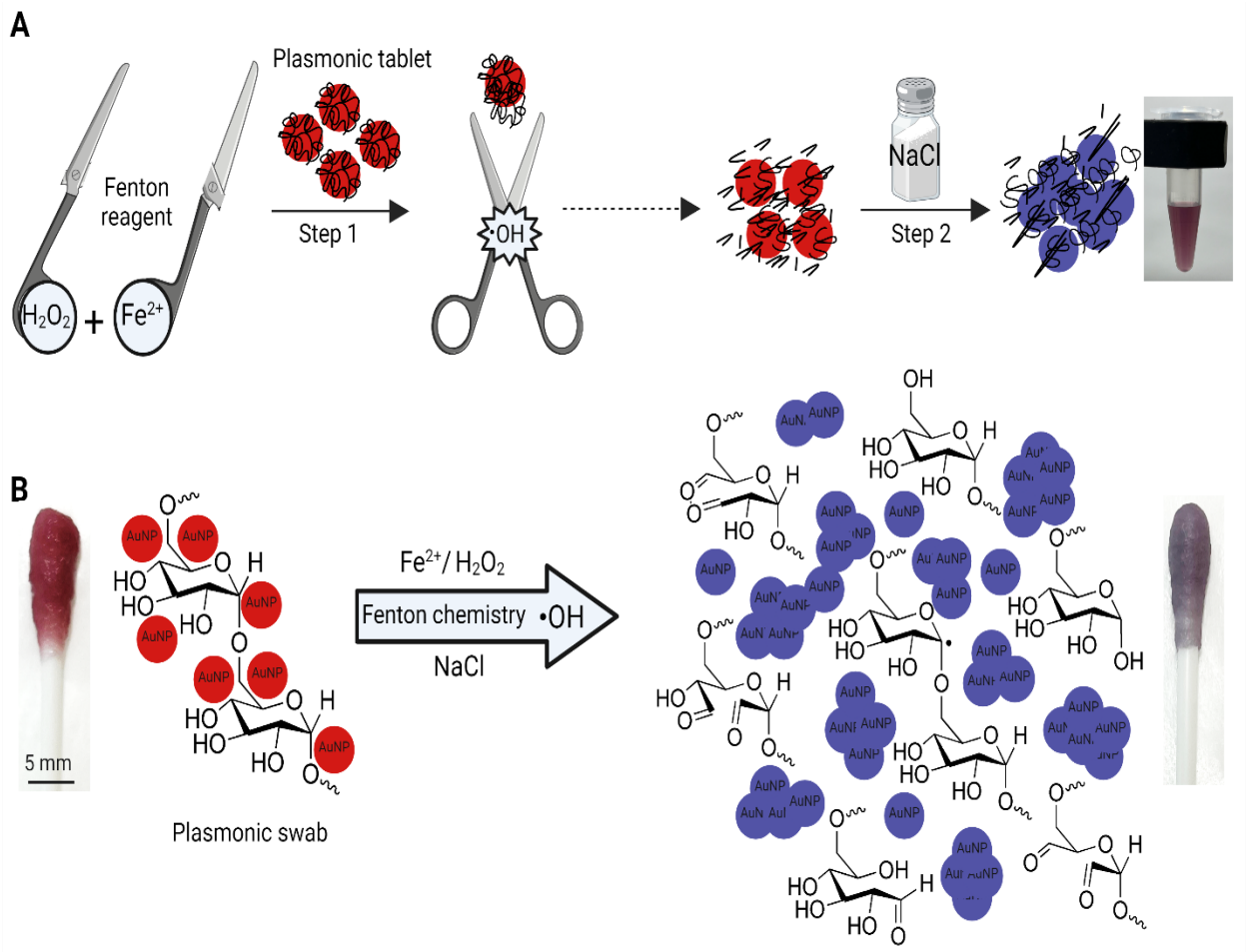


Figure 5.3 Fenton-mediated colorimetric detection of $H_2O_2$ *via* •OH-assisted dextran degradation around dAuNPs resulting in aggregation of dAuNPs. A) A Fenton reagent consisting of $H_2O_2$ and ferrous ions ($Fe^{2+}$) produces •OH radical which oxidizes dextran chains around dAuNPs in the first step. The oxidized dextran cannot protect dAuNPs fully and leads to the aggregation of particles upon the addition of sodium chloride in the second step, producing a red-to-blue color response; B) The red color of plasmonic swab turns to blue aggregated particles by the influence of Fenton chemistry.

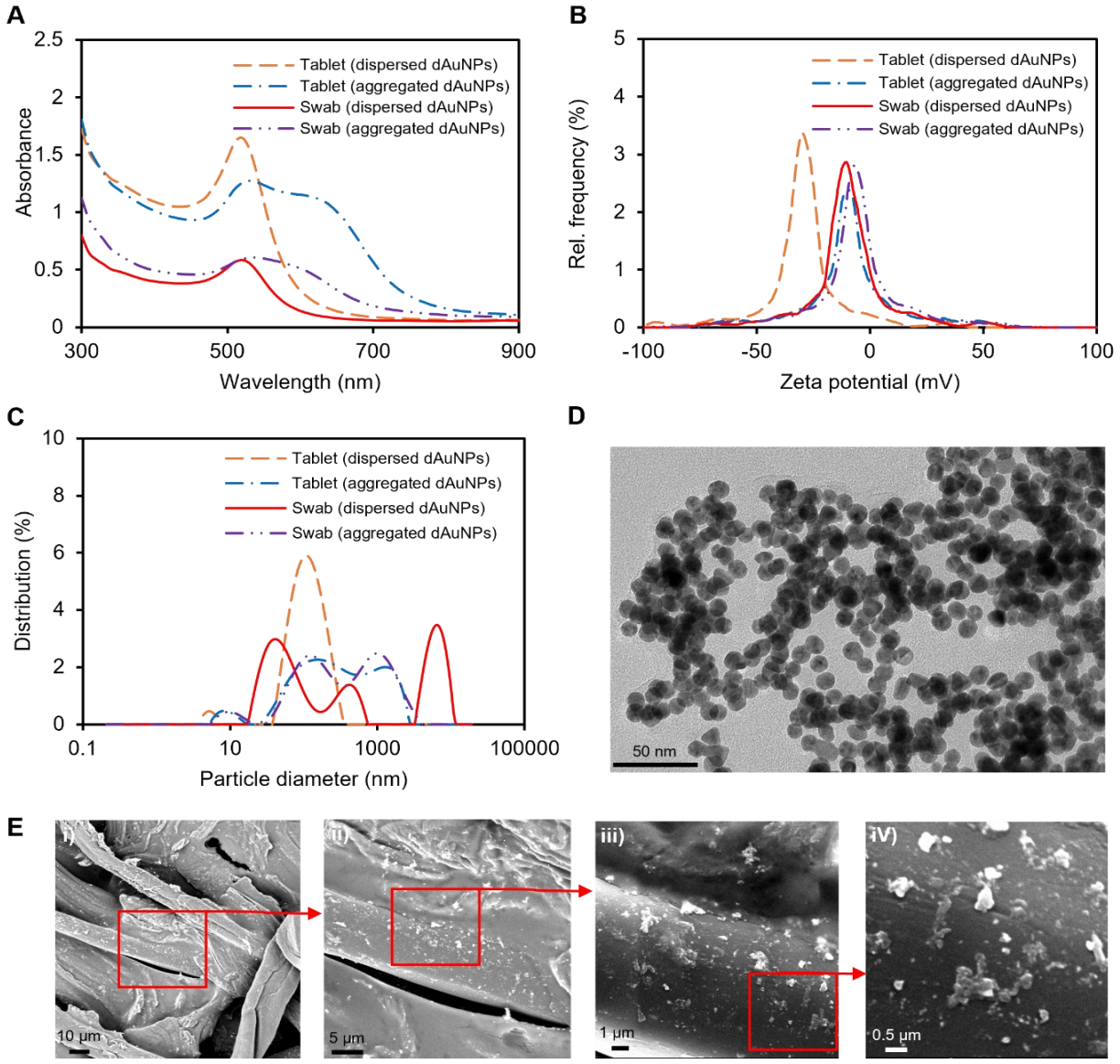


Figure 5.4 Comparison of the dAuNPs probe before (dispersed) and after (aggregated) detection of $H_2O_2$.
A) Absorption spectra; B) A graph of zeta potential values; C) A plot of hydrodynamic size; D) A TEM image of the tablet-based assay solution after nanoparticles aggregation; and E) SEM images of the dAuNPs-swab after aggregation, shown at different scales; i) 10 µm, ii) 5 µm, iii) 1 µm, and iv) 0.5 µm.

### 5.3.4 A Kinetic Study and Scavenging of •OH Radical with Ascorbic Acid

Next, by examining the rate of reaction and the effectiveness of ascorbic acid in neutralizing the radicle, we aim to deepen our understanding of the antioxidant properties of this compound. This investigation is important for implications for our plasmonic sensor technology. The generation

of •OH radicle in the detection system was confirmed by scavenging it with ascorbic acid due to its radicle-quenching nature. In this study, ascorbic acid was incubated with Fenton's reagent to quench the •OH radicle as it produced. Thus, quenching of •OH radicle inhibited the dextran degradation around dAuNPs resulting in well-dispersed stable nanoparticles. A kinetic study of $H_2O_2$ detection was executed using UV-vis spectroscopy as shown in Figure 5.5A. For this, 1 mM $H_2O_2$ in the presence and absence of ascorbic acid were screened for the gradual color change in the dAuNPs probe. An increase in $A_{650}/A_{520}$ values indicated the aggregation of dAuNPs which was prominent with time. As expected, the Fenton-ascorbic acid system showed a lower value for $A_{650}/A_{520}$ than alone $H_2O_2$ which indicated the capturing of •OH radicle by ascorbic acid resulting in less aggregation of dAuNPs. In short, direct evidence for the Fenton-induced aggregation of dAuNPs was supported by ascorbic acid-induced dispersion of dAuNPs by quenching •OH. The presence of a quencher in the system inhibits the dextran degradation, hence dAuNPs remain protected. The spectrum of dAuNPs in the presence of ascorbic acid showed $\lambda_{max}$ at 520 nm representing a state fully dispersed state of nanoparticles. However, the spectrum of 1 mM $H_2O_2$ without ascorbic acid showed a bathochromic shift due to aggregation of dAuNPs as shown in Figure 5.5B.

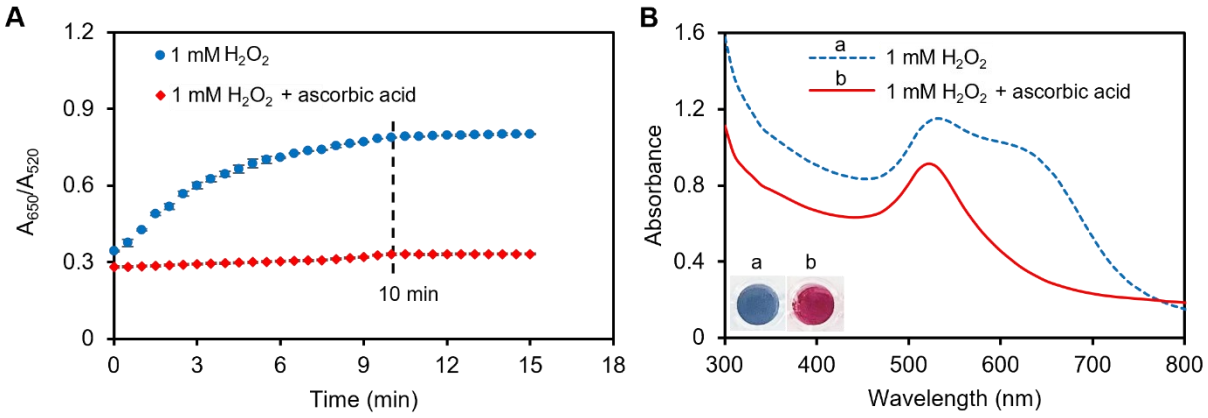


Figure 5.5 The kinetic study and hydroxyl radical (•OH) scavenging activity using a tablet sensor.
A) The kinetic study for $H_2O_2$ detection indicates 10 min time-window for the maximum color change of dAuNPs probe. The presence of ascorbic acid reduces the aggregation of dAuNPs by scavenging •OH resulting in decreased $A_{650}/A_{520}$ values; B) The spectral scan of dAuNPs detection solution after 10 min when using $H_2O_2$ alone and with ascorbic acid. An image in inset shows (a) aggregated dAuNPs and (b) dispersed dAuNPs.

### 5.3.5 Analytical Performance of Plasmonic Tablet and Swab Sensors

To evaluate the analytical performance of the plasmonic tablet and swab sensors a comprehensive analysis of sensitivity, specificity, and detection limits was conducted. This evaluation is essential for determining the reliability and accuracy of our sensor technology in real-world applications, paving the way for its potential use in point-of-care diagnostics and healthcare settings. To ensure the consistent imaging conditions, we captured the images of the swabs and tablet-based assay solutions using a custom-built imaging setup with controlled lighting and a fixed sample holder to maintain consistent height and angle positioning. This approach ensured experimental integrity and reproducibility. Moreover, for a fully developed device for point-of-care settings, an opaque box can be created and integrated with smartphone imaging to provide an affordable, portable, and user-friendly solution for end users, as reported in the literature [611]. The sensitivity of the proposed plasmonic tablet and swab probe was determined against a wide concentration range of $H_2O_2$ in water and artificial urine as shown in Figure 5.6. Under the optimal conditions (10 µL of 3 mM $Fe_2SO_4$ solution at pH 3.0, 30 µL of 1 M NaCl, reaction temperature of 20 °C, reaction time of 10 min), the absorbance intensity was measured for a series of $H_2O_2$ concentrations (30, 50, 100, 125, 250, 500, 700, and 1000 µM) in water and artificial urine. Results in water are presented in Figure 5S6. The calibration curve in artificial urine is achieved considering blue/red color intensity versus $H_2O_2$ concentrations due to •OH-induced oxidative damage of the dextran layer around nanoparticles which promoted aggregation in dAuNPs. We observed that the sensor's response was clearly visible to the naked eye at a concentration of ≥100 µM, whereas lower concentrations required the assistance of *ImageJ* for interpretation. The LoD of the proposed sensor was calculated as the lowest concentration generating to a signal that was proportional to the analyte concentration and with a value of at least three times the blank standard deviation. The tablet sensor exhibited a strong linear relationship within the range of 0.03–1.0 mM $H_2O_2$, with a correlation coefficient ($R^2$) of 0.99, as shown in Figure 5.6A. The linear equation for the tablet sensor is [y = 0.9412x + 0.2739]. The LoD was determined to be 50 µM in artificial urine. Next, the swab sensor was tested for the quantitative detection of $H_2O_2$ within a range of 0-1000 µM as shown in Figure 5.6B. All experiments were repeated three times to calculate the standard deviation. The blue/red color intensity was used as ordinates and the concentration of $H_2O_2$ as abscissa. The RGB color intensity significantly reflects the color intensity and turned to blue with the increase of $H_2O_2$

concentration, hence, achieving a visualized qualitative analysis of $H_2O_2$. The swab sensor showed a linear range of 0.05–1.0 mM $H_2O_2$ ($R^2 = 0.93$), with the corresponding linear equation being [y = 0.4322x + 0.5029]. The LoD was determined to be 100 µM in artificial urine, as depicted in Figure 5.6B. Notably, the calibrations for the tablet and swab sensors appear very similar (Figure 5.6A and 5.6B); however, the calculated LoDs in artificial urine are 50 µM and 100 µM, respectively. The higher LoD observed for the swab sensor can be attributed to the lower intensity of the color signal. This reduced signal intensity arises from the white fibrous structure of the cotton swab, which causes the deposited dAuNPs to blend into the white background. As a result, the color sharpness diminishes, leading to a less pronounced color change. In contrast, the lower LoD of the tablet sensor in artificial urine can be explained by the complete dissolution of the tablet in the liquid medium. This eliminates any interference from a substrate or medium, resulting in a sharp, high-intensity colorimetric signal. Additionally, the tablet-based assay demonstrated greater consistency in artificial urine, as evidenced by the lower standard deviation of the blank signal. Consequently, this led to a lower LoD based on our calculation method.

The stability of dAuNPs-Tablet and dAuNPs-Swab sensors is another important factor when considering the portability of these platforms because such analytical devices are very likely to be stored for a certain time before being employed in the field. Our previous studies showed that the dAuNPs-Tablet is stable for >one year [583]. The plasmonic swabs after drying were placed in an airtight glass jar and stored in ambient conditions for different intervals of time. The dAuNPs impregnated cotton swab sensing characteristic remained unchanged for 1 month followed by a gradual decrease in its stability up to 40% within three months as shown in Figure 5S7.

Our study presents a novel, nanoparticle-based approach for the detection of $H_2O_2$ using dAuNPs, which offers significant advantages over traditional chromogenic reagents such as TMB (3,3',5,5'-tetramethylbenzidine) and OPD (*o*-phenylenediamine). The traditional chromogenic reagents often present significant drawbacks, including the need for specific storage conditions, light sensitivity, high toxicity, and poor solubility, as well as limitations in portability and specificity. These solutions often need to be freshly prepared before the experiments, making them less suitable for point-of-care diagnostics in non-laboratory settings.

In contrast, the plasmonic properties of dAuNPs enable a clear, visible color change from red to blue in the presence of $H_2O_2$ through the Fenton reaction. The dAuNPs-based assay is straightforward and can be easily adapted into various formats, such as tablets and swabs, enhancing portability and making it suitable for point-of-care diagnostics. Moreover, the biocompatible nature of dAuNPs broadens the applicability of our assay. Furthermore, the dAuNPs tablets demonstrated remarkable long-term stability, retaining functionality for over a year. The high selectivity of this method also ensures minimal interference from other substances, making it a robust and practical method for colorimetric $H_2O_2$ detection.

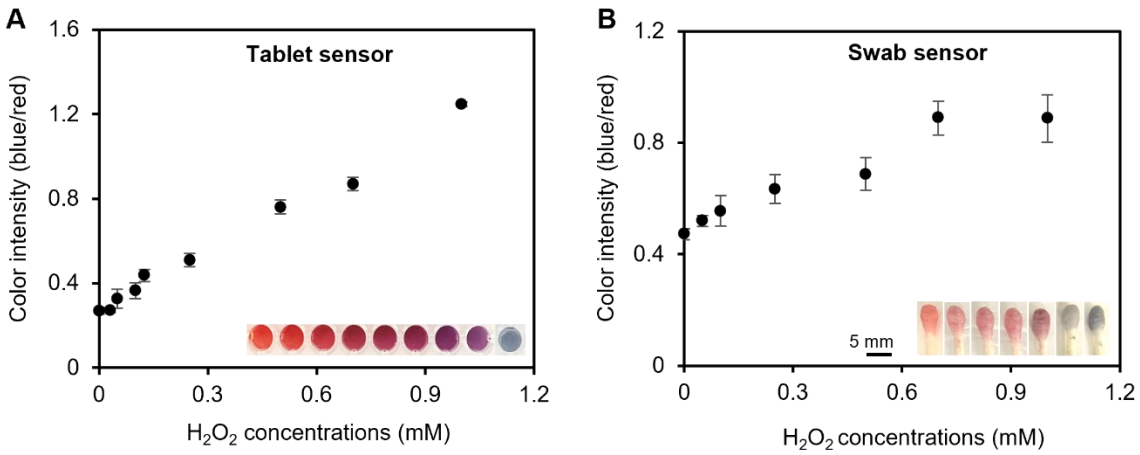


Figure 5.6 Plasmonic tablet and swab sensors for the detection of $H_2O_2$ in artificial urine.
A) The calibration curve showing a linear relationship for $H_2O_2$ detection using dAuNPs-Tablet. An inset shows a gradual color change of a sensing probe; B) The calibration curve for $H_2O_2$ detection using blue/red color intensity of dAuNPs-Swab. An inset shows the color difference in cotton swabs due to varying $H_2O_2$ concentrations.

### 5.3.6 Selectivity of the $H_2O_2$ Assay

The selectivity of the proposed $H_2O_2$ assay was investigated using several competing metal cations ($Na^+$, $K^+$, $NH_4^+$, $Ca^{2+}$, $Mg^{2+}$, $Zn^{2+}$, $Cu^{2+}$), anion ($Cl^-$), and small organic interferants (glucose, uric acid, and ascorbic acid) using plasmonic tablet and swab sensors as shown in Figure 5.7A and 5.7B, respectively. The interferant concentration of cations and $H_2O_2$ was chosen to be 1 mM while 0.1 mM of anion, glucose, uric acid, and ascorbic were added in artificial urine separately. It was observed that the Fenton reaction was unaffected by these interfering chemicals and generated •OH radicle successfully followed by selective detection of urinary $H_2O_2$. As interfering species cause negligible interferences on the aggregation of dAuNPs

by •OH radicle, both tablet and swab sensors can be used to measure urinary $H_2O_2$ which reflects the total body oxidative stress.

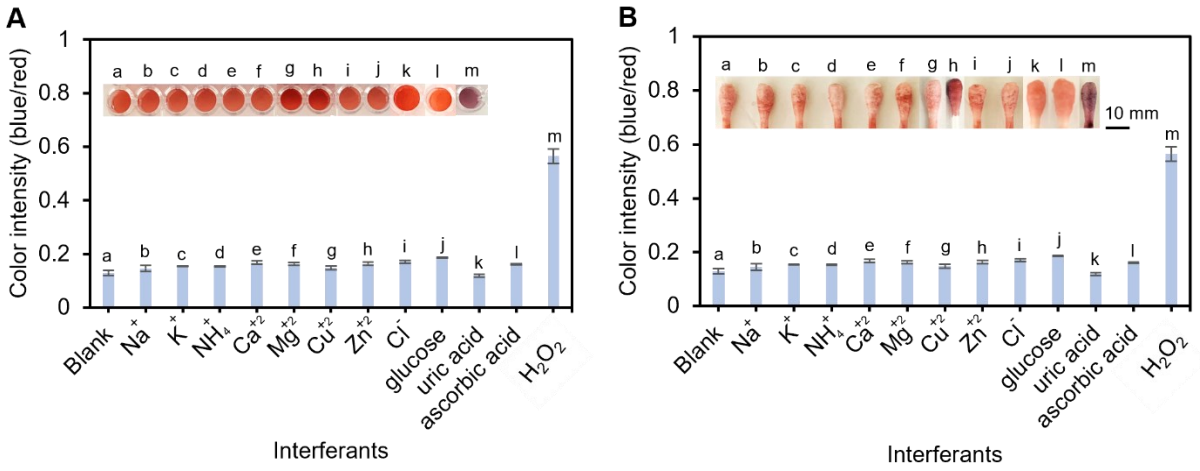


Figure 5.7 Selectivity test in the presence of different potential chemicals in artificial urine. A) Tablet sensor shows a good selectivity towards $H_2O_2$ detection. Optical image in inset showing color changes induced by corresponding interferants; B) A graph showing the selectivity of a swab sensor towards urinary $H_2O_2$ detection. Optical image in inset showing color changes induced by corresponding interferants.

### 5.3.7 Practical Application

Next, we transition from laboratory evaluations to real-world applications, exploring the practical utility of our plasmonic sensors. Our focus shifts to assessing total body oxidative stress through the analysis of urine samples collected from volunteers. Specifically, we investigate the impact of dietary interventions, such as consuming green tea, on oxidative stress levels. This real-world evaluation provides invaluable insights into the efficacy and reliability of our sensor technology in diverse physiological contexts.

The total body oxidative stress was evaluated by performing real sampling analysis against human urine samples of healthy volunteers (female and male) before and after consuming green tea for a specific period. Building upon this investigation, in a case study, we further explored the potential benefits of green tea consumption on oxidative stress levels, as green tea is renowned for its antioxidant properties and its purported ability to alleviate stress. Volunteers, who were carefully selected from the same family to better maintain consistency in dietary habits throughout the study period, were instructed to consume green tea three times a day for a week while their urine samples were collected and analyzed. The higher value of $H_2O_2$ in human urine

is associated with different diseases including urinary tract infections, diabetes, cancer, inflammatory condition, and oxidative stress. Thus, a sensor capable of detecting urinary $H_2O_2$ across a wide concentration range, from low to high levels, is crucial for providing an accurate estimation of a patient's health profile. Such a sensor could offer valuable insights into oxidative stress-related conditions and help in the early diagnosis and monitoring of diseases. Female (F) and male (M) urine samples were used within 1 h of dispense and spiked with low to high concentrations of $H_2O_2$ (160, 200, 250, and 500 μM) followed by adopting the detection procedure (Figure 5.8). This range of $H_2O_2$ concentrations was chosen to demonstrate the assay's capability across a broad spectrum, as $H_2O_2$ levels can vary significantly with the progression of different disease conditions and health scenarios. The amount of $H_2O_2$ in the real samples analyzed in this study were below the detection limit of our sensors, and no quantifiable amounts were detected in unspiked samples. The amount found in unspiked samples was up to 40 μM by calibration curve which is not quantifiable with our sensor. We employed the standard addition method and spiking recovery analysis, as detailed in Table S1, to evaluate the accuracy and applicability of our method. These approaches are critical for assessing potential matrix effects that may influence the analyte signal and for validating the calibration curve for $H_2O_2$ detection. Spiking was performed at varying concentrations to rigorously test the assay's performance and demonstrate its robustness.

The R% for F and M samples were observed in the range of 91-111% and 104-118% respectively using the plasmonic tablet sensor. It is well known that green tea reduces urinary oxidative stress due to the presence of antioxidants[612]. In this study, the same female and male volunteers consumed green tea (200 mL) three times a day for a week then their samples as F-tea (female urine sample after consuming green tea) and M-tea (male urine sample after consuming green tea) were spiked with similar $H_2O_2$ concentration. The R% was found in the range of 84-105% for F-tea and 85-107% for M-tea samples. However, green tea effectively reduced oxidative stress in both female and male. The % reduction in female samples ranged from 0.04 to 5.71%, whereas in male samples, it varied from 0.56 to 16.58% (Figure 5S8). The RSD% of the tablet sensor was in the range of 0.46-4.53 for female samples and 0.84-3.74% for male samples. In addition to RGB analysis of a tablet sensor, we have recorded absorbance values for $H_2O_2$ detection using UV-vis spectrophotometer and results are presented in Figure 5S9.

A similar experiment was repeated with the plasmonic swab sensor using 160, 250, and 500 μM $H_2O_2$ concentrations as shown in Figure 5.8B. The R% of female samples (F) were calculated as 105-120% without green tea and 90-111% after consuming green tea (F-tea) whereas it was observed as 92-119% for M samples and 80-103% for M-tea samples. The decrease in urinary oxidative stress was observed after consuming green tea which was a maximum of 5.41% for female samples and 10.14% for male samples. In brief, the % reduction in oxidative stress after green tea consumption was higher in male volunteer compared to female volunteer. The RSD% of all samples were in the range of 0.25-3.13% showing good precision of the dAuNPs-Swab sensor.

In conclusion, the findings indicate that consuming green tea leads to a reduction in urinary $H_2O_2$ levels. As illustrated in Figure 5.8A and 5.8B, the values before and after spiking in green tea samples (for both female and male subjects) are lower compared to those without green tea consumption. This suggests that the reduction in $H_2O_2$ amount in urine is due to antioxidant properties of green tea. The comparison with other $H_2O_2$ detection methods is summarized in Table 5S2. Markedly, our proposed tablet and swab sensors demonstrate the capacity to detect $H_2O_2$ across a wide range of concentrations, which is particularly significant in the context of disease conditions within the body. The excellent sensing performance can be attributed to: (i) the highly reactive nature of hydroxyl radical (•OH) that degrade the dextran chains attached to the dAuNPs, and (ii) the small size and high dispersion of dAuNPs, which result in a pronounced color change when $H_2O_2$ is used as the analyte.

Colorimetric methods often have higher detection limits (μM range) compared to more sensitive techniques like electrochemical sensors or SERS, which can achieve pM or nM levels. However, the choice of detection method depends on the application and target sample. Our tablet and swab sensor's detection limits are well-suited for detecting oxidative stress-related $H_2O_2$ variations in urine. Further studies on nanoparticle enhancement, e.g., using hybrid nanoparticles and functionalization, can also be conducted to enhance the limit of detection and sensitivity of the assay [613].

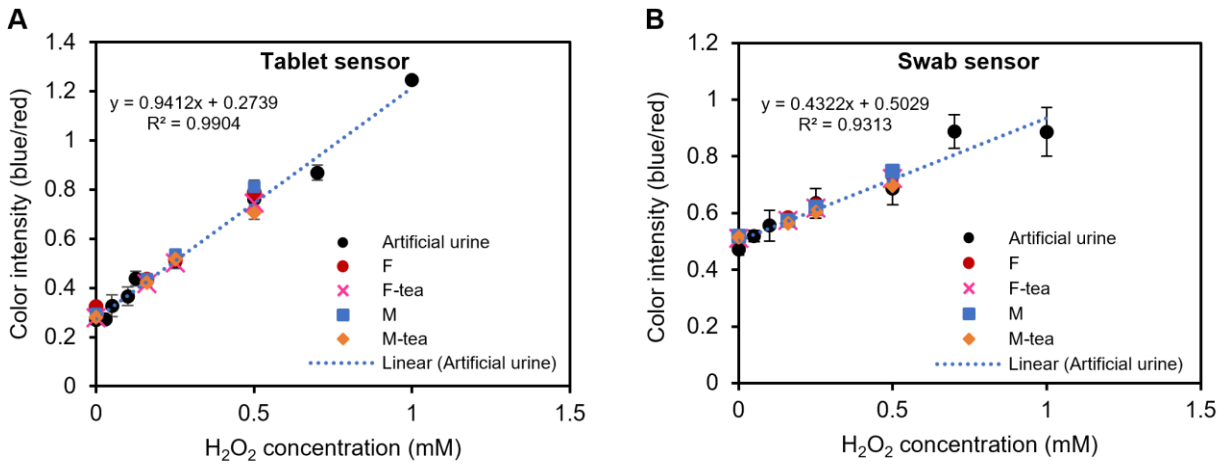


Figure 5.8 Real sample analysis to measure oxidative stress through $H_2O_2$ assay using a plasmonic tablet and swab sensors.
A) A spiking test was conducted using the tablet sensor in female (F) and male (M) urine samples before green tea consumption, along with F-tea and M-tea samples, which were collected after green tea intake; B) A spiking test with a plasmonic swab sensor was performed, showing blue/red color intensity of the swab analyzed using *ImageJ* software. Some data points are not visible on the graph due to the overlapping of data points.

## 5.4 Conclusions

In this study, we introduced a nanoscale-driven approach for determining urinary $H_2O_2$ levels as an oxidative stress biomarker, utilizing two platforms: dAuNPs-Tablet and dAuNPs-Swab. Both platforms were fabricated from the colloidal solution of dextran-gold nanoparticles (dAuNPs-Sol), with post-synthetic incorporation of 2% pristine dextran to enhance nanoparticle stability at the nanoscale. The plasmonic tablet was created through drop casting, while the plasmonic swab was prepared by depositing dAuNPs onto an alkaline-treated cotton swab. $H_2O_2$ detection relied on the aggregation of dAuNPs, initiated by the •OH radicle from $H_2O_2$ *via* the Fenton reaction. This reaction degraded the dextran chains surrounding the nanoparticles, showcasing the critical role of nanoscale interactions in sensor response. Hence, weakly shielded dAuNPs showed aggregation upon the addition of NaCl. The concentration of $H_2O_2$ was quantified by observing the color change of the dAuNPs probe for the tablet and swab using *ImageJ* software, a free open-source software for processing and analyzing scientific images. Calibration curves were established using various $H_2O_2$ concentrations in water and artificial urine, yielding a limit of detection (LoD) of 50 µM for tablet and 100 µM for swab sensor in urine. While the tablet

sensor demonstrated the high stability as compared to the swab sensor which exhibited a gradual stability decline after four weeks.

Both nanoscale platforms demonstrated excellent selectivity for urinary $H_2O_2$ detection, underscoring their potential for specific oxidative stress monitoring. Their practical utility was demonstrated by testing human urine samples (both female and male) before and after green tea consumption. Results indicated a reduction in oxidative stress levels following green tea consumption, with male volunteers showing a greater reduction (up to 16.58%) compared to female volunteers (up to 5.71%). The versatility and affordability of both platforms make them promising candidates for $H_2O_2$ assays and potential broader applications in the detection of other reactive oxygen species (ROS). Moreover, our methodology could extend to the selective detection of ascorbic acid due to its radicle scavenging activity. Overall, our nanoscale-focused approach represents an advancement in point-of-care diagnostics, contributing significantly to the field of ready-to-use colorimetric sensors and paving the way for more accessible, portable healthcare solutions.

# CHAPTER 6 Development of a Dual-Functional Nanogold Tablet for Biomedical Sensing of Glucose and Uric acid

**This chapter is reproduced from the article published in *Nanoscale Advances* (2025).**

This chapter presents an advancement in tablet technology, transitioning from a plasmonic tablet to a dual-functional tablet that enables a highly selective colorimetric-chromogenic assay. Leveraging the plasmonic and nanozyme properties of dextran-gold nanoparticles (dAuNPs), the dual-functional tablet is used for the detection and quantification of uric acid and glucose in urine. This tablet sensor contributes to the advancement of point-of-care devices, offering a user-friendly assay for rapid diagnosis.

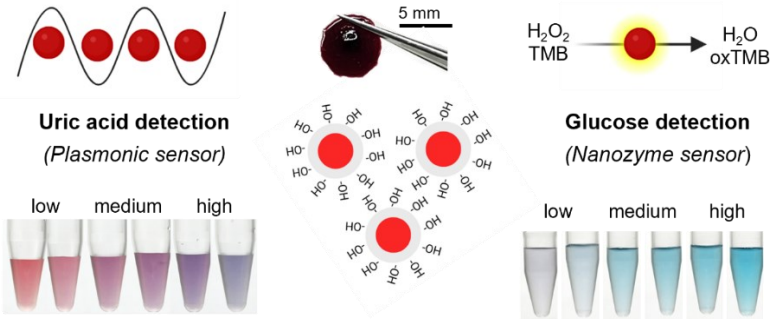

## 6.1 Introduction

The tablet platform presents a versatile and attractive tool for point-of-use detection across various fields, including food industry, environmental monitoring, forensic analysis, and disease diagnostics [614]. Tablets containing solid reagents can be produced through direct compaction of powder mixtures, while liquid reagents are encapsulated by polysaccharides using a drop-casting method. For instance, Udugama et al. developed compressed tablets by blending lyophilized powder with mannitol sugar, chosen for its bulking properties, to create chemical diagnostic assays such as nucleic acid and protein tests [614]. In the drop-casting technique, pioneered in 2014 by our group, different detection reagents, including enzymes and its substrates, and nanoparticles are encapsulated within polysaccharides such as pullulan and dextran to give tablets [615]. This approach enabled the release of reagents for point-of-use applications such as pesticide and hypochlorite detection in water, as well as glucose and cysteamine detection in bio-fluids [34,616–618].

Compressed tablets offer benefits such as high throughput and enhanced dissolution rates, but uniform mixing of reagents necessitates either specialized equipment or labor-intensive processes, along with the use of molds for fabrication. In contrast, the drop-casting approach is simpler, requiring only the pipetting of solutions with pre-optimized concentrations. Overall, tableting technology allows for customizable tablets that hold premeasured quantities of components. Furthermore, labile reagents can be preserved within tablets, preventing reagent degradation due to hydrolysis or oxidation. The tablet form also facilitates safe transportation of chemicals, while making it a user-friendly detection platform for point-of-care (POC) applications.

Hyperuricemia, a condition characterized by elevated uric acid levels, can be measured using both enzyme-based and enzyme-free methods [619]. While enzyme-based methods are sensitive, they are also indirect and expensive, relying on the uricase enzyme to catalyze uric acid, with the resulting hydrogen peroxide ($H_2O_2$) detected to quantify uric acid concentration [620,621]. In enzyme-based approaches, electrochemical sensing in sweat and saliva samples is frequently employed, utilizing materials such as uricase embedded zeolitic metal azolate framework-7 [622], silver nanowires-Prussian blue composite aerogel [621], and uricase-immobilized paper [620]. These methods, however, necessitate labor-intensive preparation of the conducting

electrodes and require an electrochemical workstation for signal read-out. On the other side, enzyme-free methods, though less explored, pose a greater challenge due to their dependence on direct chemical interactions between uric acid and sensing agents [623,624]. In one such approach, uric acid was detected using 2-thiouracil functionalized gold nanoparticles (TU-AuNPs), where hydrogen bonding and π-π interactions between TU-AuNPs and uric acid served as molecular recognition elements. The plasmonic property of TU-AuNPs enabled colorimetric detection [624]. However, the high concentration of 2-thiouracil used during functionalization caused self-aggregation of the particles, reducing their stability and limiting their utility in uric acid sensing. Conversely, a high concentration of uric acid led to an opposite effect due to anti-aggregation or etching behavior resulting in blue to red coloration [623]. Hence, this sensor requires extensive optimization and careful observation of the detection mechanism.

Glycosuria, characterized by elevated levels of glucose in the urine, occurs when blood glucose concentration surpasses the renal threshold or when the renal tubular reabsorption capacity is diminished. In such cases, excess glucose is excreted into urine without being metabolized by the body. Therefore, monitoring urine glucose levels is crucial for diagnosing diabetes and assessing potential declines in kidney function [625]. The hybrid glucose oxidase (GOx)/horseradish peroxidase (HRP) assay remains the gold standard for glucose detection. Recently, our group encapsulated both enzymes (GOx and HRP) within a dextran-based tablet sensor for detecting glucose in urine [626]. In another study, we replaced HRP with an inorganic enzyme-mimic nanomaterial—pullulan-gold nanoparticles (pAuNPs)—which exhibited peroxidase-like nanozyme activity in the oxidation of 3,3′,5,5′-tetramethylbenzidine (TMB) during glucose assay [616]. This tablet sensor demonstrated potential as a point-of-care (POC) tool for single-analyte detection, though further optimization is needed to advance the technology. In another report, a bifunctional sensing platform composed of polylactic acid and polyethylene glycol fiber mats has been developed for detecting urinary glucose in the range of 1.0 to 6.0 mM [627]. However, the electrochemical deposition of Prussian blue nanoparticles on the treated mat involves complex pretreatment, complicating the sensing process. Given these limitations, there is an increasing demand for a more user-friendly glucose assay in POC settings. Urine, being a non-invasive sample that maintains its integrity over time, presents an ideal biofluid for POC glucose monitoring, offering both convenience and practicality.

Dual-detection sensors developed for monitoring both uric acid and glucose must exhibit sensitivity within physiologically relevant ranges, with limits of detection (LoD) low enough to differentiate between pathological conditions such as hypouricemia and hypoglycemia from normal levels. In urine, the physiological range for uric acid is 1.40 - 4.44 mM [628], while glucose levels should not exceed 2.8 mM *(see Table 6S1 for details)* [629]. Maintaining healthy uric acid and glucose levels is essential to prevent conditions such as kidney stones, gout, diabetes, hypertension, and cardiovascular diseases [630]. Dual detection of uric acid and glucose has been employed using carboxyl functionalized multiwall carbon nanotubes and Prussian blue-glucose oxidase composite electrodes printed on a rubber glove [630]. This electrochemical sensor offers simultaneous detection but involves lots of chemicals and requires time-consuming multistep procedure to prepare the electrode. In another study, luminescent sweat tape was introduced to detect uric acid and glucose using enzyme-embedded gold nanoclusters wrapped by $MnO_2$ nanosheets as the sensing probe [631]. Utilization of uricase and GOx besides the requirement of an external light source for signal read-out makes this sensor less practical. Such wearable biosensors are not ideal for POC settings. Therefore, a simple dual-functional POC device capable of measuring both hyperuricemia and glycosuria are crucial for tracking an individual's overall health profile.

In our previous work, we demonstrated that dextran-gold nanoparticles (dAuNPs) could be encapsulated in tablet form to simplify assay procedures and eliminate the need for specific storage conditions [33]. These customizable tablets were successfully applied for in-field detection of hypochlorite [34], as well as point-of-care detection of glucose and cysteamine [616,632]. In this study, we present the first showcase of a dual-functional tablet for the detection of two analytes: uric acid and glucose. We produced these dual-functional tablets using dAuNPs through a simple, one-pot method without requiring reflux conditions. The dAuNPs solution was prepared under ambient conditions and used directly to cast tablets without any additional chemicals. The as-prepared dAuNPs solution contained an optimized amount of dextran, sufficient to produce solid, stable tablets capable of detecting both uric acid and glucose colorimetrically. This was achieved by leveraging the plasmonic and nanozyme properties of the dAuNPs (Figure 6.1). The colorimetric results were digitized using a UV-vis spectrophotometer, and the concentrations were calculated based on a calibration curve. Our dual-functional tablet

proved to be highly efficient for both plasmonic and nanozyme-based sensing, paving the way for future designs of POC diagnostic devices.

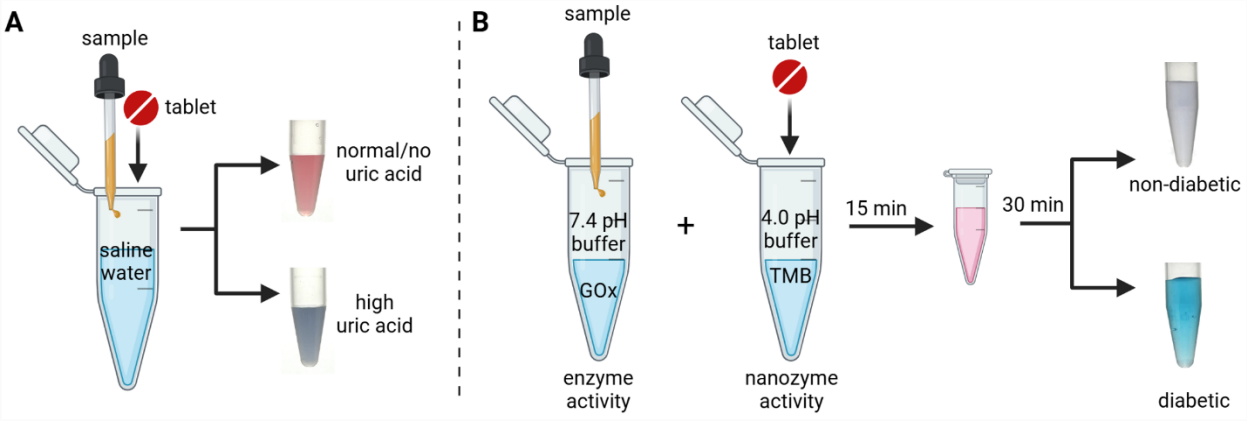


Figure 6.1 Assay workflow with a dual-functional tablet sensor for uric acid and glucose detection in urine samples.
A) The tablet acts as a plasmonic sensor showing a blue color read-out due to the aggregation of dAuNPs when uric acid is high; B) The same tablet acts as peroxidase mimetic nanozyme showing a blue color read-out due to by oxidizing a chromogenic substance when the glucose level is high.

## 6.2 Experimental Section

### Chemicals and Instruments

Full details are provided in the Supporting Information (SI) file for Chapter 6.

### 6.2.1 Synthesis of dAuNPs and Formation of Direct and Indirect Tablets

The dAuNPs were prepared according to a previously reported method with considerable modifications [633]. First, dextran (400 mg) was dissolved in 20 mL of alkaline water (1 M NaOH, 300 µL) under magnetic stirring followed by the addition of $HAuCl_4$ (1 mM, 13.8 µL). The resulting mixture remained at room temp (20 °C) under stirring for 10 min to prepare dAuNPs colloidal solution. The tablet was fabricated directly from this colloidal solution using the drop-casting method as per our previously established protocols [33]. The tablet produced from this method is called a direct tablet. We also produced indirect tablets following our pre-established procedure [34]. In short, the dAuNPs solution was synthesized under reflux conditions using $HAuCl_4$ (1 mM, 17.22 uL in 25 mL water), dextran solution (5%, 50 µL), and NaOH solution (1 M, 50 µL). Next, an additional amount of dextran (497 mg) was added post-synthetically to the gold solution followed by tablet casting. The tablet produced from this

method is called an indirect tablet. One direct or indirect tablet is formed by drop casting 100 $\mu$L of dAuNPs solution.

### 6.2.2 Procedure for the Detection of Uric Acid

To optimize the experimental conditions, the impact of different concentrations and volumes of the agglomerating agent (NaCl) was studied. A mixture of 100 µL NaCl solution (0.5, 1.0, 1.5, 2.0, 2.5, 3.0 M) and 100 µL dAuNPs solution was prepared. Also, 30, 50, 100, 150, and 200 µL of aqueous NaCl (2 M) was added to agglomerate the dAuNPs solution. After determining the optimal NaCl concentration and volume of NaCl, the uric acid amount was determined using the plasmonic characteristics of the dual-functional tablet. The stock solution of uric acid (125 mM) was prepared by dissolving 126 mg of uric acid in KOH (1M, 2 mL) followed by the addition of deionized water (4 mL). A serial dilution (up to 1.8 µM) was used in this study. In a micro tube, 100 µL of the standard uric acid solution was mixed with 50 µL of the agglomerating agent solution (2M NaCl), followed by the addition of 200 µL of deionized water and one direct tablet. The color of the dAuNPs solution gradually changed from bright red to purplish blue, indicating nanogold particle agglomeration. The UV-vis spectrometer was then used to detect uric acid in the solution. The excitation wavelength was recorded at 520 and 650 nm. Indirect tablet and dAuNPs solution were also used for uric acid determination. The selectivity of the method for uric acid detection was evaluated by adding a series of potential interfering substances (100 mM) including inorganic ions (i.e., sodium, potassium, ammonium, magnesium, calcium, chloride, phosphate, sulfate), and small molecules (i.e., maltose, fructose, lactose, trehalose, urea, glucose, ascorbic acid) to the sensing system in the absence of uric acid according to the above-mentioned procedure.

### 6.2.3 Procedure for the Detection of Glucose

Initially, the TMB solution (0.41 mM, 300 $\mu$L) was added with $H_2O_2$ (0-500 mM, 100 µL) to cetate-phosphate buffer (pH 4.0) along with one direct tablet. The mixture was incubated at 37 °C for 30 min before recording absorbance of the solution at 652 nm. Next, glucose sensing was performed in a chromogenic detection system by incubating the GOx and POx-mimetic nanozyme, separately. First, GOx (20 µL) and different glucose concentrations (0-20 mM, 80 $\mu$L) were added into 200 mL of phosphate buffer (pH 7.4) while one direct tablet as POx-mimetic nanozyme and TMB (300 µL) were added into 300 mL of citrate-phosphate buffer (pH

4.0) in a separate microtube. Both microtubes were incubated at 37 °C for 15 min. Next, the contents of both microtubes were mixed and incubated at 37 °C for another 30 min. Finally, 200 µL of the reaction solution was added to the 96-well plate, and the absorption at 652 nm was recorded in a microplate reader. A similar experiment was repeated with an indirect tablet and dAuNPs solution. To investigate the selectivity of glucose, different aqueous solutions (100 mM) of inorganic ions (sodium, potassium, ammonium, magnesium, calcium, chloride, phosphate, sulfate) and small molecules (maltose, fructose, lactose, trehalose, urea, ascorbic acid, uric acid) were chosen as the interfering substances.

### 6.2.4 Analysis of Real Samples

This work was carried out with the consent of Concordia University's Institutional Review Board, with approval number SC5823 and BioPermit number B-SJA-22–01. Additionally, both written and verbal informed consent were obtained from the subjects. The real urine samples from a female and a male volunteer were treated by centrifugation (14,000 rpm, 15 min) before detection. Uric acid with different dosages (low to high concentrations) was added to real samples to carry out the spiking experiment. Similarly, glucose was spiked to the urine samples and the detection procedure was followed as mentioned in section 2.3. The method was validated by determining the percent recovery (%R) and percent relative standard deviation (%RSD) of the results.

## 6.3 Results and Discussion

### 6.3.1 Synthesis and Characterization

A colloidal dextran-gold nanoparticles (dAuNPs) solution was prepared using a simple one-pot, one-phase wet-chemical reduction method and subsequently utilized to fabricate tablets by two methods: direct and indirect. The dAuNPs solution for the direct tablets was synthesized at room temperature using hydrogen tetrachloroaurate ($HAuCl_4$) and dextran powder in an alkaline aqueous medium (Figure 6.2A). Notably, we did not observe particle formation without the addition of sodium hydroxide, which served as the initiator for Au particle formation. The absorption value of the dAuNPs gradually increased with reaction time, with the suspension turning wine red, reaching maximum absorption after 10 minutes, which remained unchanged thereafter.

During the first 2 minutes, the reduction of the gold salt by dextran results in the formation of gold nuclei, which then begin to aggregate. Particle growth occurred through both aggregation and the deposition of additional gold atoms onto the particles [634]. Over the next 3 minutes, the degree of aggregation increased, resulting in a bright red solution, with stable dAuNPs forming shortly thereafter and remaining unchanged. Dextran played a dual role in the synthesis, acting as both a reducing agent and a stabilizer, preventing agglomeration of the Au particles. As per the IUPAC definition, an agglomeration refers to a situation where dispersed particles are bound by weak physical interactions, resulting in phase separation through the development of precipitates bigger than colloidal size, with the entire process being reversible. On the other hand, aggregation is characterized by the presence of tightly bound colloidal particles, and the clustering process is irreversible [635]. Aggregation or agglomeration is a dynamic process influenced by various elements, including temperature, light, surrounding environment, and the chemical properties of the surface ligand. Solution-phase synthetic approach prevents agglomeration through surface functionalization and regulation of surface charge [636].

The ratio of gold to dextran controlled the size variation of the dAuNPs, with higher dextran concentrations producing smaller particles. Additionally, dextran's tablet-forming properties allowed for the direct formation of tablets from the dAuNPs solution, providing the colloidal solution containing at least 2% dextran (w/v). For our synthesis, we used 2% dextran, maintained a basic pH (~8), and successfully fabricated solid tablets directly from the dAuNPs solution. The concentration of the dAuNPs solution was estimated to be ~261 nM by Beer's-Lambert law using a UV-vis spectrophotometer based on an approximate extinction coefficient (ε) of $8.56 \times 10^6$ $M^{-1}$ $cm^{-1}$ at 520 nm for 5 nm particles [637]. The weight of a direct tablet is 1.8 ± 0.2 mg. The resonance absorption band of the dAuNPs solution appeared at 520 nm with a narrow size distribution, indicating the monodispersity of the particles. This result was consistent with transmission electron microscopy (TEM) images, which revealed a uniform distribution of spherical Au particles with a size of 5 nm. The zeta potential of the Au species in solution was -11.18 mV, and the hydrodynamic size was measured to be 276 nm (Figure 6.2B).

We captured high-resolution surface images of a direct tablet without stains using the AFM scanning probe microscopy, as shown in Figure 6.2C. The images showed that the nanogold particles were fully embedded with their surroundings and almost uniformly distributed

throughout the solid tablet, as evidenced by the phase trace (6.2Ci). The phase trace image indicates that the particles have a spherical shape, as confirmed by the TEM image. The two-dimensional height profile of a direct tablet demonstrates surface roughness and waviness attributes. The maximum roughness is 2.7 nm, and maximum waviness is 2.3 nm. The dextran matrix stabilizes the dAuNPs due to the interaction between the gold nanoparticles and dextran's free alcoholic hydroxyl groups [33]. This interaction enhances the stability and dispersion of the dAuNPs. So, AFM analysis showed that the particles are fully spread on the polysaccharide surface. As previously reported, the morphology of the Au particles in the solid tablet remained consistent with those in solution, demonstrating the usefulness of this method for sensing and detection applications [33]. Our approach provides a direct method for tablet formation, eliminating the need for post-synthetic mixing, and making it a straightforward and efficient alternative to solution-phase dAuNPs.

In contrast to the direct tablet preparation, reflux conditions were required to synthesize the dAuNPs solution for indirect tablets, which were formed after the post-synthetic addition of dextran to the dAuNPs solution (Figure 6S1). Initially, 0.01% dextran was employed as both a reducing and capping agent in an alkaline medium to synthesize the colloidal dAuNPs solution. Dextran, a reductive polysaccharide with abundant hydroxyl and ether functionalities, surrounds the Au ions, providing stabilization and preventing agglomeration. Dextran chains provide a repulsive surface capping layer around Au nanoparticles. If the capping layer is disrupted, the dAuNPs will agglomerate to form aggregates [35]. During the reaction, the $HAuCl_4$ is reduced by dextran, leading to the formation of stable dAuNPs.

Subsequently, additional dextran was added to the synthesized dAuNPs solution to achieve an overall concentration of 2%. This post-synthetic addition of dextran is essential for the formation of a rigid solid tablet, referred to as an indirect tablet. The formation of such indirect tablets has been reported in our previous work [34]. The values of zeta potential and hydrodynamic size in indirect tablets primarily depend on the concentration of dextran in dAuNPs solution. With increasing the dextran contents in the nanogold colloidal solution, zeta potential decreases and hydrodynamic size increases. The as-synthesized nanogold colloidal solution with 0.01% dextran has a zeta potential of -41.83 mV and a hydrodynamic diameter of 79.95 nm. The post-synthetic addition of 1.99% dextran shifts the value to -10.80 mV and 292.30 nm. The decrease of

negative charge at the surface of dAuNPs results from external neutral dextran that gradually establishes a diffuse layer around dAuNPs surface, partially neutralizing their negative charge. The increased hydrodynamic size results from the thickening of the dextran layer surrounding the Au particles, as previously reported by our group [34]. Optimal sensitivity in detection is attained with reduced dextran content [34]. This study utilizes a 2% dextran concentration in colloidal solution, which is the minimum necessary for tablet casting in both direct and indirect methods. The distinction between direct and indirect tablets lies in the incorporation of dextran; direct tablets include the entire amount of dextran all at once, whereas indirect tablets involve a two-steps addition, with 0.01% dextran introduced during synthesis and 1.99% added after synthesis. The zeta potential and hydrodynamic diameter values are comparable in both tablets.

It is noteworthy that the position of the maximum absorption peaks remained unchanged, regardless of the preparation method of the dAuNPs solution. Furthermore, the sizes of the dAuNPs were difficult to distinguish using UV–Vis spectra when both samples were synthesized in aqueous media with dextran as the capping agent. In this work, dextran-coated Au particles require no further surface modification for sensing applications. As a result, dAuNPs act as fully functional nanoprobes and are well-suited for sensor fabrication, offering an efficient platform for various sensing applications. Throughout this study, we used tablets created using the previously mentioned direct method, otherwise mentioned. Both the direct and indirect tablets exhibit high inertness to atmospheric conditions and can be stored at room temperature, maintaining stability for over a year, as previously reported [33,616]. The distinguishing features of direct and indirect tablets can be found in Table 6S2.

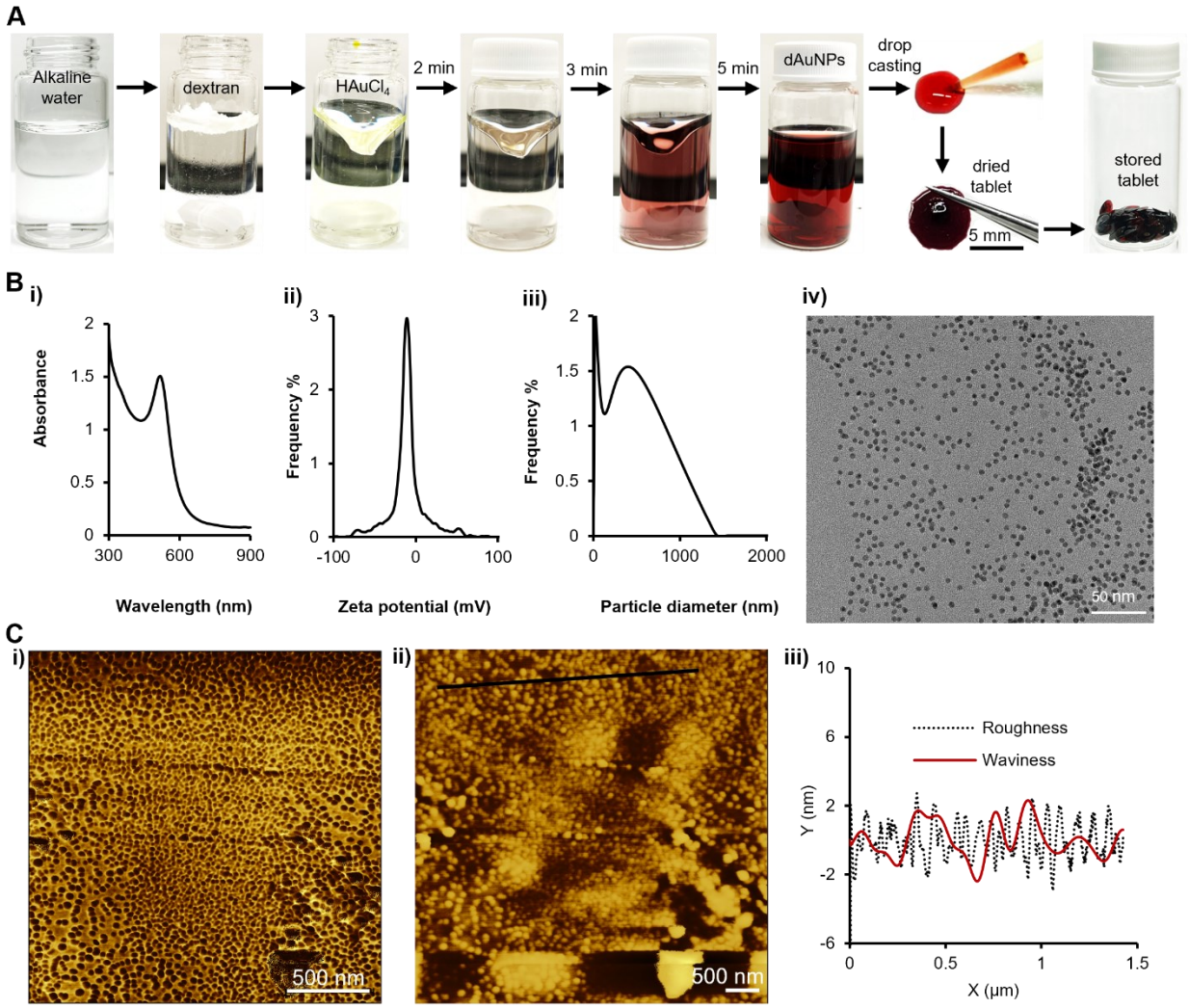


Figure 6.2 Preparation and characterization of a dual-functional tablet.
A) The dAuNPs solution is synthesized at room temperature using a chemical reduction method followed by a tablet formation directly from the colloidal solution through drop casting technique; B) Morphology characterization of nanomaterial in the tablet as i) UV-vis spectrum, ii) zeta potential, iii) hydrodynamic size of particles, and iv) TEM analysis; C) AFM images showing the surface morphology of the direct tablet as i) the phase trace image showing the dispersed state of nanoparticles, ii) the height trace 2D topographic image, iii) height distribution as surface roughness and waviness in graph along the black line area of image (ii).

### 6.3.2 Mechanistic Insights of the Dual-Functional Tablet Sensor

Gold nanoparticles are excellent nanoscale material for colorimetric detection due to their unique optical properties [10,638,639]. After successful fabrication and thorough characterization of the tablets, the dAuNPs have been extensively studied for their sensing and catalytic capabilities. Our dual-functional tablet incorporates ~5 nm spherical dAuNPs, which exhibit both plasmonic

response and peroxidase (POx)-mimetic activity for the detection of uric acid and glucose, respectively. We leveraged these dual-functionalities in our sensing system. The plasmonic colorimetric response is based on a uric acid-induced color change in the dAuNPs, as illustrated in Figure 6.3A. The carbonyl moieties of uric acid to form hydrogen bonds with the hydroxyl groups of dextran, cause dAuNPs aggregation. The existence of $\pi$-$\pi$ interactions and hydrophobic forces further reduce the interparticle distance, promoting this aggregation [624]. Additionally, the ionic nature of salt (i.e., sodium chloride) enhances this aggregation. The aggregation of nanoparticles alters their optical properties, causing a visible red-to-blue color shift that aids in the colorimetric identification of target agents. The gold nanoparticles undergo agglomeration at lower analyte concentrations but aggregation at higher concentrations, as reported in the literature [640]. The visible color change in the solution corresponds to the change in the spectral profile of dAuNPs, which allows for the quantification of uric acid. This method is highly sensitive and selective, effectively distinguishing uric acid even in the presence of coexisting interferents in urine samples.

For glucose detection, the dual-functional tablet operates as a nanozyme sensor *via* a chromogenic reaction with TMB (Figure 6.3B). The peroxidase-like activity of dAuNPs catalyzes the oxidation of TMB substrate in the presence of hydrogen peroxide ($H_2O_2$). The $H_2O_2$ and TMB adsorb on the surface of dAuNPs and their proximity on the surface enhances the reaction efficiency. Also, nanogold particles' intrinsic nanozyme activity depends on the nature of their surface charges, which can be either positive or negative. The negative surface charge significantly enhances the affinity of nanoparticles for the peroxidase substrate (TMB) *via* electrostatic attraction in mildly acidic conditions [616]. Initially, $H_2O_2$ decomposes into reactive oxygen species (e.g., hydroxyl radicals (•OH), superoxide anions ($O_2^{\bullet -}$), which oxidize TMB due to the two readily oxidizable amino groups on its benzidine core. The negative charge on dAuNPs, owing to the presence of the hydroxyl group, attracts the positively charged amino group of oxTMB, thereby facilitating the nanozyme process. The resulting oxTMB is a colored product, formed through a one-electron route which shows an absorption peak at 652 nm [616]. The intensity of this peak directly correlates with the amount of $H_2O_2$, which in turn reflects the glucose concentration in the sample. Our dual-functional tablet sensor demonstrates excellent performance in detecting both uric acid and glucose. The plasmonic response is driven by the

high molar extinction coefficient of dAuNPs, while the nanozyme activity is enhanced by their small particle size, ensuring a highly efficient and sensitive detection method for both analytes.

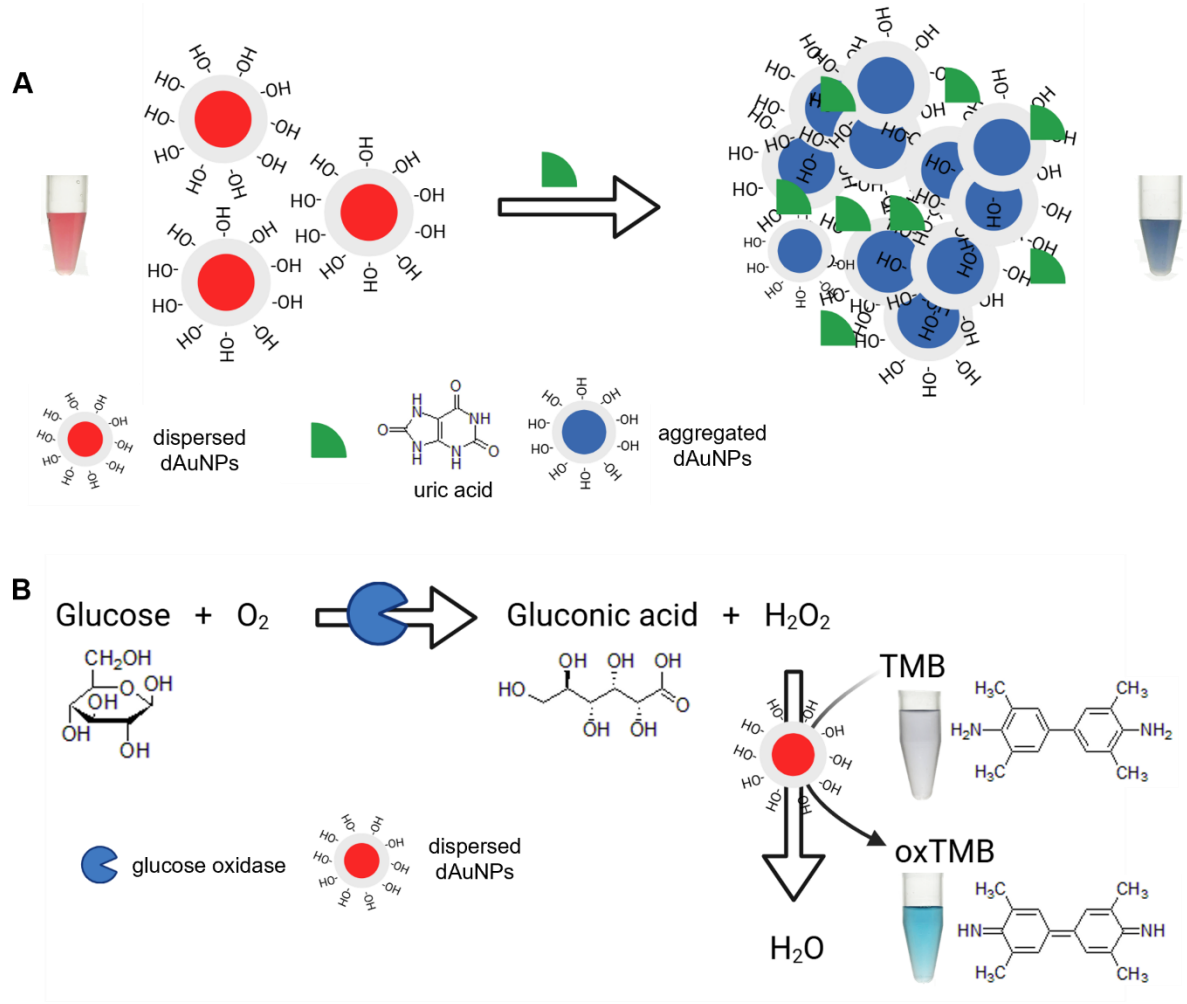


Figure 6.3 Schematic mechanism for dual-functional tablet sensor.
A) The tablet acts as a plasmonic sensor detecting uric acid; B) The tablet acts as a nanozyme sensor detecting glucose.

### 6.3.3 Dual-Functional Tablet Sensor for Uric Acid Detection

This section focuses on the optimization studies and the detection of uric acid using the plasmonic properties of a dual-functional tablet, followed by an analysis of selectivity and spiking results.

*6.3.3.1. Optimization studies*

The direct tablet was employed to optimize reaction conditions, including variables such as the concentration and volume of NaCl, as well as the kinetics of the uric acid assay (Figure 6.4).

Optimal experimental conditions were determined by measuring absorbance at 520 nm and 650 nm, which represent the dispersed and aggregated states of Au nanoparticles, respectively. It was found that 2M NaCl (100 µL) did not cause a visible color change in the dAuNPs tablet, indicating that this condition did not interfere with the uric acid assay but rather enhanced signal intensity. The salt concentration >2M induced aggregation without analyte, hence unsuitable for the detection system. Next, the volume of 2M NaCl was optimized to obtain the best working ratio. The volume of 100 µL of NaCl was selected to enhance the signal intensity. Finally, the reaction kinetics revealed a 20-minute window for maximum color development (Figure 6.4).

It is important to mention that we have examined the impact of varying pH levels on uric acid detection. We have evaluated various buffer solutions with pH levels from neutral to alkaline, including phosphate buffer at pH 7.0, Tris-HCl buffer at pH 7.4, and $KH_2PO_4$-NaOH buffer at pH 8.2. Since acidic conditions cause aggregation of the dAuNPs tablet, we refrained from utilising an acidic buffer. None of the buffer system were effective for uric acid detection, as we did not see a gradual colorimetric response with varying concentrations of uric acid. The failure of the buffer system in this assay is attributed to the significant pH variation induced by varying amounts of uric acid in the test solution. The pH of a standard uric acid solution is ~12, while the pH of the dAuNPs colloidal solution is ~8 due to its alkaline-assisted synthesis. The pH of the test solution remained ~11 up to the uric acid content of 1.95 mM. However, at higher uric acid concentration, the pH increased, reaching ~13 at 62.50 mM. This significant pH change within the uric acid concentration range makes uric acid detection impractical in a buffered system.

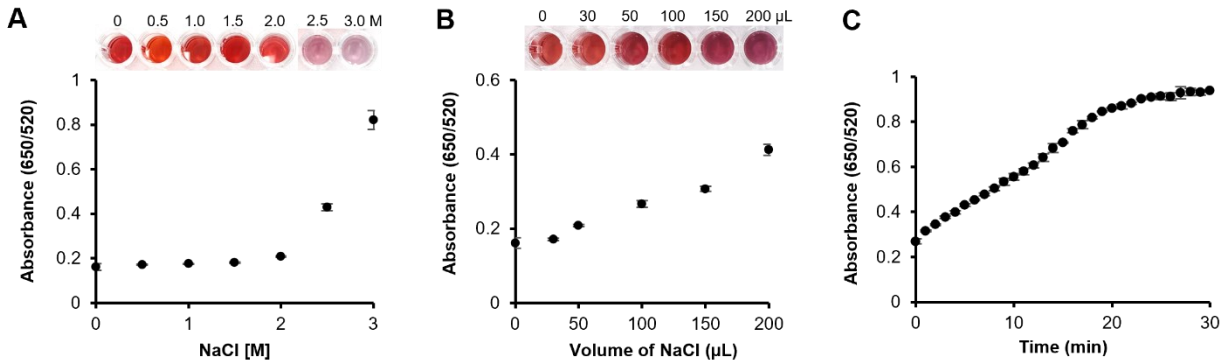


Figure 6.4 Optimization of assay for uric acid detection using a direct tablet.
A) Variable concentrations of NaCl were tested; B) Different volumes of NaCl were used; C) Kinetic study.

*6.3.3.2. Quantitative analysis of uric acid*

A calibration plot for uric acid detection was generated using the absorbance ratio (650/520), as shown in Figure 6.5. The bright red color of Au nanoparticles shifts to violet-blue in the presence of uric acid and the optimized amount of NaCl. The dextran chains surrounding the dAuNPs not only provide particle stability but also serve as functional units, facilitating interactions with uric acid. In particular, the carbonyl group of uric acid may form hydrogen bonds with the hydroxyl group of dextran, reducing the interparticle distance and inducing aggregation of the dAuNPs. As shown in Figure 6.5B, the absorbance ratio (650/520) increases proportionally with the concentration of uric acid. Sodium chloride enhances the intensity of particle aggregation, improving the sensitivity of the assay. A Hill function was used to fit the data of the calibration curve, giving an $R^2$ value of 0.98, indicating a strong fit with the data. This confirms that the data follows a typical saturation behavior, consistent with the sensor's expected performance. The limit of detection (LoD) was calculated as three times the standard deviation of the blank signal added to the mean signal of the blank. The direct tablet sensor demonstrated a working range of 0.00375 to 7.8 mM, with an LoD of 0.0037 mM, which is in the biologically relevant range and makes it a reliable tool for uric acid detection. The ultra-wide working range and low LoD are attributed to the strong plasmonic response of dAuNPs, which amplifies the sensitivity of uric acid detection, resulting in a lower LoD. The use of NaCl as a signal amplifier further improves signal transduction, rendering absorbance changes highly responsive to variations in uric acid concentration. Furthermore, the surface of dAuNPs is optimized with dextran chains to ensure selective binding with uric acid, hence minimizing non-specific interactions and enhancing both the sensitivity and range. The sensor's distinct color change from red to blue, caused by dAuNPs aggregation in the presence of uric acid, is easily detectable even at minimal concentrations.

Our proposed uric acid assay is suitable for POC applications. We employed smartphone-assisted quantification of uric acid with ImageJ software to illustrate this. The color intensity of each uric acid working solution was quantified, and a calibration curve was generated, as illustrated in Figure 6S2. A sigmoidal curve was obtained for the concentration range of 0–62.50 mM, with an LoD of 0.0037 mM. A gradual change in color intensity is evident in the logarithmic scale graph (Figure 6S2B). To guarantee precise colour selection and uphold uniformity in height and angle throughout image acquisition, we utilized our laboratory-constructed imaging apparatus with

regulated lighting and a stationary sample holder. Therefore, a dual-functional tablet sensor is applicable for uric acid detection in POC scenarios.

The working range of uric acid detection can be adjusted by utilizing different nanoprobes, such as indirect tablets and as-prepared dAuNPs solution. The indirect tablet exhibited a working range of 0.0075 to 15.6 mM, with a limit of detection (LoD) of 0.0075 mM, while the dAuNPs solution demonstrated a range of 0.03 to 1.95 mM with an LoD of 0.03 mM (Figure 6S3). Calibration plots include data represented as the mean and standard deviation from three independent measurements.

*6.3.3.3. Selectivity analysis*

To assess the selectivity of the dual-functional sensor, several potential interfering substances commonly found in human urine, including various inorganic ions ($Na^+$, $K^+$, $NH_4^+$, $Mg^{2+}$, $Ca^{2+}$, $Cl^-$, $HPO_4^-$, $SO_4^{2-}$) and small molecules (maltose, fructose, lactose, trehalose, urea, glucose, ascorbic acid), were tested at 100 mM concentrations in the detection system without uric acid. As shown in Figure 6.5C, none of these interferants affected the absorbance ratio, confirming the high selectivity of the sensor for uric acid.

*6.3.3.4. Validation with real samples*

The plasmonic properties of the dual-functional tablet sensor were further utilized for uric acid detection in real urine samples. First-morning urine samples were collected from a male and female volunteer, centrifuged at 14000 rpm for 15 min, and the supernatant after spiking with 0.48, 3.9, and 15.6 mM uric acid was used for analysis (Figure 6.5B). The recovery percentage (%R) for male urine samples were 116 ± 2.2, 108 ± 3.3, and 103 ± 1.9, while those for female urine samples were 103 ± 3.1, 111 ± 1.4, and 110 ± 1.7, confirming the assay's accuracy. The assay showed excellent precision and reproducibility, with percent relative standard deviations (%RSD) values below 3% for all samples, each analyzed in triplicate. The spiking analysis confirmed the successful application of the proposed sensor for uric acid detection in real urine samples, showing its potential for clinical applications and daily monitoring. Moreover, this sensor is not limited to detecting uric acid in urine; with the appropriate dAuNPs nanoprobe, it can be adapted to detect uric acid in other biofluids. For instance, uric acid detection in serum can be achieved using direct or indirect tablets, as their operational ranges (0.00375-7.8 mM or

0.0075-15.6 mM) align with the required uric acid level in serum (0.120–0.400 mM). This optimal detection capability makes the tablet sensor highly suitable for serum analysis, thereby expanding its utility in POC settings.

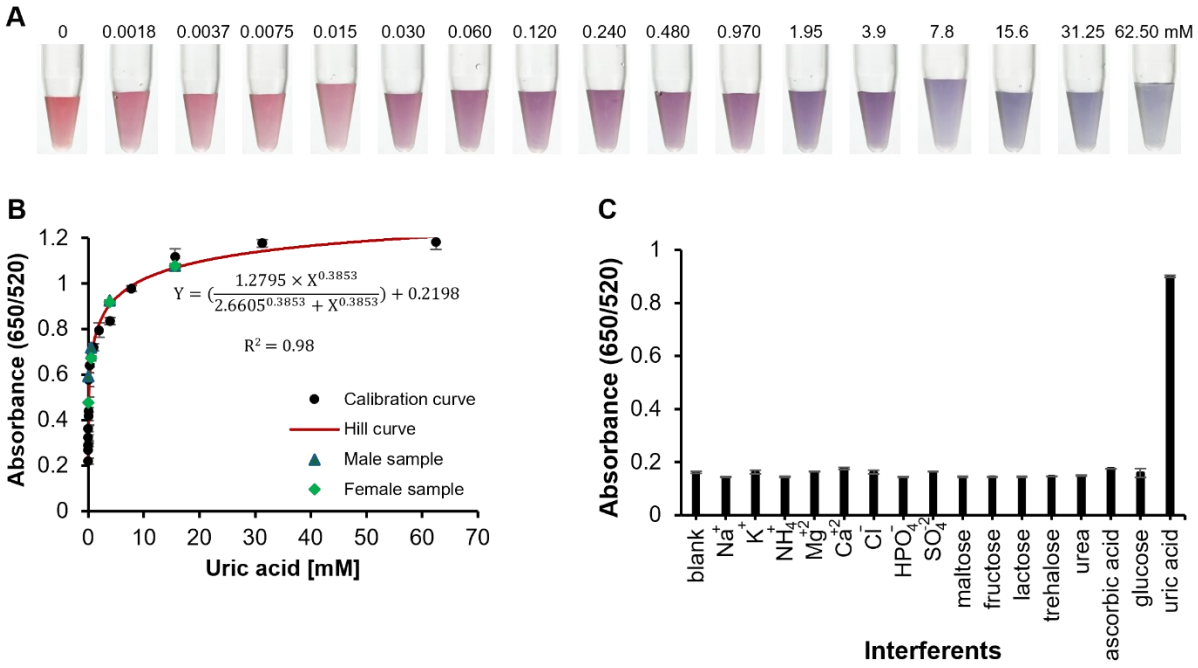


Figure 6.5 Detection of uric acid using dual-functional tablet sensor.
A) Optimal images of color transition in a reaction vial; B) A calibration plot indicating a concentration-dependent response of a direct tablet for uric acid along with real-sample spiking results; C) Selectivity of the proposed dual-functional tablet sensor.

### 6.3.4 Dual-functional Tablet Sensor for Glucose Detection

Glucose levels in body fluids serve as crucial biomarkers for various diseases, including diabetes and vascular conditions. Thus, developing nanostructures capable of glucose monitoring is an important strategy for early and accurate disease detection. In this study, we employed the peroxidase (POx)-mimetic properties of a dual-functional tablet to quantify glucose levels.

*6.3.4.1. Optimization studies*

The optimization of reaction conditions, including varying TMB concentrations, pH, reaction time, and temperature, was performed. TMB concentrations of 0.4, 0.6, 0.8, 1.0, and 1.2 mM were tested, and 0.8 mM was found as the best amount required for this reaction. Oxidised TMB (oxTMB) exhibited a blue hue at 652 nm, while unreacted TMB remained colourless, which was

measured using a UV-vis spectrophotometer. Similarly, both reaction time and temperature were monitored, revealing that an increase in temperature correlates with a decrease in reaction time, as supported by literature [616]. A 30-minute incubation at 37 °C produced the optimal results. Glucose oxidase is active within a pH range of 4–8; therefore, the experiment was conducted at pH levels from 3.0 to 8.0 using acetate-phosphate and phosphate buffers. The optimal pH for full peroxidase activity in the acetate-phosphate buffer was 4.0, while the optimal pH for glucose oxidase activity in the phosphate buffer was 7.4. The absorbance spectra of dAuNPs in the presence of various reagents are illustrated in Figure 6.6A. Fully dispersed dAuNPs exhibit a characteristic peak at 520 nm, which broadens and shifts to 530 nm in acetate buffer (pH 4.0). No change in particle dispersion was observed with 1M $H_2O_2$. However, TMB induced aggregation of the dAuNPs, marked by an absorbance peak at 570 nm. The POx-mimetic activity of the dAuNPs was confirmed by the appearance of a blue color at 652 nm ($\lambda_{652}$) when TMB was oxidized by $H_2O_2$ (Figure 6.6A-v). This catalytic reaction was terminated using a stop solution (e.g., $H_2SO_4$), which produced a yellow color with an absorbance peak at 450 nm ($\lambda_{450}$).

After confirming the POx-mimetic behavior of the dAuNPs tablet, we proceeded to calculate the steady-state kinetics of the catalytic reaction using the Michaelis-Mention plots. To provide an in-depth understanding of the POx-mimetic activity of the tablet, the kinetic parameters were assessed by altering the concentrations of TMB and $H_2O_2$. The kinetic parameters, including the Michaelis-Menten constant ($K_m$) and maximum reaction velocity ($V_{max}$), were determined to evaluate the reaction's efficiency. The reaction rates for TMB oxidation were calculated and used to produce standard Michaelis-Menten curves (Figure 6.6C). Through nonlinear fitting of the Michaelis-Menten plot, we ascertained the kinetic parameters ($V_{\max}$ and $K_{\mathrm{m}}$) using website (mycurvefit.com). A high $K_m$ signifies weak enzyme-substrate affinity, while a low $K_m$ indicates strong affinity. The calculated $K_m$ value for the direct tablet is 0.106 mM with TMB, which is lower than that of the pullulan-gold nanoparticles tablet ($K_m$ = 0.142 mM) [616] and the natural HRP enzyme ($K_{m,\ \mathrm{TMB}}$ = 0.434 mM) [641], indicating a strong affinity of the direct tablet for TMB. However, the $K_m$ value with $H_2O_2$ was higher (1182 mM) compared to that of HRP (3.7 mM), suggesting that a higher $H_2O_2$ concentration is needed to achieve the maximum activity of dAuNPs, as supported by the literature[642]. The calculated $V_{max}$ with TMB for the direct tablet is 369.72 mM/min. The Michaelis-Menten plots for the dAuNPs displayed a hyperbolic curve

when TMB and $H_2O_2$ were used as substrates. These results highlight the rapid catalytic kinetics of dAuNPs, underscoring their potential for POx-mimetic activity in glucose detection.

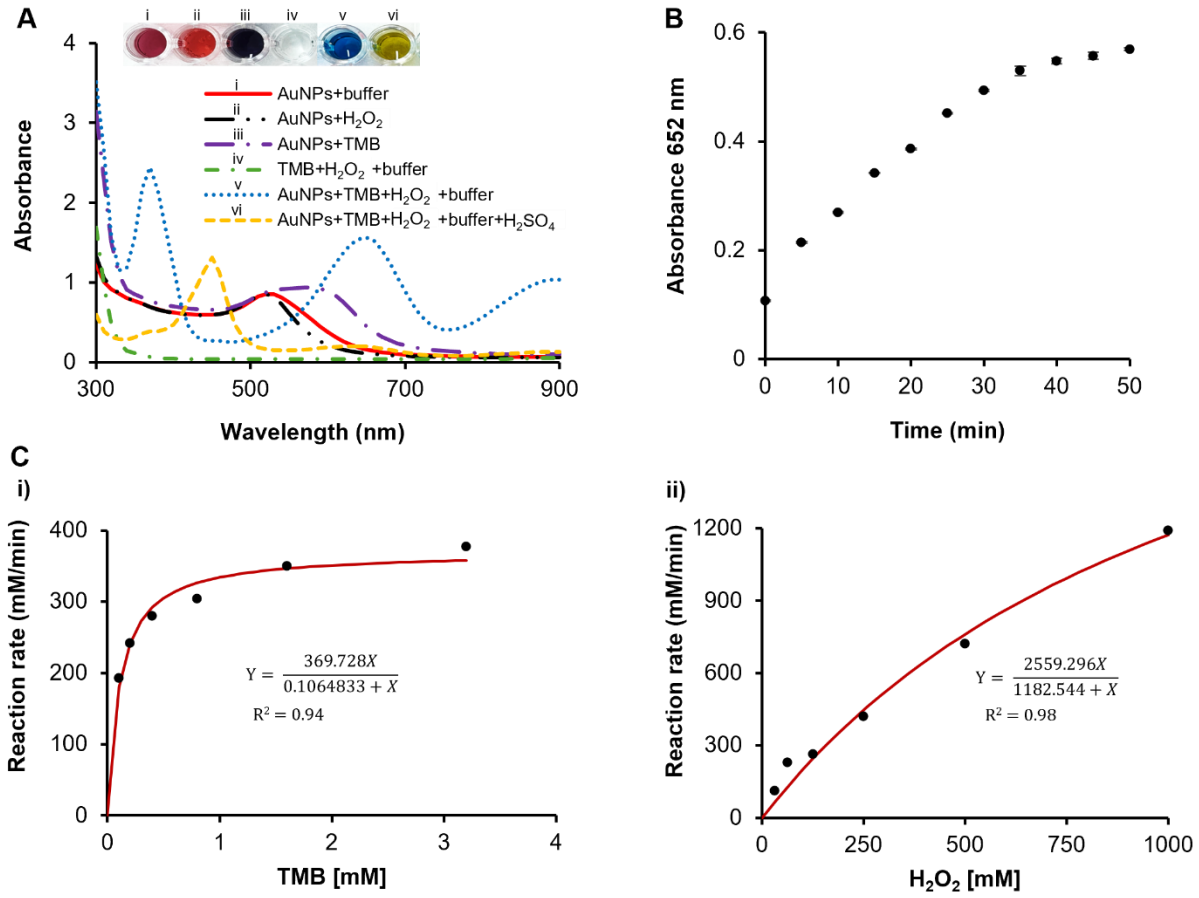


Figure 6.6 Optimization and kinetic studies for glucose detection using a direct tablet.
A) Absorbance spectra; B) A graph showing a gradual increase in the concentration of oxTMB with time; C) Steady-state kinetics of a dAuNPs tablet.

*6.3.4.2. Quantitative analysis of glucose*

Following this, quantitative colorimetric detection of the $H_2O_2$ level is evaluated by the POx-mimetic activity of a direct tablet. The characteristic absorption peak at 652 nm increases gradually with rising concentrations of $H_2O_2$ in the presence of TMB as a substrate (Figure 6S4). Subsequently, glucose detection was performed in a two-step reaction process. In the first step, glucose oxidase (GOx) catalyzes the oxidation of glucose into gluconic acid, releasing $H_2O_2$ as a by-product. In the second step, the peroxidase-mimetic (POD-mimetic) activity of the dAuNPs oxidizes TMB in the presence of the generated $H_2O_2$, leading to a detectable colorimetric change.

A positive correlation between absorbance intensity and glucose concentration was observed, confirming the method's high sensitivity for glucose detection (Figure 6.7). The LoD for the direct tablet was determined to be 0.625 mM with a working range of 0.625–10 mM. A similar working range (0.625 – 20 mM) was reported by Sun *et al.* for glucose assay using the peroxidase-mimetic activity of core-shell Cu/Au nanoparticles [643]. Another study recorded a linear range of 0.05-20 mM for glucose assay using Au-Ag heterogeneous nanorods [644].

On the other hand, smartphone-assisted quantification of glucose was achieved *via ImageJ* analysis (Figure 6S5). Digital photos were captured through a smartphone in a controlled environment and a fixed distance, adhering to the principles of colorimetric research. These results are consistent with those obtained with UV-vis system (working range of 0.625-10 mM, LoD of 0.625 mM), demonstrate the compatibility of ImageJ analysis for glucose detection. Previously, our group reported glucose oxidase encapsulation in a solid tablet which solves the storage and stability challenges related to enzymes [626]. The enzyme encapsulated tablets exhibit heat stability up to 60 °C and have been effectively utilized for glucose detection in urine. Thus, tablet-based sensors provide user-friendly tool for POC applications [35]. The comparison of the current method with previously reported assays is outlined in Table 6S3.

Further evaluations of glucose detection using the indirect tablet and as-prepared dAuNPs solution were conducted, with results presented in Figure 6S6. Both systems demonstrated a proportional linear relationship between absorbance intensity and glucose concentration. The indirect tablet exhibited a working range of 0.31–5 mM, while the as-prepared dAuNPs solution had a range of 0.31–10 mM. The working range of the dual-functional tablet is broader compared to the working range (0-6 mM) of our previously reported tablet assay [626]. These findings highlight the versatility and effectiveness of the dual-functional tablet system for glucose detection across different nanoprobe formats.

*6.3.4.3. Selectivity analysis*

Human urine is a complex matrix containing a variety of inorganic salts and organic compounds, which can complicate the precise identification of the target biomarker. Therefore, eradicating any potential interfering substances ensures reliable signal output. Common strategies to mitigate interference in complex samples include dilution and the use of masking agents. In this study, we centrifuged the urine sample to minimise the matrix effect. The absorbance intensity of oxTMB

followed a similar trend as the control when various potential interfering substances (maltose, fructose, lactose, trehalose, urea, ascorbic acid, uric acid) and inorganic ions (sodium, potassium, ammonium, magnesium, calcium, chloride, phosphate, sulfate) were tested. This confirms the excellent selectivity of the direct tablet sensor for glucose detection (Figure 6.7C).

*6.3.4.4. Validation with real samples*

Finally, to evaluate the practical applicability of our proposed glucose assay in real-world scenarios, human urine samples from both male and female volunteers were spiked with glucose concentrations of 0.31, 1.25, and 2.50 mM glucose and tested using with the dual-functional tablet sensor. As shown in Figure 6.7D, the blue triangles representing male samples indicate that the measured intensities for the blank and spiked samples followed the calibration curve trend, with calculated recovery values of 103 ± 3.1, 105 ± 1.7, and 116 ± 1.3% for the 0.31, 1.25, and 2.50 mM spiked samples, respectively. Similarly, the green diamonds for female samples show the calculated recovery values of 101 ± 3.1, 99 ± 0.9, and 105 ± 2.3%. The assay also demonstrated excellent precision, with %RSD values below 2% for all data points across three replicates. These findings highlight the assay's applicability in complex matrices, underscoring the high feasibility and reliability of the dual-functional tablet sensor for glucose detection in real biological samples, with significant potential for clinical and routine monitoring applications. To develop a complete device suitable for POC settings, an opaque box can be designed and combined with smartphone imaging to offer an affordable, portable, and user-friendly solution, as highlighted in the literature [611].

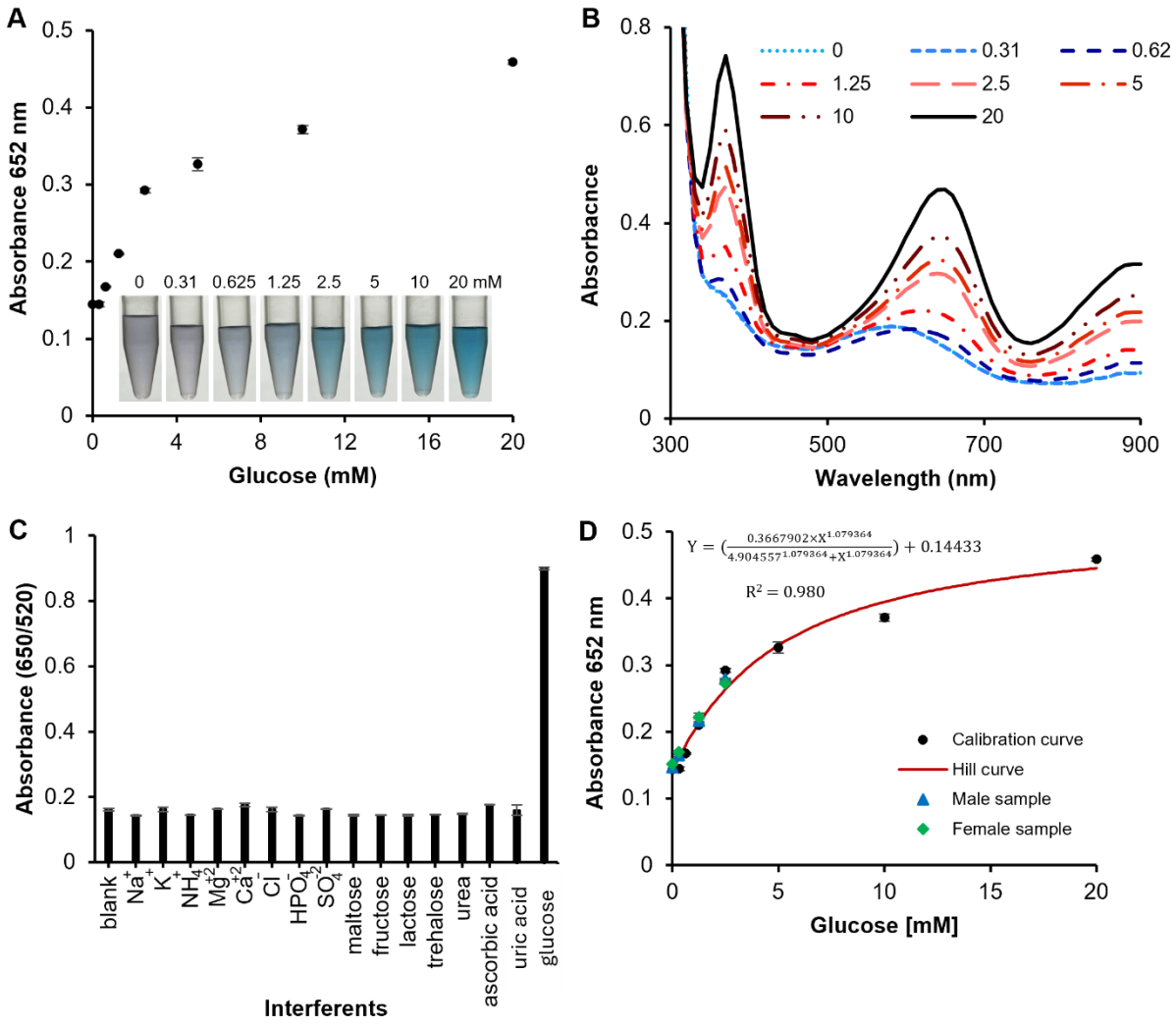


Figure 6.7 Peroxidase (POx) mimetic nanozyme performances of a dual functional tablet sensor for glucose detection.
A) A calibration curve indicating a concentration-dependent response of a tablet sensor using TMB substrate; B) The absorbance spectra indicating a gradual increase in peak intensity with raising glucose concentration; C) Selectivity analysis; D) Spiking analysis.

## 6.4 Conclusions

In this work, we highlight the use of dextran-gold nanoparticles (dAuNPs) as a complete nanoprobe, emphasizing their tablet-forming property and dual-functional colorimetric detection capabilities. The dAuNPs exhibit both plasmonic and peroxidase (POx)-mimetic nanozyme characteristics, which were utilized to develop a dual-functional sensor for the detection of uric acid and glucose in the urine, respectively. A concentration-dependent plasmonic response toward uric acid was achieved within the range of 0.00375 - 7.8 mM, which falls within the

biologically relevant range of 1.4 – 4.44 mM. Similarly, the tablet sensor demonstrated nanozymatic activity in the range of 0.625 – 10 mM for glucose, suitable for glucose monitoring in urine. Our dual-functional tablet sensor is highly sensitive, and selective that remains stable for over a year. The advantage of this technology lies in its ability to combine both plasmonic and nanozyme properties within a single tablet, enabling portable testing for field use. This tablet-based approach offers a simple and effective method for developing self-monitoring testing kits with visual readouts. The promising performance of this tablet sensor indicates its potential for fast, safe, and convenient monitoring of uric acid and glucose in clinical settings and for self-care testing.

# CHAPTER 7 Conclusion and Future Directions

This thesis introduces a tablet platform as an affordable, portable, sensitive, and user-friendly detection platform for point-of-use applications. We fabricated the tablet by encapsulating dextran-gold nanoparticles (dAuNPs) and fully characterized it using spectroscopic and microscopic techniques. Initially, we developed a plasmonic tablet for a single detection assay. Next, the tablet technology is enhanced by exploring the nanozyme properties of dAuNPs, which provide the tablet with two functions: the detection of two different analytes. To achieve this, extensive optimization was carried out in terms of dextran amount, synthetic procedure, and sensing protocols towards different targeted analytes, which is summarized below.

## 7.1 Summary and Conclusions

We developed a plasmonic tablet from a colloidal solution of dAuNPs using a simple pipetting-out method. Initially, we prepared citrate-gold nanoparticles under reflux conditions through the Turkevich approach, followed by a ligand exchange reaction with dextran at room temperature. Dextran easily replaces citrate, a weak ligand, without affecting the particle morphology and provides enhanced stability to nanoparticles against aggregation. The optimal dextran concentration was selected so that it would be stable enough to support tablet formation while still letting the plasmonic response work. Next, the plasmonic tablet was tested in three different pH environments using sodium chloride (neutral), hydrochloric acid (acidic), and sodium hydroxide (alkaline) solutions to evaluate the potential response of dAuNPs after encapsulation. The tablet's pH-responsive behavior was shown by its stable dispersion in neutral and alkaline conditions and its controlled aggregation in acidic conditions, which could be seen with the naked eye. The study concludes that the plasmonic tablet has the potential to detect acid-labile analytes for in-field applications. The tablet, which was made using a wet chemical reduction method and post-synthetic dextran addition, is low-cost (about 1.22 CAD per 100 tablets of 100 μL dAuNPs-Solution) and is an easy to carry device. It remains stable for over four years (to date) and serves as a user-friendly alternative to the solution phase of dAuNPs. The tablets are easy to prepare, handle, transport, and store at room temperature. This approach highlights simple fabrication and concentration-dependent aggregation in low pH environments, making

these tablets suitable for diverse applications in diagnostics and environmental monitoring (Chapter 3).

Progressing further, we simplified the tablet formation procedure by eliminating the ligand exchange step. Instead of citrate, we used dextran as a ligand/capping agent to synthesize the dAuNPs solution, which provides high stability to the gold particles. Next, we optimize the sensing behavior by varying the dextran content in the dAuNPs solution. We observe that an increase in the dextran amount leads to a corresponding increase in the hydrodynamic size of dAuNPs, while the magnitude of surface charge on Au particles is decreased from -43.89 to -0.52 mV with 0.01 to 30.01% dextran due to the charge-neutral nature of pristine dextran. We achieved a tunable plasmonic probe to detect hypochlorite ($OCl^-$) as an environmental analyte. Low dextran content (0.01%) enabled highly sensitive $OCl^-$ detection (LoD 50 μM) in real swimming pool water. Scalable and cost-effective production of concentrated dAuNPs (20 times) was achieved without compromising particle integrity (Chapter 4).

Once a fully functional plasmonic tablet was fabricated for environmental analyte, we stepped forward to explore the utilization of this tablet in health care applications. This study presents a portable, nanoscale sensor for detecting urinary hydrogen peroxide ($H_2O_2$), an oxidative stress biomarker, using plasmonic tablet and swab sensors. The red color of the tablet solution or plasmonic swab turns to blue in the presence of $H_2O_2$ in the sample due to salt-induced nanoparticle aggregation. The transition in color is observed due to •OH-assisted degradation of the dextran layer around dAuNPs, leading to the loss of colloidal stability and subsequent aggregation of dAuNPs. This colorimetric assay involves Fenton chemistry and relies on an aggregation mechanism, demonstrating high selectivity as indicated by interference analysis. We analyzed the $H_2O_2$ concentrations in urine samples from healthy male and female volunteers before and after consuming green tea. The observed decrease in urinary $H_2O_2$ level after green tea consumption suggests a potential role of green tea antioxidants in reducing oxidative stress (Chapter 5).

Finally, the tablet technology was advanced by upgrading the plasmonic tablet into a dual-functional tablet that combines the plasmonic and nanozyme characteristics of dAuNPs. This research further simplifies the synthetic procedure in terms of the number of steps involved, heat, and time. We prepared the colloidal gold solution with 2% dextran all at once, eliminating the

need for post-synthetic dextran addition, which was necessary for tablet formation. Hence, we fabricated the "direct" tablet directly from the dAuNPs solution, while the "indirect" tablet involves an extra step of dextran addition. The dextran acts as a reducing agent, a stabilizing agent, and a tablet-forming agent. Also, the reflux condition required for the conventional synthetic set-up was replaced with stirring at room temperature, making the procedure energy efficient, cost-effective, and eco-friendly. The reaction time for the synthesis of dAuNPs solution for direct tablet production was reduced to 83%. This direct tablet sensor was used for the detection of uric acid and glucose in urine under the biologically relevant ranges, which makes it practical for real-world sample testing. It advances the point-of-care devices due to its dual functionality within the same tablet: plasmonic response for uric acid detection and nanozyme property for glucose detection. The direct tablet sensor is highly sensitive, selective, and cost-effective. This innovative, portable, dual-functional tablet is a potential candidate for point-of-use assays for resource-limited settings and in-field applications (Chapter 6).

In short, the encapsulated dAuNPs are ultra-stable at room temperature, low-cost, available in variable concentrations, and user-friendly in handling and transportation. The dAuNPs-Tablet provides easy retrieval of dAuNPs upon quick dissolution into aqueous media, which responds to the detection system comparable to the dAuNPs solution. Furthermore, the dAuNPs-Tablet is a dual-functional nanoprobe showing plasmonic and nanozyme characteristics within the same tablet. Hence, the tablet sensor is a potential candidate for a point-of-use detection system.

## 7.2 Future Work

This research has laid the foundation for the scientific community engaged in the development of user-friendly point-of-use sensors for the detection of toxic substances. The objective of this thesis was successfully achieved by developing a novel, affordable, and efficient tablet-based platform for point-of-use applications. Initially, we fabricated a plasmonic tablet and advanced it to a dual-functional tablet, taking into account the plasmonic and nanozyme properties of the nanogold. Several steps have been accomplished in the fabrication, optimization, stability, and testing of a reliable assay with analytes such as hypochlorite, hydrogen peroxide, uric acid, and glucose. However, as the research continues, there are some recommendations for future investigations.

- ✓ As tablet technology has advanced to dual-functional tablet, future development could lead to a multiplex tablet. Multiplex sensing capabilities would enable multi-analyte detection in a single assay, improving efficiency for field applications.
- ✓ Encapsulation of other materials (e.g., chromogenic substances, buffer media) would help to develop a fully integrated point-of-use kit. Also, encapsulation of hybrid gold nanoparticles such as quantum dot-gold nanoparticles, gold-silica core-shell nanoparticles, gold-magnetic nanoparticles, and gold-DNA nanoconjugates would advance the point-of-use assays by improving the sensitivity and selectivity of the method.
- ✓ Efforts should be made to improve the sensitivity of the detection method. Encapsulation using a variety of dextran scaffolds, such as acetate dextran and amine dextran, could enhance sensitivity. In addition, using a lower molecular weight dextran could also contribute to improved detection performance.
- ✓ The proposed tablet methodology can be applied to detecting other disease biomarkers and pathogens, as well as monitoring analytes for food quality assessment and forensic analysis. Expanding the target analytes such as pesticides and heavy metals could be an intriguing future direction.
- ✓ The plasmonic tablet shows excellent tolerance to saline conditions and long-term environmental stability, so it can be a potential candidate in the drug delivery field.
- ✓ Coupling the plasmonic tablet with a smartphone-based imaging and AI-driven data processing system could allow real-time, user-friendly, and quantitative analysis.
- ✓ Extensive field testing in real environmental, industrial, or clinical settings is needed to validate the tablet's accuracy and robustness under practical conditions.
- ✓ Investigating regulatory approvals, mass production techniques, and cost-effective manufacturing strategies will be crucial for translating this research into a market-ready product.

## REFERENCES


[1] Sensor Market: Global Industry Analysis and Forecast (2024-2030) by Type, Component, Technology, End User and Region, (2024).

[2] T. Zhao, X. Liang, X. Guo, X. Yang, J. Guo, X. Zhou, X. Huang, W. Zhang, Y. Wang, Z. Liu, Z. Jiang, H. Zhou, H. Zhou, Smartphone-based colorimetric sensor array using gold nanoparticles for rapid distinguishment of multiple pesticides in real samples, Food Chem 404 (2023). https://doi.org/10.1016/j.foodchem.2022.134768.

[3] A. Behera, S.R. Mahapatra, S. Majhi, N. Misra, R. Sharma, J. Singh, R.P. Singh, S.S. Pandey, K.R. Singh, R.G. Kerry, Gold nanoparticle assisted colorimetric biosensors for rapid polyethylene terephthalate (PET) sensing for sustainable environment to monitor microplastics, Environ Res 234 (2023). https://doi.org/10.1016/j.envres.2023.116556.

[4] G. Adedokun, M. Alipanah, Z.H. Fan, Sample preparation and detection methods in point-of-care devices towards future at-home testing, Lab Chip 24 (2024) 3626–3650. https://doi.org/10.1039/d3lc00943b.

[5] H. Yousefi, H.M. Su, S.M. Imani, K. Alkhaldi, C.D. Filipe, T.F. Didar, Intelligent Food Packaging: A Review of Smart Sensing Technologies for Monitoring Food Quality, ACS Sens 4 (2019) 808–821. https://doi.org/10.1021/acssensors.9b00440.

[6] S. Chen, S. Brahma, J. Mackay, C. Cao, B. Aliakbarian, The role of smart packaging system in food supply chain, J Food Sci 85 (2020) 517–525. https://doi.org/10.1111/1750-3841.15046.

[7] J.A. Otoo, T.S. Schlappi, REASSURED Multiplex Diagnostics: A Critical Review and Forecast, Biosensors (Basel) 12 (2022). https://doi.org/10.3390/bios12020124.

[8] M. Baldeh, F.K. Bawa, F.U. Bawah, M. Chamai, F. Dzabeng, W.M.A. Jebreel, J.B.B. Kabuya, S.K. Molemodile Dele-Olowu, E. Odoyo, D. Rakotomalala Robinson, A.J. Cunnington, Lessons from the pandemic: new best practices in selecting molecular diagnostics for point-of-care testing of infectious diseases in sub-Saharan Africa, Expert Rev Mol Diagn 24 (2024) 153–159. https://doi.org/10.1080/14737159.2023.2277368.

[9] M.R. Kumalasari, R. Alfanaar, A.S. Andreani, Gold nanoparticles (AuNPs): A versatile material for biosensor application, Talanta Open 9 (2024). https://doi.org/10.1016/j.talo.2024.100327.

[10] Z. Sadiq, S.H. Safiabadi Tali, H. Hajimiri, M. Al-Kassawneh, S. Jahanshahi-Anbuhi, Gold Nanoparticles-Based Colorimetric Assays for Environmental Monitoring and Food Safety Evaluation, Crit Rev Anal Chem 54 (2022) 2209–2244. https://doi.org/10.1080/10408347.2022.2162331.

[11] S.H. Safiabadi Tali, H. Hajimiri, Z. Sadiq, S. Jahanshahi-Anbuhi, Engineered detection zone to enhance color uniformity on paper microfluidics fabricated via Parafilm®-heating-laser-cutting, Sens Actuators B Chem 380 (2023) 133324. https://doi.org/10.1016/j.snb.2023.133324.

[12] Y. Chen, Y. Liu, J. Liu, Y. Li, Y. Liu, W. Zhang, L. Han, D. Wang, S. Cao, H. Liu, Q. Xie, X. Wang, M. Zhang, Porous PDMS–ZnO Wearable Gas Sensor for Acetone Biomarker Detection and Breath Analysis, ACS Appl Mater Interfaces (2024). https://doi.org/10.1021/acsami.4c16209.

[13] G. Wu, H. Du, Y.L. Cha, D. Lee, W. Kim, F. Feyzbar-Khalkhali-Nejad, T.S. Oh, X. Zhang, D.J. Kim, A wearable mask sensor based on polyaniline/CNT nanocomposites for monitoring ammonia gas and human breathing, Sens Actuators B Chem 375 (2023). https://doi.org/10.1016/j.snb.2022.132858.

[14] K. Teekayupak, N. Ruecha, O. Chailapakul, N. Rodthongkum, Flexible cotton-AuNP thread electrode for non-enzymatic sensor of uric acid in urine, Cellulose 28 (2021) 10501–10515. https://doi.org/10.1007/s10570-021-04169-y.

[15] American Chemical Society National Historic Chemical Landmarks, 2010. Development of Diagnostic Test Strips, Http://Www.Acs.Org/Content/Acs/En/Education/Whatischemistry/Landmarks/Diagnosticteststrips.Html (Accessed 7.9.24). (2010).

[16] S. Jahanshahi-Anbuhi, K. Pennings, V. Leung, M. Liu, C. Carrasquilla, B. Kannan, Y. Li, R. Pelton, J.D. Brennan, C.D.M.M. Filipe, Pullulan Encapsulation of Labile Biomolecules to Give Stable Bioassay Tablets, Angewandte Chemie International Edition 53 (2014) 6155–6158. https://doi.org/10.1002/anie.201403222.

[17] B. Udugama, P. Kadhiresan, A. Samarakoon, W.C.W. Chan, Simplifying Assays by Tableting Reagents, J Am Chem Soc 139 (2017) 17341–17349. https://doi.org/10.1021/jacs.7b07055.

[18] M. Al-Kassawneh, Z. Sadiq, S. Jahanshahi-Anbuhi, Pullulan-stabilized gold nanoparticles tablet as a nanozyme sensor for point-of-care applications, Sens Biosensing Res 38 (2022) 100526. https://doi.org/10.1016/j.sbsr.2022.100526.

[19] V.Y.C. Li, B. Udugama, P. Kadhiresan, W.C.W. Chan, Sequential Reagent Release from a Layered Tablet for Multistep Diagnostic Assays, Anal Chem 94 (2022) 17102–17111. https://doi.org/10.1021/acs.analchem.2c03315.

[20] Z. Sadiq, S.H. Safiabadi Tali, H. Hajimiri, M. Al-Kassawneh, S. Jahanshahi-Anbuhi, Gold Nanoparticles-Based Colorimetric Assays for Environmental Monitoring and Food Safety Evaluation, Crit Rev Anal Chem (2022). https://doi.org/10.1080/10408347.2022.2162331.

[21] R. Arvizo, R. Bhattacharya, P. Mukherjee, Gold nanoparticles: Opportunities and challenges in nanomedicine, Expert Opin Drug Deliv 7 (2010) 753–763. https://doi.org/10.1517/17425241003777010.

[22] I. Gessner, J.H. Park, H.Y. Lin, H. Lee, R. Weissleder, Magnetic Gold Nanoparticles with Idealized Coating for Enhanced Point-Of-Care Sensing, Adv Healthc Mater 11 (2022). https://doi.org/10.1002/adhm.202102035.

[23] M. Hegde, P. Pai, M.G. Shetty, K.S. Babitha, Gold nanoparticle based biosensors for rapid pathogen detection: A review, Environ Nanotechnol Monit Manag 18 (2022). https://doi.org/10.1016/j.enmm.2022.100756.

[24] Y. Xu, C. Lu, Y. Sun, Y. Shao, Y. Cai, Y. Zhang, J. Miao, P. Miao, A colorimetric aptasensor for the antibiotics oxytetracycline and kanamycin based on the use of magnetic beads and gold nanoparticles, Microchimica Acta 185 (2018). https://doi.org/10.1007/s00604-018-3077-y.

[25] H.B. Ahmed, Recruitment of various biological macromolecules in fabrication of gold nanoparticles: Overview for preparation and applications, Int J Biol Macromol 140 (2019) 265–277. https://doi.org/10.1016/j.ijbiomac.2019.08.138.

[26] G.R. Vázquez-Martínez, M.A. Meraz-Rios, J.A. Balderas-López, Synthesis of glyco-gold nanoparticles stabilized with non-thioled disaccharides, MRS Adv 7 (2022) 678–682. https://doi.org/10.1557/s43580-022-00333-z.

[27] J. Tang, X. Fu, Q. Ou, K. Gao, S.Q. Man, J. Guo, Y. Liu, Hydroxide assisted synthesis of monodisperse and biocompatible gold nanoparticles with dextran, Materials Science and Engineering C 93 (2018) 759–767. https://doi.org/10.1016/j.msec.2018.08.045.

[28] K.R. Sreelakshmi, C.O. Mohan, K.K. Anas, R.K. Renjith, S. Remya, P.M. Ashraf, Synthesis and stability of chitosan gold nanocomposites: Effect of time of heating and concentration of reactant, Int J Food Sci Technol 57 (2022) 1333–1339. https://doi.org/10.1111/ijfs.15467.

[29] P.H.N. Diem, D.T.T. Thao, D. Van Phu, N.N. Duy, H.T.D. Quy, T.T. Hoa, N.Q. Hien, Synthesis of gold nanoparticles stabilized in dextran solution by gamma Co-60 ray irradiation and preparation of gold nanoparticles/dextran powder, J Chem 2017 (2017). https://doi.org/10.1155/2017/6836375.

[30] F.S. Tenório, T.L. do Amaral Montanheiro, A.M.I. dos Santos, M. dos Santos Silva, A.P. Lemes, D.B. Tada, Chitosan hydrogel covalently crosslinked by gold nanoparticle: Eliminating the use of toxic crosslinkers, J Appl Polym Sci 138 (2021). https://doi.org/10.1002/app.49819.

[31] J. Liu, X. Xu, A. Wu, Z. Wang, S. Song, H. Kuang, L. Liu, C. Xu, Development of a gold nanoparticle-based lateral flow immunoassay for the detection of pyridaben, Microchemical Journal 170 (2021). https://doi.org/10.1016/j.microc.2021.106762.

[32] A.N. Baker, G.W. Hawker-Bond, P.G. Georgiou, S. Dedola, R.A. Field, M.I. Gibson, Glycosylated gold nanoparticles in point of care diagnostics: from aggregation to lateral flow, Chem Soc Rev 51 (2022) 7238–7259. https://doi.org/10.1039/d2cs00267a.

[33] Z. Sadiq, S.H. Safiabadi Tali, S. Jahanshahi-Anbuhi, Gold Tablets: Gold Nanoparticles Encapsulated into Dextran Tablets and Their pH-Responsive Behavior as an Easy-to-Use Platform for Multipurpose Applications, ACS Omega 7 (2022) 11177–11189. https://doi.org/10.1021/acsomega.1c07393.

[34] Z. Sadiq, M. Al-Kassawneh, S.H. Safiabadi Tali, S. Jahanshahi-Anbuhi, Tailoring plasmonic sensing strategies for the rapid and sensitive detection of hypochlorite in swimming water samples, Microchimica Acta 191 (2024) 183. https://doi.org/10.1007/s00604-024-06246-y.

[35] Z. Sadiq, M. Al-Kassawneh, S.H. Safiabadi Tali, S. Jahanshahi-Anbuhi, Dextran-Gold Nanoparticle-Based Tablets and Swabs for Colorimetric Detection of Urinary $H_2O_2$, ACS Appl Nano Mater 8 (2025) 1008–1020. https://doi.org/10.1021/acsanm.4c05691.

[36] Z. Sadiq, S.H. Safiabadi Tali, M. Mansouri, S. Jahanshahi-Anbuhi, Dual-functional nanogold tablet as a plasmonic and nanozyme sensor for point-of-care applications, Nanoscale Adv (2025). https://doi.org/10.1039/D5NA00082C.

[37] C. Louis, O. Pluchery, Gold Nanoparticles for Physics, Chemistry and Biology, Imperial College Press, 2012. https://doi.org/10.1142/p815.

[38] F. Dekker, L. Kool, A. Bunschoten, A.H. Velders, V. Saggiomo, Syntheses of gold and silver dichroic nanoparticles; Looking at the Lycurgus cup colors, Chemistry Teacher International 3 (2021) 1–6. https://doi.org/10.1515/cti-2019-0011.

[39] M. Faraday, Experimental Relations o f Gold (and other Metals) to Light., Philos Trans R Soc Lond 147 (1857) 145–181. https://doi.org/https://doi.org/10.1098/rstl.1857.0011.

[40] I. Letchumanan, S.C.B. Gopinath, M.K. Md Arshad, M.S. Mohamed Saheed, V. Perumal, C.H. Voon, U. Hashim, Gold-Nanohybrid Biosensors for Analyzing Blood Circulating Clinical Biomacromolecules: Current Trend toward Future Remote Digital Monitoring, Crit. Rev. Anal. Chem. 52 (2022) 577–592. https://doi.org/10.1080/10408347.2020.1812373.

[41] A. De, D. Kalita, Bio-Fabricated Gold and Silver Nanoparticle Based Plasmonic Sensors for Detection of Environmental Pollutants: An Overview, Crit. Rev. Anal. Chem. (2021) 1–17. https://doi.org/10.1080/10408347.2021.1970507.

[42] C. Daruich De Souza, B. Ribeiro Nogueira, M.E.C.M. Rostelato, Review of the methodologies used in the synthesis gold nanoparticles by chemical reduction, J. Alloys Compd. 798 (2019) 714–740. https://doi.org/10.1016/j.jallcom.2019.05.153.

[43] L. Qin, G. Zeng, C. Lai, D. Huang, P. Xu, C. Zhang, M. Cheng, X. Liu, S. Liu, B. Li, H. Yi, “Gold rush” in modern science: Fabrication strategies and typical advanced applications of gold nanoparticles in sensing, Coord. Chem. Rev. 359 (2018) 1–31. https://doi.org/10.1016/j.ccr.2018.01.006.

[44] D.A. Giljohann, D.S. Seferos, W.L. Daniel, M.D. Massich, P.C. Patel, C.A. Mirkin, Gold nanoparticles for Biology and Medicine, Angew. Chem. Int. Ed. 49 (2010) 3280–3294. https://doi.org/10.1002/anie.200904359.

[45] C. Daruich De Souza, B. Ribeiro Nogueira, M.E.C.M. Rostelato, Review of the methodologies used in the synthesis gold nanoparticles by chemical reduction, J. Alloys Compd. 798 (2019) 714–740. https://doi.org/10.1016/j.jallcom.2019.05.153.

[46] J. yuan Li, J. Zhu, G. jun Weng, J. jun Li, J. wu Zhao, Multiplex Sensing Based on Plasmonic Optics of Noble Metallic Nanostructures, Crit. Rev. Anal. Chem. (2022) 1–13. https://doi.org/10.1080/10408347.2022.2122692.

[47] P.L. Venugopalan, B. Esteban-Fernández De Ávila, M. Pal, A. Ghosh, J. Wang, Fantastic Voyage of Nanomotors into the Cell, ACS Nano 14 (2020) 9423–9439. https://doi.org/10.1021/acsnano.0c05217.

[48] W.A. Ameku, W.R. De Araujo, C.J. Rangel, R.A. Ando, T.R.L.C. Paixão, Gold Nanoparticle Paper-Based Dual-Detection Device for Forensics Applications, ACS Appl. Nano Mater. 2 (2019) 5460–5468. https://doi.org/10.1021/acsanm.9b01057.

[49] Z. Hua, T. Yu, D. Liu, Y. Xianyu, Recent advances in gold nanoparticles-based biosensors for food safety detection, Biosens. Bioelectron. 179 (2021) 113076. https://doi.org/10.1016/j.bios.2021.113076.

[50] R. Wilson, The use of gold nanoparticles in diagnostics and detection, Chem. Soc. Rev. 37 (2008) 2028–2045. https://doi.org/10.1039/b712179m.

[51] M.S. Draz, H. Shafiee, Applications of gold nanoparticles in virus detection, Theranostics 8 (2018) 1985–2017. https://doi.org/10.7150/thno.23856.

[52] Annalen der Physik - 1908 - Mie - Beitr ge zur Optik tr ber Medien  speziell kolloidaler Metall sungen, (n.d.).

[53] H. Horvath, Gustav Mie and the scattering and absorption of light by particles: Historic developments and basics, J Quant Spectrosc Radiat Transf 110 (2009) 787–799. https://doi.org/10.1016/j.jqsrt.2009.02.022.

[54] J. Turkevich, P.C. Stevenson, J. Hillier, A study of the nucleation and growth processes in the synthesis of colloidal gold, Discuss Faraday Soc 11 (1951) 55. https://doi.org/10.1039/df9511100055.

[55] R.P. Feynman, There’s Plenty of Room at the Bottom, 1960.

[56] W. Page Faulk, G. Malcolm Taylor, Immunocolloid method for the electron microscope, Immunochemistry 8 (1971) 1081–1083. https://doi.org/10.1016/0019-2791(71)90496-4.

[57] G. FRENS, Controlled Nucleation for the Regulation of the Particle Size in Monodisperse Gold Suspensions, Nature Physical Science 241 (1973) 20–22. https://doi.org/10.1038/physci241020a0.

[58] M. Brust, M. Walker, D. Bethell, D.J. Schiffrin, R. Whyman, Synthesis of Thiol-derivatised Gold Nanoparticles in a Two-phase Liquid-Liquid System, 1994.

[59] A.P. Alivisatos, K.P. Johnsson, X. Peng, T.E. Wilson, C.J. Loweth, M.P. Bruchez, P.G. Schultz, Organization of “nanocrystal molecules” using DNA, Nature 382 (1996) 609–611. https://doi.org/10.1038/382609a0.

[60] C.A. Mirkin, R.L. Letsinger, R.C. Mucic, J.J. Storhoff, A DNA-based method for rationally assembling nanoparticles into macroscopic materials, n.d.

[61] H. Li, L.J. Rothberg, Label-free colorimetric detection of specific sequences in genomic DNA amplified by the polymerase chain reaction, J Am Chem Soc 126 (2004) 10958–10961. https://doi.org/10.1021/ja048749n.

[62] P. Velusamy, C.H. Su, P. Ramasamy, V. Arun, N. Rajnish, P. Raman, V. Baskaralingam, S.M. Senthil Kumar, S.C.B. Gopinath, Volatile Organic Compounds as Potential Biomarkers for Noninvasive Disease Detection by Nanosensors: A Comprehensive Review, Crit. Rev. Anal. Chem. (2022) 1–12. https://doi.org/10.1080/10408347.2022.2043145.

[63] D. Rawtani, M. Tharmavaram, G. Pandey, C.M. Hussain, Functionalized nanomaterial for forensic sample analysis, TrAC - Trends Anal. Chem. 120 (2019) 115661. https://doi.org/10.1016/j.trac.2019.115661.

[64] O.D. Oyewunmi, S.H. Safiabadi-Tali, S. Jahanshahi-Anbuhi, Dual-modal assay kit for the qualitative and quantitative determination of the total water hardness using a permanent marker fabricated microfluidic paper-based analytical device, Chemosensors 8 (2020) 97. https://doi.org/10.3390/chemosensors8040097.

[65] S.H. Safiabadi Tali, J.J. LeBlanc, Z. Sadiq, O.D. Oyewunmi, C. Camargo, B. Nikpour, N. Armanfard, S.M. Sagan, S. Jahanshahi-Anbuhi, Tools and Techniques for Severe Acute Respiratory Syndrome Coronavirus 2 (SARS-CoV-2)/COVID-19 Detection., Clin. Microbiol. Rev. 34 (2021) 1–63. https://doi.org/10.1128/CMR.00228-20.

[66] Z. Hua, T. Yu, D. Liu, Y. Xianyu, Recent advances in gold nanoparticles-based biosensors for food safety detection, Biosens. Bioelectron. 179 (2021) 113076. https://doi.org/10.1016/j.bios.2021.113076.

[67] Y. Li, Z. Wang, L. Sun, L. Liu, C. Xu, H. Kuang, Nanoparticle-based sensors for food contaminants, TrAC - Trends Anal. Chem. 113 (2019) 74–83. https://doi.org/10.1016/j.trac.2019.01.012.

[68] K. Saha, S.S. Agasti, C. Kim, X. Li, V.M. Rotello, Gold nanoparticles in chemical and biological sensing, Chem. Rev. 112 (2012) 2739–2779. https://doi.org/10.1021/cr2001178.

[69] N. Elahi, M. Kamali, M.H. Baghersad, Recent biomedical applications of gold nanoparticles: A review, Talanta 184 (2018) 537–556. https://doi.org/10.1016/j.talanta.2018.02.088.

[70] Y. Li, Z. Wang, L. Sun, L. Liu, C. Xu, H. Kuang, Nanoparticle-based sensors for food contaminants, TrAC - Trends Anal. Chem. 113 (2019) 74–83. https://doi.org/10.1016/j.trac.2019.01.012.

[71] X. Hong, J. Bai, Y. Peng, X. Zhang, Z. Gao, B. Ning, M. Li, Y. Pu, Y. Ying, F. Su, X. Zhang, Au-doped photonic crystal allows naked-eye determination of small organic molecules, Sens. Actuators B Chem. 321 (2020) 128493. https://doi.org/10.1016/j.snb.2020.128493.

[72] W. Xiao, Z. Deng, J. Huang, Z. Huang, M. Zhuang, Y. Yuan, J. Nie, Y. Zhang, Highly sensitive colorimetric detection of a variety of analytes via the Tyndall effect, Anal. Chem. 91 (2019) 15114–15122. https://doi.org/10.1021/acs.analchem.9b03824.

[73] A. Sánchez-Visedo, B. Gallego, L.J. Royo, A. Soldado, M. Valledor, F.J. Ferrero, J.C. Campo, J.M. Costa-Fernández, M.T. Fernández-Argüelles, Visual detection of microRNA146a by using RNA-functionalized gold nanoparticles, Microchimica Acta 187 (2020) 192. https://doi.org/10.1007/s00604-020-4148-4.

[74] T. Dong, X. Ma, N. Sheng, X. Qi, Y. Chu, Q. Song, B. Zou, G. Zhou, Point-of-care DNA testing by automatically and sequentially performing extraction, amplification and identification in a closed-type cassette, Sens. Actuators B Chem. 327 (2021) 128919. https://doi.org/10.1016/j.snb.2020.128919.

[75] L. Li, Y. Liang, Y. Zhao, Z. Chen, Target binding and DNA hybridization-induced gold nanoparticle aggregation for colorimetric detection of thrombin, Sens. Actuators B Chem. 262 (2018) 733–738. https://doi.org/10.1016/j.snb.2018.02.061.

[76] S. Giorgi-Coll, M.J. Marín, O. Sule, P.J. Hutchinson, K.L.H. Carpenter, Aptamer-modified gold nanoparticles for rapid aggregation-based detection of inflammation: an optical assay for interleukin-6, Microchimica Acta 187 (2020) 1–11. https://doi.org/10.1007/s00604-019-3975-7.

[77] Z. Gul, S. Ullah, S. Khan, H. Ullah, M.U. Khan, M. Ullah, S. Ali, A.A. Altaf, Recent Progress in Nanoparticles Based Sensors for the Detection of Mercury (II) Ions in Environmental and Biological Samples, Crit. Rev. Anal. Chem. (2022) 1–17. https://doi.org/10.1080/10408347.2022.2049676.

[78] S. Ali, X. Chen, W. Shi, G. Huang, L. ming Yuan, L. Meng, S. Chen, X. Zhonghao, X. Chen, Recent Advances in Silver and Gold Nanoparticles-Based Colorimetric Sensors for Heavy Metal Ions Detection: A Review, Crit. Rev. Anal. Chem. (2021) 1–33. https://doi.org/10.1080/10408347.2021.1973886.

[79] F. Wang, Y. Lu, Y. Chen, J. Sun, Y. Liu, Colorimetric nanosensor based on the aggregation of AuNP triggered by carbon quantum dots for detection of Ag+ ions, ACS Sustain. Chem. Eng. 6 (2018) 3706–3713. https://doi.org/10.1021/acssuschemeng.7b04067.

[80] M. Cordeiro, F.F. Carlos, P. Pedrosa, A. Lopez, P.V. Baptista, Gold nanoparticles for diagnostics: Advances towards points of care, Diagnostics 6 (2016) 43. https://doi.org/10.3390/diagnostics6040043.

[81] M.I.G.S. Almeida, B.M. Jayawardane, S.D. Kolev, I.D. McKelvie, Developments of microfluidic paper-based analytical devices (μPADs) for water analysis: A review, Talanta 177 (2018) 176–190. https://doi.org/10.1016/j.talanta.2017.08.072.

[82] C. Te Kung, C.Y. Hou, Y.N. Wang, L.M. Fu, Microfluidic paper-based analytical devices for environmental analysis of soil, air, ecology and river water, Sens. Actuators B Chem. 301 (2019) 126855. https://doi.org/10.1016/j.snb.2019.126855.

[83] A. Lapresta-Fernández, A. Fernández, J. Blasco, Nanoecotoxicity effects of engineered silver and gold nanoparticles in aquatic organisms, TrAC - Trends Anal. Chem. 32 (2012) 40–59. https://doi.org/10.1016/j.trac.2011.09.007.

[84] S. Rinaldi, L. Tarpani, L. Latterini, UV Treatment of the Stabilizing Shell for Improving the Photostability of Silver Nanoparticles, J. Nanomater. 2016 (2016). https://doi.org/https://doi.org/10.1155/2016/7510563.

[85] X. Lin, Z. Zhu, C. Zhao, S. Li, Q. Liu, A. Liu, L. Lin, X. Lin, Robust oxidase mimicking activity of protamine-stabilized platinum nanoparticles units and applied for colorimetric sensor of trypsin and inhibitor, Sens. Actuators B Chem. 284 (2019) 346–353. https://doi.org/10.1016/j.snb.2018.12.109.

[86] L. Sun, Z. Fu, E. Ma, J. Guo, Z. Zhang, W. Li, L. Li, Z. Liu, X. Guo, Ultrasmall Pt Nanozymes Immobilized on Spherical Polyelectrolyte Brushes with Robust Peroxidase-like Activity for Highly Sensitive Detection of Cysteine, Langmuir 38 (2022) 12915–12923. https://doi.org/10.1021/acs.langmuir.2c02056.

[87] N. Elahi, M. Kamali, M.H. Baghersad, Recent biomedical applications of gold nanoparticles: A review, Talanta 184 (2018) 537–556. https://doi.org/10.1016/j.talanta.2018.02.088.

[88] L. Qin, G. Zeng, C. Lai, D. Huang, P. Xu, C. Zhang, M. Cheng, X. Liu, S. Liu, B. Li, H. Yi, “Gold rush” in modern science: Fabrication strategies and typical advanced applications of gold nanoparticles in sensing, Coord. Chem. Rev. 359 (2018) 1–31. https://doi.org/10.1016/j.ccr.2018.01.006.

[89] G. Sriram, M.P. Bhat, P. Patil, U.T. Uthappa, H.Y. Jung, T. Altalhi, T. Kumeria, T.M. Aminabhavi, R.K. Pai, Madhuprasad, M.D. Kurkuri, Paper-based microfluidic analytical devices for colorimetric detection of toxic ions: A review, TrAC - Trends Anal. Chem. 93 (2017) 212–227. https://doi.org/10.1016/j.trac.2017.06.005.

[90] M.I.G.S. Almeida, B.M. Jayawardane, S.D. Kolev, I.D. McKelvie, Developments of microfluidic paper-based analytical devices (μPADs) for water analysis: A review, Talanta 177 (2018) 176–190. https://doi.org/10.1016/j.talanta.2017.08.072.

[91] M. Shah, V. Badwaik, Y. Kherde, H.K. Waghwani, T. Modi, Z.P. Aguilar, H. Rodgers, W. Hamilton, T. Marutharaj, C. Webb, M.B. Lawrenz, R. Dakshinamurthy, Gold nanoparticles: various methods of synthesis and antibacterial applications., Front. Biosci. (Landmark Ed) 19 (2014) 1320–44. https://doi.org/10.2741/4284.

[92] R. Sardar, A.M. Funston, P. Mulvaney, R.W. Murray, Gold Nanoparticles: Past, Present, and Future, Langmuir 25 (2009) 13840–13851. https://doi.org/10.1021/la9019475.

[93] S. Sun, P. Mendes, K. Critchley, S. Diegoli, M. Hanwell, S.D. Evans, G.J. Leggett, J.A. Preece, T.H. Richardson, Fabrication of Gold Micro- and Nanostructures by Photolithographic Exposure of Thiol-Stabilized Gold Nanoparticles, Nano Lett. 6 (2006) 345–350. https://doi.org/10.1021/nl052130h.

[94] B. Tangeysh, K. Moore Tibbetts, J.H. Odhner, B.B. Wayland, R.J. Levis, Gold Nanoparticle Synthesis Using Spatially and Temporally Shaped Femtosecond Laser Pulses: Post-Irradiation Auto-Reduction of Aqueous [AuCl 4 ]−, J. Phys. Chem. C 117 (2013) 18719–18727. https://doi.org/10.1021/jp4056494.

[95] R.C. Birtcher, M.A. Kirk, K. Furuya, G.R. Lumpkin, M.-O. Ruault, In situ Transmission Electron Microscopy Investigation of Radiation Effects, J. Mater. Res. Technol. 20 (2005) 1654–1683. https://doi.org/10.1557/JMR.2005.0242.

[96] M. Shah, V. Badwaik, Y. Kherde, H.K. Waghwani, T. Modi, Z.P. Aguilar, H. Rodgers, W. Hamilton, T. Marutharaj, C. Webb, M.B. Lawrenz, R. Dakshinamurthy, Gold nanoparticles: various methods of synthesis and antibacterial applications., Front. Biosci. (Landmark Ed) 19 (2014) 1320–44. https://doi.org/10.2741/4284.

[97] J. Turkevich, P.C. Stevenson, J. Hillier, A study of the nucleation and growth processes in the synthesis of colloidal gold, Discuss. Faraday Soc. 11 (1951) 55. https://doi.org/10.1039/df9511100055.

[98] M. Wuithschick, A. Birnbaum, S. Witte, M. Sztucki, U. Vainio, N. Pinna, K. Rademann, F. Emmerling, R. Kraehnert, J. Polte, Turkevich in new robes: key questions answered for the most common gold nanoparticle synthesis, ACS Nano 9 (2015) 7052–7071. https://doi.org/10.1021/acsnano.5b01579.

[99] J. Turkevich, P.C. Stevenson, J. Hillier, A study of the nucleation and growth processes in the synthesis of colloidal gold, Discuss. Faraday Soc. 11 (1951) 55. https://doi.org/10.1039/df9511100055.

[100] G. Frens, Controlled nucleation for the regulation of the particle size in monodisperse gold suspensions, Nat. Phys. Sci. 241 (1973) 20–22.

[101] M. Brust, M. Walker, D. Bethell, D.J. Schiffrin, R. Whyman, Synthesis of thiol-derivatised gold nanoparticles in a two-phase liquid-liquid system, J. Chem. Soc., Chem. Commun. (1994) 801–802. https://doi.org/10.1039/C39940000801.

[102] X. Yang, M. Yang, B. Pang, M. Vara, Y. Xia, Gold nanomaterials at work in biomedicine, Chem. Rev. 115 (2015) 10410–10488. https://doi.org/10.1021/acs.chemrev.5b00193.

[103] A. Wieckowska, M. Dzwonek, Ultrasmall Au nanoparticles coated with hexanethiol and anthraquinone/hexanethiol for enzyme-catalyzed oxygen reduction, Sens. Actuators B Chem. 224 (2016) 514–520. https://doi.org/10.1016/j.snb.2015.10.073.

[104] R. Sardar, J.S. Shumaker-Parry, 9-BBN Induced Synthesis of Nearly Monodisperse ω-Functionalized Alkylthiol Stabilized Gold Nanoparticles, Chem. Mater. 21 (2009) 1167–1169. https://doi.org/10.1021/cm802942x.

[105] R.K. Gupta, M.P. Srinivasan, R. Dharmarajan, Synthesis of short chain thiol capped gold nanoparticles, their stabilization and immobilization on silicon surface, Colloids Surf. A: Physicochem. Eng. Asp. 390 (2011) 149–156. https://doi.org/10.1016/j.colsurfa.2011.09.019.

[106] A.F.G. Leontowich, C.F. Calver, M. Dasog, R.W.J. Scott, Surface Properties of Water-Soluble Glycine-Cysteamine-Protected Gold Clusters, Langmuir 26 (2010) 1285–1290. https://doi.org/10.1021/la902465b.

[107] O. Zaluzhna, Y. Li, C. Zangmeister, T.C. Allison, Y.Y.J. Tong, Mechanistic insights on one-phase vs. Two-phase Brust-Schiffrin method synthesis of Au nanoparticles with dioctyl-diselenides, Chem. Commun. 48 (2012) 362–364. https://doi.org/10.1039/c1cc15955k.

[108] J. Wiesner, A. Wokaun, Anisometric gold colloids. Preparation, characterization, and optical properties, Chem. Phys. Lett. 157 (1989) 569–575. https://doi.org/10.1016/S0009-2614(89)87413-5.

[109] Y.C. Yang, C.H. Wang, Y.K. Hwu, J.H. Je, Synchrotron X-ray synthesis of colloidal gold particles for drug delivery, Mater. Chem. Phys. 100 (2006) 72–76. https://doi.org/10.1016/j.matchemphys.2005.12.007.

[110] B. Akar, K. Pushpavanam, E. Narayanan, K. Rege, J.J. Heys, Mechanistic investigation of radiolysis-induced gold nanoparticle formation for radiation dose prediction, Biomed. Phys. Eng. Express. 4 (2018) 065011. https://doi.org/10.1088/2057-1976/aac280.

[111] A.M. Abdelghany, E.M. Abdelrazek, S.I. Badr, M.S. Abdel-Aziz, M.A. Morsi, Effect of Gamma-irradiation on biosynthesized gold nanoparticles using Chenopodium murale leaf extract, J. Saudi Chem. Soc. 21 (2017) 528–537. https://doi.org/10.1016/j.jscs.2015.10.002.

[112] N. Hanžić, T. Jurkin, A. Maksimović, M. Gotić, The synthesis of gold nanoparticles by a citrate-radiolytical method, Radiat. Phys. Chem. 106 (2015) 77–82. https://doi.org/10.1016/j.radphyschem.2014.07.006.

[113] S. Chen, Y. Liu, G. Wu, Stabilized and size-tunable gold nanoparticles formed in a quaternary ammonium-based room-temperature ionic liquid under γ-irradiation, Nanotechnology 16 (2005) 2360–2364. https://doi.org/10.1088/0957-4484/16/10/061.

[114] X. Li, L. Liu, Z. Xu, W. Wang, J. Shi, L. Liu, M. Jing, F. Li, X. Zhang, Gamma irradiation and microemulsion assisted synthesis of monodisperse flower-like platinum-gold nanoparticles/reduced graphene oxide nanocomposites for ultrasensitive detection of carcinoembryonic antigen, Sens. Actuators B Chem. 287 (2019) 267–277. https://doi.org/10.1016/j.snb.2019.02.026.

[115] C. Fan, W. Li, S. Zhao, J. Chen, X. Li, Efficient one pot synthesis of chitosan-induced gold nanoparticles by microwave irradiation, Mater. Lett. 62 (2008) 3518–3520. https://doi.org/10.1016/j.matlet.2008.03.040.

[116] V.K.T. Ngo, D.G. Nguyen, T.P. Huynh, Q.V. Lam, A low cost technique for synthesis of gold nanoparticles using microwave heating and its application in signal amplification for detecting Escherichia Coli O157:H7 bacteria, Adv. Nat. Sci.: Nanosci. Nanotechnol. 7 (2016) 035016. https://doi.org/10.1088/2043-6262/7/3/035016.

[117] M.E. El-Naggar, T.I. Shaheen, M.M.G. Fouda, A.A. Hebeish, Eco-friendly microwave-assisted green and rapid synthesis of well-stabilized gold and core–shell silver–gold nanoparticles, Carbohydr. Polym. 136 (2016) 1128–1136. https://doi.org/10.1016/j.carbpol.2015.10.003.

[118] M. Morad, M.A. Karim, H.M. Altass, A.E.R.S. Khder, Microwave-assisted synthesis of gold nanoparticles supported on Mn3O4 catalyst for low temperature CO oxidation, Environ. Technol. (U. K.) 42 (2021) 2680–2689. https://doi.org/10.1080/09593330.2019.1709988.

[119] M. Alle, S.H. Lee, J.C. Kim, Ultrafast synthesis of gold nanoparticles on cellulose nanocrystals via microwave irradiation and their dyes-degradation catalytic activity, J. Mater. Sci. Technol. 41 (2020) 168–177. https://doi.org/10.1016/j.jmst.2019.11.003.

[120] C.D.W. Chin, L.J. Treadwell, J.B. Wiley, Microwave synthetic routes for shape-controlled catalyst nanoparticles and nanocomposites, Molecules 26 (2021) 1–16. https://doi.org/10.3390/molecules26123647.

[121] M.D.P. Rodríguez-Torres, L.A. Diaz -Torres, M. Olmos-López, P. Salas, C. Gutiérrez, UVA mediated synthesis of gold nanoparticles in pharmaceutical-grade heparin sodium solutions, in: Plasmonics: Metallic Nanostructures and Their Optical Properties XI, 2013: p. 88092R. https://doi.org/10.1117/12.2024441.

[122] D. Braguer, F. Correard, K. Maximova, C. Villard, M. Roy, A. Al-Kattan, M. Sentis, M. Gingras, A. Kabashin, M.-A. Esteve, Gold nanoparticles prepared by laser ablation in aqueous biocompatible solutions: assessment of safety and biological identity for nanomedicine applications, Int. J. Nanomed. 9 (2014) 5415. https://doi.org/10.2147/IJN.S65817.

[123] H.R. Tiyyagura, P. Majerič, I. Anžel, R. Rudolf, Low-cost synthesis of AuNPs through ultrasonic spray pyrolysis, Mater. Res. Express 7 (2020). https://doi.org/10.1088/2053-1591/ab80ea.

[124] L. Gao, S. Mei, H. Ma, X. Chen, Ultrasound-assisted green synthesis of gold nanoparticles using citrus peel extract and their enhanced anti-inflammatory activity, Ultrason. Sonochemistry 83 (2022) 105940. https://doi.org/10.1016/j.ultsonch.2022.105940.

[125] K.D.N. Vo, C. Kowandy, L. Dupont, X. Coqueret, N.Q. Hien, Radiation synthesis of chitosan stabilized gold nanoparticles comparison between e− beam and γ irradiation, Radiat. Phys. Chem. 94 (2014) 84–87. https://doi.org/10.1016/j.radphyschem.2013.04.015.

[126] A. Kumar, M. Bhatt, G. Vyas, S. Bhatt, P. Paul, Sunlight Induced Preparation of Functionalized Gold Nanoparticles as Recyclable Colorimetric Dual Sensor for Aluminum and Fluoride in Water, ACS Appl. Mater. Interfaces 9 (2017) 17359–17368. https://doi.org/10.1021/acsami.7b02742.

[127] M.D.P. Rodríguez-Torres, L.A. Diaz -Torres, M. Olmos-López, P. Salas, C. Gutiérrez, UVA mediated synthesis of gold nanoparticles in pharmaceutical-grade heparin sodium solutions, in: Plasmonics: Metallic Nanostructures and Their Optical Properties XI, 2013: p. 88092R. https://doi.org/10.1117/12.2024441.

[128] C. Fan, W. Li, S. Zhao, J. Chen, X. Li, Efficient one pot synthesis of chitosan-induced gold nanoparticles by microwave irradiation, Mater. Lett. 62 (2008) 3518–3520. https://doi.org/10.1016/j.matlet.2008.03.040.

[129] V.K.T. Ngo, D.G. Nguyen, T.P. Huynh, Q.V. Lam, A low cost technique for synthesis of gold nanoparticles using microwave heating and its application in signal amplification for detecting Escherichia Coli O157:H7 bacteria, Adv. Nat. Sci.: Nanosci. Nanotechnol. 7 (2016) 035016. https://doi.org/10.1088/2043-6262/7/3/035016.

[130] M.E. El-Naggar, T.I. Shaheen, M.M.G. Fouda, A.A. Hebeish, Eco-friendly microwave-assisted green and rapid synthesis of well-stabilized gold and core–shell silver–gold nanoparticles, Carbohydr. Polym. 136 (2016) 1128–1136. https://doi.org/10.1016/j.carbpol.2015.10.003.

[131] J. Qiao, L. Qi, Recent progress in plant-gold nanoparticles fabrication methods and bio-applications, Talanta 223 (2021) 121396. https://doi.org/10.1016/j.talanta.2020.121396.

[132] T.H.A. Nguyen, V.C. Nguyen, T.N.H. Phan, V.T. Le, Y. Vasseghian, M.A. Trubitsyn, A.T. Nguyen, T.P. Chau, V.D. Doan, Novel biogenic silver and gold nanoparticles for multifunctional applications: Green synthesis, catalytic and antibacterial activity, and colorimetric detection of Fe(III) ions, Chemosphere 287 (2022) 132271. https://doi.org/10.1016/j.chemosphere.2021.132271.

[133] V.D. Badwaik, J.J. Bartonojo, J.W. Evans, S. V. Sahi, C.B. Willis, R. Dakshinamurthy, Single-Step Biofriendly Synthesis of Surface Modifiable, Near-Spherical Gold Nanoparticles for Applications in Biological Detection and Catalysis, Langmuir 27 (2011) 5549–5554. https://doi.org/10.1021/la105041d.

[134] M. Gholami-Shabani, M. Shams-Ghahfarokhi, Z. Gholami-Shabani, A. Akbarzadeh, G. Riazi, S. Ajdari, A. Amani, M. Razzaghi-Abyaneh, Enzymatic synthesis of gold nanoparticles using sulfite reductase purified from Escherichia coli: A green eco-friendly approach, Process Biochem. 50 (2015) 1076–1085. https://doi.org/10.1016/j.procbio.2015.04.004.

[135] T. Maruyama, Y. Fujimoto, T. Maekawa, Synthesis of gold nanoparticles using various amino acids, J. Colloid Interface Sci. 447 (2015) 254–257. https://doi.org/10.1016/j.jcis.2014.12.046.

[136] S. Roy, T.K. Das, G.P. Maiti, U. Basu, Microbial biosynthesis of nontoxic gold nanoparticles, Mater. Sci. Eng. B 203 (2016) 41–51. https://doi.org/10.1016/j.mseb.2015.10.008.

[137] M. Gholami-Shabani, M. Shams-Ghahfarokhi, Z. Gholami-Shabani, A. Akbarzadeh, G. Riazi, S. Ajdari, A. Amani, M. Razzaghi-Abyaneh, Enzymatic synthesis of gold nanoparticles using sulfite reductase purified from Escherichia coli: A green eco-friendly approach, Process Biochem. 50 (2015) 1076–1085. https://doi.org/10.1016/j.procbio.2015.04.004.

[138] T. Maruyama, Y. Fujimoto, T. Maekawa, Synthesis of gold nanoparticles using various amino acids, J. Colloid Interface Sci. 447 (2015) 254–257. https://doi.org/10.1016/j.jcis.2014.12.046.

[139] V.D. Badwaik, J.J. Bartonojo, J.W. Evans, S. V. Sahi, C.B. Willis, R. Dakshinamurthy, Single-Step Biofriendly Synthesis of Surface Modifiable, Near-Spherical Gold Nanoparticles for

Applications in Biological Detection and Catalysis, Langmuir 27 (2011) 5549–5554. https://doi.org/10.1021/la105041d.

[140] S. Ying, Z. Guan, P.C. Ofoegbu, P. Clubb, C. Rico, F. He, J. Hong, Green synthesis of nanoparticles: Current developments and limitations, Environ. Technol. Innov. 26 (2022) 102336. https://doi.org/10.1016/j.eti.2022.102336.

[141] S. Ying, Z. Guan, P.C. Ofoegbu, P. Clubb, C. Rico, F. He, J. Hong, Green synthesis of nanoparticles: Current developments and limitations, Environ. Technol. Innov. 26 (2022) 102336. https://doi.org/10.1016/j.eti.2022.102336.

[142] F. Dumur, E. Dumas, C.R. Mayer, Functionalization of gold nanoparticles by Inorganic entities, Nanomaterials 10 (2020) 548. https://doi.org/10.3390/nano10030548.

[143] A.P. Alivisatos, K.P. Johnsson, X. Peng, T.E. Wilson, C.J. Loweth, M.P. Bruchez, P.G. Schultz, Organization of "nanocrystal molecules" using DNA, Nature 382 (1996) 609–611. https://doi.org/10.1038/382609a0.

[144] C.A. Mirkin, R.L. Letsinger, R.C. Mucic, J.J. Storhoff, A DNA-based method for rationally assembling nanoparticles into macroscopic materials, Nature 382 (1996) 607–609. https://doi.org/10.1038/382607a0.

[145] J.R. Nicol, D. Dixon, J.A. Coulter, Gold nanoparticle surface functionalization: a necessary requirement in the development of novel nanotherapeutics, Nanomedicine 10 (2015) 1315–1326. https://doi.org/10.2217/nnm.14.219.

[146] Z. Wang, J.H. Lee, Y. Lu, Label-free colorimetric detection of lead ions with a nanomolar detection limit and tunable dynamic range by using gold nanoparticles and DNAzyme, Adv. Mater. 20 (2008) 3263–3267. https://doi.org/10.1002/adma.200703181.

[147] H. Li, L.J. Rothberg, Label-free colorimetric detection of specific sequences in genomic DNA amplified by the polymerase chain reaction, J. Am. Chem. Soc. 126 (2004) 10958–10961. https://doi.org/10.1021/ja048749n.

[148] T. Fellows, L. Ho, S. Flanagan, R. Fogel, D. Ojo, J. Limson, Gold nanoparticle-streptavidin conjugates for rapid and efficient screening of aptamer function in lateral flow sensors using novel CD4-binding aptamers identified through Crossover-SELEX, Analyst 145 (2020) 5180–5193. https://doi.org/10.1039/d0an00634c.

[149] J.R. Nicol, D. Dixon, J.A. Coulter, Gold nanoparticle surface functionalization: a necessary requirement in the development of novel nanotherapeutics, Nanomedicine 10 (2015) 1315–1326. https://doi.org/10.2217/nnm.14.219.

[150] Y.C. Shih, C.Y. Ke, C.J. Yu, C.Y. Lu, W.L. Tseng, Combined tween 20-stabilized gold nanoparticles and reduced graphite oxide-Fe3O4 nanoparticle composites for rapid and efficient removal of mercury species from a complex matrix, ACS Appl. Mater. Interfaces 6 (2014) 17437–17445. https://doi.org/10.1021/am5033988.

[151] Y. Zhao, Z. Wang, W. Zhang, X. Jiang, Adsorbed Tween 80 is unique in its ability to improve the stability of gold nanoparticles in solutions of biomolecules, Nanoscale 2 (2010) 2114–2119. https://doi.org/10.1039/c0nr00309c.

[152] Y. Wang, J.E.Q. Quinsaat, T. Ono, M. Maeki, M. Tokeshi, T. Isono, K. Tajima, T. Satoh, S. ichiro Sato, Y. Miura, T. Yamamoto, Enhanced dispersion stability of gold nanoparticles by the physisorption of cyclic poly(ethylene glycol), Nat. Commun. 11 (2020) 1–12. https://doi.org/10.1038/s41467-020-19947-8.

[153] M. Brust, M. Walker, D. Bethell, D.J. Schiffrin, R. Whyman, Synthesis of thiol-derivatised gold nanoparticles in a two-phase liquid-liquid system, J. Chem. Soc., Chem. Commun. (1994) 801–802. https://doi.org/10.1039/C39940000801.

[154] F. Chai, C. Wang, T. Wang, L. Li, Z. Su, Colorimetric detection of Pb2+ using glutathione functionalized gold nanoparticles, ACS Appl. Mater. Interfaces 2 (2010) 1466–1470. https://doi.org/10.1021/am100107k.

[155] J.P. Hermes, F. Sander, T. Peterle, R. Urbani, T. Pfohl, D. Thompson, M. Mayor, Gold nanoparticles stabilized by thioether dendrimers, Chem. - Eur. J. 17 (2011) 13473–13481. https://doi.org/10.1002/chem.201101837.

[156] T. Yonezawa, K. Yasui, N. Kimizuka, Controlled formation of smaller gold nanoparticles by the use of four-chained disulfide stabilizer, Langmuir 17 (2001) 271–273. https://doi.org/10.1021/la001247c.

[157] O. Tzhayik, P. Sawant, S. Efrima, E. Kovalev, J.T. Klug, Xanthate capping of silver, copper, and gold colloids, Langmuir 18 (2002) 3364–3369. https://doi.org/10.1021/la015653n.

[158] X. Zhang, M.R. Servos, J. Liu, Instantaneous and quantitative functionalization of gold nanoparticles with thiolated DNA using a pH-assisted and surfactant-free route, J. Am. Chem. Soc. 134 (2012) 7266–7269. https://doi.org/10.1021/ja3014055.

[159] C. Luo, W. Wen, F. Lin, X. Zhang, H. Gu, S. Wang, Simplified aptamer-based colorimetric method using unmodified gold nanoparticles for the detection of carcinoma embryonic antigen, RSC Adv 5 (2015) 10994–10999. https://doi.org/10.1039/c4ra14833a.

[160] H.D. Chirra, T. Sexton, D. Biswal, L.B. Hersh, J.Z. Hilt, Catalase-coupled gold nanoparticles: Comparison between the carbodiimide and biotin–streptavidin methods, Acta Biomater. 7 (2011) 2865–2872. https://doi.org/10.1016/j.actbio.2011.01.003.

[161] Á. Martínez, P. Scrimin, Gold nanoparticles crosslinking by peptides and amino acids: A tool for the colorimetric identification of amino acids, Biopolymers 109 (2018) e23111. https://doi.org/10.1002/bip.23111.

[162] X. Lin, X. Chen, Gold nanoparticles stabilized with four kinds of amino acid-derived carbon dots for colorimetric and visual discrimination of proteins and microorganisms, Microchimica Acta 186 (2019) 1–9. https://doi.org/10.1007/s00604-019-3602-7.

[163] Á. Martínez, P. Scrimin, Gold nanoparticles crosslinking by peptides and amino acids: A tool for the colorimetric identification of amino acids, Biopolymers 109 (2018) e23111. https://doi.org/10.1002/bip.23111.

[164] N. Zohora, D. Kumar, M. Yazdani, V.M. Rotello, R. Ramanathan, V. Bansal, Rapid colorimetric detection of mercury using biosynthesized gold nanoparticles, Colloids Surf. A: Physicochem. Eng. Asp. 532 (2017) 451–457. https://doi.org/10.1016/j.colsurfa.2017.04.036.

[165] F. Dumur, E. Dumas, C.R. Mayer, Functionalization of gold nanoparticles by Inorganic entities, Nanomaterials 10 (2020) 548. https://doi.org/10.3390/nano10030548.

[166] E. Harrison, J.A. Coulter, D. Dixon, Gold nanoparticle surface functionalization: Mixed monolayer versus hetero bifunctional peg linker, Nanomedicine 11 (2016) 851–865. https://doi.org/10.2217/nnm.16.28.

[167] E. Harrison, J.A. Coulter, D. Dixon, Gold nanoparticle surface functionalization: Mixed monolayer versus hetero bifunctional peg linker, Nanomedicine 11 (2016) 851–865. https://doi.org/10.2217/nnm.16.28.

[168] V. Poonthiyil, T.K. Lindhorst, V.B. Golovko, A.J. Fairbanks, Recent applications of click chemistry for the functionalization of gold nanoparticles and their conversion to glyco-gold nanoparticles, Beilstein J. Org. Chem. 14 (2017) 11–24. https://doi.org/10.3762/bjoc.14.2.

[169] T.K. Mandal, M.S. Fleming, D.R. Walt, Preparation of Polymer Coated Gold Nanoparticles by Surface-Confined Living Radical Polymerization at Ambient Temperature, Nano Lett. 2 (2002) 3–7. https://doi.org/10.1021/nl015582c.

[170] K.R. Yoon, S.M. Lee, B. Ramaraj, D.-P. Kim, Surface initiated-atom transfer radical polymerization of a sugar methacrylate on gold nanoparticles, Surf. Interface Anal. 40 (2008) 1139–1143. https://doi.org/10.1002/sia.2847.

[171] K. Saha, S.S. Agasti, C. Kim, X. Li, V.M. Rotello, Gold nanoparticles in chemical and biological sensing, Chem. Rev. 112 (2012) 2739–2779. https://doi.org/10.1021/cr2001178.

[172] Y.H. Kim, J. Jeon, S.H. Hong, W.K. Rhim, Y.S. Lee, H. Youn, J.K. Chung, M.C. Lee, D.S. Lee, K.W. Kang, J.M. Nam, Tumor targeting and imaging using cyclic RGD-PEGylated gold nanoparticle probes with directly conjugated iodine-125, Small 7 (2011) 2052–2060. https://doi.org/10.1002/smll.201100927.

[173] C.J. Mu, D.A. LaVan, R.S. Langer, B.R. Zetter, Self-Assembled Gold Nanoparticle Molecular Probes for Detecting Proteolytic Activity In Vivo, ACS Nano 4 (2010) 1511–1520. https://doi.org/10.1021/nn9017334.

[174] T.C. Chiu, C.C. Huang, Aptamer-functionalized nano-biosensors, 2009. https://doi.org/10.3390/s91210356.

[175] B. Ding, Z. Deng, H. Yan, S. Cabrini, R.N. Zuckermann, J. Bokor, Gold nanoparticle self-similar chain structure organized by DNA origami, J. Am. Chem. Soc. 132 (2010) 3248–3249. https://doi.org/10.1021/ja9101198.

[176] D.Y. Choi, S. Kim, J.W. Oh, J.M. Nam, Conjugation strategies of DNA to gold nanoparticles, Bull. Korean Chem. Soc. (2022) 1–9. https://doi.org/10.1002/bkcs.12621.

[177] B. Liu, J. Liu, Interface-Driven Hybrid Materials Based on DNA-Functionalized Gold Nanoparticles, Matter 1 (2019) 825–847. https://doi.org/10.1016/j.matt.2019.08.008.

[178] S.J. Hurst, A.K.R. Lytton-Jean, C.A. Mirkin, Maximizing DNA loading on a range of gold nanoparticle sizes, Anal. Chem. 78 (2006) 8313–8318. https://doi.org/10.1021/ac0613582.

[179] S.N. Mthembu, A. Sharma, F. Albericio, B.G. de la Torre, Breaking a Couple: Disulfide Reducing Agents, ChemBioChem 21 (2020) 1947–1954. https://doi.org/10.1002/cbic.202000092.

[180] D.Y. Choi, S. Kim, J.W. Oh, J.M. Nam, Conjugation strategies of DNA to gold nanoparticles, Bull. Korean Chem. Soc. (2022) 1–9. https://doi.org/10.1002/bkcs.12621.

[181] B. Liu, J. Liu, Methods for preparing DNA-functionalized gold nanoparticles, a key reagent of bioanalytical chemistry, Analytical Methods 9 (2017) 2633–2643. https://doi.org/10.1039/c7ay00368d.

[182] B. Moreira-Alvarez, L. Cid-Barrio, H.S. Ferreira, J.M. Costa-Fernández, J.R. Encinar, Integrated analytical platforms for the comprehensive characterization of bioconjugated inorganic nanomaterials aiming at biological applications, J. Anal. At. Spectrom. 35 (2020) 1518–1529. https://doi.org/10.1039/d0ja00147c.

[183] A.R. Esfahani, Z. Sadiq, O.D. Oyewunmi, S.H. Safiabadi Tali, N. Usen, D.C.C. Boffito, S. Jahanshahi-Anbuhi, S.H. Safiabadi-Tali, N. Usen, D.C.C. Boffito, S. Jahanshahi-Anbuhi, Portable, stable, and sensitive assay to detect phosphate in water with gold nanoparticles (AuNPs) and dextran tablet, Analyst 146 (2021) 3697–3708. https://doi.org/10.1039/D0AN02063J.

[184] E. Buhr, N. Senftleben, T. Klein, D. Bergmann, D. Gnieser, C.G. Frase, H. Bosse, Characterization of nanoparticles by scanning electron microscopy in transmission mode, Meas. Sci. Technol. 20 (2009) 084025. https://doi.org/10.1088/0957-0233/20/8/084025.

[185] J. Liu, R. Papadakis, H. Li, Experimental observation of size-dependent behavior in surface energy of gold nanoparticles through atomic force microscope, Appl. Phys. Lett. 113 (2018) 083108. https://doi.org/10.1063/1.5046736.

[186] A. Ramanaviciene, J. Voronovic, A. Popov, R. Drevinskas, A. Kausaite-Minkstimiene, A. Ramanavicius, Investigation of biocatalytic enlargement of gold nanoparticles using dynamic light scattering and atomic force microscopy, Colloids Surf. A: Physicochem. Eng. Asp. 510 (2016) 183–189. https://doi.org/10.1016/j.colsurfa.2016.07.078.

[187] T. Zheng, S. Bott, Q. Huo, Techniques for Accurate Sizing of Gold Nanoparticles Using Dynamic Light Scattering with Particular Application to Chemical and Biological Sensing Based on Aggregate Formation, ACS Appl. Mater. Interfaces 8 (2016) 21585–21594. https://doi.org/10.1021/acsami.6b06903.

[188] A.R. Esfahani, Z. Sadiq, O.D. Oyewunmi, S.H. Safiabadi Tali, N. Usen, D.C.C. Boffito, S. Jahanshahi-Anbuhi, S.H. Safiabadi-Tali, N. Usen, D.C.C. Boffito, S. Jahanshahi-Anbuhi, Portable, stable, and sensitive assay to detect phosphate in water with gold nanoparticles (AuNPs) and dextran tablet, Analyst 146 (2021) 3697–3708. https://doi.org/10.1039/D0AN02063J.

[189] C.L. Nehl, J.H. Hafner, Shape-dependent plasmon resonances of gold nanoparticles, J. Mater. Chem. 18 (2008) 2415. https://doi.org/10.1039/b714950f.

[190] T. Pellegrino, R.A. Sperling, A.P. Alivisatos, W.J. Parak, Gel electrophoresis of gold-DNA nanoconjugates., J. Biomed. Biotechnol. 2007 (2007) 26796. https://doi.org/10.1155/2007/26796.

[191] P.K. Harimech, S.R. Gerrard, A.H. El-Sagheer, T. Brown, A.G. Kanaras, Reversible Ligation of Programmed DNA-Gold Nanoparticle Assemblies, J. Am. Chem. Soc. 137 (2015) 9242–9245. https://doi.org/10.1021/jacs.5b05683.

[192] B. Abbasgholi N. Asbaghi, A. Alsadig, L. Casalis, P. Parisse, J. Niemela, S. Bellucci, H. Cabrera, An electrophoresis approach with online thermal lens detection to monitoring DNA surface coatings on gold nanoparticles, Microchem. J. 173 (2022) 106961. https://doi.org/10.1016/j.microc.2021.106961.

[193] S. Nara, V. Tripathi, H. Singh, T.G. Shrivastav, Colloidal gold probe based rapid immunochromatographic strip assay for cortisol, Anal. Chim. Acta 682 (2010) 66–71. https://doi.org/10.1016/j.aca.2010.09.041.

[194] S.A. Akintelu, S.C. Olugbeko, A.S. Folorunso, A review on synthesis, optimization, characterization and antibacterial application of gold nanoparticles synthesized from plants, Int. Nano Lett. 10 (2020) 237–248. https://doi.org/10.1007/s40089-020-00317-7.

[195] F. Arockiya Aarthi Rajathi, C. Parthiban, V. Ganesh Kumar, P. Anantharaman, Biosynthesis of antibacterial gold nanoparticles using brown alga, Stoechospermum marginatum (kützing), Spectrochim. Acta A Mol. Biomol. Spectrosc. 99 (2012) 166–173. https://doi.org/10.1016/j.saa.2012.08.081.

[196] A. von Bohlen, M. Brücher, B. Holland, R. Wagner, R. Hergenröder, X-ray standing waves and scanning electron microscopy — Energy dispersive X-ray emission spectroscopy study of gold nanoparticles, Spectrochim. Acta B: At. Spectrosc. 65 (2010) 409–414. https://doi.org/10.1016/j.sab.2010.04.017.

[197] M.Y. Chan, W. Leng, P.J. Vikesland, Surface-enhanced raman spectroscopy characterization of salt-induced aggregation of gold nanoparticles, ChemPhysChem 19 (2018) 24–28. https://doi.org/10.1002/cphc.201700798.

[198] D. Mozhayeva, C. Engelhard, A critical review of single particle inductively coupled plasma mass spectrometry-A step towards an ideal method for nanomaterial characterization, J. Anal. At. Spectrom. 35 (2020) 1740–1783. https://doi.org/10.1039/c9ja00206e.

[199] P. Pengo, S. Polizzi, M. Battagliarin, L. Pasquato, P. Scrimin, Synthesis, characterization and properties of water-soluble gold nanoparticles with tunable core size, J. Mater. Chem. 13 (2003) 2471–2478. https://doi.org/10.1039/B306366F.

[200] S. Nicolardi, Y.E.M. van der Burgt, J.D.C. Codée, M. Wuhrer, C.H. Hokke, F. Chiodo, Structural Characterization of Biofunctionalized Gold Nanoparticles by Ultrahigh-Resolution Mass Spectrometry, ACS Nano 11 (2017) 8257–8264. https://doi.org/10.1021/acsnano.7b03402.

[201] S. Link, M.A. El-Sayed, Size and temperature dependence of the plasmon absorption of colloidal gold nanoparticles, J. Phys. Chem. B 103 (1999) 4212–4217. https://doi.org/10.1021/jp984796o.

[202] P.N. Njoki, I.-I.S. Lim, D. Mott, H.-Y. Park, B. Khan, S. Mishra, R. Sujakumar, J. Luo, C.-J. Zhong, Size Correlation of Optical and Spectroscopic Properties for Gold Nanoparticles, The Journal of Physical Chemistry C 111 (2007) 14664–14669. https://doi.org/10.1021/jp074902z.

[203] H. Jans, Q. Huo, Gold nanoparticle-enabled biological and chemical detection and analysis, Chem. Soc. Rev. 41 (2012) 2849–2866. https://doi.org/10.1039/c1cs15280g.

[204] C.L. Nehl, J.H. Hafner, Shape-dependent plasmon resonances of gold nanoparticles, J. Mater. Chem. 18 (2008) 2415. https://doi.org/10.1039/b714950f.

[205] S. Zeng, K.T. Yong, I. Roy, X.Q. Dinh, X. Yu, F. Luan, A Review on Functionalized Gold Nanoparticles for Biosensing Applications, Plasmonics 6 (2011) 491–506. https://doi.org/10.1007/s11468-011-9228-1.

[206] W. Zhao, M.A. Brook, Y. Li, Design of gold nanoparticle-based colorimetric biosensing assays, ChemBioChem 9 (2008) 2363–2371. https://doi.org/10.1002/cbic.200800282.

[207] G. Frens, Particle size and sol stability in metal colloids, Kolloid-Zeitschrift & Zeitschrift Für Polymere 250 (1972) 736–741. https://doi.org/10.1007/BF01498565.

[208] F. Zhang, S. Wang, J. Liu, Gold nanoparticles adsorb DNA and aptamer probes too strongly and a comparison with graphene oxide for biosensing, Anal Chem 91 (2019) 14743–14750. https://doi.org/10.1021/acs.analchem.9b04142.

[209] F. Zhang, J. Liu, Label-Free Colorimetric Biosensors Based on Aptamers and Gold Nanoparticles: A Critical Review, Analysis & Sensing 1 (2021) 30–43. https://doi.org/10.1002/anse.202000023.

[210] W. Zhao, M.A. Brook, Y. Li, Design of gold nanoparticle-based colorimetric biosensing assays, ChemBioChem 9 (2008) 2363–2371. https://doi.org/10.1002/cbic.200800282.

[211] Y. Zhou, S. Wang, K. Zhang, X. Jiang, Visual detection of copper(II) by azide- and alkyne-functionalized gold nanoparticles using click chemistry, Angew. Chem. Int. Ed. 47 (2008) 7454–7456. https://doi.org/10.1002/anie.200802317.

[212] Y. Xie, Y. Huang, J. Li, J. Wu, A trigger-based aggregation of aptamer-functionalized gold nanoparticles for colorimetry: An example on detection of Escherichia coli O157:H7, Sens. Actuators B Chem. 339 (2021) 129865. https://doi.org/10.1016/j.snb.2021.129865.

[213] R. Pamies, J.G.H. Cifre, V.F. Espín, M. Collado-González, F.G.D. Baños, J.G. De La Torre, Aggregation behaviour of gold nanoparticles in saline aqueous media, J. Nanoparticle Res. 16 (2014) 1–11. https://doi.org/10.1007/s11051-014-2376-4.

[214] N.R. Tiwari, A. Rathore, A. Prabhune, S.K. Kulkarni, Gold Nanoparticles for Colorimetric detection of hydrolysis of antibiotics by penicillin G acylase, Adv. Biol. Biotechnol. 01 (2010) 322–329. https://doi.org/10.4236/abb.2010.14042.

[215] J. Zhang, Y. Wang, X. Yang, X. Xu, X. Yang, Specifically colorimetric recognition of calcium, strontium, and barium ions using 2-mercaptosuccinic acid-functionalized gold nanoparticles and its use in reliable detection of calcium ion in water, Analyst 136 (2011) 3865–3868. https://doi.org/10.1039/c1an15175d.

[216] K. Kim, Y.S. Nam, Y. Lee, K.B. Lee, Highly Sensitive Colorimetric Assay for Determining Fe3+ Based on Gold Nanoparticles Conjugated with Glycol Chitosan, J. Anal. Methods Chem. 2017 (2017). https://doi.org/10.1155/2017/3648564.

[217] M. Reyes, M. Piotrowski, S.K. Ang, J. Chan, S. He, J.J.H. Chu, J.C.Y. Kah, Exploiting the anti-aggregation of gold nanostars for rapid detection of hand, foot, and mouth disease causing enterovirus 71 using surface-enhanced raman spectroscopy, Anal. Chem. 89 (2017) 5373–5381. https://doi.org/10.1021/acs.analchem.7b00066.

[218] Y. Wan, J. Zhao, J. He, X. Lou, Nano-Affi: A solution-phase, label-free, colorimetric aptamer affinity assay based on binding-inhibited aggregation of gold nanoparticles, Analyst 145 (2020) 4276–4282. https://doi.org/10.1039/d0an00827c.

[219] M.R. Hormozi-Nezhad, S. Abbasi-Moayed, A sensitive and selective colorimetric method for detection of copper ions based on anti-aggregation of unmodified gold nanoparticles, Talanta 129 (2014) 227–232. https://doi.org/10.1016/j.talanta.2014.05.022.

[220] L. Mao, Q. Wang, Y. Luo, Y. Gao, Detection of Ag+ ions via an anti-aggregation mechanism using unmodified gold nanoparticles in the presence of thiamazole, Talanta 222 (2021) 121506. https://doi.org/10.1016/j.talanta.2020.121506.

[221] S. Plaisen, W. Cheewasedtham, T. Rujiralai, Robust colorimetric detection based on the anti-aggregation of gold nanoparticles for bromide in rice samples, RSC Adv. 8 (2018) 21566–21576. https://doi.org/10.1039/c8ra03497d.

[222] J. Song, P.C. Huang, Y.Q. Wan, F.Y. Wu, Colorimetric detection of thiocyanate based on anti-aggregation of gold nanoparticles in the presence of cetyltrimethyl ammonium bromide, Sens. Actuators B Chem. 222 (2016) 790–796. https://doi.org/10.1016/j.snb.2015.09.006.

[223] P.C. Huang, N. Gao, J.F. Li, F.Y. Wu, Colorimetric detection of methionine based on anti-aggregation of gold nanoparticles in the presence of melamine, Sens. Actuators B Chem. 255 (2018) 2779–2784. https://doi.org/10.1016/j.snb.2017.09.092.

[224] Y. Xianyu, Y. Lin, Q. Chen, A. Belessiotis-Richards, M.M. Stevens, M.R. Thomas, Iodide-Mediated Rapid and Sensitive Surface Etching of Gold Nanostars for Biosensing, Angew. Chem. Int. Ed. 60 (2021) 9891–9896. https://doi.org/10.1002/anie.202017317.

[225] J. Pérez-Juste, I. Pastoriza-Santos, L.M. Liz-Marzán, P. Mulvaney, Gold nanorods: Synthesis, characterization and applications, Coord. Chem. Rev. 249 (2005) 1870–1901. https://doi.org/10.1016/j.ccr.2005.01.030.

[226] Z. Zhang, H. Wang, Z. Chen, X. Wang, J. Choo, L. Chen, Plasmonic colorimetric sensors based on etching and growth of noble metal nanoparticles: Strategies and applications, Biosens. Bioelectron. 114 (2018) 52–65. https://doi.org/10.1016/j.bios.2018.05.015.

[227] Z. Zhang, H. Wang, Z. Chen, X. Wang, J. Choo, L. Chen, Plasmonic colorimetric sensors based on etching and growth of noble metal nanoparticles: Strategies and applications, Biosens. Bioelectron. 114 (2018) 52–65. https://doi.org/10.1016/j.bios.2018.05.015.

[228] S.A. Lone, K.K. Sadhu, Time-Dependent Growth of Gold Nanoparticles: Experimental Correlation of van der Waals Contact between DNA and Amino Acids with Polar Uncharged Side Chains, J. Phys. Chem. C 123 (2019) 20319–20324. https://doi.org/10.1021/acs.jpcc.9b04911.

[229] O.C. Compton, F.E. Osterloh, Evolution of size and shape in the colloidal crystallization of gold nanoparticles, J. Am. Chem. Soc. 129 (2007) 7793–7798. https://doi.org/10.1021/ja069033q.

[230] T.J. Jayeoye, U. Sirimahachai, T. Rujiralai, Sensitive colorimetric detection of ascorbic acid based on seed mediated growth of sodium alginate reduced/stabilized gold nanoparticles, Carbohydr. Polym. 255 (2021) 117376. https://doi.org/10.1016/j.carbpol.2020.117376.

[231] Y. Zhao, L. Gui, Z. Chen, Colorimetric detection of Hg2+ based on target-mediated growth of gold nanoparticles, Sens. Actuators B Chem. 241 (2017) 262–267. https://doi.org/10.1016/j.snb.2016.10.084.

[232] B. Liu, Y. Tang, Y. Yang, Y. Wu, Design an aptamer-based sensitive lateral flow biosensor for rapid determination of isocarbophos pesticide in foods, Food Control 129 (2021) 108208. https://doi.org/10.1016/j.foodcont.2021.108208.

[233] M. Zhao, X. Yao, S. Liu, H. Zhang, L. Wang, X. Yin, L. Su, B. Xu, J. Wang, Q. Lan, D. Zhang, Antibiotic and mammal IgG based lateral flow assay for simple and sensitive detection of Staphylococcus aureus, Food Chem. 339 (2021) 127955. https://doi.org/10.1016/j.foodchem.2020.127955.

[234] B.N. Khlebtsov, R.S. Tumskiy, A.M. Burov, T.E. Pylaev, N.G. Khlebtsov, Quantifying the Numbers of Gold Nanoparticles in the Test Zone of Lateral Flow Immunoassay Strips, ACS Appl. Nano Mater. 2 (2019) 5020–5028. https://doi.org/10.1021/acsanm.9b00956.

[235] W. Liu, L. Tian, J. Du, J. Wu, Y. Liu, G. Wu, X. Lu, Triggered peroxidase-like activity of Au decorated carbon dots for colorimetric monitoring of Hg2+enrichment in: Chlorella vulgaris, Analyst 145 (2020) 5500–5507. https://doi.org/10.1039/d0an00930j.

[236] R. Das, A. Dhiman, A. Kapil, V. Bansal, T.K. Sharma, Aptamer-mediated colorimetric and electrochemical detection of Pseudomonas aeruginosa utilizing peroxidase-mimic activity of gold NanoZyme, Anal. Bioanal. Chem. 411 (2019) 1229–1238. https://doi.org/10.1007/s00216-018-1555-z.

[237] J. Lou Franco, B. Das, C. Elliott, C. Cao, Gold nanozymes : From concept to biomedical applications, Springer Singapore, 2021. https://doi.org/10.1007/s40820-020-00532-z.

[238] Y. Xu, C. Lu, Y. Sun, Y. Shao, Y. Cai, Y. Zhang, J. Miao, P. Miao, A colorimetric aptasensor for the antibiotics oxytetracycline and kanamycin based on the use of magnetic beads and gold nanoparticles, Microchimica Acta 185 (2018) 1–8. https://doi.org/10.1007/s00604-018-3077-y.

[239] J. Lou Franco, B. Das, C. Elliott, C. Cao, Gold nanozymes : From concept to biomedical applications, Springer Singapore, 2021. https://doi.org/10.1007/s40820-020-00532-z.

[240] C.P. Liu, K.C. Chen, C.F. Su, P.Y. Yu, P.W. Lee, Revealing the active site of gold nanoparticles for the peroxidase-like activity: The determination of surface accessibility, Catalysts 9 (2019) 517. https://doi.org/10.3390/catal9060517.

[241] Y. Liu, Y. Xiang, Y. Zhen, R. Guo, Halide ion-induced switching of gold nanozyme activity based on Au-X interactions, Langmuir 33 (2017) 6372–6381. https://doi.org/10.1021/acs.langmuir.7b00798.

[242] D. Zhao, C. Chen, L. Lu, F. Yang, X. Yang, A label-free colorimetric sensor for sulfate based on the inhibition of peroxidase-like activity of cysteamine-modified gold nanoparticles, Sens. Actuators B Chem. 215 (2015) 437–444. https://doi.org/10.1016/j.snb.2015.04.010.

[243] Z. Chen, S. Qian, J. Chen, J. Cai, S. Wu, Z. Cai, Protein-templated gold nanoclusters based sensor for off-on detection of ciprofloxacin with a high selectivity, Talanta 94 (2012) 240–245. https://doi.org/10.1016/j.talanta.2012.03.033.

[244] C. Te Kung, C.Y. Hou, Y.N. Wang, L.M. Fu, Microfluidic paper-based analytical devices for environmental analysis of soil, air, ecology and river water, Sens. Actuators B Chem. 301 (2019) 126855. https://doi.org/10.1016/j.snb.2019.126855.

[245] J. Briffa, E. Sinagra, R. Blundell, Heavy metal pollution in the environment and their toxicological effects on humans, Heliyon 6 (2020) e04691. https://doi.org/10.1016/j.heliyon.2020.e04691.

[246] J. Briffa, E. Sinagra, R. Blundell, Heavy metal pollution in the environment and their toxicological effects on humans, Heliyon 6 (2020) e04691. https://doi.org/10.1016/j.heliyon.2020.e04691.

[247] M. Wang, Z. Chen, X. Jing, H. Zhou, Y. Wang, J. Ye, Q. Chu, Tween 20-capped gold nanoparticles for selective extraction of free low-molecular-weight thiols in saliva followed by capillary electrophoresis with contactless conductivity detection, J. Chromatogr. B: Anal. Technol. Biomed. Life Sci. 1176 (2021) 122756. https://doi.org/10.1016/j.jchromb.2021.122756.

[248] F. Chen, G. Li, H. Liu, C.H. Leung, D.L. Ma, G-quadruplex-based detection of glyphosate in complex biological systems by a time-resolved luminescent assay, Sens. Actuators B Chem. 320 (2020) 128393. https://doi.org/10.1016/j.snb.2020.128393.

[249] J.T. Zhang, T.S. Kang, S.Y. Wong, R.J. Pei, D.L. Ma, C.H. Leung, An iridium(III) complex/G-quadruplex ensemble for detection of ochratoxin A based on long-lifetime luminescent, Anal. Biochem. 580 (2019) 49–55. https://doi.org/10.1016/j.ab.2019.06.005.

[250] D.L. Ma, C. Wu, Z.Z. Dong, W.S. Tam, S.W. Wong, C. Yang, G. Li, C.H. Leung, The Development of G-Quadruplex-Based Assays for the Detection of Small Molecules and Toxic Substances, Chem. - Asian J. 12 (2017) 1851–1860. https://doi.org/10.1002/asia.201700533.

[251] A. Escarpa, Lights and shadows on Food Microfluidics, Lab Chip 14 (2014) 3213–3224. https://doi.org/10.1039/c4lc00172a.

[252] E. Della Gaspera, M. Guglielmi, S. Agnoli, G. Granozzi, M.L. Post, V. Bello, G. Mattei, A. Martucci, Au nanoparticles in nanocrystalline tio2-nio films for SPR-based, selective H2S gas sensing, Chem. Mater. 22 (2010) 3407–3417. https://doi.org/10.1021/cm100297q.

[253] E. Della Gaspera, M. Guglielmi, S. Agnoli, G. Granozzi, M.L. Post, V. Bello, G. Mattei, A. Martucci, Au nanoparticles in nanocrystalline tio2-nio films for SPR-based, selective H2S gas sensing, Chem. Mater. 22 (2010) 3407–3417. https://doi.org/10.1021/cm100297q.

[254] Z. Zhang, Z. Chen, S. Wang, C. Qu, L. Chen, On-site visual detection of hydrogen sulfide in air based on enhancing the stability of gold nanoparticles, ACS Appl. Mater. Interfaces 6 (2014) 6300–6307. https://doi.org/10.1021/am500564w.

[255] A. Martí, A.M. Costero, P. Gaviña, M. Parra, Selective colorimetric NO(g) detection based on the use of modified gold nanoparticles using click chemistry, Chem. Commun. 51 (2015) 3077–3079. https://doi.org/10.1039/c4cc10149a.

[256] D. Feng, Y. Zhang, W. Shi, X. Li, H. Ma, A simple and sensitive method for visual detection of phosgene based on the aggregation of gold nanoparticles, Chem. Commun. 46 (2010) 9203–9205. https://doi.org/10.1039/c0cc02703k.

[257] Z. Zhang, Z. Chen, S. Wang, C. Qu, L. Chen, On-site visual detection of hydrogen sulfide in air based on enhancing the stability of gold nanoparticles, ACS Appl. Mater. Interfaces 6 (2014) 6300–6307. https://doi.org/10.1021/am500564w.

[258] C. Martínez-Aquino, A.M. Costero, S. Gil, P. Gaviña, Resorcinol functionalized gold nanoparticles for formaldehyde colorimetric detection, Nanomaterials 9 (2019) 302. https://doi.org/10.3390/nano9020302.

[259] M. Harada, Minamata disease: Methylmercury poisoning in Japan caused by environmental pollution, Crit. Rev. Toxicol. 25 (1995) 1–24. https://doi.org/10.3109/10408449509089885.

[260] C.Y. Lin, C.J. Yu, Y.H. Lin, W.L. Tseng, Colorimetric sensing of silver(I) and mercury(II) ions based on an assembly of tween 20-stabilized gold nanoparticles, Anal. Chem. 82 (2010) 6830–6837. https://doi.org/10.1021/ac1007909.

[261] X. Wang, C. Shen, C. Zhou, Y. Bu, X. Yan, Methods , principles and applications of optical detection of metal ios, Chem. Eng. J. 417 (2021) 129125. https://doi.org/10.1016/j.cej.2021.129125.

[262] A.N. Berlina, D. V. Sotnikov, N.S. Komova, A. V. Zherdev, B.B. Dzantiev, Limitations for colorimetric aggregation assay of metal ions and ways of their overcoming, Anal. Methods 13 (2021) 250–257. https://doi.org/10.1039/d0ay02068k.

[263] S. Hu, P.-J.J.J. Huang, J. Wang, J. Liu, Dissecting the effect of salt for more sensitive label-free colorimetric detection of DNA using gold nanoparticles, Anal. Chem. 92 (2020) 13354–13360. https://doi.org/10.1021/acs.analchem.0c02688.

[264] M. Naderi, M. Hosseini, M.R. Ganjali, Naked-eye detection of potassium ions in a novel gold nanoparticle aggregation-based aptasensor, Spectrochim. Acta A Mol. Biomol. Spectrosc. 195 (2018) 75–83. https://doi.org/10.1016/j.saa.2018.01.051.

[265] J. Qiu, L. Fu, H. Wang, R. Zou, Y. Zhang, X. Li, A. Wu, Colorimetric detection of Cs+ based on the nonmorphological transition mechanism of gold nanoparticles in the presence of Prussian blue, New J. Chem. 44 (2020) 2241–2246. https://doi.org/10.1039/c9nj05301h.

[266] P. Duenchay, O. Chailapakul, W. Siangproh, A transparency sheet-based colorimetric device for simple determination of calcium ions using induced aggregation of modified gold nanoparticles, Int. J. Mol. Sci. 20 (2019) 2954. https://doi.org/10.3390/ijms20122954.

[267] L. Zhang, D. Huang, G. Yue, J. Zhu, L. Yang, L. Yang, W. Dan, P. Zhao, Effective colorimetric detection of Ni2+ using gold nanoparticles functionalized with phytate, Chem. Phys. Lett. 784 (2021) 139101. https://doi.org/10.1016/j.cplett.2021.139101.

[268] S. Ali, X. Chen, W. Shi, G. Huang, L. ming Yuan, L. Meng, S. Chen, X. Zhonghao, X. Chen, Recent Advances in Silver and Gold Nanoparticles-Based Colorimetric Sensors for Heavy Metal Ions Detection: A Review, Crit. Rev. Anal. Chem. (2021) 1–33. https://doi.org/10.1080/10408347.2021.1973886.

[269] G.H. Chen, W.Y. Chen, Y.C. Yen, C.W. Wang, H.T. Chang, C.F. Chen, Detection of mercury(II) ions using colorimetric gold nanoparticles on paper-based analytical devices, Anal. Chem. 86 (2014) 6843–6849. https://doi.org/10.1021/ac5008688.

[270] Y. Hu, Z. Huang, B. Liu, J. Liu, Hg(II) Adsorption on Gold Nanoparticles Dominates DNA-Based Label-Free Colorimetric Sensing, ACS Appl. Nano Mater. 4 (2021) 1377–1384. https://doi.org/10.1021/acsanm.0c02923.

[271] Y. Hu, Z. Huang, B. Liu, J. Liu, Hg(II) Adsorption on Gold Nanoparticles Dominates DNA-Based Label-Free Colorimetric Sensing, ACS Appl. Nano Mater. 4 (2021) 1377–1384. https://doi.org/10.1021/acsanm.0c02923.

[272] Y. Gan, T. Liang, Q. Hu, L. Zhong, X. Wang, H. Wan, P. Wang, In-situ detection of cadmium with aptamer functionalized gold nanoparticles based on smartphone-based colorimetric system, Talanta 208 (2020) 120231. https://doi.org/10.1016/j.talanta.2019.120231.

[273] J.R. Bhamore, A.R. Gul, S.K. Kailasa, K.W. Kim, J.S. Lee, H. Park, T.J. Park, Functionalization of gold nanoparticles using guanidine thiocyanate for sensitive and selective visual detection of Cd2+, Sens. Actuators B Chem. 334 (2021) 129685. https://doi.org/10.1016/j.snb.2021.129685.

[274] Y. Qi, J. Ma, F.R. Xiu, X. Gao, Determination of Cr(VI) based on the peroxidase mimetic catalytic activity of citrate-capped gold nanoparticles, Microchimica Acta 188 (2021). https://doi.org/10.1007/s00604-021-04942-7.

[275] A. Mohamed, X. Li, C. Li, X. Li, C. Yuan, H. Barakat, Smartphone-based colorimetric detection of chromium (Vi) by maleic acid-functionalized gold nanoparticles, Appl. Sci. (Switz.) 11 (2021) 10894. https://doi.org/10.3390/app112210894.

[276] S.Y. Ejeta, T. Imae, Selective colorimetric and electrochemical detections of Cr(III) pollutant in water on 3-mercaptopropionic acid-functionalized gold plasmon nanoparticles, Anal. Chim. Acta 1152 (2021) 338272. https://doi.org/10.1016/j.aca.2021.338272.

[277] M. Shellaiah, N. Thirumalaivasan, K.W. Sun, S.P. Wu, A pH cooperative strategy for enhanced colorimetric sensing of Cr(III) ions using biocompatible L-glutamic acid stabilized gold nanoparticles, Microchem. J. 160 (2021). https://doi.org/10.1016/j.microc.2020.105754.

[278] F. Jia, Q. Liu, Z. Chen, W. Wei, Colorimetric determination of nine metal ions based on the de-aggregation of papain-functionalized gold nanoparticles and using three chelating agents, Microchimica Acta 186 (2019) 1–7. https://doi.org/10.1007/s00604-019-4028-y.

[279] L. Yu, Y. Pang, Z. Mo, Y. Huang, X. Shen, Coordination array for accurate colorimetric sensing of multiple heavy metal ions, Talanta 231 (2021) 122357. https://doi.org/10.1016/j.talanta.2021.122357.

[280] X. Li, S. Li, Q. Liu, Z. Chen, Electronic-Tongue Colorimetric-Sensor Array for Discrimination and Quantitation of Metal Ions Based on Gold-Nanoparticle Aggregation, Anal. Chem. 91 (2019) 6315–6320. https://doi.org/10.1021/acs.analchem.9b01139.

[281] F. Sang, X. Li, Z. Zhang, J. Liu, G. Chen, Recyclable colorimetric sensor of Cr3 + and Pb2 + ions simultaneously using a zwitterionic amino acid modified gold nanoparticles, Spectrochim. Acta - A: Mol. Biomol. Spectrosc. 193 (2018) 109–116. https://doi.org/10.1016/j.saa.2017.11.048.

[282] S.J. Yoon, Y.S. Nam, Y. Lee, I.H. Oh, K.B. Lee, A dual colorimetric probe for rapid environmental monitoring of Hg2+and As3+using gold nanoparticles functionalized withd-penicillamine, RSC Adv. 11 (2021) 5456–5465. https://doi.org/10.1039/d0ra08525a.

[283] S. Marquez, E. Morales-Narváez, Nanoplasmonics in paper-based analytical devices, Front. Bioeng. Biotechnol. 7 (2019) 1–10. https://doi.org/10.3389/fbioe.2019.00069.

[284] A. Hyder, J.A. Buledi, M. Nawaz, D.B. Rajpar, Z.-H. Shah, Y. Orooji, M.L. Yola, H. Karimi-Maleh, H. Lin, A.R. Solangi, Identification of heavy metal ions from aqueous environment through gold, Silver and Copper Nanoparticles: An excellent colorimetric approach, Environ. Res. 205 (2022) 112475. https://doi.org/10.1016/j.envres.2021.112475.

[285] T. Lou, L. Chen, Z. Chen, Y. Wang, L. Chen, J. Li, Colorimetric detection of trace copper ions based on catalytic leaching of silver-coated gold nanoparticles, ACS Appl. Mater. Interfaces 3 (2011) 4215–4220. https://doi.org/10.1021/am2008486.

[286] M.R. Hormozi-Nezhad, S. Abbasi-Moayed, A sensitive and selective colorimetric method for detection of copper ions based on anti-aggregation of unmodified gold nanoparticles, Talanta 129 (2014) 227–232. https://doi.org/10.1016/j.talanta.2014.05.022.

[287] R. Liu, Z. Chen, S. Wang, C. Qu, L. Chen, Z. Wang, Colorimetric sensing of copper(II) based on catalytic etching of gold nanoparticles, Talanta 112 (2013) 37–42. https://doi.org/10.1016/j.talanta.2013.01.065.

[288] Y. Liu, D. Ding, Y. Zhen, R. Guo, Amino acid-mediated 'turn-off/turn-on' nanozyme activity of gold nanoclusters for sensitive and selective detection of copper ions and histidine, Biosens. Bioelectron. 92 (2017) 140–146. https://doi.org/10.1016/j.bios.2017.01.036.

[289] Y.F. Xie, Y.Y. Cheng, M.L. Liu, H.Y. Zou, C.Z. Huang, A single gold nanoprobe for colorimetric detection of silver(i) ions with dark-field microscopy, Analyst 144 (2019) 2011–2016. https://doi.org/10.1039/c8an02397b.

[290] X. Jiang, W. Xu, X. Chen, Y. Liang, Colorimetric assay for ultrasensitive detection of Ag(I) ions based on the formation of gold nanoparticle oligomers, Anal. Bioanal. Chem. 411 (2019) 2439–2445. https://doi.org/10.1007/s00216-019-01685-6.

[291] L. Mao, Q. Wang, Y. Luo, Y. Gao, Detection of Ag+ ions via an anti-aggregation mechanism using unmodified gold nanoparticles in the presence of thiamazole, Talanta 222 (2021) 121506. https://doi.org/10.1016/j.talanta.2020.121506.

[292] A. Safavi, R. Ahmadi, Z. Mohammadpour, Colorimetric sensing of silver ion based on anti aggregation of gold nanoparticles, Sens. Actuators B Chem. 242 (2017) 609–615. https://doi.org/10.1016/j.snb.2016.11.043.

[293] X. Li, Z. Wu, X. Zhou, J. Hu, Colorimetric response of peptide modified gold nanoparticles: An original assay for ultrasensitive silver detection, Biosens. Bioelectron. 92 (2017) 496–501. https://doi.org/10.1016/j.bios.2016.10.075.

[294] L. Zhao, Y. Wang, Z. Li, Y. Deng, X. Zhao, Y. Xia, Facile synthesis of chitosan-gold nanocomposite and its application for exclusively sensitive detection of Ag+ ions, Carbohydr. Polym. 226 (2019) 115290. https://doi.org/10.1016/j.carbpol.2019.115290.

[295] P.G. Mahajan, N.C. Dige, B.D. Vanjare, S.K. Hong, K.H. Lee, K. Hwan, Gallotannin functionalized gold nanoparticles for rapid, selective and sensitive colorimetric detection of Ag+ in aqueous medium: Approach to eco-friendly water analysis, Sens. Actuators B Chem. 281 (2019) 720–729. https://doi.org/10.1016/j.snb.2018.10.116.

[296] A. Zuber, M. Purdey, E. Schartner, C. Forbes, B. Van Der Hoek, D. Giles, A. Abell, T. Monro, H. Ebendorff-Heidepriem, Detection of gold nanoparticles with different sizes using absorption and fluorescence based method, Sens. Actuators B Chem. 227 (2016) 117–127. https://doi.org/10.1016/j.snb.2015.12.044.

[297] N. Bagheri, V. Mazzaracchio, S. Cinti, N. Colozza, C. Di Natale, P.A. Netti, M. Saraji, S. Roggero, D. Moscone, F. Arduini, Electroanalytical Sensor Based on Gold-Nanoparticle-Decorated Paper for Sensitive Detection of Copper Ions in Sweat and Serum, Anal. Chem. 93 (2021) 5225–5233. https://doi.org/10.1021/acs.analchem.0c05469.

[298] E. Priyadarshini, N. Pradhan, P.K. Panda, B.K. Mishra, Biogenic unmodified gold nanoparticles for selective and quantitative detection of cerium using UV-vis spectroscopy and photon correlation spectroscopy (DLS), Biosens. Bioelectron. 68 (2015) 598–603. https://doi.org/10.1016/j.bios.2015.01.048.

[299] X. Liu, W. Ouyang, Y. Shu, Y. Tian, Y. Feng, T. Zhang, W. Chen, Incorporating bioaccessibility into health risk assessment of heavy metals in particulate matter originated from different sources of atmospheric pollution, Environ. Pollut. 254 (2019) 113113. https://doi.org/10.1016/j.envpol.2019.113113.

[300] M. Rogosnitzky, S. Branch, Gadolinium-based contrast agent toxicity: a review of known and proposed mechanisms, BioMetals 29 (2016) 365–376. https://doi.org/10.1007/s10534-016-9931-7.

[301] K. Park, J. Park, H. Lee, J. Choi, W.J. Yu, J. Lee, Toxicity and tissue distribution of cerium oxide nanoparticles in rats by two different routes: single intravenous injection and single oral administration, Arch. Pharmacal Res. 41 (2018) 1108–1116. https://doi.org/10.1007/s12272-018-1074-7.

[302] B. He, J. Wang, J. Lin, J. Chen, Z. Zhuang, Y. Hong, L. Yan, L. Lin, B. Shi, Y. Qiu, L. Pan, X. Zheng, F. Liu, F. Chen, Association Between Rare Earth Element Cerium and the Risk of Oral Cancer: A Case-Control Study in Southeast China, Front. Public Health 9 (2021) 647120. https://doi.org/10.3389/fpubh.2021.647120.

[303] Y. Ma, P. Li, L. Zhao, J. Liu, J. Yu, Y. Huang, Y. Zhu, Z. Li, R. Zhao, S. Hua, Y. Zhu, Z. Zhang, Size-dependent cytotoxicity and reactive oxygen species of cerium oxide nanoparticles in human retinal pigment epithelia cells, Int. J. Nanomed. 16 (2021) 5333–5341. https://doi.org/10.2147/IJN.S305676.

[304] X. Liu, W. Ouyang, Y. Shu, Y. Tian, Y. Feng, T. Zhang, W. Chen, Incorporating bioaccessibility into health risk assessment of heavy metals in particulate matter originated from different sources

of atmospheric pollution, Environ. Pollut. 254 (2019) 113113. https://doi.org/10.1016/j.envpol.2019.113113.

[305] C.E. Lisowski, J.E. Hutchison, Malonamide-functionalized gold nanoparticles for selective, colorimetric sensing of trivalent lanthanide ions, Anal. Chem. 81 (2009) 10246–10253. https://doi.org/10.1021/ac902271t.

[306] R.M. Pallares, K.P. Carter, S.E. Zeltmann, T. Tratnjek, A.M. Minor, R.J. Abergel, Selective Lanthanide Sensing with Gold Nanoparticles and Hydroxypyridinone Chelators, Inorg. Chem. 59 (2020) 2030–2036. https://doi.org/10.1021/acs.inorgchem.9b03393.

[307] E. Priyadarshini, N. Pradhan, P.K. Panda, B.K. Mishra, Biogenic unmodified gold nanoparticles for selective and quantitative detection of cerium using UV-vis spectroscopy and photon correlation spectroscopy (DLS), Biosens. Bioelectron. 68 (2015) 598–603. https://doi.org/10.1016/j.bios.2015.01.048.

[308] P. Mondal, J.L. Yarger, Colorimetric Dual Sensors of Metal Ions Based on 1,2,3-Triazole-4,5-Dicarboxylic Acid-Functionalized Gold Nanoparticles, J. Phys. Chem. C 123 (2019) 20459–20467. https://doi.org/10.1021/acs.jpcc.9b03721.

[309] P. Mondal, J.L. Yarger, Colorimetric Dual Sensors of Metal Ions Based on 1,2,3-Triazole-4,5-Dicarboxylic Acid-Functionalized Gold Nanoparticles, J. Phys. Chem. C 123 (2019) 20459–20467. https://doi.org/10.1021/acs.jpcc.9b03721.

[310] A. Ducatman, M. Luster, T. Fletcher, Perfluoroalkyl substance excretion: Effects of organic anion-inhibiting and resin-binding drugs in a community setting, Environ. Toxicol. Pharmacol. 85 (2021) 103650. https://doi.org/10.1016/j.etap.2021.103650.

[311] P.D. Beer, P.A. Gale, Anion Recognition and Sensing : The State of the Art and Future Perspectives, Angew. Chem. Int. Ed. 40 (2001) 486–516.

[312] M. Sepahvand, F. Ghasemi, H.M. Seyed Hosseini, Plasmonic nanoparticles for colorimetric detection of nitrite and nitrate, Food Chem. Toxicol. 149 (2021) 112025. https://doi.org/10.1016/j.fct.2021.112025.

[313] F. Mamatioğlu, A. Üzer, E. Erçağ, R. Apak, Development of a gold nanoparticles-based colorimetric sensor for the indirect determination of ammonium dinitramide and tetryl, Talanta 226 (2021). https://doi.org/10.1016/j.talanta.2021.122187.

[314] Z. He, L. Zhang, G. Peng, G. Wang, X. Liang, Chemical redox-modulated etching of plasmonic nanoparticles for nitrite detection: Comparison among gold nanosphere, nanorod, and nanotriangle, J. Anal. Test. 5 (2021) 350–359. https://doi.org/10.1007/s41664-021-00153-4.

[315] Z. He, L. Zhang, G. Peng, G. Wang, X. Liang, Chemical redox-modulated etching of plasmonic nanoparticles for nitrite detection: Comparison among gold nanosphere, nanorod, and nanotriangle, J. Anal. Test. 5 (2021) 350–359. https://doi.org/10.1007/s41664-021-00153-4.

[316] O. Adegoke, S. Zolotovskaya, A. Abdolvand, N. Nic, Talanta Rapid and highly selective colorimetric detection of nitrite based on the catalytic-enhanced reaction of mimetic Au nanoparticle-CeO 2 nanoparticle-graphene oxide hybrid nanozyme, Talanta 224 (2021) 121875. https://doi.org/10.1016/j.talanta.2020.121875.

[317] O. Adegoke, S. Zolotovskaya, A. Abdolvand, N. Nic, Talanta Rapid and highly selective colorimetric detection of nitrite based on the catalytic-enhanced reaction of mimetic Au nanoparticle-CeO 2 nanoparticle-graphene oxide hybrid nanozyme, Talanta 224 (2021) 121875. https://doi.org/10.1016/j.talanta.2020.121875.

[318] W. Liu, Z. Du, Y. Qian, F. Li, A specific colorimetric probe for phosphate detection based on anti-aggregation of gold nanoparticles, Sens. Actuators B Chem. 176 (2013) 927–931. https://doi.org/10.1016/j.snb.2012.10.074.

[319] S. Plaisen, W. Cheewasedtham, T. Rujiralai, Robust colorimetric detection based on the anti-aggregation of gold nanoparticles for bromide in rice samples, RSC Adv. 8 (2018) 21566–21576. https://doi.org/10.1039/c8ra03497d.

[320] R. Rajamanikandan, K. Shanmugaraj, M. Ilanchelian, H. Ju, Cysteamine-decorated gold nanoparticles for plasmon-based colorimetric on-site sensors for detecting cyanide ions using the smart-phone color ratio and for catalytic reduction of 4-nitrophenol, Chemosphere 316 (2023). https://doi.org/10.1016/j.chemosphere.2023.137836.

[321] L. Wu, X. Qiu, T. Wang, K. Tao, L. Bao, E.Y. Zeng, Water Quality and Organic Pollution with Health Risk Assessment in China: A Short Review, ACS ES&T Water 2 (2022) 1279–1288. https://doi.org/10.1021/acsestwater.2c00137.

[322] A. Mishra, M. Kumari, R. Kumar, K. Iqbal, I. Shekhar, Bioresource Technology Reports Persistent organic pollutants in the environment : Risk assessment , hazards , and mitigation strategies, Bioresour. Technol. Rep. 19 (2022) 101143. https://doi.org/10.1016/j.biteb.2022.101143.

[323] X. Fan, Z. Wang, Y. Li, H. Wang, W. Fan, Z. Dong, Estimating the dietary exposure and risk of persistent organic pollutants in China: A national analysis, Environ. Pollut. 288 (2021) 117764. https://doi.org/10.1016/j.envpol.2021.117764.

[324] N. Stratakis, S. Rock, M.A. La Merrill, M. Saez, O. Robinson, D. Fecht, M. Vrijheid, D. Valvi, D. V. Conti, R. McConnell, V.L. Chatzi, Prenatal exposure to persistent organic pollutants and childhood obesity: A systematic review and meta-analysis of human studies, Obes. Rev. 23 (2022) 1–16. https://doi.org/10.1111/obr.13383.

[325] H.K. Okoro, S. Pandey, C.O. Ogunkunle, C.J. Ngila, C. Zvinowanda, I. Jimoh, I.A. Lawal, M.M. Orosun, A.G. Adeniyi, Nanomaterial-based biosorbents: Adsorbent for efficient removal of selected organic pollutants from industrial wastewater, Emerg. Contam. 8 (2022) 46–58. https://doi.org/10.1016/j.emcon.2021.12.005.

[326] M. Wagner, K.Y. Andrew Lin, W. Da Oh, G. Lisak, Metal-organic frameworks for pesticidal persistent organic pollutants detection and adsorption – A mini review, J. Hazard. Mater. 413 (2021) 125325. https://doi.org/10.1016/j.jhazmat.2021.125325.

[327] W. Bin Tseng, M.M. Hsieh, C.H. Chen, T.C. Chiu, W.L. Tseng, Functionalized gold nanoparticles for sensing of pesticides: A review, J. Food Drug Anal. 28 (2020) 521–538. https://doi.org/10.38212/2224-6614.1092.

[328] D.M. Liu, B. Xu, C. Dong, Recent advances in colorimetric strategies for acetylcholinesterase assay and their applications, TrAC - Trends Anal. Chem. 142 (2021) 116320. https://doi.org/10.1016/j.trac.2021.116320.

[329] G. Ozcelikay, A. Cetinkaya, S.I. Kaya, M. Yence, P.E. Canavar Eroğlu, M.A. Unal, S.A. Ozkan, Novel Sensor Approaches of Aflatoxins Determination in Food and Beverage Samples, Crit. Rev. Anal. Chem. (2022) 1–20. https://doi.org/10.1080/10408347.2022.2105136.

[330] S. Erarpat, S. Bodur, S. Bakırdere, Nanoparticles Based Extraction Strategies for Accurate and Sensitive Determination of Different Pesticides, Crit. Rev. Anal. Chem. 52 (2021) 1–16. https://doi.org/10.1080/10408347.2021.1876552.

[331] B.M. da Costa Filho, A.C. Duarte, T.A.P.R. Santos, Environmental monitoring approaches for the detection of organic contaminants in marine environments: A critical review, Trends Environ. Anal. Chem. 33 (2022) e00154. https://doi.org/10.1016/j.teac.2022.e00154.

[332] Y. Zhou, C. Li, R. Liu, Z. Chen, L. Li, W. Li, Y. He, L. Yuan, Label-free colorimetric detection of prothioconazole using gold nanoparticles based on one-step reaction, ACS Biomater. Sci. Eng. 6 (2020) 2805–2811. https://doi.org/10.1021/acsbiomaterials.0c00208.

[333] K. Rana, J.R. Bhamore, J. V. Rohit, T.J. Park, S.K. Kailasa, Ligand exchange reactions on citrate-gold nanoparticles for a parallel colorimetric assay of six pesticides, New J. Chem. 42 (2018) 9080–9090. https://doi.org/10.1039/c8nj01294f.

[334] S.K. Kailasa, T.P. Nguyen, S.H. Baek, L.M. Tu Phan, R. Rafique, T.J. Park, Assembly of 6-aza-2-thiothymine on gold nanoparticles for selective and sensitive colorimetric detection of pencycuron in water and food samples, Talanta 205 (2019) 120087. https://doi.org/10.1016/j.talanta.2019.06.087.

[335] S. Wang, L. Su, L. Wang, D. Zhang, G. Shen, Y. Ma, Colorimetric determination of carbendazim based on the specific recognition of aptamer and the poly-diallyldimethylammonium chloride aggregation of gold nanoparticles, Spectrochim. Acta A Mol. Biomol. Spectrosc. 228 (2020) 117809. https://doi.org/10.1016/j.saa.2019.117809.

[336] H. Chen, Q. Shi, H. Fu, O. Hu, Y. Fan, L. Xu, L. Zhang, W. Lan, D. Sun, T. Yang, Y. She, Rapid detection of five pesticide residues using complexes of gold nanoparticle and porphyrin combined with ultraviolet visible spectrum, J. Sci. Food Agric. 100 (2020) 4464–4473. https://doi.org/10.1002/jsfa.10487.

[337] C. Kuitio, S. Klangprapan, N. Chingkitti, S. Boonthavivudhi, K. Choowongkomon, Aptasensor for paraquat detection by gold nanoparticle colorimetric method, J. Environ. Sci. Health - B Pestic. Food Contam. Agric. Wastes 56 (2021) 370–377. https://doi.org/10.1080/03601234.2021.1888615.

[338] Y. Zhang, Y. Huang, L. Fu, J. Qiu, Z. Wang, A. Wu, Colorimetric detection of paraquat in aqueous and fruit juice samples based on functionalized gold nanoparticles, J. Food Compos. Anal. 92 (2020) 103574. https://doi.org/10.1016/j.jfca.2020.103574.

[339] S. Wang, Z. Ye, X. Wang, L. Xiao, Etching of single-MnO2-coated gold nanoparticles for the colorimetric detection of organophosphorus pesticides, ACS Appl. Nano Mater. 2 (2019) 6646–6654. https://doi.org/10.1021/acsanm.9b01517.

[340] S. Wang, Z. Ye, X. Wang, L. Xiao, Etching of single-MnO2-coated gold nanoparticles for the colorimetric detection of organophosphorus pesticides, ACS Appl. Nano Mater. 2 (2019) 6646–6654. https://doi.org/10.1021/acsanm.9b01517.

[341] M.M. Shah, W. Ren, J. Irudayaraj, A.A. Sajini, M.I. Ali, B. Ahmad, Colorimetric detection of organophosphate pesticides based on acetylcholinesterase and cysteamine capped gold nanoparticles as nanozyme, Sensors 21 (2021) 8050. https://doi.org/10.3390/s21238050.

[342] Y. Hu, J. Wang, Y. Wu, A simple and rapid chemosensor for colorimetric detection of dimethoate pesticide based on the peroxidase-mimicking catalytic activity of gold nanoparticles, Analytical Methods 11 (2019) 5337–5347. https://doi.org/10.1039/c9ay01506j.

[343] S.K. Kailasa, J.R. Koduru, M.L. Desai, T.J. Park, R.K. Singhal, H. Basu, Recent progress on surface chemistry of plasmonic metal nanoparticles for colorimetric assay of drugs in pharmaceutical and biological samples, TrAC - Trends Anal. Chem. 105 (2018) 106–120. https://doi.org/10.1016/j.trac.2018.05.004.

[344] X. Zhou, L. Wang, G. Shen, D. Zhang, J. Xie, A. Mamut, W. Huang, S. Zhou, Colorimetric determination of ofloxacin using unmodified aptamers and the aggregation of gold nanoparticles, Microchimica Acta 185 (2018) 1–9. https://doi.org/10.1007/s00604-018-2895-2.

[345] H. Han, J. Liu, J. Zhou, Y. Li, W. Wang, Z. Lu, Kanamycin adsorption on gold nanoparticles dominates its label-free colorimetric sensing with its aptamer, Langmuir 36 (2020) 11490–11498. https://doi.org/10.1021/acs.langmuir.0c01786.

[346] Z. Zhang, Y. Tian, P. Huang, F.Y. Wu, Using target-specific aptamers to enhance the peroxidase-like activity of gold nanoclusters for colorimetric detection of tetracycline antibiotics, Talanta 208 (2020) 120342. https://doi.org/10.1016/j.talanta.2019.120342.

[347] D.A. Raja, S.G. Musharraf, M.R. Shah, A. Jabbar, M.I. Bhanger, M.I. Malik, Poly(propylene glycol) stabilized gold nanoparticles: An efficient colorimetric assay for ceftriaxone, J. Ind. Eng. Chem. 87 (2020) 180–186. https://doi.org/10.1016/j.jiec.2020.03.041.

[348] S. Khurana, S. Kukreti, M. Kaushik, Designing a two-stage colorimetric sensing strategy based on citrate reduced gold nanoparticles: Sequential detection of Sanguinarine (anticancer drug) and

visual sensing of DNA, Spectrochim. Acta A Mol. Biomol. Spectrosc. 246 (2021) 119039. https://doi.org/10.1016/j.saa.2020.119039.

[349] Y.Y. Wu, P. Huang, F.Y. Wu, A label-free colorimetric aptasensor based on controllable aggregation of AuNPs for the detection of multiplex antibiotics, Food Chem. 304 (2020) 125377. https://doi.org/10.1016/j.foodchem.2019.125377.

[350] Q. Ma, Y. Wang, J. Jia, Y. Xiang, Colorimetric aptasensors for determination of tobramycin in milk and chicken eggs based on DNA and gold nanoparticles, Food Chem. 249 (2018) 98–103. https://doi.org/10.1016/j.foodchem.2018.01.022.

[351] X. Zhou, L. Wang, G. Shen, D. Zhang, J. Xie, A. Mamut, W. Huang, S. Zhou, Colorimetric determination of ofloxacin using unmodified aptamers and the aggregation of gold nanoparticles, Microchimica Acta 185 (2018) 1–9. https://doi.org/10.1007/s00604-018-2895-2.

[352] Y.Y. Wu, P. Huang, F.Y. Wu, A label-free colorimetric aptasensor based on controllable aggregation of AuNPs for the detection of multiplex antibiotics, Food Chem. 304 (2020) 125377. https://doi.org/10.1016/j.foodchem.2019.125377.

[353] B. Liu, J. Liu, Interface-Driven Hybrid Materials Based on DNA-Functionalized Gold Nanoparticles, Matter 1 (2019) 825–847. https://doi.org/10.1016/j.matt.2019.08.008.

[354] W. Huang, Y. Wang, L. Wang, C. Pan, G. Shen, Colorimetric detection of ciprofloxacin in aqueous solution based on an unmodified aptamer and the aggregation of gold nanoparticles, Anal. Methods 13 (2021) 90–98. https://doi.org/10.1039/d0ay01811b.

[355] H. Han, J. Liu, J. Zhou, Y. Li, W. Wang, Z. Lu, Kanamycin adsorption on gold nanoparticles dominates its label-free colorimetric sensing with its aptamer, Langmuir 36 (2020) 11490–11498. https://doi.org/10.1021/acs.langmuir.0c01786.

[356] K. Birader, P. Kumar, Y. Tammineni, J.A. Barla, S. Reddy, P. Suman, Colorimetric aptasensor for on-site detection of oxytetracycline antibiotic in milk, Food Chem. 356 (2021) 129659. https://doi.org/10.1016/j.foodchem.2021.129659.

[357] S. Ramalingam, C.M. Collier, A. Singh, A Paper-Based Colorimetric Aptasensor for the Detection of Gentamicin, Biosensors (Basel) 11 (2021) 29.

[358] Y. Xu, C. Lu, Y. Sun, Y. Shao, Y. Cai, Y. Zhang, J. Miao, P. Miao, A colorimetric aptasensor for the antibiotics oxytetracycline and kanamycin based on the use of magnetic beads and gold nanoparticles, Microchimica Acta 185 (2018) 1–8. https://doi.org/10.1007/s00604-018-3077-y.

[359] S. Ramalingam, C.M. Collier, A. Singh, A Paper-Based Colorimetric Aptasensor for the Detection of Gentamicin, Biosensors (Basel) 11 (2021) 29.

[360] W. Huang, Y. Wang, L. Wang, C. Pan, G. Shen, Colorimetric detection of ciprofloxacin in aqueous solution based on an unmodified aptamer and the aggregation of gold nanoparticles, Anal. Methods 13 (2021) 90–98. https://doi.org/10.1039/d0ay01811b.

[361] N. Pourreza, M. Ghomi, A network composed of gold nanoparticles and a poly(vinyl alcohol) hydrogel for colorimetric determination of ceftriaxone, Microchimica Acta 187 (2020) 1–10. https://doi.org/10.1007/s00604-019-4039-8.

[362] D.A. Raja, F. Munir, M.R. Shah, M.I. Bhanger, M.I. Malik, Colorimetric sensing of cephradine through polypropylene glycol functionalized gold nanoparticles, R. Soc. Open Sci. 8 (2021) 210185. https://doi.org/10.1098/rsos.210185.

[363] D.A. Raja, S.G. Musharraf, M.R. Shah, A. Jabbar, M.I. Bhanger, M.I. Malik, Poly(propylene glycol) stabilized gold nanoparticles: An efficient colorimetric assay for ceftriaxone, J. Ind. Eng. Chem. 87 (2020) 180–186. https://doi.org/10.1016/j.jiec.2020.03.041.

[364] N. Pourreza, M. Ghomi, A network composed of gold nanoparticles and a poly(vinyl alcohol) hydrogel for colorimetric determination of ceftriaxone, Microchimica Acta 187 (2020) 1–10. https://doi.org/10.1007/s00604-019-4039-8.

[365] V. Turcanu, H.A. Brough, G. Du Toit, R.X. Foong, T. Marrs, A.F. Santos, G. Lack, Immune mechanisms of food allergy and its prevention by early intervention, Curr. Opin. Immunol. 48 (2017) 92–98. https://doi.org/10.1016/j.coi.2017.08.009.

[366] T. Ramesh, P. Hong, L. Maqsood, A. Soomro, H. Zheng, X. Li, K. Wang, Visual detection of tropomyosin , a major shrimp allergenic protein using gold nanoparticles ( AuNPs )- assisted colorimetric aptasensor, Mar. Life Sci. Technol. 3 (2021) 382–394. https://doi.org/10.1007/s42995-020-00085-5.

[367] K. Xing, J. Peng, W. Chen, B. Fang, D. Liu, S. Shan, G. Zhang, Y. Huang, W. Lai, Development of a label-free plasmonic gold nanoparticles aggregates sensor on the basis of charge neutralization for the detection of zearalenone, Food Chem. 370 (2022) 131365. https://doi.org/10.1016/j.foodchem.2021.131365.

[368] E. Kim, J. Hahn, C. Ban, Y. Jo, H. Han, S. Lim, Y.J. Choi, Visible on-site detection of Ara h 1 by the switchable-linker-mediated precipitation of gold nanoparticles, Food Chem. 352 (2021) 129354. https://doi.org/10.1016/j.foodchem.2021.129354.

[369] D. Yuan, X. Fang, Y. Liu, J. Kong, Q. Chen, A hybridization chain reaction coupled with gold nanoparticles for allergen gene detection in peanut, soybean and sesame DNAs, Analyst 144 (2019) 3886–3891. https://doi.org/10.1039/c9an00394k.

[370] T. Ramesh, P. Hong, L. Maqsood, A. Soomro, H. Zheng, X. Li, K. Wang, Visual detection of tropomyosin , a major shrimp allergenic protein using gold nanoparticles ( AuNPs )- assisted colorimetric aptasensor, Mar. Life Sci. Technol. 3 (2021) 382–394. https://doi.org/10.1007/s42995-020-00085-5.

[371] J.I. Lee, S.C. Jang, J. Chung, W.K. Choi, C. Hong, G.R. Ahn, S.H. Kim, B.Y. Lee, W.J. Chung, Colorimetric allergenic fungal spore detection using peptide-modified gold nanoparticles, Sens. Actuators B Chem. 327 (2021) 128894. https://doi.org/10.1016/j.snb.2020.128894.

[372] E. Kim, J. Hahn, C. Ban, Y. Jo, H. Han, S. Lim, Y.J. Choi, Visible on-site detection of Ara h 1 by the switchable-linker-mediated precipitation of gold nanoparticles, Food Chem. 352 (2021) 129354. https://doi.org/10.1016/j.foodchem.2021.129354.

[373] D. Yuan, X. Fang, Y. Liu, J. Kong, Q. Chen, A hybridization chain reaction coupled with gold nanoparticles for allergen gene detection in peanut, soybean and sesame DNAs, Analyst 144 (2019) 3886–3891. https://doi.org/10.1039/c9an00394k.

[374] C.C. Chang, G. Wang, T. Takarada, M. Maeda, Target-recycling-Amplified colorimetric detection of pollen allergen using non-cross-linking aggregation of dna-modified gold nanoparticles, ACS Sens. 4 (2019) 363–369. https://doi.org/10.1021/acssensors.8b01156.

[375] C.C. Chang, G. Wang, T. Takarada, M. Maeda, Target-recycling-Amplified colorimetric detection of pollen allergen using non-cross-linking aggregation of dna-modified gold nanoparticles, ACS Sens. 4 (2019) 363–369. https://doi.org/10.1021/acssensors.8b01156.

[376] J. Singh, A. Mehta, Rapid and sensitive detection of mycotoxins by advanced and emerging analytical methods: A review, Food Sci. Nutr. 8 (2020) 2183–2204. https://doi.org/10.1002/fsn3.1474.

[377] X. Huang, T. Huang, X. Li, Z. Huang, Flower-like gold nanoparticles-based immunochromatographic test strip for rapid simultaneous detection of fumonisin B1 and deoxynivalenol in Chinese traditional medicine, J. Pharm. Biomed. Anal. 177 (2020) 112895. https://doi.org/10.1016/j.jpba.2019.112895.

[378] T. Bu, M. Zhang, X. Sun, Y. Tian, F. Bai, P. Jia, Y. Bai, T. Zhe, L. Wang, Gold nanoparticles-functionalized microorganisms assisted construction of immunobiosensor for sensitive detection of ochratoxin A in food samples, Sens. Actuators B Chem. 299 (2019) 126969. https://doi.org/10.1016/j.snb.2019.126969.

[379] Y. Wu, Y. Zhou, H. Huang, X. Chen, Y. Leng, W. Lai, X. Huang, Y. Xiong, Engineered gold nanoparticles as multicolor labels for simultaneous multi-mycotoxin detection on the immunochromatographic test strip nanosensor, Sens. Actuators B Chem. 316 (2020) 128107. https://doi.org/10.1016/j.snb.2020.128107.

[380] Y. Yu, Y. Li, Q. Zhang, Y. Zha, S. Lu, Y. Yang, P. Li, Y. Zhou, Colorimetric immunoassay via smartphone based on Mn2+-Mediated aggregation of AuNPs for convenient detection of fumonisin B1, Food Control 132 (2022) 108481. https://doi.org/10.1016/j.foodcont.2021.108481.

[381] W. Ren, Z. Huang, Y. Xu, Y. Li, Y. Ji, B. Su, Urchin-like gold nanoparticle-based immunochromatographic strip test for rapid detection of fumonisin B1 in grains, Anal. Bioanal. Chem. 407 (2015) 7341–7348. https://doi.org/10.1007/s00216-015-8896-7.

[382] W. Zhang, Y.Y. Wang, M. Nan, Y. Li, J. Yun, Y.Y. Wang, Y. Bi, Novel colorimetric aptasensor based on unmodified gold nanoparticle and ssDNA for rapid and sensitive detection of T-2 toxin, Food Chem. 348 (2021) 129128. https://doi.org/10.1016/j.foodchem.2021.129128.

[383] V.A. Miron-Merida, Y. Gonzalez-Espinosa, M. Collado-gonzalez, Y.Y. Gong, Y. Guo, F.M. Goycoolea, Aptamer–Target–Gold nanoparticle conjugates for the quantification of Fumonisin B1, Biosensors (Basel) 11 (2021) 1–18. https://doi.org/https://doi.org/10.3390/bios11010018.

[384] J. Lerdsri, J. Soongsong, P. Laolue, J. Jakmunee, Reliable colorimetric aptasensor exploiting 72-Mers ssDNA and gold nanoprobes for highly sensitive detection of aflatoxin M1 in milk, J. Food Compos. Anal. 102 (2021) 103992. https://doi.org/10.1016/j.jfca.2021.103992.

[385] J. Lerdsri, W. Chananchana, J. Upan, T. Sridara, J. Jakmunee, Label-free colorimetric aptasensor for rapid detection of aflatoxin B1 by utilizing cationic perylene probe and localized surface plasmon resonance of gold nanoparticles, Sens. Actuators B Chem. 320 (2020) 128356. https://doi.org/10.1016/j.snb.2020.128356.

[386] J. Qian, C. Ren, C. Wang, K. An, H. Cui, N. Hao, K. Wang, Gold nanoparticles mediated designing of versatile aptasensor for colorimetric/electrochemical dual-channel detection of aflatoxin B1, Biosens. Bioelectron. 166 (2020) 112443. https://doi.org/10.1016/j.bios.2020.112443.

[387] Y. He, F. Tian, J. Zhou, Q. Zhao, R. Fu, B. Jiao, Colorimetric aptasensor for ochratoxin A detection based on enzyme-induced gold nanoparticle aggregation, J. Hazard. Mater. 388 (2020) 121758. https://doi.org/10.1016/j.jhazmat.2019.121758.

[388] Y. He, F. Tian, J. Zhou, Q. Zhao, R. Fu, B. Jiao, Colorimetric aptasensor for ochratoxin A detection based on enzyme-induced gold nanoparticle aggregation, J. Hazard. Mater. 388 (2020) 121758. https://doi.org/10.1016/j.jhazmat.2019.121758.

[389] F. Tian, J. Zhou, R. Fu, Y. Cui, Q. Zhao, B. Jiao, Y. He, Multicolor colorimetric detection of ochratoxin A via structure-switching aptamer and enzyme-induced metallization of gold nanorods, Food Chem. 320 (2020) 126607. https://doi.org/10.1016/j.foodchem.2020.126607.

[390] W. Zhu, L. Li, Z. Zhou, X. Yang, N. Hao, Y. Guo, K. Wang, A colorimetric biosensor for simultaneous ochratoxin A and aflatoxins B1 detection in agricultural products, Food Chem. 319 (2020) 126544. https://doi.org/10.1016/j.foodchem.2020.126544.

[391] S. Sun, Y. Xie, An enhanced enzyme-linked aptamer assay for the detection of zearalenone based on gold nanoparticles, Anal. Methods 13 (2021) 1255–1260. https://doi.org/10.1039/d0ay02173c.

[392] A. Sheini, Colorimetric aggregation assay based on array of gold and silver nanoparticles for simultaneous analysis of aflatoxins, ochratoxin and zearalenone by using chemometric analysis and paper based analytical devices, Microchimica Acta 187 (2020). https://doi.org/10.1007/s00604-020-4147-5.

[393] A. Sheini, Colorimetric aggregation assay based on array of gold and silver nanoparticles for simultaneous analysis of aflatoxins, ochratoxin and zearalenone by using chemometric analysis and paper based analytical devices, Microchimica Acta 187 (2020). https://doi.org/10.1007/s00604-020-4147-5.

[394] Y. Wu, Y. Zhou, H. Huang, X. Chen, Y. Leng, W. Lai, X. Huang, Y. Xiong, Engineered gold nanoparticles as multicolor labels for simultaneous multi-mycotoxin detection on the immunochromatographic test strip nanosensor, Sens. Actuators B Chem. 316 (2020) 128107. https://doi.org/10.1016/j.snb.2020.128107.

[395] S. Cerra, T.A. Salamone, F. Sciubba, M. Marsotto, C. Battocchio, S. Nappini, F.A. Scaramuzzo, R. Li Voti, C. Sibilia, R. Matassa, A.M. Beltrán, G. Familiari, I. Fratoddi, Study of the interaction mechanism between hydrophilic thiol capped gold nanoparticles and melamine in aqueous medium, Colloids Surf. B: Biointerfaces 203 (2021) 111727. https://doi.org/10.1016/j.colsurfb.2021.111727.

[396] M. Jia, J. Sha, Z. Li, W. Wang, H. Zhang, High affinity truncated aptamers for ultra-sensitive colorimetric detection of bisphenol A with label-free aptasensor, Food Chem. 317 (2020) 126459. https://doi.org/10.1016/j.foodchem.2020.126459.

[397] J. Yang, Q. Sun, C. Huang, S. Qin, S. Han, Z. Huo, Y. Li, X. Sun, J. Chen, 3-Aminophenylboronic acid-mediated aggregation of gold nanoparticles for colorimetric sensing of iohexol in environmental and biological samples, Spectrochim. Acta A Mol. Biomol. Spectrosc. 261 (2021) 120004. https://doi.org/10.1016/j.saa.2021.120004.

[398] F. Takahashi, Y. Kazui, H. Miyaguchi, T. Ohmori, R. Tanaka, J. Jin, Simple colorimetric screening of the nerve agent VX using gold nanoparticles and a hand-powered extraction device, Sens. Actuators B Chem. 327 (2021) 128902. https://doi.org/10.1016/j.snb.2020.128902.

[399] X. Liu, F. He, F. Zhang, Z. Zhang, Z. Huang, J. Liu, Dopamine and Melamine Binding to Gold Nanoparticles Dominates Their Aptamer-Based Label-Free Colorimetric Sensing, Anal. Chem. 92 (2020) 9370–9378. https://doi.org/10.1021/acs.analchem.0c01773.

[400] M. Jia, J. Sha, Z. Li, W. Wang, H. Zhang, High affinity truncated aptamers for ultra-sensitive colorimetric detection of bisphenol A with label-free aptasensor, Food Chem. 317 (2020) 126459. https://doi.org/10.1016/j.foodchem.2020.126459.

[401] F. Takahashi, Y. Kazui, H. Miyaguchi, T. Ohmori, R. Tanaka, J. Jin, Simple colorimetric screening of the nerve agent VX using gold nanoparticles and a hand-powered extraction device, Sens. Actuators B Chem. 327 (2021) 128902. https://doi.org/10.1016/j.snb.2020.128902.

[402] J. Yang, Q. Sun, C. Huang, S. Qin, S. Han, Z. Huo, Y. Li, X. Sun, J. Chen, 3-Aminophenylboronic acid-mediated aggregation of gold nanoparticles for colorimetric sensing of iohexol in environmental and biological samples, Spectrochim. Acta A Mol. Biomol. Spectrosc. 261 (2021) 120004. https://doi.org/10.1016/j.saa.2021.120004.

[403] J. Ma, C. Liu, J. Li, Z. An, B. Zhang, W. Hong, C. Ye, M. Li, L.H. Guo, Colorimetric visualization detection of perfluorooctanoic acid based on host-guest interactions with cyclodextrin-modified gold nanoparticles, Environ Sci Nano (2025). https://doi.org/10.1039/d4en01096e.

[404] B. Brasiunas, A. Popov, A. Ramanavicius, A. Ramanaviciene, Gold nanoparticle based colorimetric sensing strategy for the determination of reducing sugars, Food Chem. 351 (2021) 129238. https://doi.org/10.1016/j.foodchem.2021.129238.

[405] W. Liang, Y. Wei, M. Gao, X. Yan, X. Zhu, W. Guo, Detection of Melamine Adulteration in Milk Powder by Using Optical Spectroscopy Technologies in the Last Decade—a Review, Food Anal. Methods 13 (2020) 2059–2069. https://doi.org/10.1007/s12161-020-01822-3.

[406] R.M. Harahap, M. Lutfi Firdaus, Nanomaterial-based colorimetric sensors for melamine and polymers analysis: A review, Proceeding International Conference on Science (ICST) 2 (2021) 1–9.

[407] S. Siddiquee, S. Saallah, N.A. Bohari, G. Ringgit, J. Roslan, L. Naher, N.F.H. Nudin, Visual and optical absorbance detection of melamine in milk by melamine-induced aggregation of gold nanoparticles, Nanomaterials 11 (2021) 1–11. https://doi.org/10.3390/nano11051142.

[408] S. Cerra, T.A. Salamone, F. Sciubba, M. Marsotto, C. Battocchio, S. Nappini, F.A. Scaramuzzo, R. Li Voti, C. Sibilia, R. Matassa, A.M. Beltrán, G. Familiari, I. Fratoddi, Study of the interaction mechanism between hydrophilic thiol capped gold nanoparticles and melamine in aqueous medium, Colloids Surf. B: Biointerfaces 203 (2021) 111727. https://doi.org/10.1016/j.colsurfb.2021.111727.

[409] T. Xie, J. Ma, M. Zhou, Y. Fu, T. Jiao, Comparison of visual detection of melamine by AuNPs sol prepared in marine and terrestrial plant extracts, Colloids Surf. A: Physicochem. Eng. Asp. 614 (2021) 126133. https://doi.org/10.1016/j.colsurfa.2021.126133.

[410] M. Elliott, Biological pollutants and biological pollution - An increasing cause for concern, Mar. Pollut. Bull. 46 (2003) 275–280. https://doi.org/10.1016/S0025-326X(02)00423-X.

[411] N.A. Rosário Filho, M. Urrutia-Pereira, G. D'Amato, L. Cecchi, I.J. Ansotegui, C. Galán, A. Pomés, M. Murrieta-Aguttes, L. Caraballo, P. Rouadi, H.J. Chong-Neto, D.B. Peden, Air pollution and indoor settings, World Allergy Organ. J. 14 (2021) 100499. https://doi.org/10.1016/j.waojou.2020.100499.

[412] W. Wang, S. Gunasekaran, Nanozymes-based biosensors for food quality and safety, TrAC - Trends Anal. Chem. 126 (2020) 115841. https://doi.org/10.1016/j.trac.2020.115841.

[413] M.M. Hassan, Y. Xu, M. Zareef, H. Li, Q. Chen, Recent progress in chemometrics driven biosensors for food application, TrAC - Trends Anal. Chem. 156 (2022) 116707. https://doi.org/10.1016/j.trac.2022.116707.

[414] K. Akshaya, C. Arthi, A.J. Pavithra, P. Poovizhi, S.S. Antinate, G.S. Hikku, K. Jeyasubramanian, R. Murugesan, Bioconjugated gold nanoparticles as an efficient colorimetric sensor for cancer diagnostics, Photodiagnosis Photodyn. Ther. 30 (2020) 101699. https://doi.org/10.1016/j.pdpdt.2020.101699.

[415] T. Yang, Z. Luo, Y. Tian, C. Qian, Y. Duan, Design strategies of AuNPs-based nucleic acid colorimetric biosensors, TrAC - Trends Anal. Chem. 124 (2020) 115795. https://doi.org/10.1016/j.trac.2019.115795.

[416] L.R. Gerber, H. McCallum, K.D. Lafferty, J.L. Sabo, A. Dobson, Exposing extinction risk analysis to pathogens: Is disease just another form of density dependence?, Ecol. Appl. 15 (2005) 1402–1414. https://doi.org/10.1890/04-0880.

[417] N. Yadav, A.K. Chhillar, J.S. Rana, Detection of pathogenic bacteria with special emphasis to biosensors integrated with AuNPs, Sensors International 1 (2020) 100028. https://doi.org/10.1016/j.sintl.2020.100028.

[418] Y. Man, M. Ban, A. Li, X. Jin, Y. Du, L. Pan, A microfluidic colorimetric biosensor for in-field detection of Salmonella in fresh-cut vegetables using thiolated polystyrene microspheres, hose-based microvalve and smartphone imaging APP, Food Chem. 354 (2021). https://doi.org/10.1016/j.foodchem.2021.129578.

[419] N. Yadav, A.K. Chhillar, J.S. Rana, Detection of pathogenic bacteria with special emphasis to biosensors integrated with AuNPs, Sensors International 1 (2020) 100028. https://doi.org/10.1016/j.sintl.2020.100028.

[420] Z. He, S. Ding, L. Wang, G. Wang, X. Liang, T. Takarada, M. Maeda, Introducing DNA Nanosensor to Undergraduate Students: Rapid Non-Cross-Linking Aggregation of DNA-Functionalized Gold Nanoparticles for Colorimetric DNA Assay, J. Chem. Educ. 98 (2021) 3553–3559. https://doi.org/10.1021/acs.jchemed.1c00605.

[421] M. Marin, M.V. Nikolic, J. Vidic, Rapid point-of-need detection of bacteria and their toxins in food using gold nanoparticles, Compr. Rev. Food Sci. Food Saf. 20 (2021) 5880–5900. https://doi.org/10.1111/1541-4337.12839.

[422] Y. Jiao, Q. Liu, H. Qiang, Z. Chen, Colorimetric detection of L-histidine based on the target-triggered self-cleavage of swing-structured DNA duplex-induced aggregation of gold nanoparticles, Microchimica Acta 185 (2018) 1–6. https://doi.org/10.1007/s00604-018-2987-z.

[423] M. Marin, M.V. Nikolic, J. Vidic, Rapid point-of-need detection of bacteria and their toxins in food using gold nanoparticles, Compr. Rev. Food Sci. Food Saf. 20 (2021) 5880–5900. https://doi.org/10.1111/1541-4337.12839.

[424] R. Gupta, A. Kumar, S. Kumar, A.K. Pinnaka, N.K. Singhal, Naked eye colorimetric detection of Escherichia coli using aptamer conjugated graphene oxide enclosed Gold nanoparticles, Sens. Actuators B Chem. 329 (2021) 129100. https://doi.org/10.1016/j.snb.2020.129100.

[425] S. Yao, J. Li, B. Pang, X. Wang, Y. Shi, X. Song, K. Xu, J. Wang, C. Zhao, Colorimetric immunoassay for rapid detection of Staphylococcus aureus based on etching-enhanced peroxidase-like catalytic activity of gold nanoparticles, Microchimica Acta 187 (2020) 1–8. https://doi.org/10.1007/s00604-020-04473-7.

[426] J. Du, Z. Yu, Z. Hu, J. Chen, J. Zhao, Y. Bai, A low pH-based rapid and direct colorimetric sensing of bacteria using unmodified gold nanoparticles, J. Microbiol. Methods 180 (2021) 106110. https://doi.org/10.1016/j.mimet.2020.106110.

[427] Q. You, X. Zhang, F.G. Wu, Y. Chen, Colorimetric and test stripe-based assay of bacteria by using vancomycin-modified gold nanoparticles, Sens. Actuators B Chem. 281 (2019) 408–414. https://doi.org/10.1016/j.snb.2018.10.103.

[428] J. Du, Z. Yu, Z. Hu, J. Chen, J. Zhao, Y. Bai, A low pH-based rapid and direct colorimetric sensing of bacteria using unmodified gold nanoparticles, J. Microbiol. Methods 180 (2021) 106110. https://doi.org/10.1016/j.mimet.2020.106110.

[429] Y. Xie, Y. Huang, J. Li, J. Wu, A trigger-based aggregation of aptamer-functionalized gold nanoparticles for colorimetry: An example on detection of Escherichia coli O157:H7, Sens. Actuators B Chem. 339 (2021) 129865. https://doi.org/10.1016/j.snb.2021.129865.

[430] Q. Chen, R. Gao, L. Jia, Enhancement of the peroxidase-like activity of aptamers modified gold nanoclusters by bacteria for colorimetric detection of Salmonella typhimurium, Talanta 221 (2021) 121476. https://doi.org/10.1016/j.talanta.2020.121476.

[431] Y. Man, M. Ban, A. Li, X. Jin, Y. Du, L. Pan, A microfluidic colorimetric biosensor for in-field detection of Salmonella in fresh-cut vegetables using thiolated polystyrene microspheres, hose-based microvalve and smartphone imaging APP, Food Chem. 354 (2021). https://doi.org/10.1016/j.foodchem.2021.129578.

[432] S. Ahmadi, H. Kamaladini, F. Haddadi, M.R. Sharifmoghadam, Thiol-Capped Gold Nanoparticle Biosensors for Rapid and Sensitive Visual Colorimetric Detection of Klebsiella pneumoniae, J. Fluoresc. 28 (2018) 987–998. https://doi.org/10.1007/s10895-018-2262-z.

[433] I.A. Quintela, B.G. De Los Reyes, C.S. Lin, V.C.H. Wu, Simultaneous colorimetric detection of a variety of Salmonella spp. In food and environmental samples by optical biosensing using oligonucleotide-gold nanoparticles, Front. Microbiol. 10 (2019) 1–12. https://doi.org/10.3389/fmicb.2019.01138.

[434] G.B.L. Silva, L.A.C. Alvarez, F. V. Campos, M.C.C. Guimarães, J.P. Oliveira, A sensitive gold nanoparticle-based lateral flow immunoassay for quantitative on-site detection of Salmonella in foods, Microchemical Journal 199 (2024). https://doi.org/10.1016/j.microc.2024.109952.

[435] K. Fu, Y. Zheng, J. Li, Y. Liu, B. Pang, X. Song, K. Xu, J. Wang, C. Zhao, Colorimetric Immunoassay for Rapid Detection of Vibrio parahemolyticus Based on Mn2+ Mediates the Assembly of Gold Nanoparticles, J. Agric. Food Chem. 66 (2018) 9516–9521. https://doi.org/10.1021/acs.jafc.8b02494.

[436] S. Yao, J. Li, B. Pang, X. Wang, Y. Shi, X. Song, K. Xu, J. Wang, C. Zhao, Colorimetric immunoassay for rapid detection of Staphylococcus aureus based on etching-enhanced peroxidase-like catalytic activity of gold nanoparticles, Microchimica Acta 187 (2020) 1–8. https://doi.org/10.1007/s00604-020-04473-7.

[437] C.N. Elliott, M.C. Becerra, J.C. Bennett, L. Graham, M.J. Silvero C., G.L. Hallett-Tapley, Facile synthesis of antibiotic-functionalized gold nanoparticles for colorimetric bacterial detection, RSC Adv. 11 (2021) 14161–14168. https://doi.org/10.1039/d1ra01316e.

[438] Q. You, X. Zhang, F.G. Wu, Y. Chen, Colorimetric and test stripe-based assay of bacteria by using vancomycin-modified gold nanoparticles, Sens. Actuators B Chem. 281 (2019) 408–414. https://doi.org/10.1016/j.snb.2018.10.103.

[439] Y. Liu, X. Wang, X. Shi, M. Sun, L. Wang, Z. Hu, F. Liu, Q. Liu, P. Wang, J. Li, C. Zhao, A colorimetric sensor for Staphylococcus aureus detection based on controlled click chemical-induced aggregation of gold nanoparticles and immunomagnetic separation, Microchimica Acta 189 (2022). https://doi.org/10.1007/s00604-022-05211-x.

[440] M. Sankar, Q. He, R. V Engel, M.A. Sainna, A.J. Logsdail, A. Roldan, D.J. Willock, N. Agarwal, C.J. Kiely, G.J. Hutchings, Role of the support in gold-containing nanoparticles as heterogeneous catalysts, Chem Rev 120 (2020) 3890–3938. https://doi.org/10.1021/acs.chemrev.9b00662.

[441] C.A. dos Santos, A.P. Ingle, M. Rai, The emerging role of metallic nanoparticles in food, Appl Microbiol Biotechnol 104 (2020) 2373–2383. https://doi.org/10.1007/s00253-020-10372-x.

[442] P. Phummirat, N. Mann, D. Preece, D. Preece, Applications of optically controlled gold nanostructures in biomedical engineering, Front Bioeng Biotechnol 8 (2021) 1–8. https://doi.org/10.3389/fbioe.2020.602021.

[443] S.A. Bansal, V. Kumar, Role of gold nanoparticles in advanced biomedical applications, Nanoscale Adv 2 (2020) 3764–3787. https://doi.org/10.1039/d0na00472c.

[444] K. Nejati, M. Dadashpour, T. Gharibi, H. Mellatyar, A. Akbarzadeh, Biomedical applications of functionalized gold nanoparticles: A Review, J Clust Sci 9 (2021). https://doi.org/10.1007/s10876-020-01955-9.

[445] K.-C. Lee, W.-J. Chen, Y.-C. Chen, Using dextran-encapsulated gold nanoparticles as insulin carriers to prolong insulin activity, Nanomedicine 12 (2017) 1823–1834. https://doi.org/10.2217/nnm-2017-0019.

[446] F. Wang, Y.C. Wang, S. Dou, M.H. Xiong, T.M. Sun, J. Wang, Doxorubicin-tethered responsive gold nanoparticles facilitate intracellular drug delivery for overcoming multidrug resistance in cancer cells, ACS Nano 5 (2011) 3679–3692. https://doi.org/10.1021/nn200007z.

[447] M. Retout, P. Blond, I. Jabin, G. Bruylants, Ultrastable PEGylated calixarene-coated gold nanoparticles with a tunable bioconjugation density for biosensing applications, Bioconjug Chem 32 (2021) 290–300. https://doi.org/10.1021/acs.bioconjchem.0c00669.

[448] Y. Yu, G. Su, W.S. Zhang, J. Pan, F. Li, M. Zhu, M. Xu, H. Zhu, Reverse transcription recombinase polymerase amplification coupled with CRISPR-Cas12a for facile and highly sensitive colorimetric SARS-CoV-2 detection, Anal Chem 93 (2021) 4126–4133. https://doi.org/10.1021/acs.analchem.1c00013.

[449] S. Hu, P.-J.J. Huang, J. Wang, J. Liu, Dissecting the effect of salt for more sensitive label-free colorimetric detection of DNA using gold nanoparticles, Anal Chem 92 (2020) 13354–13360. https://doi.org/10.1021/acs.analchem.0c02688.

[450] T. Pinheiro, A.C. Marques, P. Carvalho, R. Martins, E. Fortunato, Paper microfluidics and tailored gold nanoparticles for nonenzymatic, colorimetric multiplex biomarker detection, ACS Appl Mater Interfaces 13 (2021) 3576–3590. https://doi.org/10.1021/acsami.0c19089.

[451] P. Si, N. Razmi, O. Nur, S. Solanki, C.M. Pandey, R.K. Gupta, B.D. Malhotra, M. Willander, A. de la Zerda, Gold nanomaterials for optical biosensing and bioimaging, Nanoscale Adv 3 (2021) 2679–2698. https://doi.org/10.1039/D0NA00961J.

[452] K. Kalimuthu, B.S. Cha, S. Kim, K.S. Park, Eco-friendly synthesis and biomedical applications of gold nanoparticles: A review, Microchemical Journal 152 (2020) 104296. https://doi.org/10.1016/j.microc.2019.104296.

[453] F. Schulz, T. Homolka, N.G. Bastús, V. Puntes, H. Weller, T. Vossmeyer, Little adjustments significantly improve the Turkevich synthesis of gold nanoparticles, Langmuir 30 (2014) 10779–10784. https://doi.org/10.1021/la503209b.

[454] H. Liu, K. Ikeda, M.T. Nguyen, S. Sato, N. Matsuda, H. Tsukamoto, T. Tokunaga, T. Yonezawa, Alginate-Stabilized Gold Nanoparticles Prepared Using the Microwave-Induced Plasma-in-Liquid Process with Long-Term Storage Stability for Potential Biomedical Applications, ACS Omega (2022) acsomega.1c06769. https://doi.org/10.1021/acsomega.1c06769.

[455] N. Sarfraz, I. Khan, Plasmonic Gold Nanoparticles (AuNPs): Properties, Synthesis and their Advanced Energy, Environmental and Biomedical Applications, Chem Asian J 16 (2021) 720–742. https://doi.org/10.1002/asia.202001202.

[456] S. Chowdhury, Y.L. Teoh, K.M. Ong, N.S. Rafflisman Zaidi, S.K. Mah, Poly(vinyl) alcohol crosslinked composite packaging film containing gold nanoparticles on shelf life extension of banana, Food Packag Shelf Life 24 (2020) 100463. https://doi.org/10.1016/j.fpsl.2020.100463.

[457] K.A. Sarpong, K. Zhang, Y. Luan, Y. Cao, W. Xu, Development and application of a novel electrochemical sensor based on AuNPS and difunctional monomer-MIPs for the selective determination of Tetrabromobisphenol-S in water samples, Microchemical Journal 154 (2020) 104526. https://doi.org/10.1016/j.microc.2019.104526.

[458] Z. Hua, T. Yu, D. Liu, Y. Xianyu, Recent advances in gold nanoparticles-based biosensors for food safety detection, Biosens Bioelectron 179 (2021) 113076. https://doi.org/10.1016/j.bios.2021.113076.

[459] E. Priyadarshini, N. Pradhan, Gold nanoparticles as efficient sensors in colorimetric detection of toxic metal ions: A review, Sens Actuators B Chem 238 (2017) 888–902. https://doi.org/10.1016/j.snb.2016.06.081.

[460] W. Zhang, Y. Wang, M. Nan, Y. Li, J. Yun, Y. Wang, Y. Bi, Novel colorimetric aptasensor based on unmodified gold nanoparticle and ssDNA for rapid and sensitive detection of T-2 toxin, Food Chem 348 (2021) 129128. https://doi.org/10.1016/j.foodchem.2021.129128.

[461] A. Kasoju, N.S. Shrikrishna, D. Shahdeo, A.A. Khan, A.M. Alanazi, S. Gandhi, Microfluidic paper device for rapid detection of aflatoxin B1 using an aptamer based colorimetric assay, RSC Adv 10 (2020) 11843–11850. https://doi.org/10.1039/D0RA00062K.

[462] A. Kasoju, D. Shahdeo, A.A. Khan, N.S. Shrikrishna, S. Mahari, A.M. Alanazi, M.A. Bhat, J. Giri, S. Gandhi, Fabrication of microfluidic device for Aflatoxin M1 detection in milk samples with specific aptamers, Sci Rep 10 (2020) 1–8. https://doi.org/10.1038/s41598-020-60926-2.

[463] Q. ul A. Zahra, Z. Luo, R. Ali, M.I. Khan, F. Li, B. Qiu, Advances in gold nanoparticles-based colorimetric aptasensors for the detection of antibiotics: An overview of the past decade, Nanomaterials 11 (2021) 840. https://doi.org/10.3390/nano11040840.

[464] Y. Zha, S. Lu, P. Hu, H. Ren, Z. Liu, W. Gao, C. Zhao, Y. Li, Y. Zhou, Dual-Modal Immunosensor with Functionalized Gold Nanoparticles for Ultrasensitive Detection of Chloroacetamide Herbicides, ACS Appl Mater Interfaces 13 (2021) 6091–6098. https://doi.org/10.1021/acsami.0c21760.

[465] P. Shrivastava, B.P. Singh, S.K. Jain, V.K. Jain, S. Nagpal, A novel approach to detect barium in gunshot residue using a handheld device: a forensic application, Analytical Methods 13 (2021) 4379–4389. https://doi.org/10.1039/D1AY01272J.

[466] H. Jang, S. Ryoo, K. Kostarelos, S. Woo, D. Min, Biomaterials The effective nuclear delivery of doxorubicin from dextran-coated gold nanoparticles larger than nuclear pores, Biomaterials 34 (2013) 3503–3510. https://doi.org/10.1016/j.biomaterials.2013.01.076.

[467] S.H. Safiabadi Tali, J.J. LeBlanc, Z. Sadiq, O.D. Oyewunmi, C. Camargo, B. Nikpour, N. Armanfard, S.M. Sagan, S. Jahanshahi-Anbuhi, Tools and techniques for severe acute respiratory syndrome coronavirus 2 (SARS-CoV-2)/COVID-19 detection, Clin Microbiol Rev 34 (2021). https://doi.org/10.1128/CMR.00228-20.

[468] W. Lv, S. Liu, X. Fan, S. Wang, G. Zhang, F. Zhang, Gold nanoparticles functionalized by a dextran-based pH- And temperature-sensitive polymer, Macromol Rapid Commun 31 (2010) 454–458. https://doi.org/10.1002/marc.200900624.

[469] A.M. Jazani, J.K. Oh, Development and disassembly of single and multiple acid-cleavable block copolymer nanoassemblies for drug delivery, Polym Chem 11 (2020) 2934–2954. https://doi.org/10.1039/D0PY00234H.

[470] Y. Zhang, L. Yang, C. Yang, J. Liu, Recent advances of smart acid-responsive gold nanoparticles in tumor therapy, WIREs Nanomedicine and Nanobiotechnology 12 (2020) 1–16. https://doi.org/10.1002/wnan.1619.

[471] F. Chen, G. Huang, H. Huang, Preparation and application of dextran and its derivatives as carriers, Int J Biol Macromol 145 (2020) 827–834. https://doi.org/10.1016/j.ijbiomac.2019.11.151.

[472] R. Analysis, Y. Wang, L. Zhan, C.Z. Huang, One-pot preparation of dextran-capped gold nanoparticles at room temperature and colorimetric detection of dihydralazine sulfate in uric samples, Analytical Methods 2 (2010) 1982–1988. https://doi.org/10.1039/c0ay00470g.

[473] S. Davidović, V. Lazić, I. Vukoje, J. Papan, S.P. Anhrenkiel, S. Dimitrijević, J.M. Nedeljković, Dextran coated silver nanoparticles — Chemical sensor for selective cysteine detection, Colloids Surf B Biointerfaces 160 (2017) 184–191. https://doi.org/10.1016/j.colsurfb.2017.09.031.

[474] K. Prusty, S.K. Swain, Nanostructured gold dispersed polyethylmethaacrylate / dextran hybrid composites for packaging applications, Polymer-Plastics Technology and Materials 58 (2019) 2019–2030. https://doi.org/10.1080/25740881.2019.1602140.

[475] P.H.N. Diem, D.T.T. Thao, D. Van Phu, N.N. Duy, H.T.D. Quy, T.T. Hoa, N.Q. Hien, Synthesis of gold nanoparticles stabilized in dextran solution by gamma Co-60 ray irradiation and preparation of gold nanoparticles/dextran powder, J Chem 2017 (2017) 1–8. https://doi.org/10.1155/2017/6836375.

[476] H. Cai, P. Yao, In situ preparation of gold nanoparticle-loaded lysozyme-dextran nanogels and applications for cell imaging and drug delivery, Nanoscale 5 (2013) 2892–2900. https://doi.org/10.1039/c3nr00178d.

[477] C. Xia, B. Ren, N. Liu, Y. Zheng, A feasible strategy of fabricating of gold-encapsulated dextran/polyvinyl alcohol nanoparticles for the treatment and care of wound healing, J Clust Sci 2 (2021). https://doi.org/10.1007/s10876-021-02132-2.

[478] S. Nath, C. Kaittanis, A. Tinkham, J.M. Perez, Dextran-coated gold nanoparticles for the assessment of antimicrobial susceptibility, Anal Chem 80 (2008) 1033–1038. https://doi.org/10.1021/ac701969u.

[479] A.R. Esfahani, Z. Sadiq, O.D. Oyewunmi, S.H. Safiabadi Tali, N. Usen, D.C.C. Boffito, S. Jahanshahi-Anbuhi, S.H. Safiabadi-Tali, N. Usen, D.C.C. Boffito, S. Jahanshahi-Anbuhi, Portable, stable, and sensitive assay to detect phosphate in water with gold nanoparticles (AuNPs) and dextran tablet, Analyst 146 (2021) 3697–3708. https://doi.org/10.1039/D0AN02063J.

[480] S. Jahanshahi-Anbuhi, K. Pennings, V. Leung, M. Liu, C. Carrasquilla, B. Kannan, Y. Li, R. Pelton, J.D. Brennan, C.D.M.M. Filipe, Pullulan encapsulation of labile biomolecules to give stable bioassay tablets, Angewandte Chemie - International Edition 53 (2014) 6155–6158. https://doi.org/10.1002/anie.201403222.

[481] F. Kettemann, A. Birnbaum, S. Witte, M. Wuithschick, N. Pinna, R. Kraehnert, K. Rademann, J. Polte, Missing piece of the mechanism of the turkevich method: The critical role of citrate

protonation, Chemistry of Materials 28 (2016) 4072–4081. https://doi.org/10.1021/acs.chemmater.6b01796.

[482] J. Tang, X. Fu, Q. Ou, K. Gao, S. Man, J. Guo, Y. Liu, Hydroxide assisted synthesis of monodisperse and biocompatible gold nanoparticles with dextran, Materials Science and Engineering: C 93 (2018) 759–767. https://doi.org/10.1016/j.msec.2018.08.045.

[483] H. Nur, S. Md. Nasir, Gold nanoparticles embedded on the surface of polyvinyl alcohol layer, Malaysian Journal of Fundamental and Applied Sciences 4 (2014). https://doi.org/10.11113/mjfas.v4n1.33.

[484] P. Tripathy, A. Mishra, S. Ram, H.J. Fecht, J. Bansmann, R.J. Behm, X-ray photoelectron spectrum in surface interfacing of gold nanoparticles with polymer molecules in a hybrid nanocomposite structure, Nanotechnology 20 (2009). https://doi.org/10.1088/0957-4484/20/7/075701.

[485] L. Huang, M. Zhai, J. Peng, L. Xu, J. Li, G. Wei, Synthesis, size control and fluorescence studies of gold nanoparticles in carboxymethylated chitosan aqueous solutions, J Colloid Interface Sci 316 (2007) 398–404. https://doi.org/10.1016/j.jcis.2007.07.039.

[486] A. Sung, I. Piirma, Electrosteric stabilization of polymer colloids, Langmuir 1 (1994) 1393–1398. https://doi.org/0743-7463/94/2410-1393$04.50/0.

[487] R.Y.T. Chiu, P.T. Nguyen, J. Wang, E. Jue, B.M. Wu, D.T. Kamei, Dextran-coated gold nanoprobes for the concentration and detection of protein biomarkers, Ann Biomed Eng 42 (2014) 2322–2332. https://doi.org/10.1007/s10439-014-1043-3.

[488] J. Schubert, M. Chanana, Coating matters: review on colloidal stability of nanoparticles with biocompatible coatings in biological media, living cells and organisms, Curr Med Chem 25 (2018) 4553–4586. https://doi.org/10.2174/0929867325666180601101859.

[489] V. Kumar, D. Bano, D.K. Singh, S. Mohan, V.K. Singh, S.H. Hasan, Size-dependent synthesis of gold nanoparticles and their peroxidase-like activity for the colorimetric detection of glutathione from human blood serum, ACS Sustain Chem Eng 6 (2018) 7662–7675. https://doi.org/10.1021/acssuschemeng.8b00503.

[490] Z.N. Abdul-Ameer, Novelty Au nanoparticles with different nano sizes as an acidity sensor, Revue Des Composites et Des Materiaux Avances 31 (2021) 169–173. https://doi.org/10.18280/rcma.310308.

[491] EPA, Products with Emerging Viral Pathogens AND Human Coronavirus claims for use against SARS-CoV-2, Products with Emerging Viral Pathogens AND Human Coronavirus Claims for Use against SARS-CoV-2\ (2020) 1–38.

[492] R.J. Slaughter, M. Watts, J.A. Vale, J.R. Grieve, L.J. Schep, The clinical toxicology of sodium hypochlorite, Clin Toxicol 57 (2019) 303–311. https://doi.org/10.1080/15563650.2018.1543889.

[493] I. Santos, S. Lucas, R. Seixas, I. Lino, Organizing pneumonia after exposure to sodium hypochlorite: a case report, Cureus 12 (2020) 1–6. https://doi.org/10.7759/cureus.12025.

[494] B. Nemery, P.H.M. Hoet, D. Nowak, Indoor swimming pools, water chlorination and respiratory health., Eur Respir J 19 (2002) 790–3. https://doi.org/10.1183/09031936.02.00308602.

[495] R.J. Slaughter, M. Watts, J.A. Vale, J.R. Grieve, L.J. Schep, The clinical toxicology of sodium hypochlorite, Clin Toxicol 57 (2019) 303–311. https://doi.org/10.1080/15563650.2018.1543889.

[496] J.V.M. Santini, J.A. Barbosa, I.J.Z. Filho, F.P.L. de Castro, L.M. Tempest, Use of Sodium Hypochlorite versus Chlorexidine Gluconate as an Irrigating Solution in Endodontic Treatment: A Literature Review of the Period from 2006 to 2016, Dentistry: Advanced Research 2017 (2017) 1–5.

[497] O.M. Panasenko, V.I. Sergienko, Hypochlorite, oxidative modification of plasma lipoproteins, and atherosclerosis, Bull Exp Biol Med 131 (2001) 407–415. https://doi.org/10.1023/A:1017926309665.

[498] Y.W. Yap, M. Whiteman, N.S. Cheung, Chlorinative stress: an under appreciated mediator of neurodegeneration, Cell Signal 19 (2007) 219–228. https://doi.org/10.1016/j.cellsig.2006.06.013.

[499] C.H. Sam, H.K. Lu, The role of hypochlorous acid as one of the reactive oxygen species in periodontal disease, J Dent Sci 4 (2009) 45–54. https://doi.org/10.1016/S1991-7902(09)60008-8.

[500] World Health Organization., Guidelines for safe recreational water environments, Volume 2, Swimming pools and similar environments, World Health Organization, 2006.

[501] World health organization, Guidelines for drinking-water quality, 2022.

[502] S. Majewski, T. Bhattacharya, M. Asztalos, B. Bohaty, K.C. Durham, D.P. West, A.A. Hebert, A.S. Paller, Sodium hypochlorite body wash in the management of Staphylococcus aureus–colonized moderate-to-severe atopic dermatitis in infants, children, and adolescents, Pediatr Dermatol 36 (2019) 442–447. https://doi.org/10.1111/pde.13842.

[503] M. Johnson, P. Melbourne, Photolytic Spectroscopic Quantification of Residual Chlorine in Potable Waters, 121 (1996) 1075–1078.

[504] D. V. Girenko, A.A. Gyrenko, N. V. Nikolenko, Potentiometric determination of chlorate impurities in Hypochlorite solutions, Int J Anal Chem 2019 (2019) 1–7. https://doi.org/10.1155/2019/2360420.

[505] L.C. Adam, G. Gordon, Direct and sequential potentiometric determination of hypochlorite, chlorite, and chlorate ions when hypochlorite ion is present in large excess, Anal Chem 67 (1995) 535–540. https://doi.org/10.1021/ac00099a009.

[506] L. Lu, J. Zhang, X. Yang, Simple and selective colorimetric detection of hypochlorite based on anti-aggregation of gold nanoparticles, Sens Actuators B Chem 184 (2013) 189–195. https://doi.org/10.1016/j.snb.2013.04.073.

[507] Y. Ma, Y. Zhu, B. Liu, G. Quan, L. Cui, Colorimetric determination of hypochlorite based on the oxidative leaching of gold nanorods, Materials 11 (2018) 9–14. https://doi.org/10.3390/ma11091629.

[508] L. Wonjung, H. Youn, J. Bae, D.H. Kim, Solid-phase colorimetric sensor for hypochlorite, Analyst 146 (2021) 2301–2306. https://doi.org/10.1039/d0an02448a.

[509] J. Zhang, X. Wang, X. Yang, Colorimetric determination of hypochlorite with unmodified gold nanoparticles through the oxidation of a stabilizer thiol compound, Analyst 137 (2012) 2806–2812. https://doi.org/10.1039/c2an35239g.

[510] X. Li, X. Lin, S. Lin, X. Sun, D. Gao, B. Liu, H. Zhao, J. Zhang, S. Cong, L. Wang, Au Nanospheres@Ag Nanorods for Wide Linear Range Colorimetric Determination of Hypochlorite, ACS Appl Nano Mater 2 (2019) 3161–3168. https://doi.org/10.1021/acsanm.9b00475.

[511] Y. Guo, Q. Ma, F. Cao, Q. Zhao, X. Ji, Colorimetric detection of hypochlorite in tap water based on the oxidation of 3,3′,5,5′-tetramethyl benzidine, Analytical Methods 7 (2015) 4055–4058. https://doi.org/10.1039/c5ay00735f.

[512] L.S. Walekar, S.P. Pawar, A.H. Gore, V.D. Suryawanshi, S.S. Undare, P. V. Anbhule, S.R. Patil, G.B. Kolekar, Surfactant stabilized AgNPs as a colorimetric probe for simple and selective detection of hypochlorite anion (ClO-) in aqueous solution: Environmental sample analysis, Colloids Surf A Physicochem Eng Asp 491 (2016) 78–85. https://doi.org/10.1016/j.colsurfa.2015.11.016.

[513] A.R. Esfahani, Z. Sadiq, O.D. Oyewunmi, S.H. Safiabadi Tali, N. Usen, D.C. Boffito, S. Jahanshahi-Anbuhi, Portable, stable, and sensitive assay to detect phosphate in water with gold nanoparticles (AuNPs) and dextran tablet, Analyst 146 (2021) 3697–3708. https://doi.org/10.1039/D0AN02063J.

[514] R.P. Edachana, A. Kumaresan, V. Balasubramanian, R. Thiagarajan, B.G. Nair, S.B. Thekkedath Gopalakrishnan, Paper-based device for the colorimetric assay of bilirubin based on in-situ formation of gold nanoparticles, Microchimica Acta 187 (2020). https://doi.org/10.1007/s00604-019-4051-z.

[515] D. Zhang, Y. Liu, J. Ding, K. Hayat, X. Zhan, P. Zhou, D. Zhang, Label-free colorimetric assay for arsenic(III) determination based on a truncated short ssDNA and gold nanoparticles, (n.d.). https://doi.org/10.1007/s00604-020-04697-7/Published.

[516] H. Ravan, A. Norouzi, N. Sanadgol, E. Hosseinzadeh, Colorimetric nanoplatform for visual determination of cancer cells via target-catalyzed hairpin assembly actuated aggregation of gold nanoparticles, Microchimica Acta 187 (2020). https://doi.org/10.1007/s00604-020-04368-7.

[517] Z. Niu, Y. Liu, X. Li, H. Zhu, M. Zhang, K. Yan, H. Chen, Colorimetric detection of sulfamethazine based on target resolved calixarene derivative stabilized gold nanoparticles aggregation, Microchimica Acta 189 (2022). https://doi.org/10.1007/s00604-022-05176-x.

[518] C. Chen, J. Wang, Optical biosensors: An exhaustive and comprehensive review, Analyst 145 (2020) 1605–1628. https://doi.org/10.1039/c9an01998g.

[519] Z. Sadiq, S.H. Safiabadi Tali, H. Hajimiri, M. Al-Kassawneh, S. Jahanshahi-Anbuhi, Gold Nanoparticles-Based Colorimetric Assays for Environmental Monitoring and Food Safety Evaluation, Crit Rev Anal Chem (2022). https://doi.org/10.1080/10408347.2022.2162331.

[520] H. Chen, K. Zhou, G. Zhao, Gold nanoparticles: From synthesis, properties to their potential application as colorimetric sensors in food safety screening, Trends Food Sci Technol 78 (2018) 83–94. https://doi.org/10.1016/j.tifs.2018.05.027.

[521] J. Zhang, X. Xu, X. Yang, Role of Tris on the colorimetric recognition of anions with melamine-modified gold nanoparticle probe and the visual detection of sulfite and hypochlorite, Analyst 137 (2012) 3437–3440. https://doi.org/10.1039/c2an35609k.

[522] Y. Ma, Y. Zhu, B. Liu, G. Quan, L. Cui, Colorimetric determination of hypochlorite based on the oxidative leaching of gold nanorods, Materials 11 (2018) 9–14. https://doi.org/10.3390/ma11091629.

[523] K. Shanmugaraj, M. Ilanchelian, Visual and optical detection of hypochlorite in water samples based on etching of gold/silver alloy nanoparticles, New Journal of Chemistry 41 (2017) 14130–14136. https://doi.org/10.1039/c7nj02682j.

[524] C.-F. Huang, G.-H. Yao, R.-P. Liang, J.-D. Qiu, Graphene oxide and dextran capped gold nanoparticles based surface plasmon resonance sensor for sensitive detection of concanavalin A., Biosens Bioelectron 50 (2013) 305–10. https://doi.org/10.1016/j.bios.2013.07.002.

[525] P.H.N. Diem, D.T.T. Thao, D. Van Phu, N.N. Duy, H.T.D. Quy, T.T. Hoa, N.Q. Hien, Synthesis of gold nanoparticles stabilized in dextran solution by gamma Co-60 ray irradiation and preparation of gold nanoparticles/dextran powder, J Chem 2017 (2017). https://doi.org/10.1155/2017/6836375.

[526] M. Al-Kassawneh, Z. Sadiq, S. Jahanshahi-Anbuhi, Pullulan-stabilized gold nanoparticles tablet as a nanozyme sensor for point-of-care applications, Sens Biosensing Res 38 (2022) 100526. https://doi.org/10.1016/j.sbsr.2022.100526.

[527] M. Al-Kassawneh, Z. Sadiq, S. Jahanshahi-Anbuhi, User-friendly and ultra-stable all-inclusive gold tablets for cysteamine detection, RSC Adv 13 (2023) 19638–19650. https://doi.org/10.1039/d3ra03073c.

[528] Z. Sadiq, S.H. Safiabadi Tali, S. Jahanshahi-Anbuhi, Gold Tablets: Gold Nanoparticles Encapsulated into Dextran Tablets and Their pH-Responsive Behavior as an Easy-to-Use Platform for Multipurpose Applications, ACS Omega 7 (2022) 11177–11189. https://doi.org/10.1021/acsomega.1c07393.

[529] C.-F. Huang, G.-H. Yao, R.-P. Liang, J.-D. Qiu, Graphene oxide and dextran capped gold nanoparticles based surface plasmon resonance sensor for sensitive detection of concanavalin A., Biosens Bioelectron 50 (2013) 305–10. https://doi.org/10.1016/j.bios.2013.07.002.

[530] M. He, X. Liu, B. Liu, J. Yang, Investigation of antisolvent effect on gold nanoparticles during postsynthesis purification, J Colloid Interface Sci 537 (2019) 414–421. https://doi.org/10.1016/j.jcis.2018.11.043.

[531] Z. Liu, O.L. Lanier, A. Chauhan, Poly (vinyl alcohol) assisted synthesis and anti-solvent precipitation of gold nanoparticles, Nanomaterials 10 (2020) 1–16. https://doi.org/10.3390/nano10122359.

[532] J. Tang, X. Fu, Q. Ou, K. Gao, S.Q. Man, J. Guo, Y. Liu, Hydroxide assisted synthesis of monodisperse and biocompatible gold nanoparticles with dextran, Materials Science and Engineering C 93 (2018) 759–767. https://doi.org/10.1016/j.msec.2018.08.045.

[533] X. Liu, M. Atwater, J. Wang, Q. Huo, Extinction coefficient of gold nanoparticles with different sizes and different capping ligands, Colloids Surf B Biointerfaces 58 (2007) 3–7. https://doi.org/10.1016/j.colsurfb.2006.08.005.

[534] Z. Sadiq, S.H. Safiabadi Tali, S. Jahanshahi-Anbuhi, Gold tablets: gold nanoparticles encapsulated into dextran tablets and their pH-responsive behavior as an easy-to-use platform for multipurpose applications, ACS Omega 7 (2022) 11177–11189. https://doi.org/10.1021/acsomega.1c07393.

[535] P.H.N. Diem, D.T.T. Thao, D. Van Phu, N.N. Duy, H.T.D. Quy, T.T. Hoa, N.Q. Hien, Synthesis of gold nanoparticles stabilized in dextran solution by gamma Co-60 ray irradiation and preparation of gold nanoparticles/dextran powder, J Chem 2017 (2017) 1–8. https://doi.org/10.1155/2017/6836375.

[536] M. Pohanka, Toxicology and the biological role of methanol and Ethanol: Current view, Biomedical Papers 160 (2016) 54–63. https://doi.org/10.5507/bp.2015.023.

[537] P. Baptista, E. Pereira, P. Eaton, G. Doria, A. Miranda, I. Gomes, P. Quaresma, R. Franco, Gold nanoparticles for the development of clinical diagnosis methods, Anal Bioanal Chem 391 (2008) 943–950. https://doi.org/10.1007/s00216-007-1768-z.

[538] Y. Wang, L. Zhan, C.Z. Huang, One-pot preparation of dextran-capped gold nanoparticles at room temperature and colorimetric detection of dihydralazine sulfate in uric samples, Analytical Methods 2 (2010) 1982–1988. https://doi.org/10.1039/c0ay00470g.

[539] P.S. Popovetskiy, A.I. Bulavchenko, Determination of effective hydrodynamic diameters of biopolymer molecules in high-viscosity mixtures by photon-correlation spectroscopy, Colloid Journal 78 (2016) 196–203. https://doi.org/10.1134/S1061933X16010142.

[540] R. Tantra, P. Schulze, P. Quincey, Effect of nanoparticle concentration on zeta-potential measurement results and reproducibility, Particuology 8 (2010) 279–285. https://doi.org/10.1016/j.partic.2010.01.003.

[541] C. Kulsing, Y. Yang, C. Munera, C. Tse, M.T. Matyska, J.J. Pesek, R.I. Boysen, M.T.W. Hearn, Correlations between the zeta potentials of silica hydride-based stationary phases, analyte

retention behaviour and their ionic interaction descriptors, Anal Chim Acta 817 (2014) 48–60. https://doi.org/10.1016/j.aca.2014.01.054.

[542] L. Qing, S. Zhao, Z.G. Wang, Surface charge density in electrical double layer capacitors with nanoscale cathode-anode separation, Journal of Physical Chemistry B 125 (2021) 625–636. https://doi.org/10.1021/acs.jpcb.0c09332.

[543] F. Varenne, J.B. Coty, J. Botton, F.X. Legrand, H. Hillaireau, G. Barratt, C. Vauthier, Evaluation of zeta potential of nanomaterials by electrophoretic light scattering: Fast field reversal versus Slow field reversal modes, Talanta 205 (2019) 120062. https://doi.org/10.1016/j.talanta.2019.06.062.

[544] C.J. Chin, S.C. Lu, S. Yiacoumi, C. Tsouris, Fractal dimension of particle aggregates in magnetic fields, Sep Sci Technol 39 (2004) 2839–2862. https://doi.org/10.1081/SS-200028768.

[545] X. Wang, Y.L. Xiong, Oxidative polyaldehyde production: a novel approach to the conjugation of dextran with soy peptides for improved emulsifying properties, J Food Sci Technol 53 (2016) 3215–3224. https://doi.org/10.1007/s13197-016-2296-7.

[546] H. Wu, D. cong Shang-guan, Q. meng Lu, X. qin Hu, J. wen Yang, H. bin Zhang, Oxidation of dextran using H2O2 and NaClO/NaBr and their applicability in iron chelation, Int J Biol Macromol 144 (2020) 615–623. https://doi.org/10.1016/j.ijbiomac.2019.12.104.

[547] S. Jailani, G. V. Franks, T.W. Healy, ζ-Potential of nanoparticle suspensions: effect of electrolyte concentration, particle size, and volume fraction, Journal of the American Ceramic Society 91 (2008) 1141–1147. https://doi.org/10.1111/j.1551-2916.2008.02277.x.

[548] X. Xu, J. Ji, P. Chen, J. Wu, Y. Jin, L. Zhang, S. Du, Salt-induced gold nanoparticles aggregation lights up fluorescence of DNA-silver nanoclusters to monitor dual cancer markers carcinoembryonic antigen and carbohydrate antigen 125, Anal Chim Acta 1125 (2020) 41–49. https://doi.org/10.1016/j.aca.2020.05.027.

[549] R.D. Wesley, T. Cosgrove, L. Thompson, S.P. Armes, N.C. Billingham, F.L. Baines, Hydrodynamic layer thickness of a polybase brush in the presence of salt, Langmuir 16 (2000) 4467–4469. https://doi.org/10.1021/la991263d.

[550] R. Epsztein, E. Shaulsky, M. Qin, M. Elimelech, Activation behavior for ion permeation in ion-exchange membranes: Role of ion dehydration in selective transport, J Memb Sci 580 (2019) 316–326. https://doi.org/10.1016/j.memsci.2019.02.009.

[551] N.T. Kim Thanh, Z. Rosenzweig, Development of an aggregation-based immunoassay for anti-protein A using gold nanoparticles, Anal Chem 74 (2002) 1624–1628. https://doi.org/10.1021/ac011127p.

[552] Z. Zhang, S. Maji, A.B.D.F. Antunes, R. De Rycke, Q. Zhang, R. Hoogenboom, B.G. De Geest, Salt plays a pivotal role in the temperature-responsive aggregation and layer-by-layer assembly of polymer-decorated gold nanoparticles, Chemistry of Materials 25 (2013) 4297–4303. https://doi.org/10.1021/cm402414u.

[553] J.M. Andrade, M.G. Estévez-Pérez, Statistical comparison of the slopes of two regression lines: A tutorial, Anal Chim Acta 838 (2014) 1–12. https://doi.org/10.1016/j.aca.2014.04.057.

[554] A. Gallina, P. Pastore, F. Magno, The use of nitrite ion in the chromatographic determination of large amounts of hypochlorite ion and of traces of chlorite and chlorate ions, Analyst 124 (1999) 1439–1442. https://doi.org/10.1039/a904562g.

[555] R. Chen, S. Xing, T. Hu, Y. Li, J. Chen, Q. Niu, T. Li, Highly sensitive fluorescent sensor for hypochlorite in nearly 100% aqueous solution and its application for live-cell, plant and zebrafish imaging, Anal Chim Acta 1237 (2023) 340557. https://doi.org/10.1016/j.aca.2022.340557.

[556] S. Ata, F.H. Wattoo, M. Ahmed, M.H.S. Wattoo, S.A. Tirmizi, A. Wadood, A method optimization study for atomic absorption spectrophotometric determination of total zinc in insulin using direct aspiration technique, Alexandria Journal of Medicine 51 (2015) 19–23. https://doi.org/10.1016/j.ajme.2014.03.004.

[557] G. Pizzino, N. Irrera, M. Cucinotta, G. Pallio, F. Mannino, V. Arcoraci, F. Squadrito, D. Altavilla, A. Bitto, Oxidative stress: harms and benefits for human health, Oxid Med Cell Longev 2017 (2017) 1–13. https://doi.org/10.1155/2017/8416763.

[558] S.K. Raut, M. Khullar, Oxidative stress in metabolic diseases: current scenario and therapeutic relevance, Mol Cell Biochem 478 (2023) 185–196. https://doi.org/10.1007/s11010-022-04496-z.

[559] Y. Wang, H. Zhang, Z. Wang, Z. Geng, H. Liu, H. Yang, P. Song, Q. Liu, Therapeutic effect of nerve growth factor on cerebral infarction in dogs using the hemisphere anomalous volume ratio of diffusion-weighted magnetic resonance imaging, Neural Regen Res 7 (2012) 1873–1880. https://doi.org/10.3969/j.issn.1673-5374.

[560] H. Tsutsui, S. Kinugawa, S. Matsushima, Oxidative stress and heart failure, J Physiol Heart Circ Physiol 301 (2011) 2181–2190. https://doi.org/10.1152/ajpheart.00554.2011.-Oxidative.

[561] M. Sharifi-Rad, N. V. Anil Kumar, P. Zucca, E.M. Varoni, L. Dini, E. Panzarini, J. Rajkovic, P.V. Tsouh Fokou, E. Azzini, I. Peluso, A. Prakash Mishra, M. Nigam, Y. El Rayess, M. El Beyrouthy, L. Polito, M. Iriti, N. Martins, M. Martorell, A.O. Docea, W.N. Setzer, D. Calina, W.C. Cho, J. Sharifi-Rad, Lifestyle, oxidative stress, and antioxidants: back and forth in the pathophysiology of chronic diseases, Front Physiol 11 (2020) 694. https://doi.org/10.3389/fphys.2020.00694.

[562] M. Graille, P. Wild, J.-J. Sauvain, M. Hemmendinger, I. Guseva Canu, N.B. Hopf, Urinary 8-OHdG as a Biomarker for Oxidative Stress: A Systematic Literature Review and Meta-Analysis, Int J Mol Sci 21 (2020) 3743. https://doi.org/10.3390/ijms21113743.

[563] A. Toto, P. Wild, M. Graille, V. Turcu, C. Crézé, M. Hemmendinger, J.-J. Sauvain, E. Bergamaschi, I. Guseva Canu, N.B. Hopf, Urinary malondialdehyde (MDA) concentrations in the general population—A systematic literature review and meta-analysis, Toxics 10 (2022) 160. https://doi.org/10.3390/toxics10040160.

[564] S. Pennathur, V. Jackson-Lewis, S. Przedborski, J.W. Heinecke, Mass spectrometric quantification of 3-nitrotyrosine, ortho-tyrosine, and o,o'-dityrosine in brain tissue of 1-methyl-4-phenyl-1,2,3,6- tetrahydropyridine-treated mice, a model of oxidative stress in Parkinson's disease, Journal of Biological Chemistry 274 (1999) 34621–34628. https://doi.org/10.1074/jbc.274.49.34621.

[565] H. Kaur, B. Halliwell, Detection of hydroxyl radicals by aromatic hydroxylation, in: Methods Enzymol, 1994: pp. 67–82. https://doi.org/10.1016/S0076-6879(94)33009-3.

[566] G.M. Rosen, M.S. Cohen, B.E. Britigan, S. Pou, Application of spin traps to biological systems, Free Radic Res Commun 9 (1990) 187–195. https://doi.org/10.3109/10715769009145676.

[567] H. Kasai, Analysis of a form of oxidative DNA damage, 8-hydroxy-2′-deoxyguanosine, as a marker of cellular oxidative stress during carcinogenesis, Mutation Research/Reviews in Mutation Research 387 (1997) 147–163. https://doi.org/10.1016/S1383-5742(97)00035-5.

[568] J.W.M. Yuen, I.F.F. Benzie, Hydrogen peroxide in urine as a potential biomarker of whole body oxidative stress, Free Radic Res 37 (2003) 1209–1213. https://doi.org/10.1080/10715760310001616032.

[569] Y. Sato, K. Ogino, N. Sakano, D.H. Wang, J. Yoshida, Y. Akazawa, S. Kanbara, K. Inoue, M. Kubo, H. Takahashi, Evaluation of urinary hydrogen peroxide as an oxidative stress biomarker in a healthy Japanese population, Free Radic Res 47 (2013) 181–191. https://doi.org/10.3109/10715762.2012.759218.

[570] S.D. Varma, P.S. Devamanoharan, Excretion of hydrogen peroxide in human urine, Free Radic Res Commun 8 (1990) 73–78. https://doi.org/10.3109/10715769009087976.

[571] V.R. Preedy, V.B. Patel, General methods in biomarker research and their applications, Springer Netherlands, 2018. https://doi.org/10.1007/978-94-007-7696-8.

[572] G.W. Dryden, I. Deaciuc, G. Arteel, C.J. McClain, Clinical implications of oxidative stress and antioxidant therapy, Curr Gastroenterol Rep 7 (2005) 308–316. https://doi.org/10.1007/s11894-005-0024-y.

[573] V.S. Watwe, S.D. Kulkarni, P.S. Kulkarni, Cr(VI)-mediated homogeneous Fenton oxidation for decolorization of methylene blue dye: sludge free and pertinent to a wide pH range, ACS Omega 6 (2021) 27288–27296. https://doi.org/10.1021/acsomega.1c04090.

[574] O. Legrini, E. Oliveros, A.M. Braun, Photochemical Processes for Water Treatment, Chem Rev 93 (1993) 671–698. https://doi.org/10.1021/cr00018a003.

[575] W. Ben, Z. Qiang, X. Pan, M. Chen, Removal of veterinary antibiotics from sequencing batch reactor (SBR) pretreated swine wastewater by Fenton's reagent, Water Res 43 (2009) 4392–4402. https://doi.org/10.1016/j.watres.2009.06.057.

[576] C.P. Rubio, J.J. Cerón, Spectrophotometric assays for evaluation of Reactive Oxygen Species (ROS) in serum: general concepts and applications in dogs and humans, BMC Vet Res 17 (2021) 226. https://doi.org/10.1186/s12917-021-02924-8.

[577] Z. Zhang, Z. Chen, F. Cheng, Y. Zhang, L. Chen, Highly sensitive on-site detection of glucose in human urine with naked eye based on enzymatic-like reaction mediated etching of gold nanorods, Biosens Bioelectron 89 (2017) 932–936. https://doi.org/10.1016/j.bios.2016.09.090.

[578] E. Chamarro, A. Marco, S. Esplugas, Use of Fenton reagent to improve organic chemical biodegradability, Water Res 35 (2001) 1047–1051. https://doi.org/10.1016/S0043-1354(00)00342-0.

[579] S.A.G. Evans, J.M. Elliott, L.M. Andrews, P.N. Bartlett, P.J. Doyle, G. Denuault, Detection of hydrogen peroxide at mesoporous platinum microelectrodes, Anal Chem 74 (2002) 1322–1326. https://doi.org/10.1021/ac011052p.

[580] W. Chen, J. Chen, Y. Bin Feng, L. Hong, Q.Y. Chen, L.F. Wu, X.H. Lin, X.H. Xia, Peroxidase-like activity of water-soluble cupric oxide nanoparticles and its analytical application for detection of hydrogen peroxide and glucose, Analyst 137 (2012) 1706–1712. https://doi.org/10.1039/c2an35072f.

[581] X. Cao, Z. Zeng, W. Shi, P. Yep, Q. Yan, H. Zhang, Three-dimensional graphene network composites for detection of hydrogen peroxide, Small 9 (2013) 1703–1707. https://doi.org/10.1002/smll.201200683.

[582] Q. Liu, Y. Huang, S. Wang, S. Yang, Z. Jiang, S. Huang, Monodispersed Au nanoparticles decorated MoS2 nanosheets with enhanced peroxidase-like activity based electrochemical H2O2 sensing for anticancer drug evaluations, Anal Chim Acta 1320 (2024) 342996. https://doi.org/10.1016/j.aca.2024.342996.

[583] Z. Sadiq, S.H. Safiabadi Tali, S. Jahanshahi-Anbuhi, Gold Tablets: Gold Nanoparticles Encapsulated into Dextran Tablets and Their pH-Responsive Behavior as an Easy-to-Use Platform for Multipurpose Applications, ACS Omega 7 (2022) 11177–11189. https://doi.org/10.1021/acsomega.1c07393.

[584] Z. Chen, A. Cao, D. Liu, Z. Zhu, F. Yang, Y. Fan, R. Liu, Z. Huang, Y. Li, Self-Confined Dewetting Mechanism in Wafer-Scale Patterning of Gold Nanoparticle Arrays with Strong Surface Lattice Resonance for Plasmonic Sensing, Advanced Science 11 (2024). https://doi.org/10.1002/advs.202306239.

[585] A.N. Frickenstein, N. Means, Y. He, L. Whitehead, T. Harcourt, Z. Malik, V. Sheth, L. Longacre, H. Taffe, L. Wang, I. McSpadden, C. Baroody, W. Yang, Y.D. Zhao, S. Wilhelm, The Predictive Synthesis of Monodisperse and Biocompatible Gold Nanoparticles, ACS Appl Nano Mater (2024). https://doi.org/10.1021/acsanm.4c04838.

[586] J. Ye, Z. Chen, W. Chen, Y. Zhao, C. Ding, Y. Huang, Gold Nanoparticles Coated with Silica Shells as High-Performance Fluorescence Nanoprobe, ACS Appl Nano Mater 7 (2024) 5543–5553. https://doi.org/10.1021/acsanm.4c00243.

[587] X. Liu, D. Huang, C. Lai, Y. Chen, X. Zhou, F. Xu, Functionalized Gold Nanoparticles for Visual Determination of Dopamine in Biological Fluids, ACS Appl Nano Mater 5 (2022) 7357–7364. https://doi.org/10.1021/acsanm.2c01294.

[588] T. Ishida, T. Murayama, A. Taketoshi, M. Haruta, Importance of Size and Contact Structure of Gold Nanoparticles for the Genesis of Unique Catalytic Processes, Chem Rev 120 (2020) 464–525. https://doi.org/10.1021/acs.chemrev.9b00551.

[589] T. Mitsudome, K. Kaneda, Gold nanoparticle catalysts for selective hydrogenations, Green Chemistry 15 (2013) 2636. https://doi.org/10.1039/c3gc41360h.

[590] S.X. Oszwaldowski, R. Lipka, M. Jarosz, Sensitive reversed-phase liquid chromatographic determination of hydrogen peroxide and glucose based on ternary vanadium(V)-hydrogen peroxide- 2-(5-bromo-2-pyridylazo)-5-diethylaminophenol system, Anal Chim Acta 421 (2000) 35–43. https://doi.org/10.1016/S0003-2670(00)01031-X.

[591] X. Tian, Y. Qin, Y. Jiang, X. Guo, Y. Wen, H. Yang, Chemically renewable SERS sensor for the inspection of H2O2 residue in food stuff, Food Chem 438 (2024) 137777. https://doi.org/10.1016/j.foodchem.2023.137777.

[592] Z. Han, L. Zhang, X. Lu, Sensitive detection of trace hydrogen peroxide via dual-emissive electrochemiluminescence from a luminol/porphyrin system: comprehensive innovative experiments on analytical instruments for undergraduates, J Chem Educ 101 (2024) 1248–1256. https://doi.org/10.1021/acs.jchemed.3c01240.

[593] J.Y. Huang, H.T. Lin, T.H. Chen, C.A. Chen, H.T. Chang, C.F. Chen, Signal amplified gold nanoparticles for cancer diagnosis on paper-based analytical devices, ACS Sens 3 (2018) 174–182. https://doi.org/10.1021/acssensors.7b00823.

[594] D. Agustini, F.R. Caetano, R.F. Quero, J.A. Fracassi da Silva, M.F. Bergamini, L.H. Marcolino-Junior, D.P. de Jesus, Microfluidic devices based on textile threads for analytical applications: state of the art and prospects, Analytical Methods 13 (2021) 4830–4857. https://doi.org/10.1039/D1AY01337H.

[595] N.A. Suhaidi, M.I.E. Halmi, A.A. Rashidi, M.F.M. Anuar, K. Mahmud, N. Kusnin, S.S.A. Gani, M.Y.A. Shukor, Colorimetric detection of mercury (Hg2+) using UV–vis spectroscopy and digital image analysis based on gold nanoparticles functionalized with bromelain enzyme, 3 Biotech 13 (2023) 121. https://doi.org/10.1007/s13205-023-03532-z.

[596] W.-Z. Lin, C.-Y. Yeung, C.-K. Liang, Y.-H. Huang, C.-C. Liu, S.-Y. Hou, A colorimetric sensor for the detection of hydrogen peroxide using DNA-modified gold nanoparticles, J Taiwan Inst Chem Eng 89 (2018) 49–55. https://doi.org/10.1016/j.jtice.2018.05.005.

[597] S. Wu, S.Y. Tan, C.Y. Ang, Z. Luo, Y. Zhao, Oxidation-triggered aggregation of gold nanoparticles for naked-eye detection of hydrogen peroxide, Chemical Communications 52 (2016) 3508–3511. https://doi.org/10.1039/c5cc09447j.

[598] M. Al-Kassawneh, Z. Sadiq, S. Jahanshahi-Anbuhi, User-friendly and ultra-stable all-inclusive gold tablets for cysteamine detection, RSC Adv 13 (2023) 19638–19650. https://doi.org/10.1039/d3ra03073c.

[599] H. Hajimiri, S.H. Safiabadi Tali, M. Al-Kassawneh, Z. Sadiq, S. Jahanshahi-Anbuhi, Tablet-based sensor: A stable and user-friendly tool for point-of-care detection of glucose in urine, Biosensors (Basel) 13 (2023) 893. https://doi.org/10.3390/bios13090893.

[600] S. Jahanshahi-Anbuhi, B. Kannan, V. Leung, K. Pennings, M. Liu, C. Carrasquilla, D. White, Y. Li, R.H. Pelton, J.D. Brennan, C.D.M. Filipe, Simple and ultrastable all-inclusive pullulan tablets for challenging bioassays, Chem Sci 7 (2016) 2342–2346. https://doi.org/10.1039/c5sc04184h.

[601] Z. Sadiq, M. Al-Kassawneh, S.H. Safiabadi Tali, S. Jahanshahi-Anbuhi, Tailoring plasmonic sensing strategies for the rapid and sensitive detection of hypochlorite in swimming water samples, Microchimica Acta 191 (2024) 183. https://doi.org/10.1007/s00604-024-06246-y.

[602] J. Tang, X. Fu, Q. Ou, K. Gao, S.Q. Man, J. Guo, Y. Liu, Hydroxide assisted synthesis of monodisperse and biocompatible gold nanoparticles with dextran, Materials Science and Engineering C 93 (2018) 759–767. https://doi.org/10.1016/j.msec.2018.08.045.

[603] B. Halliwell, L.H. Long, T.P. Yee, S. Lim, R. Kelly, Establishing biomarkers of oxidative stress: the measurement of hydrogen peroxide in human urine, Curr Med Chem 11 (2004) 1085–1092. https://doi.org/10.2174/0929867043365404.

[604] Y.D. Li, W.Y. Li, H.H. Chai, C. Fang, Y.J. Kang, C.M. Li, L. Yu, Chitosan functionalization to prolong stable hydrophilicity of cotton thread for thread-based analytical device application, Cellulose 25 (2018) 4831–4840. https://doi.org/10.1007/s10570-018-1891-3.

[605] S. Nath, C. Kaittanis, A. Tinkham, J.M. Perez, Dextran-coated gold nanoparticles for the assessment of antimicrobial susceptibility, Anal Chem 80 (2008) 1033–1038. https://doi.org/10.1021/ac701969u.

[606] M. Sivakavinesan, M. Vanaja, G. Annadurai, Dyeing of cotton fabric materials with biogenic gold nanoparticles., Sci Rep 11 (2021) 13249. https://doi.org/10.1038/s41598-021-92662-6.

[607] M. hui Zhang, H. Dong, L. Zhao, D. xi Wang, D. Meng, A review on Fenton process for organic wastewater treatment based on optimization perspective, Science of the Total Environment 670 (2019) 110–121. https://doi.org/10.1016/j.scitotenv.2019.03.180.

[608] J. Duan, D.L. Kasper, Oxidative depolymerization of polysaccharides by reactive oxygen/nitrogen species, Glycobiology 21 (2011) 401–409. https://doi.org/10.1093/glycob/cwq171.

[609] E. V. Pronina, Y.A. Vorotnikov, T.N. Pozmogova, A.O. Solovieva, S.M. Miroshnichenko, P.E. Plyusnin, D.P. Pishchur, I. V. Eltsov, M. V. Edeleva, M.A. Shestopalov, O.A. Efremova, No catalyst added hydrogen peroxide oxidation of dextran: an environmentally friendly route to multifunctional polymers, ACS Sustain Chem Eng 8 (2020) 5371–5379. https://doi.org/10.1021/acssuschemeng.0c01030.

[610] M.D. Rees, E.C. Kennett, J.M. Whitelock, M.J. Davies, Oxidative damage to extracellular matrix and its role in human pathologies, Free Radic Biol Med 44 (2008) 1973–2001. https://doi.org/10.1016/j.freeradbiomed.2008.03.016.

[611] L.T. Anh-Dao, N. Thanh-Nho, B. Huu-Trung, N. Tien-Giagn, T. Ut Dong, N. Quoc-Duy, N. Quang-Hieu, N. Le-Vy, N.T. Thanh-Dieu, D.V.T. To, D. Minh-Huy, N. Cong-Hau, A portable colorimetric tool using a smartphone camera applied for determining total phenolic contents in coffee products, Chinese Journal of Analytical Chemistry 51 (2023) 100228. https://doi.org/10.1016/j.cjac.2023.100228.

[612] S. Coimbra, E. Castro, P. Rocha-Pereira, I. Rebelo, S. Rocha, A. Santos-Silva, The effect of green tea in oxidative stress, Clinical Nutrition 25 (2006) 790–796. https://doi.org/10.1016/j.clnu.2006.01.022.

[613] W. Ren, S.I. Mohammed, S. Wereley, J. Irudayaraj, Magnetic Focus Lateral Flow Sensor for Detection of Cervical Cancer Biomarkers, Anal Chem 91 (2019) 2876–2884. https://doi.org/10.1021/acs.analchem.8b04848.

[614] B. Udugama, P. Kadhiresan, A. Samarakoon, W.C.W. Chan, Simplifying Assays by Tableting Reagents, J Am Chem Soc 139 (2017) 17341–17349. https://doi.org/10.1021/jacs.7b07055.

[615] S. Jahanshahi-Anbuhi, K. Pennings, V. Leung, M. Liu, C. Carrasquilla, B. Kannan, Y. Li, R. Pelton, J.D. Brennan, C.D.M. Filipe, Pullulan Encapsulation of Labile Biomolecules to Give Stable Bioassay Tablets, Angewandte Chemie 53 (2014) 6155–6158. https://doi.org/10.1002/anie.201403222.

[616] M. Al-Kassawneh, Z. Sadiq, S. Jahanshahi-Anbuhi, Pullulan-stabilized gold nanoparticles tablet as a nanozyme sensor for point-of-care applications, Sens Biosensing Res 38 (2022) 100526. https://doi.org/10.1016/j.sbsr.2022.100526.

[617] A.R.R. Esfahani, Z. Sadiq, O.D. Oyewunmi, S.H. Safiabadi Tali, N. Usen, D.C. Boffito, S. Jahanshahi-Anbuhi, Portable, stable, and sensitive assay to detect phosphate in water with gold nanoparticles (AuNPs) and dextran tablet, Analyst 146 (2021) 3697–3708. https://doi.org/10.1039/d0an02063j.

[618] S. Jahanshahi-Anbuhi, B. Kannan, V. Leung, K. Pennings, M. Liu, C. Carrasquilla, D. White, Y. Li, R.H. Pelton, J.D. Brennan, C.D.M. Filipe, Simple and ultrastable all-inclusive pullulan tablets for challenging bioassays, Chem Sci 7 (2016) 2342–2346. https://doi.org/10.1039/c5sc04184h.

[619] Q. Wang, X. Wen, J. Kong, Recent Progress on Uric Acid Detection: A Review, Crit Rev Anal Chem 50 (2020) 359–375. https://doi.org/10.1080/10408347.2019.1637711.

[620] S.H. Han, Y.-J. Ha, E.H. Kang, K. Shin, Y.J. Lee, G.-J. Lee, Electrochemical detection of uric acid in undiluted human saliva using uricase paper integrated electrodes, Sci Rep 12 (2022) 12033. https://doi.org/10.1038/s41598-022-16176-5.

[621] D. Jiang, Y. Zhu, Z. Sun, Z. Zhu, Q. He, X. Huang, Y. Yang, Y. Ge, Q. Zhang, Y. Wang, A silver nanowires@Prussian blue composite aerogel-based wearable sensor for noninvasive and dynamic monitoring of sweat uric acid, Chemical Engineering Journal 486 (2024) 150220. https://doi.org/10.1016/j.cej.2024.150220.

[622] J. Xiao, Y. Luo, L. Su, J. Lu, W. Han, T. Xu, X. Zhang, Hydrophilic metal-organic frameworks integrated uricase for wearable detection of sweat uric acid, Anal Chim Acta 1208 (2022) 339843. https://doi.org/10.1016/j.aca.2022.339843.

[623] T. Pinheiro, A.C. Marques, P. Carvalho, R. Martins, E. Fortunato, Paper Microfluidics and Tailored Gold Nanoparticles for Nonenzymatic, Colorimetric Multiplex Biomarker Detection, ACS Appl Mater Interfaces 13 (2021) 3576–3590. https://doi.org/10.1021/acsami.0c19089.

[624] R.K. Bera, A. Anoop, C.R. Raj, Enzyme-free colorimetric assay of serum uric acid, Chemical Communications 47 (2011) 11498. https://doi.org/10.1039/c1cc13349g.

[625] T.-T. Wang, X.-F. Huang, H. Huang, P. Luo, L.-S. Qing, Nanomaterial-based optical- and electrochemical-biosensors for urine glucose detection: A comprehensive review, Advanced Sensor and Energy Materials 1 (2022) 100016. https://doi.org/10.1016/j.asems.2022.100016.

[626] H. Hajimiri, S.H. Safiabadi Tali, M. Al-Kassawneh, Z. Sadiq, S. Jahanshahi-Anbuhi, Tablet-Based Sensor: A Stable and User-Friendly Tool for Point-of-Care Detection of Glucose in Urine, Biosensors (Basel) 13 (2023) 893. https://doi.org/10.3390/bios13090893.

[627] N.O. Gomes, R.T. Paschoalin, S. Bilatto, A.R. Sorigotti, C.S. Farinas, L.H.C. Mattoso, S.A.S. Machado, O.N. Oliveira, P.A. Raymundo-Pereira, Flexible, Bifunctional Sensing Platform Made with Biodegradable Mats for Detecting Glucose in Urine, ACS Sustain Chem Eng 11 (2023) 2209–2218. https://doi.org/10.1021/acssuschemeng.2c05438.

[628] K. Shang, S. Wang, S. Chen, X. Wang, Sensitivity Detection of Uric Acid and Creatinine in Human Urine Based on Nanoporous Gold, Biosensors (Basel) 12 (2022) 588. https://doi.org/10.3390/bios12080588.

[629] L. Su, J. Feng, X. Zhou, C. Ren, H. Li, X. Chen, Colorimetric detection of urine glucose based ZnFe2O4 magnetic nanoparticles, Anal Chem 84 (2012) 5753–5758. https://doi.org/10.1021/ac300939z.

[630] Z. Li, Y. Wang, Z. Fan, Y. Sun, Y. Sun, Y. Yang, Y. Zhang, J. Ma, Z. Wang, Z. Zhu, A Dual-Function Wearable Electrochemical Sensor for Uric Acid and Glucose Sensing in Sweat, Biosensors (Basel) 13 (2023) 105. https://doi.org/10.3390/bios13010105.

[631] Z. Zhou, T. Shu, Y. Sun, H. Si, P. Peng, L. Su, X. Zhang, Luminescent wearable biosensors based on gold nanocluster networks for “turn-on” detection of Uric acid, glucose and alcohol in sweat, Biosens Bioelectron 192 (2021) 113530. https://doi.org/10.1016/j.bios.2021.113530.

[632] M. Al-Kassawneh, Z. Sadiq, S. Jahanshahi-Anbuhi, User-friendly and ultra-stable all-inclusive gold tablets for cysteamine detection, RSC Adv 13 (2023) 19638–19650. https://doi.org/10.1039/d3ra03073c.

[633] J. Tang, X. Fu, Q. Ou, K. Gao, S.Q. Man, J. Guo, Y. Liu, Hydroxide assisted synthesis of monodisperse and biocompatible gold nanoparticles with dextran, Materials Science and Engineering C 93 (2018) 759–767. https://doi.org/10.1016/j.msec.2018.08.045.

[634] R. Suárez-López, V.F. Puntes, N.G. Bastús, C. Hervés, C. Jaime, Nucleation and growth of gold nanoparticles in the presence of different surfactants. A dissipative particle dynamics study, Sci Rep 12 (2022) 13926. https://doi.org/10.1038/s41598-022-18155-2.

[635] S. V. Sokolov, K. Tschulik, C. Batchelor-McAuley, K. Jurkschat, R.G. Compton, Reversible or Not? Distinguishing Agglomeration and Aggregation at the Nanoscale, Anal Chem 87 (2015) 10033–10039. https://doi.org/10.1021/acs.analchem.5b02639.

[636] S. Shrestha, B. Wang, P. Dutta, Nanoparticle processing: Understanding and controlling aggregation, Adv Colloid Interface Sci 279 (2020) 102162. https://doi.org/10.1016/j.cis.2020.102162.

[637] X. Liu, M. Atwater, J. Wang, Q. Huo, Extinction coefficient of gold nanoparticles with different sizes and different capping ligands, Colloids Surf B Biointerfaces 58 (2007) 3–7. https://doi.org/10.1016/j.colsurfb.2006.08.005.

[638] H. Aldewachi, T. Chalati, M.N. Woodroofe, N. Bricklebank, B. Sharrack, P. Gardiner, Gold nanoparticle-based colorimetric biosensors, Nanoscale 10 (2018) 18–33. https://doi.org/10.1039/C7NR06367A.

[639] Y. Xu, X. Zhang, X.S. Zhu, Y.W. Shi, Silver-coated hollow fiber surface plasmon resonance sensor for glucose detection with enhanced limit of detection, Nanoscale 16 (2024) 7085–7092. https://doi.org/10.1039/d4nr00421c.

[640] X. Liu, U. Pant, N. Logan, Q. He, B. Greer, C.T. Elliott, C. Cao, Non-linear responses via agglomeration and aggregation of gold nanoparticles for surface-enhanced Raman spectroscopy (SERS) coupled with chemometric analysis for chlorpyrifos detection, Food Chem 455 (2024) 139944. https://doi.org/10.1016/j.foodchem.2024.139944.

[641] J. Sun, C. Li, Y. Qi, S. Guo, X. Liang, Optimizing Colorimetric Assay Based on V2O5 Nanozymes for Sensitive Detection of H2O2 and Glucose, Sensors 16 (2016) 584. https://doi.org/10.3390/s16040584.

[642] D. Zhou, K. Zeng, M. Yang, Gold nanoparticle-loaded hollow Prussian Blue nanoparticles with peroxidase-like activity for colorimetric determination of L-lactic acid, Microchimica Acta 186 (2019) 121. https://doi.org/10.1007/s00604-018-3214-7.

[643] R. Sun, R. Lv, Y. Zhang, T. Du, Y. Li, L. Chen, Y. Qi, Colorimetric sensing of glucose and GSH using core-shell Cu/Au nanoparticles with peroxidase mimicking activity, RSC Adv 12 (2022) 21875–21884. https://doi.org/10.1039/d2ra02375j.

[644] L. Han, C. Li, T. Zhang, Q. Lang, A. Liu, Au@Ag Heterogeneous Nanorods as Nanozyme Interfaces with Peroxidase-Like Activity and Their Application for One-Pot Analysis of Glucose at Nearly Neutral pH, ACS Appl Mater Interfaces 7 (2015) 14463–14470. https://doi.org/10.1021/acsami.5b03591.

[645] M. Naderi, M. Hosseini, M.R. Ganjali, Naked-eye detection of potassium ions in a novel gold nanoparticle aggregation-based aptasensor, Spectrochim. Acta - A: Mol. Biomol. Spectrosc. 195 (2018) 75–83. https://doi.org/10.1016/j.saa.2018.01.051.

[646] S.O. Obare, R.E. Hollowell, C.J. Murphy, Sensing strategy for lithium ion based on gold nanoparticles, Langmuir 18 (2002) 10407–10410. https://doi.org/10.1021/la0260335.

[647] M. Hsiao, S.H. Chen, J.Y. Li, P.H. Hsiao, C.Y. Chen, Unveiling the detection kinetics and quantitative analysis of colorimetric sensing for sodium salts using surface-modified Au-nanoparticle probes, Nanoscale Adv 4 (2022) 3172–3181. https://doi.org/10.1039/d2na00211f.

[648] G. Xu, N. Guo, Q. Zhang, T. Wang, P. Song, L. Xia, A sensitive surface-enhanced resonance Raman scattering sensor with bifunctional negatively charged gold nanoparticles for the determination of Cr(VI), Science of the Total Environment 830 (2022) 154598. https://doi.org/10.1016/j.scitotenv.2022.154598.

[649] C.E. Lisowski, J.E. Hutchison, Malonamide-functionalized gold nanoparticles for selective, colorimetric sensing of trivalent lanthanide ions, Anal Chem 81 (2009) 10246–10253. https://doi.org/10.1021/ac902271t.

[650] B.A. García Grajeda, S.G. Soto Acosta, S.A. Aguila, H.P. Guevara, M.E. Díaz-García, A.C. Enríquez, J.J. Campos-Gaxiola, Selective and colorimetric detection of Ba2+ ions in aqueous solutions using 11-mercaptoundecylphosphonic acid functionalized gold nanoparticles, RSC Adv 7 (2017) 31611–31618. https://doi.org/10.1039/c7ra03861e.

[651] P. Duenchay, O. Chailapakul, W. Siangproh, A transparency sheet-based colorimetric device for simple determination of calcium ions using induced aggregation of modified gold nanoparticles, Int. J. Mol. Sci. 20 (2019) 2954. https://doi.org/10.3390/ijms20122954.

[652] J. feng Guo, D. qun Huo, M. Yang, C. jun Hou, J. jie Li, H. bao Fa, H. bo Luo, P. Yang, Colorimetric detection of Cr (VI) based on the leaching of gold nanoparticles using a paper-based sensor, Talanta 161 (2016) 819–825. https://doi.org/10.1016/j.talanta.2016.09.032.

[653] G. Xu, N. Guo, Q. Zhang, T. Wang, P. Song, L. Xia, A sensitive surface-enhanced resonance Raman scattering sensor with bifunctional negatively charged gold nanoparticles for the determination of Cr(VI), Science of the Total Environment 830 (2022) 154598. https://doi.org/10.1016/j.scitotenv.2022.154598.

[654] Y. Wang, L. Wang, Z. Su, J. Xue, J. Dong, C. Zhang, X. Hua, M. Wang, F. Liu, Multipath colourimetric assay for copper(II) ions utilizing MarR functionalized gold nanoparticles, Sci Rep 7 (2017) 1–9. https://doi.org/10.1038/srep41557.

[655] Y. Zhang, R. Li, Q. Xue, H. Li, J. Liu, Colorimetric determination of copper(II) using a polyamine-functionalized gold nanoparticle probe, Microchimica Acta 182 (2015) 1677–1683. https://doi.org/10.1007/s00604-015-1498-4.

[656] J.N.B.D. Pelin, C.J.C. Edwards-Gayle, H. Martinho, B.B. Gerbelli, V. Castelletto, I.W. Hamley, W.A. Alves, Self-assembled gold nanoparticles and amphiphile peptides: a colorimetric probe for copper(ii) ion detection, Dalton Trans. 49 (2020) 16226–16237. https://doi.org/10.1039/d0dt00844c.

[657] L. Mao, Q. Wang, Y. Luo, Y. Gao, Detection of Ag+ ions via an anti-aggregation mechanism using unmodified gold nanoparticles in the presence of thiamazole, Talanta 222 (2021) 121506. https://doi.org/10.1016/j.talanta.2020.121506.

[658] Y. Qi, D. Song, Y. Chen, Colorimetric oligonucleotide-based sensor for ultra-low Hg2+ in contaminated environmental medium: Convenience, sensitivity and mechanism, Science of the Total Environment 766 (2021) 142579. https://doi.org/10.1016/j.scitotenv.2020.142579.

[659] W. Kim, G. Lee, M. Kim, J. Park, S. Jo, D.S. Yoon, Y.H. Park, J. Hong, J. Park, Al3+ ion sensing at attomole level via surface-potential mapping of gold nanoparticle complexes, Sens. Actuators B Chem. 255 (2018) 2179–2186. https://doi.org/10.1016/j.snb.2017.09.031.

[660] H. Park, W. Kim, M. Kim, G. Lee, W. Lee, J. Park, Eco-friendly and enhanced colorimetric detection of aluminum ions using pectin-rich apple extract-based gold nanoparticles, Spectrochim. Acta - A: Mol. Biomol. Spectrosc. 245 (2021) 118880. https://doi.org/10.1016/j.saa.2020.118880.

[661] S.S. Memon, A. Nafady, A.R. Solangi, A.M. Al-Enizi, Sirajuddin, M.R. Shah, S.T.H. Sherazi, S. Memon, M. Arain, M.I. Abro, M.I. Khattak, Sensitive and selective aggregation based colorimetric sensing of Fe3+ via interaction with acetyl salicylic acid derived gold nanoparticles, Sens. Actuators B Chem. 259 (2018) 1006–1012. https://doi.org/10.1016/j.snb.2017.12.162.

[662] T.T.T. Ho, C.H. Dang, T.K.C. Huynh, T.K.D. Hoang, T.D. Nguyen, In situ synthesis of gold nanoparticles on novel nanocomposite lactose/alginate: Recyclable catalysis and colorimetric detection of Fe(III), Carbohydr Polym 251 (2021) 116998. https://doi.org/10.1016/j.carbpol.2020.116998.

[663] C. Zhao, G. Zhong, D.-E. Kim, J. Liu, X. Liu, A portable lab-on-a-chip system for gold-nanoparticle-based colorimetric detection of metal ions in water, Biomicrofluidics 8 (2014) 052107. https://doi.org/10.1063/1.4894244.

[664] S. Thatai, P. Khurana, S. Prasad, S.K. Soni, D. Kumar, Trace colorimetric detection of Pb2+ using plasmonic gold nanoparticles and silica-gold nanocomposites, Microchemical Journal 124 (2016) 104–110. https://doi.org/10.1016/j.microc.2015.07.006.

[665] S. Wang, X. Huang, Q. An, R. Zhou, W. Xu, D. Xu, Q. Lin, X. Cao, Gold nanostar as an ultrasensitive colorimetric probe for picomolar detection of lead ion, Anal Chim Acta 1160 (2021) 338380. https://doi.org/10.1016/j.aca.2021.338380.

[666] M. Zhang, Y.Q. Liu, B.C. Ye, Colorimetric assay for parallel detection of Cd2+, Ni 2+ and Co2+ using peptide-modified gold nanoparticles, Analyst 137 (2012) 601–607. https://doi.org/10.1039/c1an15909g.

[667] L. Zhang, D. Huang, G. Yue, J. Zhu, L. Yang, L. Yang, W. Dan, P. Zhao, Effective colorimetric detection of Ni2+ using gold nanoparticles functionalized with phytate, Chem. Phys. Lett. 784 (2021) 139101. https://doi.org/10.1016/j.cplett.2021.139101.

[668] J.R. Kalluri, T. Arbneshi, S. Afrin Khan, A. Neely, P. Candice, B. Varisli, M. Washington, S. McAfee, B. Robinson, S. Banerjee, A.K. Singh, D. Senapati, P.C. Ray, Use of gold nanoparticles in a simple colorimetric and ultrasensitive dynamic light scattering assay: selective detection of arsenic in groundwater, Angewandte Chemie 121 (2009) 9848–9851. https://doi.org/10.1002/ange.200903958.

[669] D. Zhang, Y. Liu, J. Ding, K. Hayat, X. Zhan, P. Zhou, D. Zhang, Label-free colorimetric assay for arsenic(III) determination based on a truncated short ssDNA and gold nanoparticles, Microchimica Acta 188 (2021) 38. https://doi.org/10.1007/s00604-020-04697-7.

[670] H.H. Deng, K.Y. Huang, Q.H. Fang, Y.P. Lv, S. Bin He, H.P. Peng, X.H. Xia, W. Chen, Schiff base and Lewis acid-base interaction-regulated aggregation/dispersion of gold nanoparticles for colorimetric recognition of rare-earth Sc3+ ions, Sens. Actuators B Chem. 311 (2020) 127925. https://doi.org/10.1016/j.snb.2020.127925.

[671] P. Mondal, J.L. Yarger, Colorimetric dual sensors of metal ions based on 1,2,3-triazole-4,5-dicarboxylic acid-functionalized gold nanoparticles, J. Phys. Chem. C 123 (2019) 20459–20467. https://doi.org/10.1021/acs.jpcc.9b03721.

[672] M. Yon, C. Pibourret, J.D. Marty, D. Ciuculescu-Pradines, Easy colorimetric detection of gadolinium ions based on gold nanoparticles: key role of phosphine-sulfonate ligands, Nanoscale Adv 2 (2020) 4671–4681. https://doi.org/10.1039/d0na00374c.

[673] D. Quesada-González, G.A. Jairo, R.C. Blake, D.A. Blake, A. Merkoçi, Uranium (VI) detection in groundwater using a gold nanoparticle/paper-based lateral flow device, Sci Rep 8 (2018) 8–15. https://doi.org/10.1038/s41598-018-34610-5.

[674] A. Saha, S. Neogy, D.R.M. Rao, S.B. Deb, M.K. Saxena, B.S. Tomar, Colorimetric and visual determination of ultratrace uranium concentrations based on the aggregation of amidoxime functionalized gold nanoparticles, Microchimica Acta 186 (2019) 1–10. https://doi.org/10.1007/s00604-019-3292-1.

[675] C.E. Lisowski, J.E. Hutchison, Malonamide-functionalized gold nanoparticles for selective, colorimetric sensing of trivalent lanthanide ions, Anal Chem 81 (2009) 10246–10253. https://doi.org/10.1021/ac902271t.

[676] R.M. Pallares, K.P. Carter, S.E. Zeltmann, T. Tratnjek, A.M. Minor, R.J. Abergel, Selective lanthanide sensing with gold nanoparticles and hydroxypyridinone chelators, Inorg Chem 59 (2020) 2030–2036. https://doi.org/10.1021/acs.inorgchem.9b03393.

[677] Q. Wang, Y. Wang, M. Guan, S. Zhu, X. Yan, Y. Lei, X. Shen, L. Luo, H. He, A multicolor colorimetric assay for sensitive detection of sulfide ions based on anti-etching of triangular gold nanoplates, Microchemical Journal 159 (2020) 105429. https://doi.org/10.1016/j.microc.2020.105429.

[678] H. Wu, Y. Li, X. He, L. Chen, Y. Zhang, Colorimetric sensor based on 4-mercaptophenylboronic modified gold nanoparticles for rapid and selective detection of fluoride anion, Spectrochim. Acta - A: Mol. Biomol. Spectrosc. 214 (2019) 393–398. https://doi.org/10.1016/j.saa.2019.02.039.

[679] Z. He, L. Zhang, G. Peng, G. Wang, X. Liang, Chemical redox-modulated etching of plasmonic nanoparticles for nitrite detection: Comparison among gold nanosphere, nanorod, and nanotriangle, J. Anal. Test. 5 (2021) 350–359. https://doi.org/10.1007/s41664-021-00153-4.

[680] O. Adegoke, S. Zolotovskaya, A. Abdolvand, N.N. Daeid, Rapid and highly selective colorimetric detection of nitrite based on the catalytic-enhanced reaction of mimetic Au nanoparticle-CeO2 nanoparticle-graphene oxide hybrid nanozyme, Talanta 224 (2021) 121875. https://doi.org/10.1016/j.talanta.2020.121875.

[681] W. Liu, Z. Du, Y. Qian, F. Li, A specific colorimetric probe for phosphate detection based on anti-aggregation of gold nanoparticles, Sens. Actuators B Chem. 176 (2013) 927–931. https://doi.org/10.1016/j.snb.2012.10.074.

[682] Y. Guan, Y. Lu, J. Sun, J. Zhao, W. Huang, X. Zhang, Y. Liu, Redox recycling-activated signal amplification of peroxidase-like catalytic activity based on bare gold nanoparticle–metal ion ensembles as colorimetric sensor array for ultrasensitive discrimination of phosphates, ACS Sustain Chem Eng 9 (2021) 9802–9812. https://doi.org/10.1021/acssuschemeng.1c02265.

[683] Y. Zhou, C. Li, R. Liu, Z. Chen, L. Li, W. Li, Y. He, L. Yuan, Label-free colorimetric detection of prothioconazole using gold nanoparticles based on one-step reaction, ACS Biomater. Sci. Eng. 6 (2020) 2805–2811. https://doi.org/10.1021/acsbiomaterials.0c00208.

[684] C. Kuitio, S. Klangprapan, N. Chingkitti, S. Boonthavivudhi, K. Choowongkomon, Aptasensor for paraquat detection by gold nanoparticle colorimetric method, J. Environ. Sci. Health - B 56 (2021) 370–377. https://doi.org/10.1080/03601234.2021.1888615.

[685] P.C. Mane, M.D. Shinde, S. Varma, B.P. Chaudhari, A. Fatehmulla, M. Shahabuddin, D.P. Amalnerkar, A.M. Aldhafiri, R.D. Chaudhari, Highly sensitive label-free bio-interfacial colorimetric sensor based on silk fibroin-gold nanocomposite for facile detection of chlorpyrifos pesticide, Sci Rep 10 (2020) 1–14. https://doi.org/10.1038/s41598-020-61130-y.

[686] Y. Qu, H. Qian, Y. Mi, J. He, H. Gao, R. Lu, S. Zhang, W. Zhou, Rapid determination of the pesticide ametryn based on a colorimetric aptasensor of gold nanoparticles, Analytical Methods 12 (2020) 1919–1925. https://doi.org/10.1039/d0ay00283f.

[687] M. Qi, C. Tu, Y. Dai, W. Wang, A. Wang, J. Chen, A simple colorimetric analytical assay using gold nanoparticles for specific detection of tetracycline in environmental water samples, Analytical Methods 10 (2018) 3402–3407. https://doi.org/10.1039/c8ay00713f.

[688] K. Mao, J. Ma, X. Li, Z. Yang, Rapid duplexed detection of illicit drugs in wastewater using gold nanoparticle conjugated aptamer sensors, Science of the Total Environment 688 (2019) 771–779. https://doi.org/10.1016/j.scitotenv.2019.06.325.

[689] J.C. Gukowsky, C. Tan, Z. Han, L. He, Cysteamine-modified gold nanoparticles as a colorimetric sensor for the rapid detection of gentamicin, J Food Sci 83 (2018) 1631–1638. https://doi.org/10.1111/1750-3841.14179.

[690] H. Han, J. Liu, J. Zhou, Y. Li, W. Wang, Z. Lu, Kanamycin adsorption on gold nanoparticles dominates its label-free colorimetric sensing with its aptamer, Langmuir 36 (2020) 11490–11498. https://doi.org/10.1021/acs.langmuir.0c01786.

[691] N. Pourreza, M. Ghomi, A network composed of gold nanoparticles and a poly(vinyl alcohol) hydrogel for colorimetric determination of ceftriaxone, Microchimica Acta 187 (2020) 1–10. https://doi.org/10.1007/s00604-019-4039-8.

[692] D.A. Raja, F. Munir, M.R. Shah, M.I. Bhanger, M.I. Malik, Colorimetric sensing of cephradine through polypropylene glycol functionalized gold nanoparticles, R. Soc. Open Sci. 8 (2021) 210185. https://doi.org/10.1098/rsos.210185.

[693] T.R. Pavase, H. Lin, M.A. Soomro, H. Zheng, X. Li, K. Wang, Z. Li, Visual detection of tropomyosin, a major shrimp allergenic protein using gold nanoparticles (AuNPs)-assisted colorimetric aptasensor, Mar Life Sci Technol 3 (2021) 382–394. https://doi.org/10.1007/s42995-020-00085-5.

[694] C.C. Chang, G. Wang, T. Takarada, M. Maeda, Target-recycling-amplified colorimetric detection of pollen allergen using non-cross-linking aggregation of dna-modified gold nanoparticles, ACS Sens 4 (2019) 363–369. https://doi.org/10.1021/acssensors.8b01156.

[695] D. Yuan, X. Fang, Y. Liu, J. Kong, Q. Chen, A hybridization chain reaction coupled with gold nanoparticles for allergen gene detection in peanut, soybean and sesame DNAs, Analyst 144 (2019) 3886–3891. https://doi.org/10.1039/c9an00394k.

[696] H. Li, J. Gan, Q. Yang, L. Fu, Y. Wang, Colorimetric detection of food freshness based on amine-responsive dopamine polymerization on gold nanoparticles, Talanta 234 (2021) 122706. https://doi.org/10.1016/j.talanta.2021.122706.

[697] E. Kim, J. Hahn, C. Ban, Y. Jo, H. Han, S. Lim, Y.J. Choi, Visible on-site detection of Ara h 1 by the switchable-linker-mediated precipitation of gold nanoparticles, Food Chem. 352 (2021) 129354. https://doi.org/10.1016/j.foodchem.2021.129354.

[698] H. Zhu, C. Liu, X. Liu, Z. Quan, W. Liu, Y. Liu, A multi-colorimetric immunosensor for visual detection of ochratoxin A by mimetic enzyme etching of gold nanobipyramids, Microchimica Acta 188 (2021) 1–10. https://doi.org/10.1007/s00604-020-04699-5.

[699] Y. He, F. Tian, J. Zhou, Q. Zhao, R. Fu, B. Jiao, Colorimetric aptasensor for ochratoxin A detection based on enzyme-induced gold nanoparticle aggregation, J. Hazard. Mater. 388 (2020) 121758. https://doi.org/10.1016/j.jhazmat.2019.121758.

[700] S. Sun, R. Zhao, S. Feng, Y. Xie, Colorimetric zearalenone assay based on the use of an aptamer and of gold nanoparticles with peroxidase-like activity, Microchimica Acta 185 (2018) 1–7. https://doi.org/10.1007/s00604-018-3078-x.

[701] J. Lerdsri, J. Soongsong, P. Laolue, J. Jakmunee, Reliable colorimetric aptasensor exploiting 72-Mers ssDNA and gold nanoprobes for highly sensitive detection of aflatoxin M1 in milk, J. Food Compos. Anal. 102 (2021) 103992. https://doi.org/10.1016/j.jfca.2021.103992.

[702] X. Huang, T. Huang, X. Li, Z. Huang, Flower-like gold nanoparticles-based immunochromatographic test strip for rapid simultaneous detection of fumonisin B1 and deoxynivalenol in Chinese traditional medicine, J. Pharm. Biomed. Anal. 177 (2020) 112895. https://doi.org/10.1016/j.jpba.2019.112895.

[703] S. Siddiquee, S. Saallah, N.A. Bohari, G. Ringgit, J. Roslan, L. Naher, N.F.H. Nudin, Visual and optical absorbance detection of melamine in milk by melamine-induced aggregation of gold nanoparticles, Nanomaterials 11 (2021) 1–11. https://doi.org/10.3390/nano11051142.

[704] C. Martínez-Aquino, A.M. Costero, S. Gil, P. Gaviña, Resorcinol functionalized gold nanoparticles for formaldehyde colorimetric detection, Nanomaterials 9 (2019). https://doi.org/10.3390/nano9020302.

[705] M. Jia, J. Sha, Z. Li, W. Wang, H. Zhang, High affinity truncated aptamers for ultra-sensitive colorimetric detection of bisphenol A with label-free aptasensor, Food Chem. 317 (2020) 126459. https://doi.org/10.1016/j.foodchem.2020.126459.

[706] U.J. Kim, B.C. Kim, A colorimetric assay for detection of 6-OH-BDE-47 using 6-OH-BDE-47-specific aptamers and gold nanoparticles, Sens. Actuators B Chem. 248 (2017) 298–304. https://doi.org/10.1016/j.snb.2017.03.139.

[707] J. Yang, Q. Sun, C. Huang, S. Qin, S. Han, Z. Huo, Y. Li, X. Sun, J. Chen, 3-Aminophenylboronic acid-mediated aggregation of gold nanoparticles for colorimetric sensing of iohexol in environmental and biological samples, Spectrochim. Acta - A: Mol. Biomol. Spectrosc. 261 (2021) 120004. https://doi.org/10.1016/j.saa.2021.120004.

[708] X. Wang, Y. Liu, X. Shi, H. Chen, C. Zhao, J. Li, J. Wang, Colorimetric determination of Listeria monocytogenes using aptamer and urease dual-labeled magnetic nanoparticles and cucurbit[7]uril-mediated supramolecular assembly of gold nanoparticle, Microchimica Acta 189 (2022) 1–9. https://doi.org/10.1007/s00604-021-05130-3.

[709] Y. Liu, X. Wang, X. Shi, M. Sun, L. Wang, Z. Hu, F. Liu, Q. Liu, P. Wang, J. Li, C. Zhao, A colorimetric sensor for Staphylococcus aureus detection based on controlled click chemical-induced aggregation of gold nanoparticles and immunomagnetic separation, Microchimica Acta 189 (2022) 104. https://doi.org/10.1007/s00604-022-05211-x.

[710] L. Zeng, X. Xu, H. Ding, S. Song, L. Xu, C. Xu, H. Kuang, A gold nanoparticle based colorimetric sensor for the rapid detection of: Yersinia enterocolitica serotype O:8 in food samples, J Mater Chem B 10 (2022) 909–914. https://doi.org/10.1039/d1tb01838h.

[711] H. Zhang, S. Yao, X. Song, K. Xu, J. Wang, J. Li, C. Zhao, M. Jin, One-step colorimetric detection of Staphylococcus aureus based on target-induced shielding against the peroxidase mimicking activity of aptamer-functionalized gold-coated iron oxide nanocomposites, Talanta 232 (2021) 122448. https://doi.org/10.1016/j.talanta.2021.122448.

[712] P. Tiet, K.C. Clark, J.O. McNamara, J.M. Berlin, Colorimetric detection of staphylococcus aureus contaminated solutions without purification, Bioconjug Chem 28 (2017) 183–193. https://doi.org/10.1021/acs.bioconjchem.6b00571.

[713] J. Wen, J. Liu, J. Wu, D. He, Rapid measurement of waterborne bacterial viability based on difunctional gold nanoprobe, RSC Adv 12 (2022) 1675–1681. https://doi.org/10.1039/d1ra07287k.

[714] H. Sohrabi, M.R. Majidi, K. Asadpour-Zeynali, A. Khataee, M. Dastborhan, A. Mokhtarzadeh, A PCR-free genosensing platform for detection of Shigella dysenteriae in human plasma samples by porous and honeycomb-like biochar decorated with ultrathin flower-like MoS2 nanosheets incorporated with Au nanoparticles, Chemosphere 288 (2022) 132531. https://doi.org/10.1016/j.chemosphere.2021.132531.

[715] C. Herniou--Julien, J.R. Mendieta, T.J. Gutiérrez, Characterization of biodegradable/non-compostable films made from cellulose acetate/corn starch blends processed under reactive extrusion conditions, Food Hydrocoll 89 (2019) 67–79. https://doi.org/10.1016/j.foodhyd.2018.10.024.

[716] S. B. Aziz, M.A. Brza, I. Brevik, M.H. Hafiz, A.S.F.M. Asnawi, Y.M. Yusof, R.T. Abdulwahid, M.F.Z. Kadir, Blending and characteristics of electrochemical double-layer capacitor device assembled from plasticized proton ion conducting chitosan:dextran:NH4PF6 polymer electrolytes, Polymers (Basel) 12 (2020) 2103. https://doi.org/10.3390/polym12092103.

[717] F. dos S. Campos, D.L. Cassimiro, M.S. Crespi, A.E. Almeida, M.P.D. Gremião, Preparation and characterisation of dextran-70 hydrogel for controlled release of praziquantel, Brazilian Journal of Pharmaceutical Sciences 49 (2013) 75–83. https://doi.org/10.1590/S1984-82502013000100009.

[718] Y. Ma, Y. Zhu, B. Liu, G. Quan, L. Cui, Colorimetric determination of hypochlorite based on the oxidative leaching of gold nanorods, Materials 11 (2018). https://doi.org/10.3390/ma11091629.

[719] T. Sasikumar, M. Ilanchelian, Colorimetric detection of hypochlorite based on the morphological changes of silver nanoprisms to spherical nanoparticles, Analytical Methods 9 (2017) 3151–3158. https://doi.org/10.1039/c7ay00716g.

[720] R. You, Q. Huang, Z. Lin, W. Wang, J. Lie, J. Chen, G. Zhang, Y. Lu, Preparation of SERS base membrane with cellulose compound dopamine and determination of hypochlorite, Microchimica Acta 190 (2023). https://doi.org/10.1007/s00604-023-06006-4.

[721] K. Shanmugaraj, M. Ilanchelian, Visual and optical detection of hypochlorite in water samples based on etching of gold/silver alloy nanoparticles, New Journal of Chemistry 41 (2017) 14130–14136. https://doi.org/10.1039/c7nj02682j.

[722] L. Wonjung, H. Youn, J. Bae, D.H. Kim, Solid-phase colorimetric sensor for hypochlorite, Analyst 146 (2021) 2301–2306. https://doi.org/10.1039/d0an02448a.

[723] Z. Yang, T. Xu, X. Zhang, H. Li, X. Jia, S. Zhao, Z. Yang, X. Liu, Nitrogen–doped carbon quantum dots as fluorescent nanosensor for selective determination and cellular imaging of ClO−, Spectrochim Acta A Mol Biomol Spectrosc 271 (2022). https://doi.org/10.1016/j.saa.2022.120941.

[724] Y. Zhan, F. Luo, L. Guo, B. Qiu, Y. Lin, J. Li, G. Chen, Z. Lin, Preparation of an Efficient Ratiometric Fluorescent Nanoprobe (m-CDs at[Ru(bpy)3]2+) for Visual and Specific Detection of Hypochlorite on Site and in Living Cells, ACS Sens 2 (2017) 1684–1691. https://doi.org/10.1021/acssensors.7b00601.

[725] X. Li, X. Lin, S. Lin, X. Sun, D. Gao, B. Liu, H. Zhao, J. Zhang, S. Cong, L. Wang, Au Nanospheres@Ag Nanorods for Wide Linear Range Colorimetric Determination of Hypochlorite, ACS Appl Nano Mater 2 (2019) 3161–3168. https://doi.org/10.1021/acsanm.9b00475.

[726] K. Radhakrishnan, P. Panneerselvam, Green synthesis of surface-passivated carbon dots from the prickly pear cactus as a fluorescent probe for the dual detection of arsenic(iii) and hypochlorite ions from drinking water, RSC Adv 8 (2018) 30455–30467. https://doi.org/10.1039/c8ra05861j.

[727] G. Shen, G. Zou, X. Li, Self-cross-linking synthesis of CuO for dual-mode sensing of hydrogen peroxide, J Mol Struct 1315 (2024). https://doi.org/10.1016/j.molstruc.2024.138833.

[728] Y. Liu, Y. Cao, C. Zhang, C. Ye, Q. Bian, X. Cheng, H. Xia, J. Zheng, H. Liu, A novel colorimetric method for H2O2 sensing and its application: Fe2+-catalyzed H2O2 prevents aggregation of AuNPs by oxidizing cysteine (FeHOAuC), Anal Chim Acta 1207 (2022) 339840. https://doi.org/10.1016/j.aca.2022.339840.

[729] W.Z. Lin, C.Y. Yeung, C.K. Liang, Y.H. Huang, C.C. Liu, S.Y. Hou, A colorimetric sensor for the detection of hydrogen peroxide using DNA-modified gold nanoparticles, J Taiwan Inst Chem Eng 89 (2018) 49–55. https://doi.org/10.1016/j.jtice.2018.05.005.

[730] Y. Wei, J. Lu, Y. Xu, X. Song, Y. Yu, H. Zhang, X. Luo, Nanozyme-immobilized cellulose membranes designed by a simple hydrogen bond-dominated for colorimetric detection of hydrogen peroxide and uric acid, Microchemical Journal 193 (2023). https://doi.org/10.1016/j.microc.2023.109113.

[731] Z. Ghubish, Y.G.A. El-Reash, F.K. Algethami, N.Y. Elamin, M.A. El-Kemary, Novel nanophosphor films coated Ag nanoparticles sensor for detecting hydrogen peroxide in biological samples based on Turn off-on luminescent, J Mol Struct 1304 (2024) 137651. https://doi.org/10.1016/j.molstruc.2024.137651.

[732] W. Wang, S. Gunasekaran, MXene/Gold nanoparticles heterostructure as catalase mimic for colorimetric detection of penicillin G, Chemical Engineering Journal 482 (2024). https://doi.org/10.1016/j.cej.2024.148693.

[733] S. Chandra, V.K. Singh, P.K. Yadav, D. Bano, V. Kumar, V.K. Pandey, M. Talat, S.H. Hasan, Mustard seeds derived fluorescent carbon quantum dots and their peroxidase-like activity for colorimetric detection of H2O2 and ascorbic acid in a real sample, Anal Chim Acta 1054 (2019) 145–156. https://doi.org/10.1016/j.aca.2018.12.024.

[734] A. Jaiswal, S. Madaan, N. Acharya, S. Kumar, D. Talwar, D. Dewani, Salivary Uric Acid: A Noninvasive Wonder for Clinicians?, Cureus 11 (2021) 19649. https://doi.org/10.7759/cureus.19649.

[735] Y. Liu, J. Liu, Selection of DNA Aptamers for Sensing Uric Acid in Simulated Tears, Analysis & Sensing 2 (2022) e202200010. https://doi.org/10.1002/anse.202200010.

[736] Z. Wang, S. Dong, M. Gui, M. Asif, W. Wang, F. Wang, H. Liu, Graphene paper supported MoS2 nanocrystals monolayer with Cu submicron-buds: High-performance flexible platform for sensing in sweat, Anal Biochem 543 (2018) 82–89. https://doi.org/10.1016/j.ab.2017.12.010.

[737] X. Mao, C. Zhang, A microfluidic cloth-based photoelectrochemical analytical device for the detection of glucose in saliva, Talanta 238 (2022) 123052. https://doi.org/10.1016/j.talanta.2021.123052.

[738] H. Yao, A.J. Shum, M. Cowan, I. Lähdesmäki, B.A. Parviz, A contact lens with embedded sensor for monitoring tear glucose level, Biosens Bioelectron 26 (2011) 3290–3296. https://doi.org/10.1016/j.bios.2010.12.042.

[739] J. Cao, C. Xie, Y. Zeng, Y. Wu, Enzyme-free colorimetric assay for the detection of uric acid in urine by cobalt tetroxide, Microchemical Journal 204 (2024) 111079. https://doi.org/10.1016/j.microc.2024.111079.

[740] X. Zha, Z. Zhao, C. Ding, Z. Fan, Y. Yang, Snowflake-like Ce-BTC@MoS2 heterojunction for high-performance uric acid detection, Sens Actuators B Chem 422 (2025) 136474. https://doi.org/10.1016/j.snb.2024.136474.

[741] S. Verma, A. Sen, N. Dutta, P. Sengupta, P. Chakraborty, G. Dutta, Highly Specific Non-Enzymatic Electrochemical Sensor for the Detection of Uric Acid Using Carboxylated Multiwalled Carbon Nanotubes Intertwined with GdS-$Gd_2O_3$ Nanoplates in Human Urine and Serum, Langmuir 40 (2024) 21427–21441. https://doi.org/10.1021/acs.langmuir.4c02233.

[742] N. Baig, A.-N. Kawde, A. Elgamouz, A cost-effective disposable graphene-based sensor for sensitive and selective detection of uric acid in human urine, Biosens Bioelectron X 11 (2022) 100205. https://doi.org/10.1016/j.biosx.2022.100205.

[743] M. Caldara, J.W. Lowdon, G. van Wissen, A.G. Ferrari, R.D. Crapnell, T.J. Cleij, H. Diliën, C.E. Banks, K. Eersels, B. van Grinsven, Dipstick Sensor Based on Molecularly Imprinted Polymer-Coated Screen-Printed Electrodes for the Single-Shot Detection of Glucose in Urine Samples—From Fundamental Study toward Point-of-Care Application, Adv Mater Interfaces 10 (2023) 2300182. https://doi.org/10.1002/admi.202300182.

[744] Q. Wang, D. Sun, X. Ma, R. Huang, J. Xu, X. Xu, L. Cai, L. Xu, Surface enhanced Raman scattering active substrate based on hydrogel microspheres for pretreatment-free detection of glucose in biological samples, Talanta 260 (2023) 124657. https://doi.org/10.1016/j.talanta.2023.124657.

[745] T. Shi, D. Kou, L. Gao, Y. Xue, S. Zhang, W. Ma, One-Dimensional Responsive Photonic Crystals Assembled by Polymer Nanogels and $TiO_2$ Nanoparticles for Rapid Detection of Glucose, ACS Appl Nano Mater 7 (2024) 3116–3128. https://doi.org/10.1021/acsanm.3c05440.

# ADDITIONAL INFORMATION

## Supporting Information for Chapter 2

Table 2S1 Summary of representative inorganic ions detected by AuNPs-based colorimetric sensors

| Group | Analyte/target ion | Functionalizing moiety/ recognition unit/capping agent | Supporting/masking/aggregating agent | AuNPs size (nm) | Assay time (min) | LOD/(linear range) | Mechanism/platform | Ref. |
|---|---|---|---|---|---|---|---|---|
| Alkali earth metals (IA) | $K^+$ Potassium | 5′-GGG TTA GGG TTA GGG TTA GGG-3′ aptamer | cationic dye (Y5GL) | 13 | 45 | 4.4 nM-sol/(10 nM-50 mM) + 6.2 μM-PAD/(10 μM-40 mM) | aggregation/sol + PAD | [645] |
| | $Li^+$ Lithium | 1,10-phenanthroline ligand plus thiol | - | 4 | - | 3 mM/ (10-100 mM) | aggregation/sol | [646] |
| | $K^+$, $Na^+$, $Li^+$ | citrate | - | 15.74-20.80 | 5 | (15, 30, 45) mM | aggregation/sol | [647] |
| | $Cs^+$ cesium | citrate | prussian blue | 18 | 20 | 30 mM | anti-aggregation/sol | [648] |
| Alkaline earth metals (IIA) | $Sr^{2+}$ Strontium | 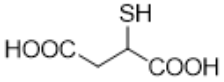 2-mercaptosuccinic acid | NaCl | 13 | - | 50 nM | aggregation/sol | [649] |
| | $Ba^{2+}$ Barium | 11-mercaptoundecylphosphonic acid | - | 20.8 | 10 | 43.27 μM/ (20–120) mM | aggregation/sol | [650] |
| | $Ca^{2+}$ Calcium | 4-amino-6-hydroxy-2-mercaptopyrimidine monohydrate | - | 20 | 5 | 3.05 ppm/(10-100) ppm | aggregation/PAD | [651] |
| Transition metals | $Cr^{6+}$ Chromium | bovine serum albumin | HBr | 14.06 ± 3.14 | 10 | 280 nM/(0.5-50.0) μM | etching/PAD | [652] |
| | $Cr^{6+}$ | citrate | $Cr^{6+}$ | 13 | 1 | 0.4 nM | peroxidase-like/sol | [653] |
| | $Cu^{2+}$ Copper | multiple antibiotic resistance regulator (MarR) | - | 20 | 5 | 1 μM | aggregation/sol | [654] |
| | | polyethyleneimine | - | 3 | 7 | 30 nM | aggregation/sol | [655] |

| | | | | | | | |
|---|---|---|---|---|---|---|---|
| | amyloid peptides | - | 10-20 | - | 0.19 μM | aggregation/sol | [656] |
| $Ag^{+}$ Silver | thiamazole | - | - | 5 | 0.042 nM/(0.1–9) μM | anti-aggregation/sol | [657] |
| $Hg^{2+}$ Mercury | graphene oxide | - | 30 | 8 | $(3.8\times10^{-10})$ M/ $(5.2\times10^{-9})$-$(1.2\times10^{-7})$ M | nanozyme/sol | [658] |
| $Al^{3+}$ Aluminum | Kelvin probe | - | 12 | - | 1 pM | aggregation/sol | [659] |
| | plant pectin | - | 24.81 ± 8.04 | 1 | 20 μM | aggregation/sol | [660] |
| $Fe^{3+}$ Iron | acetylsalicylic acid | - | 33 | 2-3 | 0.051 μM | aggregation/sol | [661] |
| | lactose/alginate | - | 357 ± 43 | 18 | 0.8 μM/(2.0–80.0) μM | aggregation/sol | [662] |
| $Pb^{2+}$ lead | 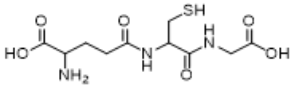 glutathione (peptide) | - | 15.26 ± 3.6 | 10 | 30 ppb | aggregation /PAD | [663] |
| | $SiO_2$ silica | - | ~360 | - | 50 nM | aggregation/sol | [664] |
| | 4-(2-hydroxyethyl)-1-piperazineethanesulfonic acid | - | 34.2 | 30 | 200 pM | etching/sol | [665] |
| $Ni^{2+}$ Nickel | cys-Ala-Leu-Asn-Asn-Asp-His-His-His-His-His-His peptide ligand | 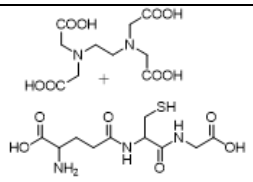 EDTA and glutathione | 8.5 | 3 | 0.3 mM | aggregation/sol | [666] |
| | phytate | - | 25.6 ± 3.1 | 15 | 5 μM | aggregation/sol | [667] |
| $As^{3+}$ arsenic | Ars-3 aptamer probe | NaCl | 5–110 | 10 | 1.26 ppb | aggregation/sol | [668] |
| | apt-21 | NaCl | 13 | 20 | 0.18 ppb/(1-30) and (30-100) ppb | aggregation/sol | [669] |
| $Sc^{3+}$ Scandium | cysteamine-pyridoxal phosphate | - | 17.5 ± 3.4 | 1 | 0.02 μM/(0.1-3) μM | anti-aggregation/sol | [670] |

| | | | | | | | | |
|---|---|---|---|---|---|---|---|---|
| **Lanthanide rare earth metals** | $Ce^{3+}$ Cerium | 1,2,3-triazole-4,5-dicarboxylic acid | - | 13-67 | 5 | 5.89 nM | aggregation/sol | [671] |
| | $Gd^{3+}$ Gadolinium | bis(*p*-sulfonatophenyl) phenyl phosphine | - | 17.2 ± 4.0 | 15 | 0.74 μM | aggregation/sol | [672] |
| **Actinides** | $U^{6+}$ Uranium | monoclonal antibody (clone 12F6) | 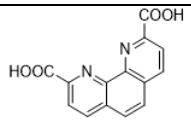 2,9-dicarboxyl-1,10-phenanthroline | 20 | 10 | 36.38 nM | aggregation/PAD | [673] |
| | | 3-mercapto propionylamidoxime | - | 4.9 ± 0.2 | 30 | 0.3 ng $mL^{-1}$ | aggregation/sol | [674] |
| | $Sm^{3+}$ samarium | 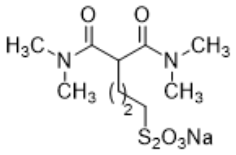 tetramethylmalonamide | $Na_2S_2O_3$ | 6.8 ± 1.7 | - | 50 nM | aggregation/sol | [675] |
| | $Eu^{3+}$ Europium | 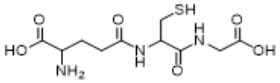 glutathione | NaCl | 13 | - | 50 nM | aggregation/sol | [675] |
| | | 3,4,3-LI(1,2-HOPO) | - | 24 ± 4 | 5 | 3 μM | aggregation/sol | [676] |
| **Chalcogens** | $S^{2-}$ sulfide | - | $Cu^{2+}$ and $I^-$ | - | 20 | 0.1 μM | anti-etching/sol | [677] |
| **Halogens** | $F^-$ Fluoride | 4-mercaptophenylboronic | - | 5-8 | 30 s | $3.45\times10^{-7}$ M/(10.0-30.0) μM | aggregation/sol | [678] |
| **Anions** | $NO_3^-$ Nitrate | - | $I^-$ | 10-15 | 20 | 4.5 μM | etching/sol | [679] |
| | | $CeO_2$ | $NO_3^-$ | 96.8 | - | 4.6 μM | peroxidase-like catalytic/sol | [680] |
| | $PO_4^{3-}$ Phosphate | 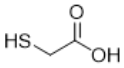 mercaptoacetic acid | $Eu^{3+}$ | 13 | 5 | 76 nM/($5.0\times10^{-7}$-$3.0\times10^{-5}$) M | anti-aggregation/sol | [681] |
| | | thiophenol | - | 20 | 10 | 0.02 μg $L^{-1}$ | peroxidase-like /sol | [682] |

Abbreviations: sol = solution; PAD = paper-based analytical device; EDTA = ethylenediaminetetraacetic acid

Table 2S2 Summary of representative organic analytes detected by AuNPs and their real sample applications

| Group | Analyte/ target | Real sample applications | Functionalizing moiety/ recognition unit/capping agent | Supporting/ masking/aggregating agent | AuNP size (nm) | Assay time (min) | LoD/(linear range) | Mechanism/platform | Ref. |
|---|---|---|---|---|---|---|---|---|---|
| **Pesticides** | prothioconazole | rice field water | citrate | NaCl | 13 | 1 | 0.38 μg $L^{-1}$ | aggregation/sol | [683] |
| | paraquat | water | 50-AGGCTTACACCTGAAAAGCGGCTTAATTTACACTACTGTAT aptamer | - | 15 | 20 | 0.267 mg $mL^{-1}$ | aggregation/sol | [684] |
| | chlorpyrifos | soil | silk fibroin | NaCl | 2-10 | 30 | 10 ppb | agglomeration/ sol | [685] |
| | ametryn | water | citrate | NaCl | 36 | 5 | 0.15 μg $L^{-1}$ /(0-80) μg $L^{-1}$ | aggregation/sol | [686] |
| **Drugs** | tetracycline | river water | TC 76 bases aptamer | NaCl | 15 | 20 | 0.071 mM/(0.10-5.00) mM | aggregation/sol | [687] |
| | methamphetamine | wastewater | DNA reporter prob (RPs) | - | 40 | - | 0.5 nM | non-aggregation/sol | [688] |
| | gentamicin | milk | cysteamine | - | 15 | 15 | 12.45 nM/(10-200) nM | aggregation/sol | [689] |
| | kanamycin | raw milk | HCR-based amplification/three hairpin DNA probes | NaCl | 13 | 20 | 0.68 μM | aggregation/sol | [690] |
| | ceftriaxone | serum and urine | poly(vinyl alcohol) and borax | - | 89 | 15 | 0.33 μg $mL^{-1}$ /(1-90) μg $mL^{-1}$ | aggregation/sol | [691] |
| | cephradine | blood plasma and urine | polypropylene glycol | - | 104.6 | 5 | 11.0 mM /(0.01-120) mM | aggregation/sol | [692] |
| **Allergens** | tropomyosin | shrimp, tofu, egg, water | ssDNA aptamer | NaCl | 13 | 5 | (70, 90, 80, 40) nM/(10-200) nM | aggregation/sol | [693] |

| | | | | | | | | | |
|---|---|---|---|---|---|---|---|---|---|
| | pollen | soil | ssDNA hairpin self-assembly | NaCl | 15 | 10 | 0.2 ng $mL^{-1}$ | non-cross linking aggregation/sol | [694] |
| | allergen gene DNA | peanut, soybean, and sesame | two hairpin probes | NaCl | - | 5 | 0.5 nM | aggregation/sol | [695] |
| | biogenic amine | shrimp, cod, and pork | polyethylene glycol | - | 20-30 | 2 | 2.8 μg $mL^{-1}$ /(1–1000) μg $mL^{-1}$ | aggregation/sol | [696] |
| | peanut Ara h 1 | cookies | streptavidin | - | 30 ± 0.5 | 30 | 0.19 mg/30 g | aggregation/sol | [697] |
| **Mycotoxin** | ochratoxin A | millet | octahedral $Cu_2O$ | - | 245 | 5 | 0.47 ng $L^{-1}$/(1 ng $L^{-1}$ - 5 μg $L^{-1}$) | etching /sol | [698] |
| | | grape juice and red wine | ochratoxin aptamer | NaCl | 13.4 ± 1.5 | 70 | 5.0 nM | aggregation/sol | [699] |
| | zearalenone | corn, corn oil | zearalenone aptamer | - | 13 | 25 | 10 ng $mL^{-1}$/(10-250) ng $mL^{-1}$ | peroxidase-like /sol | [700] |
| | aflatoxin M1 | milk | ssDNA aptamer | NaCl | 12.8 ± 0.2 | 7 | 0.002 ng $mL^{-1}$/(0.005-0.100) ng $mL^{-1}$ | aggregation/sol | [701] |
| | fumonisin B1 and deoxynivalenol | Chines traditional medicine, maize flower | FGN antibody-labeled probe | - | 20 | 5 | 5.0 ng $mL^{-1}$ | aggregation/sol and PAD | [702] |
| **Small organic toxin** | melamine | milk | - | - | 5 | 7 | $1\times10^{-9}$ M | aggregation/sol | [703] |
| | formaldehyde | water, gas from fiber and particleboard | resorcinol probe | - | 17 | 12-15 | 0.5 ppm | aggregation/sol | [704] |
| | bisphenol A | milk, orange juice, water | truncated 38-mer and 12-mer aptamers | NaCl | 15 | 20 | 7.60 pM + 14.41 pM | aggregation/sol | [705] |
| | 6-hydroxy-2,2,4,4-tetrabro | environmental water samples | ssDNA aptamer | NaCl | 10 | - | 3 ppb/(5 ppb - 1 ppm) | aggregation/sol | [706] |

| | | | | | | | | | |
|---|---|---|---|---|---|---|---|---|---|
| | modiphenyl ether (6-OH-BDE-47) | | | | | | | | |
| | iohexol | river water, human urine | 3-aminophenylboronic acid- | - | 15 | 10 | 0.005 mM | aggregation/sol | [707] |

Abbreviation: sol = solution

Table 2S3 Summary of representative biological analytes detected by AuNPs and their key findings

| Classification | Analyte/target | Real sample applications | Functionalizing moiety/ recognition unit/capping agent | Supporting/masking/aggregating agent | AuNP size (nm) | Assay time (min) | LoD/(linear range) | Mechanism/platform | Ref. |
|---|---|---|---|---|---|---|---|---|---|
| **Food-born pathogens** | *Listeria monocytogenes* | food | cucurbituril | - | 18.1 ± 1.4 | 10 | 10 cfu $mL^{-1}$/(10-106) cfu $mL^{-1}$ | aggregation /sol | [708] |
| | *Staphylococcus aureus* | pork, lake water | aptamer-functionalized and ALP-labeled $Fe_3O_4$ NPs | $Cu^{2+}$ | - | 60 | 9.7 cfu $mL^{-1}$ (pork), 8.5 cfu $mL^{-1}$ (lake water) | anti-aggregation /sol | [709] |
| | *Enterocolitica* O:8 CICC 21669, CICC 21681 and CICC 21567 | milk, pork meat | monoclonal antibody | - | 17.0 ± 1.5 | 10 | $1.3\times10^3$, $3\times10^2$ and $8\times10^2$ cfu $mL^{-1}$ | anti-aggregation /PAD | [710] |
| **Water-born pathogens** | *Staphylococcus aureus* | tap, lake, industrial wastewater | *S. aureus* aptamer -$Fe_3O_4$ | NaCl | 10.33 (AuNPs) 299.07 (*S.aureus* aptamer - $Fe_3O_4$) | 12 | 10 cfu $mL^{-1}$/(10-$10^6$) cfu $mL^{-1}$ | peroxidase-like /sol | [711] |
| | | creek, ocean water | 11-mer oligoneoclotide | - | 20 | 5 | 0.496 μM | aggregation /sol | [712] |
| | *Staphylococcus aureus, Shewanella oneidensis, Escherichia coli* | tap, lake, industrial wastewater | difunctional Au nanoprobe | - | 29.5 | 10 | - | aggregation /sol | [713] |
| | *Shigella dysenteriae* | human plasma | conjugated monoclonal antibody | NaCl | 43 | 15 | 10 cfu $mL^{-1}$ | aggregation /sol | [714] |

Abbreviation: sol = solution

**Supporting Information for Chapter 3**

**Materials and method:** Tablet thickness was recorded using stainless steel digital caliper (Neiko, China) 0.01 mm resolution with 0.02 mm accuracy. X-ray diffraction (XRD) analysis was carried out on a Rigaku Smart Lab SE diffractometer with Cu Kα radiation generated at 36 kV and 20 mA, in the range of diffraction angle 2θ = 10 to 80° at a scanning rate of 6°/min. XRD sample was a dried AuNPs-dTab on a piece of glass. The differential scanning calorimetry (DSC) analysis of the fabricated AuNPs-dTab was carried out using a DSC-250 differential scanning calorimeter (Instruments TA, USA) equipped with a computerized data station. DSC curves were obtained from 6.3 mg of AuNPs-dTab and 6.5 mg of pristine dextran in aluminium crucibles heated at 10 °C/min to 200 °C followed by isothermal for 3.0 min at 5 °C/min to 300 °C then 10 °C/min to 400 °C under a nitrogen atmosphere flowing at 25 mL/min. Prior to use the calorimeter was calibrated with metal standards; an empty aluminum pan was used as a reference. Calibration of the instrument was performed using indium as a standard.

**Procedure:** Hydrodynamic diameter was analyzed using *ImageJ* software taking twelve measurements at random positions per tablet. Thickness was determined by measuring tablet at twelve random locations using a digital caliper (Neiko, China) with an accuracy of 0.02 mm. Results were reported as average values ± SD and further considered for the calculations of ρ and Op. The dried tablet at 20 °C for 24 h was weighed as initial ($W_i$) and weighed again after drying at 105 °C for 24 h as final ($W_f$). All measurements were undertaken in triplicate and the data reported as mean values ± SD. The density was calculated as the ratio between the weight (W) and volume (V) where V is equal to area (A) x thickness (e) of a tablet using the equation (i)[715]: $p = \frac{W}{V} = \frac{W}{A*e} = \frac{W_i - W_f}{\left(\frac{\emptyset}{2}\right)^2 \pi * e}$. The opacity of the AuNPs-dTab was determined using ultraviolet (UV) and visible light barrier properties of the tablet at selected wavelength between 400 and 800 nm. Absorbance was calculated at 600 nm using the equation (ii)[715]: $Op = \frac{\mathrm{A600}}{e}$

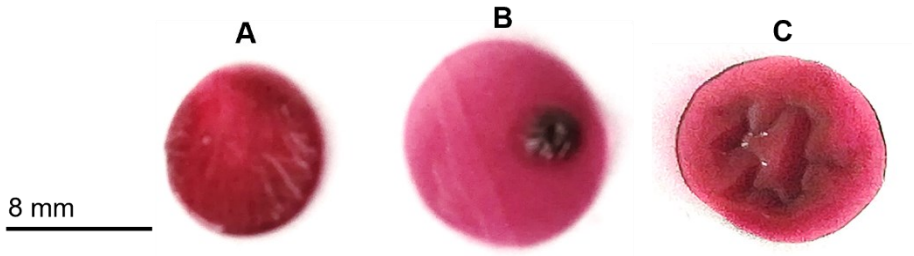


Figure 3S1 Effect of different drying conditions on casting of AuNPs-dTab.
A) Oven-dried at 50 °C for 5 h showing dense nature of tablet; B) Dried on hard hydrophobic surface at room temperature for 24 h showing well-rounded shape of tablet; C) Dried on plastic envelop at room temperature for 24 h showing wrinkles inside the tablet.

**Tablet characteristics and surface morphology:** After finding the proper range for dextran concentration to create tablets, we investigated various physical characteristics of the tablets with different dextran and AuNPs concentrations to better understand the effects of these parameters on the tablets (Figure 3S2A and S2B. As shown in Figure 3S2A, increasing the concentration of dextran from 6 to 10% resulted in the increase of the tablet thickness in all AuNP concentrations significantly. In this regard, the minimum thickness observed for the tablets was 0.31 ± 0.04 mm for the 6% dextran tablets with 8 nM AuNPs, and the maximum thickness was 0.71 ± 0.10 mm for the 10% dextran tablets with 4 nM AuNPs. Thus, the concentration of the dextran is the dominant parameter affecting the thickness of the tablets.

We also observed that the increase in the concentration of the dextran significantly increased the diameter and weight of the tablets in all AuNP concentrations (Figure 3S2Aii and 3S2Aiii). In addition, with the increase of AuNPs concentration from 2 to 8 nM in the case of 6% tablets, the diameter and weight of the tablets increased, but this increase was not observed for the case of 10% tablets. Hence, it appears that in lower concentrations of dextran, AuNPs concentration has stronger effect on the diameter and weight of the tablets. The minimum and maximum diameters recorded for the tablets were 5.79 ± 0.13 mm and 7.64 ± 0.17 mm for the 6% dextran tablets with 2 nM AuNPs and 10% dextran tablets with 2 nM AuNPs, respectively. Also, the minimum and maximum weights observed were 1.3 ± 0.06 mg and 4.3 ± 0.3 mg for the 6% dextran tablets with 2 nM AuNPs and 10% tablets with 8 nM AuNPs, respectively. Of note, we observed that the weight of the AuNPs-dTabs stored in air-tight sealed packaging was constant through out this analysis. However, there was a fluctuation in weight for those tablets placed in an open atmosphere. It appears that external environment humidity has a direct influence on the tablet's

weight, and thus, the tablets should be stored in an air-tight packaging to avoid the changes in the characteristics due to the effects of humidity.

Next, we analyzed the density of the tablets (Figure 3S2Aiv). No significant difference was observed between the tablets with 6% and 10% dextran in each concentration of AuNPs. However, an increasing trend was obtained in the case of 6% dextran tablets when the AuNP concentration was increased from 2 to 8 nM. The minimum density observed was 0.144 ± 0.005 $g/cm^3$ for the 6% dextran tablets with 2 nM AuNPs, and the maximum density was 0.247 ± 0.0.039 $g/cm^3$ for the 6% dextran tablets with 8 nM AuNPs. Finally, we assessed the opacity of the tablets. As shown in Figure 3S2Av, higher dextran content resulted in significantly lower opacity in all AuNP concentrations. This observation is justifiable by the fact that the tablets with higher dextran content had higher thickness, which has an inverse relationship with opacity. Also, increasing the AuNP concentration resulted in an increase in the opacity in both 6% and 10% dextran tablets, but the intensity of the increase was higher for the 6% dextran tablets. The minimum opacity observed was 0.762 ± 0.010 A/mm for the 10% dextran tablets with 2 nM AuNPs, and the maximum opacity was 4.009 ± 0.107 for the 6% dextran tablets with 8 nM AuNPs.

Overall, the increase in the concentration of dextran significantly increased the thickness, diameter, and weight of the tablets, while it decreased the opacity and had no significant effect on the density. Also, the increase in the concentration of AuNPs in the tablets had stronger effects on the characteristics of the tablets when the dextran content was lower. In this regard, an increasing trend was observed in diameter, weight, density, and opacity of the tablets with the increase in AuNP concentration.

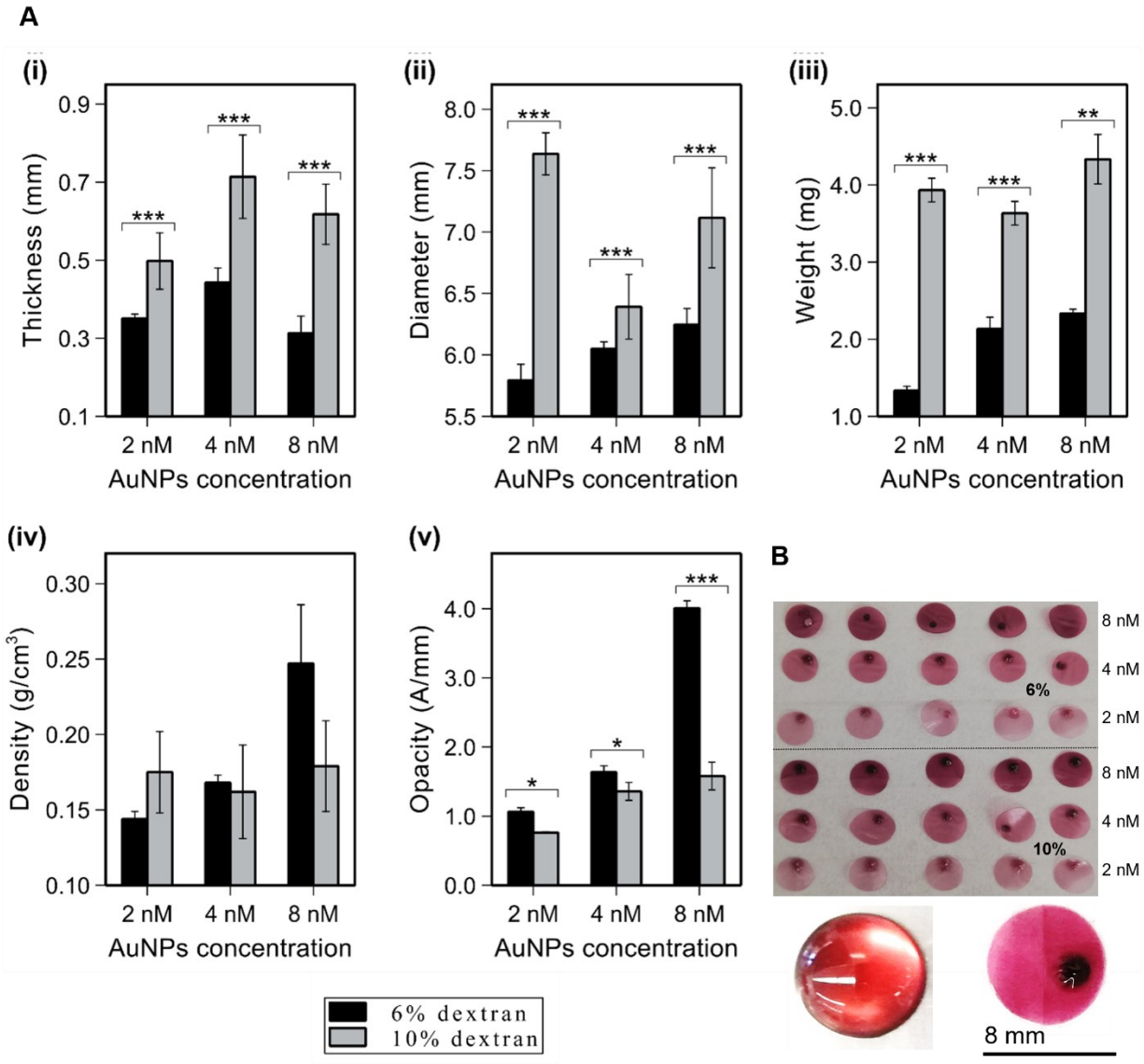


Figure 3S2 Results of the studies on the physical characteristics of the dAuNP-Tabs with 6 and 10% dextran and 2, 4, and 8 nM AuNPs.
A) The studies included i) thickness (n=12), ii) diameter (n=13), iii) weight (n=3), iv) density (n=3), and v) opacity (n=3). Each bar represents the mean value of replicated experiments ± standard deviation. Single, double, and triple asterisks signify statistically significant difference with *p*-values < 0.05, 0.01, and 0.001, respectively; B) Representation of the AuNP-dTabs with 6 and 10 wt% dextran and 2, 4, and 8 nM AuNPs used to study physical parameters of tablets. Also, an image of 100 µL drop of AuNPs-dSol solution along with an enlarged image of a dried tablet.

To present tablet surface morphology, according to the data across the line in amplitude trace AFM image Figure 3S3, the roughness average was 1.19 nm, average maximum height of the roughness was 6.76 nm, average maximum roughness valley depth 3.01 nm, maximum peak to

valley roughness was 11.59 nm and waviness average was 1.23 nm. The results demonstrated that the strong binding between dextran and AuNPs occurred.

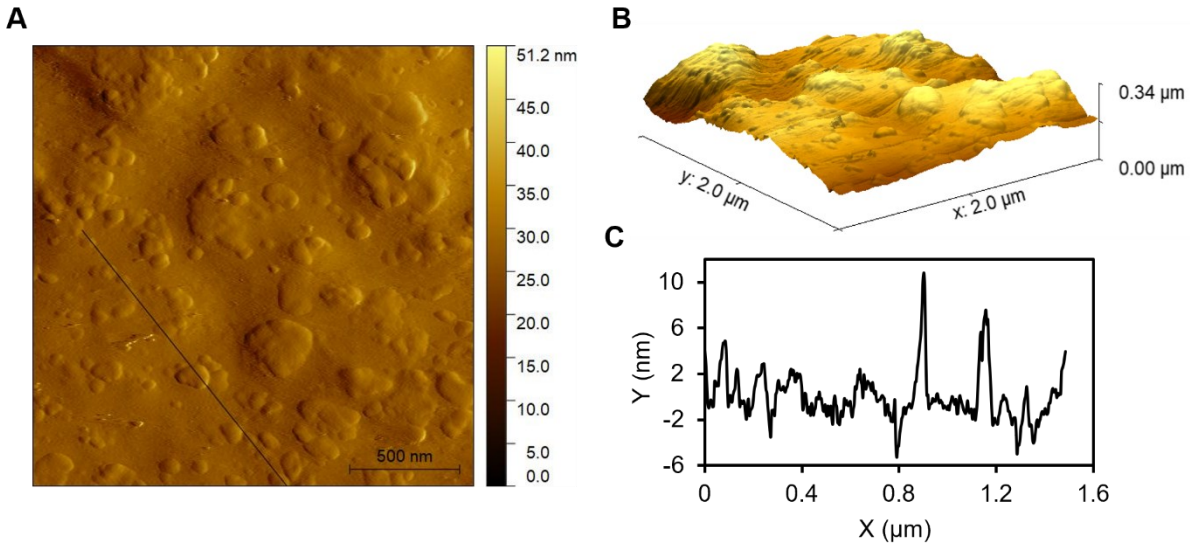


Figure 3S3 The AFM images of the AuNPs-dTab in case of dispersed particles showing height trace of tablet surface.
A) 2D image of height profile of AuNPs-dTab in an amplitude trace; B) 3D image of height prolife of A; C) Height distribution as surface roughness and texture description along the black line area of image A.

**XRD and DSC Analysis**

X-ray diffraction patterns of the fabricated AuNPs-dTab is shown in Figure 3S4A where the spectrum shows a wide hallow indicating a fully amorphous structure of a tablet due to the dextran powder as a major constituent.[716] However, there is a prominent crystalline peak at 2ɵ value 38.5° corresponding to Miller indices (1 1 1) due to the metallic gold. Small characteristic peaks at 44.3°, 64.5°, and 77.7° corresponding to Miller indices (2 0 0), (2 2 0), and (3 1 1) were vanished due to the abundance of polysaccharide as shown by the broad peak at 2ɵ 20°. Amongst the diffraction planes, plane (1 1 1) was stronger than other diffraction planes, which might be due to the major orientation of the (1 1 1) plane (JCPDF card no. 04-0784) [482]. Hence, the crystallinity of the dextran capped AuNPs in a tablet platform is affected as compared to their face centered cubic (FCC) geometry in a powdered state.[482] Results also confirm the anisotropic morphology of our tablet.

Differential scanning calorimetry is very useful in the characterization of the thermal properties of AuNPs-dTab which was compared with pure dextran. The curves of DSC data for both

samples are shown in Figure 3S4B. The value of the glass transition temperature ($T_g$) and crystallization temperature ($T_c$) was obtained taking the midpoint of the endothermic and exothermic peak respectively. In case of pristine dextran, a broad endothermic peak observed between 90 and 110 °C is due to the evaporation of residual water and another peak at 230 °C was corresponding to its glass transition temperature that indicates there is no crystalline dextran and thus confirms the amorphous structure of this biopolymer. Such high glass transition temperature could be the existence of strong hydrogen bonds between the macromolecules of dextran.[717] A sharp endothermic peak at 60 °C might be due to gold nanoparticles fractions embedded in dextran matrix whereas an exothermic peak at 328 °C might be a transition from amorphous solid to crystalline solid that refereed to crystallization temperature ($T_c$) of the AuNPs-dTab. This observation also indicates the high melting temperature ($T_m$) of AuNPs-dTab and hence its higher thermal stability. Overall, DSC analysis indicates the high thermal stability of AuNPs-dTab as well as reduction of the degree of crystallinity of AuNPs (semicrystalline) when these particles were embedded in dextran and subsequent increase in the amorphous nature of AuNPs-dTab material which is also supported by XRD data.

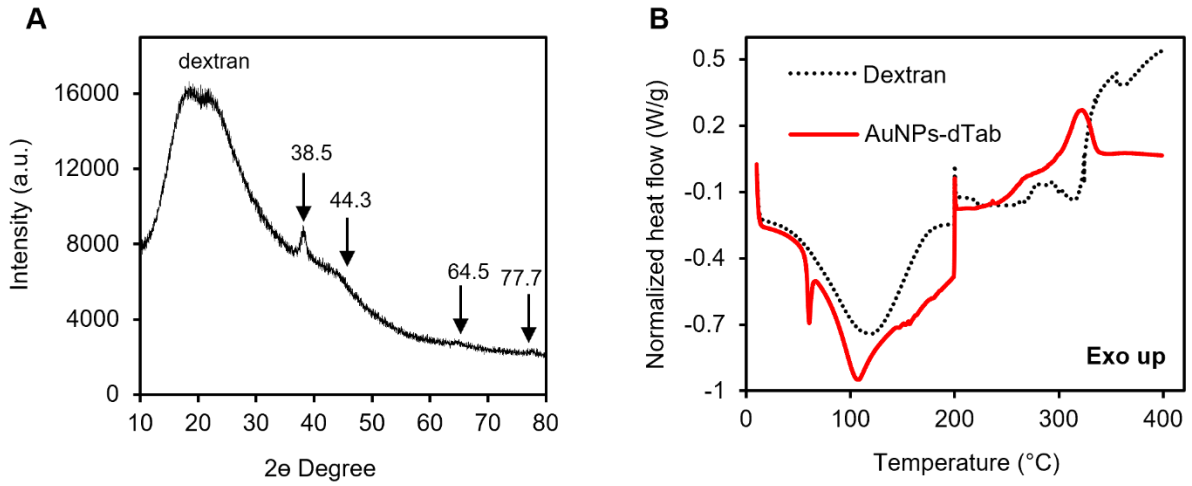


Figure 3S4 Characterization of AuNPs-dTab to see the nature of material along with its thermal stability.
A) XRD diffractogram of AuNPs-dTab showing semicrystalline nature of AuNPs-dTab; B) DSC thermogram of AuNPs-dTab and pristine dextran indicating the good thermal stability (>350 °C) of AuNPs-dTab.

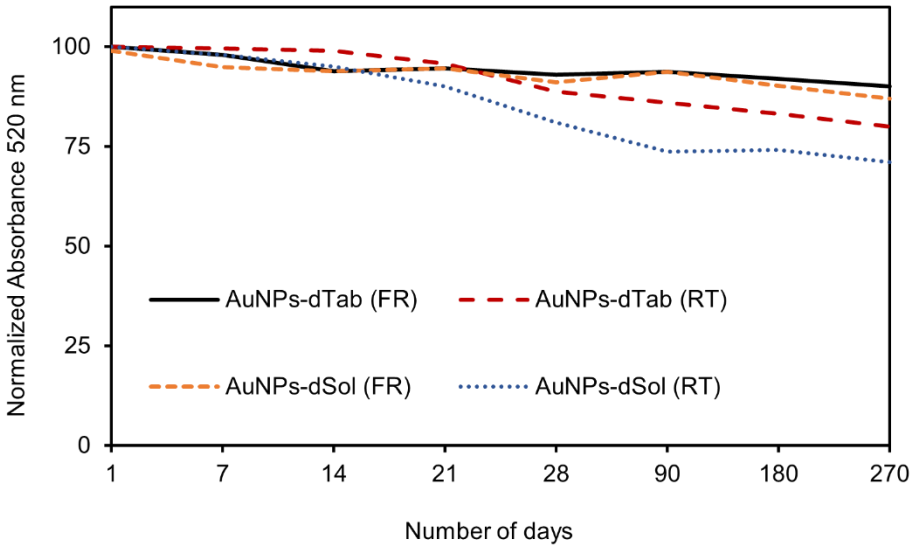


Figure 3S5 A comparative study of stability profile between AuNPs-dTab and AuNPs-dSol at room temperature (RT) 20 °C and fridge (FR) 4 °C for 9 months showing the higher stability of nanoparticles in a tablet platform than solution state under both conditions making these tablets suitable for any working environment.

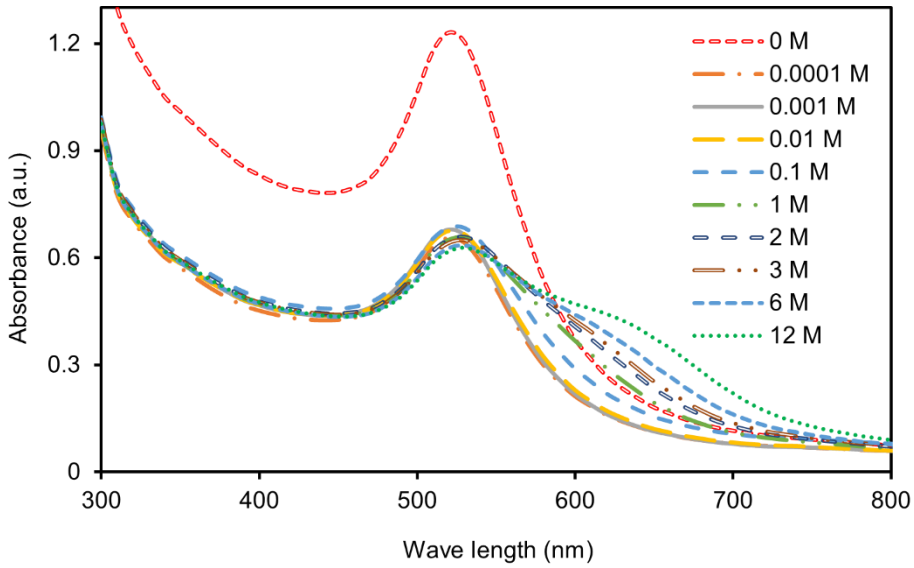


Figure 3S6 Absorption spectra of AuNPs-dTab 6% (w/v) with a range of hydrochloric acid (1:1) solution showing concentration dependent acid-promoted aggregation in tablets suitable for a broad range of sensing applications where acid sensitive linkages are responsible for colorimetric response.

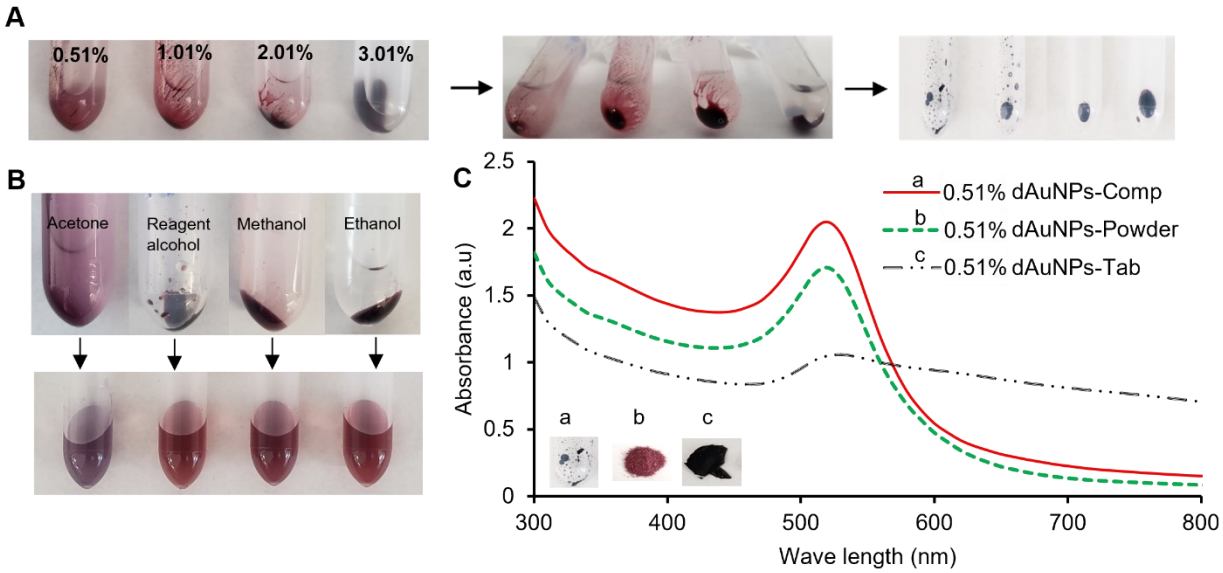


Figure 4S1 Composite formation and effect of dextran contents and solvents
A) The composite formation with different amounts of dextran (0.51-3.01%). Less dextran produced a scattered mass which is difficult to collect while a unified solid composite was collected with a high dextran amount. B) Effect of different solvents including acetone, reagent alcohol, methanol, and ethanol in composite formation indicating the equal efficiency of all alcohols, whereas acetone induces aggregation of dAuNPs as shown by purple color solution; C) The absorption spectra of composite, powder, and tablet having 0.51% dextran. The narrow and sharp peak of dAuNPs-Comp and dAuNPs-Powder has absorption maxima at 520 nm indicating well-dispersed nanoparticles while the broad peak of dAuNPs-Tab shows an unstable and aggregated nature of Au particles. This concludes that composite and powder are stable with less dextran, whereas tablet requires a higher dextran amount to keep nanoparticles stable.

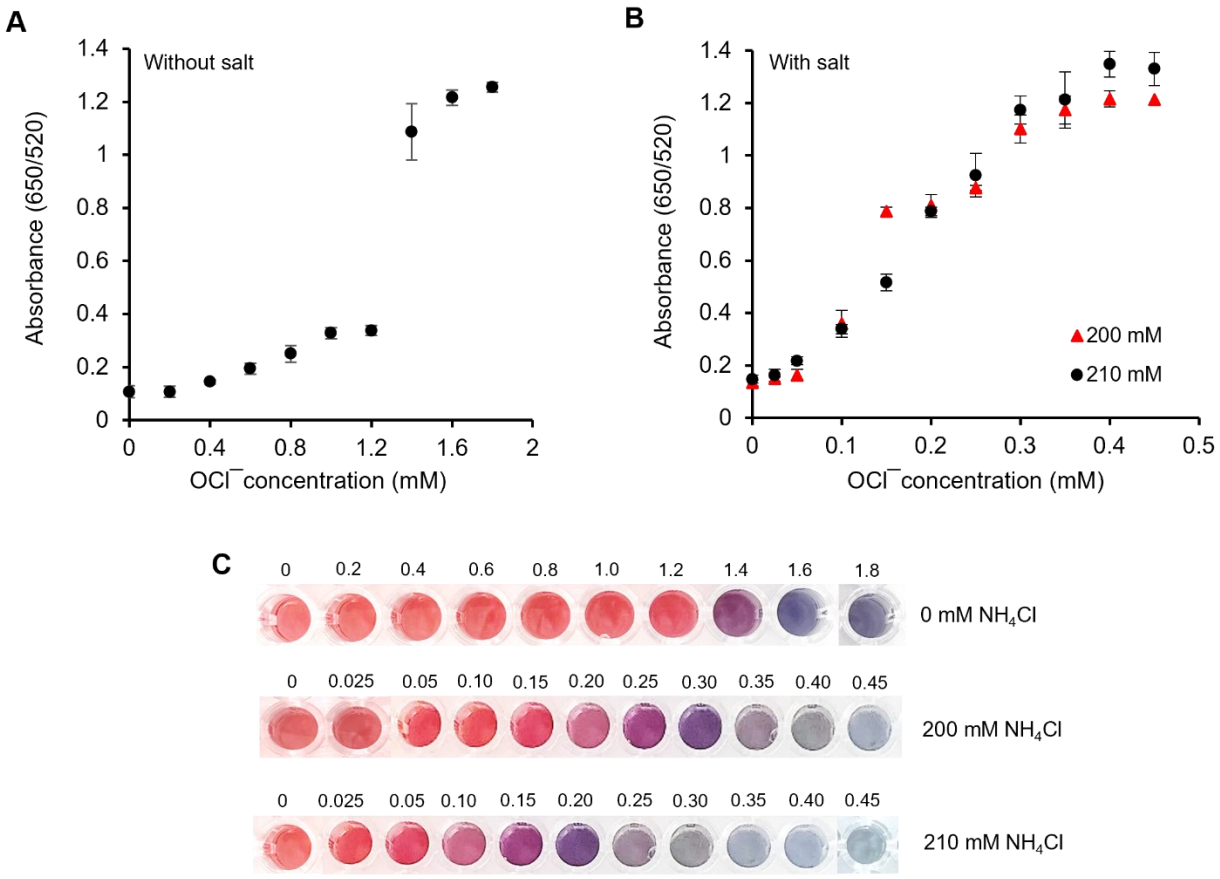


Figure 4S2 An improvement in the sensitivity of dAuNPs-Sol probe for $OCl^-$ detection with $NH_4Cl$ salt

A) The LLoD was 0.60 mM in the absence of $NH_4Cl$; B) The LLoD is improved to 0.1 and 0.05 mM using 200 and 210 mM $NH_4Cl$, respectively; C) A visual color change in dAuNPs probe showing the signal amplification effect with increasing salt concentration. The $OCl^-$ concentrations are in mM.

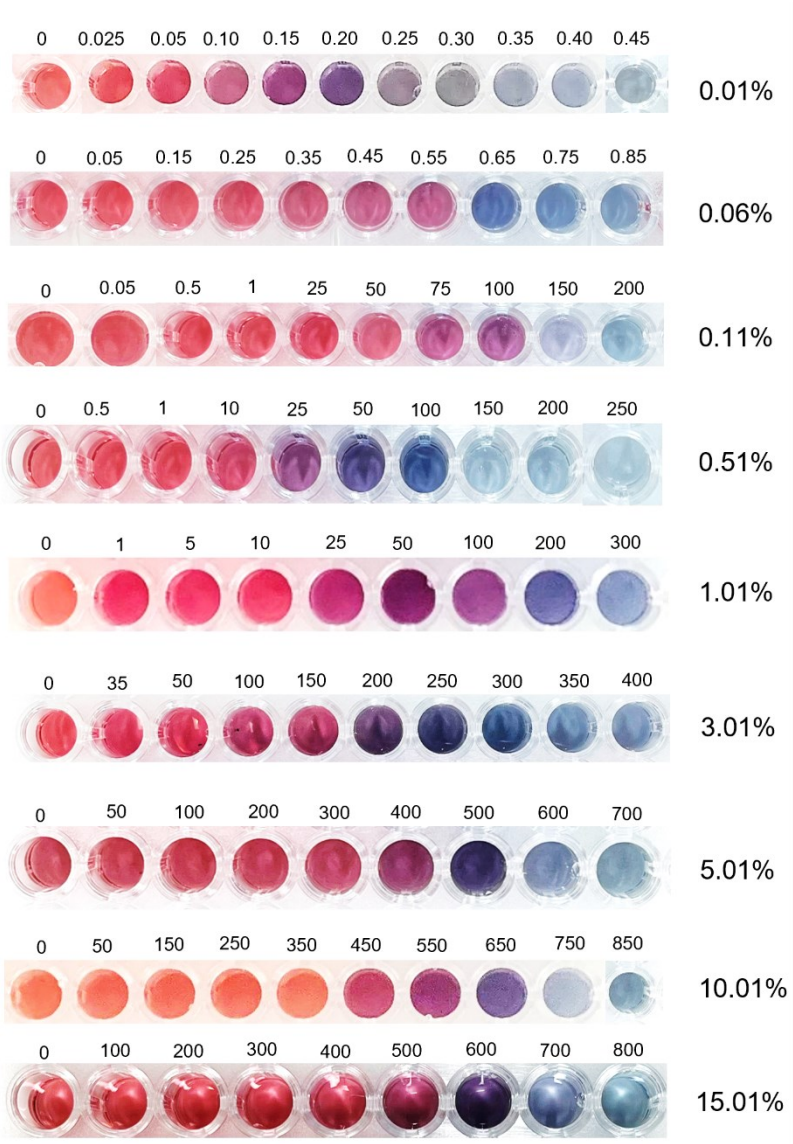


Figure 4S3 A colorimetric response of dAuNPs probes having a variable dextran amount (0.01 – 15.01%) and a broad range of $OCl^-$ concentrations (mM) in water.

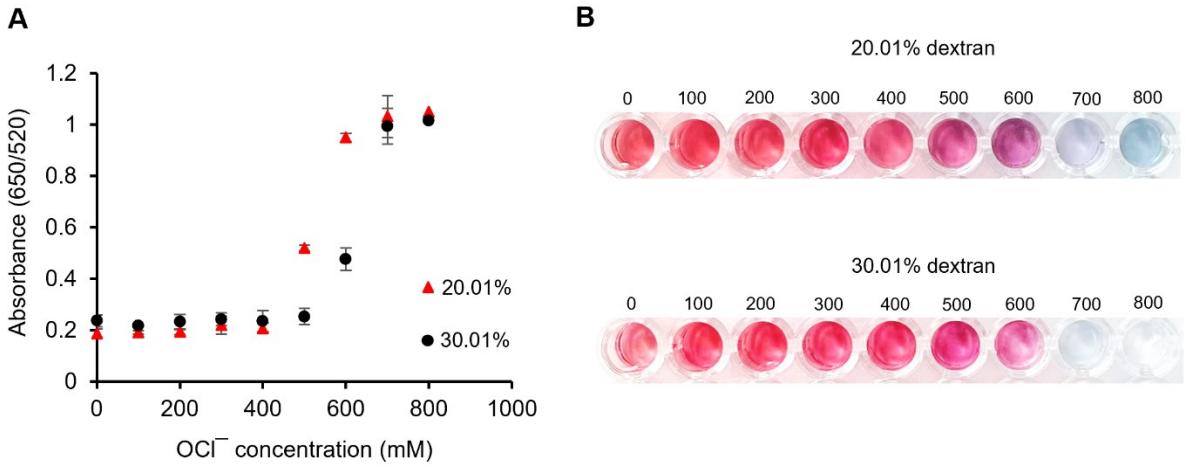


Figure 4S4 Detection of $OCl^-$ with dAuNPs solution
having 20.01 and 30.01% dextran. Calibration plots showing a sensitive response at ≥500 mM $OCl^-$ as indicates by the visual color change of dAuNPs probe.

Table 4S1 Zeta potential and hydrodynamic size against variable dextran amount in dAuNPs solution

| Amount of dextran (%) | Zeta potential (mV) | Hydrodynamic size (nm) |
|---|---|---|
| 0.01 | -43.8956 | 34.13 |
| 0.06 | -36.1762 | 58.19 |
| 0.11 | -28.7317 | 80.96 |
| 0.51 | -19.1901 | 143.55 |
| 1.01 | -17.6754 | 155.02 |
| 3.01 | -13.9771 | 236.54 |
| 5.01 | -11.6375 | 285.42 |
| 10.01 | -8.72269 | 312.62 |
| 15.01 | -5.73074 | 531.76 |
| 20.01 | -4.30253 | 875.47 |
| 30.01 | -0.52536 | 5506.69 |

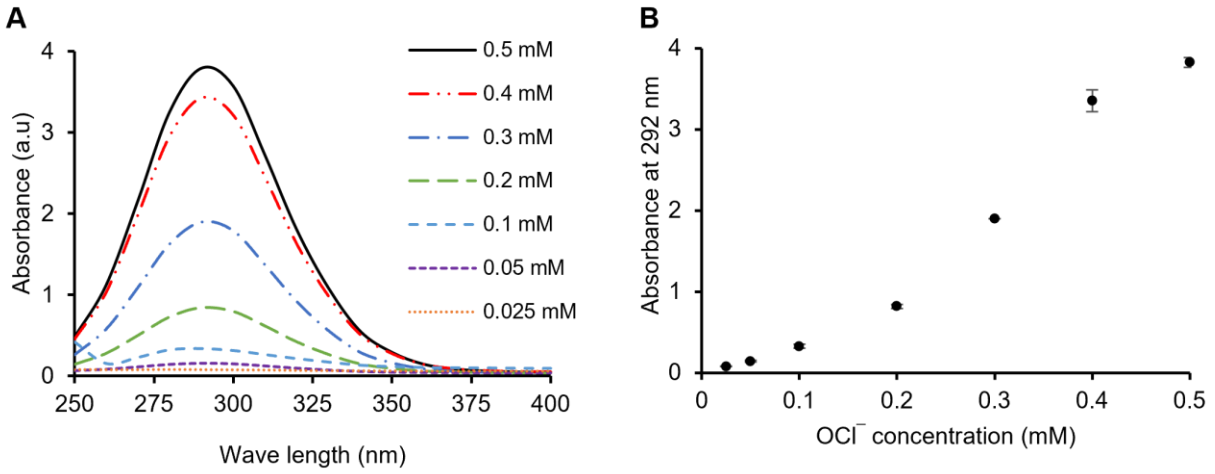


Figure 4S5 Quantification of $OCl^-$ in deionized water using conventional UV-vis spectroscopy method

A) Absorbance spectra of different concentration of $OCl^-$ solution showing $\lambda_{max}$ at 292 nm; B) Calibration plot indicates a gradual increase in absorbance value with increasing concentration of $OCl^-$.

Table 4S2 An overview of reported nanomaterial-based optical methods for the determination of $OCl^-$

| Sensing probe | Method | Response time (min) | LoD | Linear range | Tunable working range | Real sample | Match with required working range of swimming pool | References |
|---|---|---|---|---|---|---|---|---|
| Gold nanorods | colorimetry | 5 | - | 0.08–125 µM | × | tap water | ✓ | [718] |
| Silver nanoprisms | colorimetry | 15 | $2.50 \times 10^{-10}$ mol $dm^{-3}$ | $2.00 \times 10^{-7}$ mol $dm^{-3}$ – $12.00 \times 10^{-7}$ mol $dm^{-3}$ | × | tap water, swimming pool | ✓ | [719] |
| Silver nanoparticles on cellulose membrane | SERS | 2 h | 0.15 µM | 0.5–100 µM | × | cell contents, artificial urine,serum | ✓ | [720] |
| Gold/silver alloy nanoparticles | colorimetry | 15 | $0.30 \times 10^{-6}$ mol $dm^{-3}$ | 2.40–24.00 × $10^{-6}$ mol $dm^{-3}$ | × | tap water | × | [721] |
| Gold nanoparticles | colorimetry | 5 | 2.48 µM | 4.5–8.5 µM | × | tap water | × | [722] |
| Nitrogen-doped carbon quantum dots | fluorescence | real time | 0.03 µM | 0.1–50 µM | × | swimming pool, tap, distilled, and purified | × | [723] |

| | | | | | | | | |
|---|---|---|---|---|---|---|---|---|
| | | | | | | water, disinfectant samples | | |
| m-Phenylenediamine carbon dots | fluorescence | 1 | 0.012 μM | 0.05−7 μM | × | tap water | × | [724] |
| Au-nanospheres@Ag nanorods | colorimetry | 30 | 0.24 μM | 0.5−30 μM | × | tap water | × | [725] |
| Carbon dots | fluorescence | real time | 0.016 μM | 10–90 μM | × | tap, pond, river, and industrial waste water | ✓ | [726] |
| Dextran-gold nanoparticles | colorimetry | 6 | 50 μM | 0−400 μM | ✓ | swimming pool water samples | ✓ | This work |

**Supporting Information for Chapter 5**

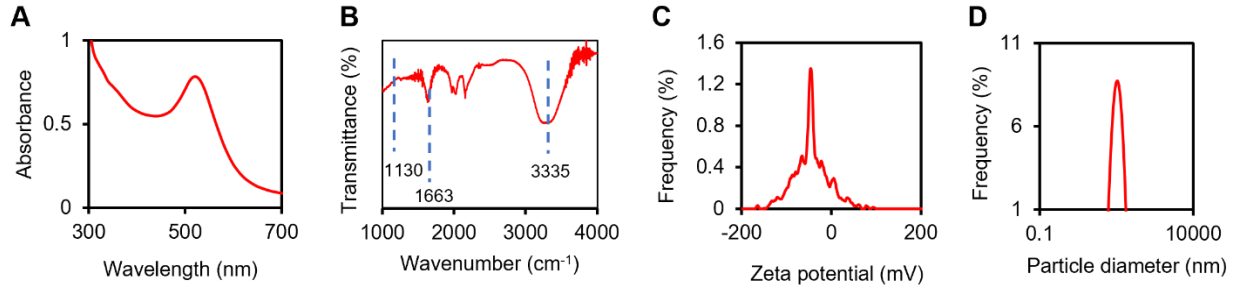


Figure 5S1 Characterization of colloidal dAuNPs-Sol.
A) absorbance spectra; B) FTIR spectra; C) zeta potential graph; D) a plot of hydrodynamic size.

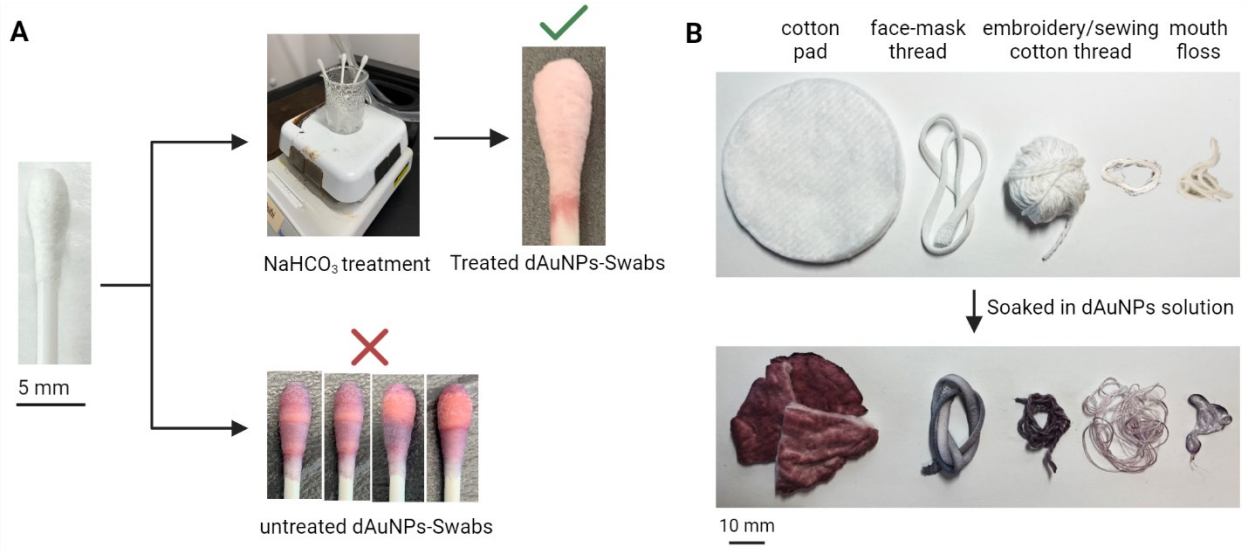


Figure 5S2 Testing the suitability of different materials (i.e. cotton, polyester) and platforms (i.e. swab, ball, thread, floss) for colorimetric assay.
A) The $NaHCO_3$ treatment removed wax layer from the cotton swab resulting in uniform spreading of dAuNPs suspension on the swab whereas untreated dAuNPs-Swabs led to the inconsistent spreading of colloidal dAuNPs giving multi-color zones; B) Incompatibility of different materials (i.e. cotton pad, face-mask thread, embroidery and sewing cotton thread, and mouth floss) to adsorb and sustain dAuNPs well-dispersed on the surface. All of them turned purplish-blue after drying, hence unsuitable for the colorimetric assay.

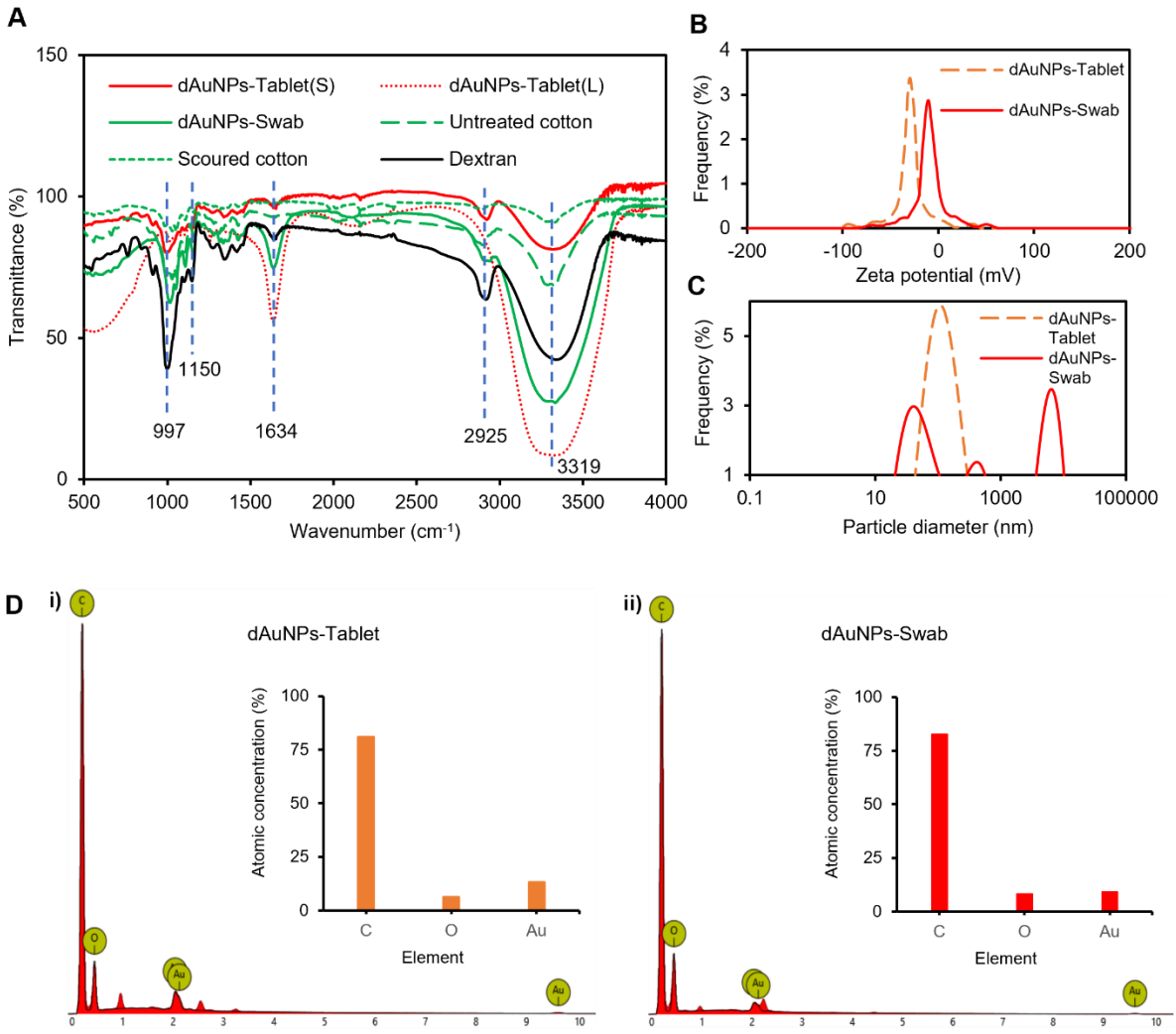


Figure 5S3 Characterization of tablet and swab sensors.
A) Infrared spectra of dAuNPs-Tablet as solid (S) and liquid (L) suspension along with dAuNPs-Swab which is compared with pure dextran and cotton; B) A graph showing zeta potential values of tablet and swab; C) A plot for the hydrodynamic size of tablet and swab; D) EDS spectra displaying the elemental composition (inset graph) of i) dAuNPs-Tablet and ii) dAuNPs-Swab.

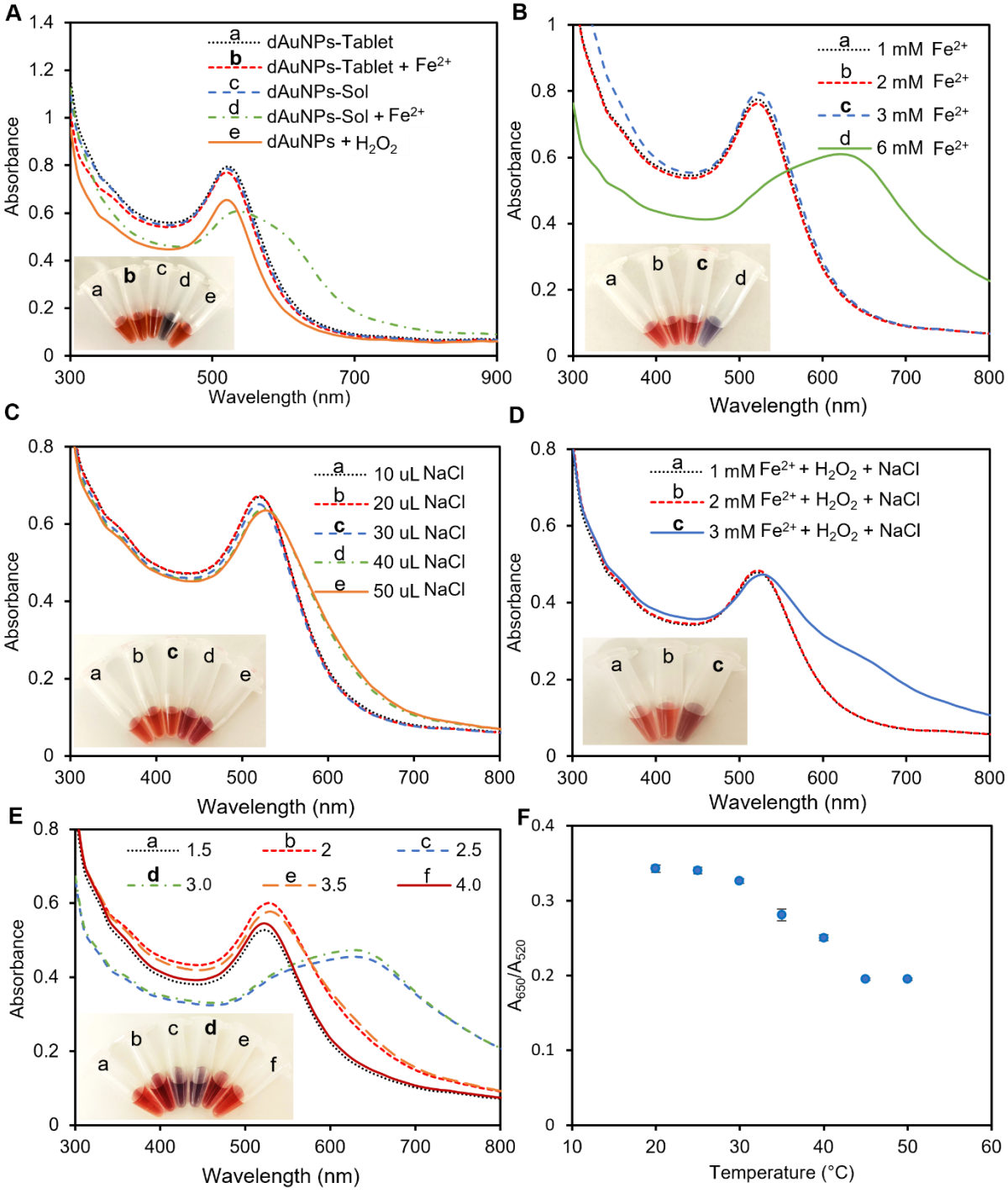


Figure 5S4 Optimization of experimental conditions for $H_2O_2$ assay using a tablet sensor and Fenton's reagent

Insets show optical images of a color change in dAuNPs solution. A) The absorption spectra of dAuNPs-Tablet (2.01% dextran) and dAuNPs-Sol (0.01% dextran) showing $\lambda_{max}$ at 520 nm but 10 µL of ferrous sulphate (1 mM) in dAuNPs-Sol solution caused the aggregation of particles which shifted the peak towards 650 nm whereas dAuNPs-Tablet solution remained intact; B) The

effect of different concentration of ferrous sulphate (1, 2, 3, 6 mM) on dAuNPs-Tablet where no aggregation was observed till 3 mM of ferrous ions while a broad peak was recorded with 6 mM ferrous ions indicating its unsuitability for the assay; C) Effect of different volumes (10, 20, 30, 40, and 50 µL) of 1 M NaCl solution on AuNPs-Tablet; D) The generation of hydroxyl radicle (·OH) using 10 µL of ferrous sulphate (1, 2, and 3 mM) and 50 µL of $H_2O_2$ (100 µM) that oxidized dextran around dAuNPs followed by salt-mediated aggregation for 3 mM ferrous ions; E) The $H_2O_2$ assay at different pHs using citrate-phosphate buffer where pH 2.5 and 3 produced a bathochromic shift; F) The $H_2O_2$ assay at variable temperature.

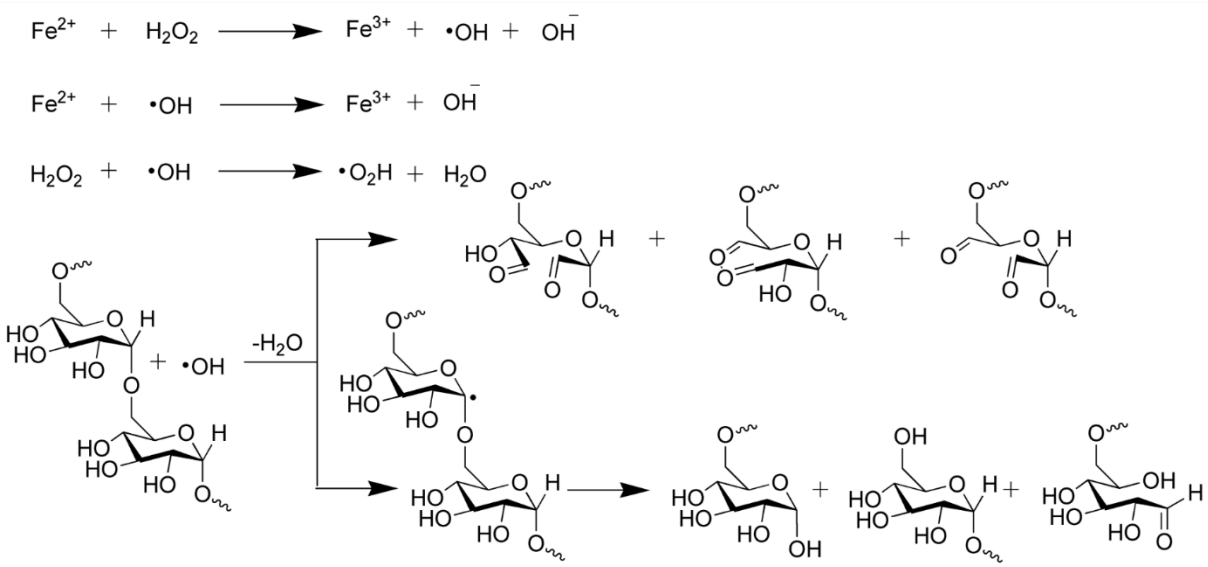


Figure 5S5 The Fenton reaction generates hydroxyl radical which involves in further reactions and oxidizes the dextran polymer either by ring opening or depolymerization

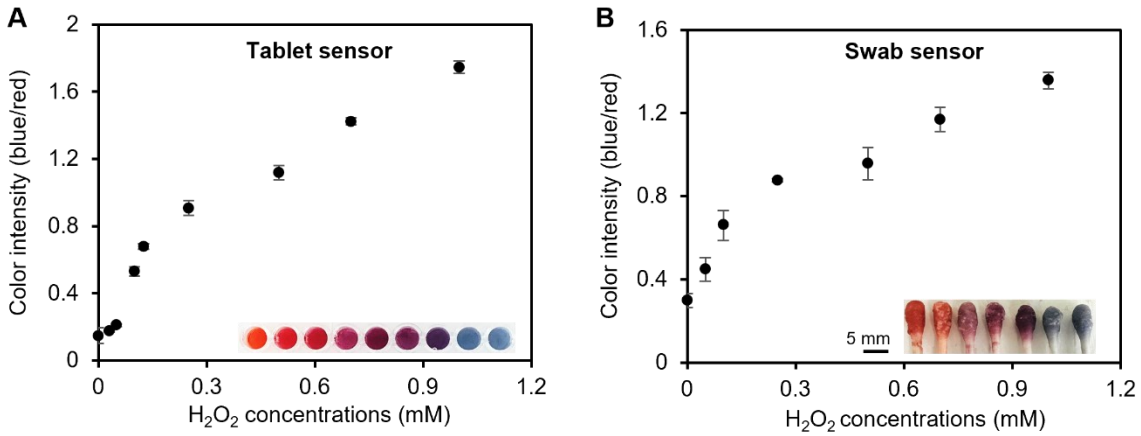


Figure 5S6 Plasmonic tablet and swab sensors for the colorimetric detection of $H_2O_2$ in water.

A) The calibration curve for $H_2O_2$ detection using dAuNPs-Tablet with LoD of 100 µM. An inset shows a gradual color change of a sensing probe; B) The calibration curve for $H_2O_2$ detection using blue/red color intensity of dAuNPs-Swab with LoD of 50 µM. An inset shows the color difference in cotton swabs due to varying $H_2O_2$ concentrations. The lower LoD in the swab sensor may be attributed to the strong signal on white cotton swab, which enabled a clear color variation between different concentrations.

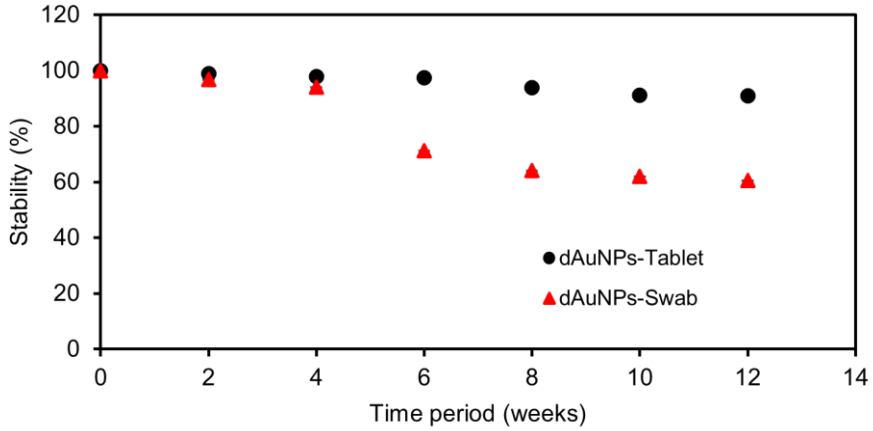


Figure 5S7 The stability profile of a tablet and a swab sensor

showed a 40% decrease in the stability of the swab over a period of 12 weeks.

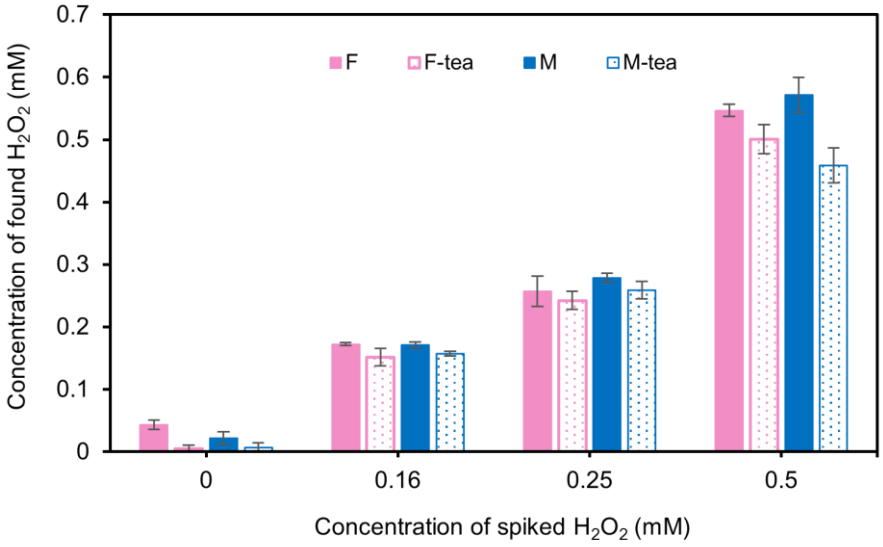


Figure 5S8 Comparison of $H_2O_2$ levels in samples before (F and M) and after green tea consumption (F-tea and M-tea).

The reduced $H_2O_2$ levels in F-tea and M-tea samples suggest a potential role of green tea in mitigating oxidative stress.

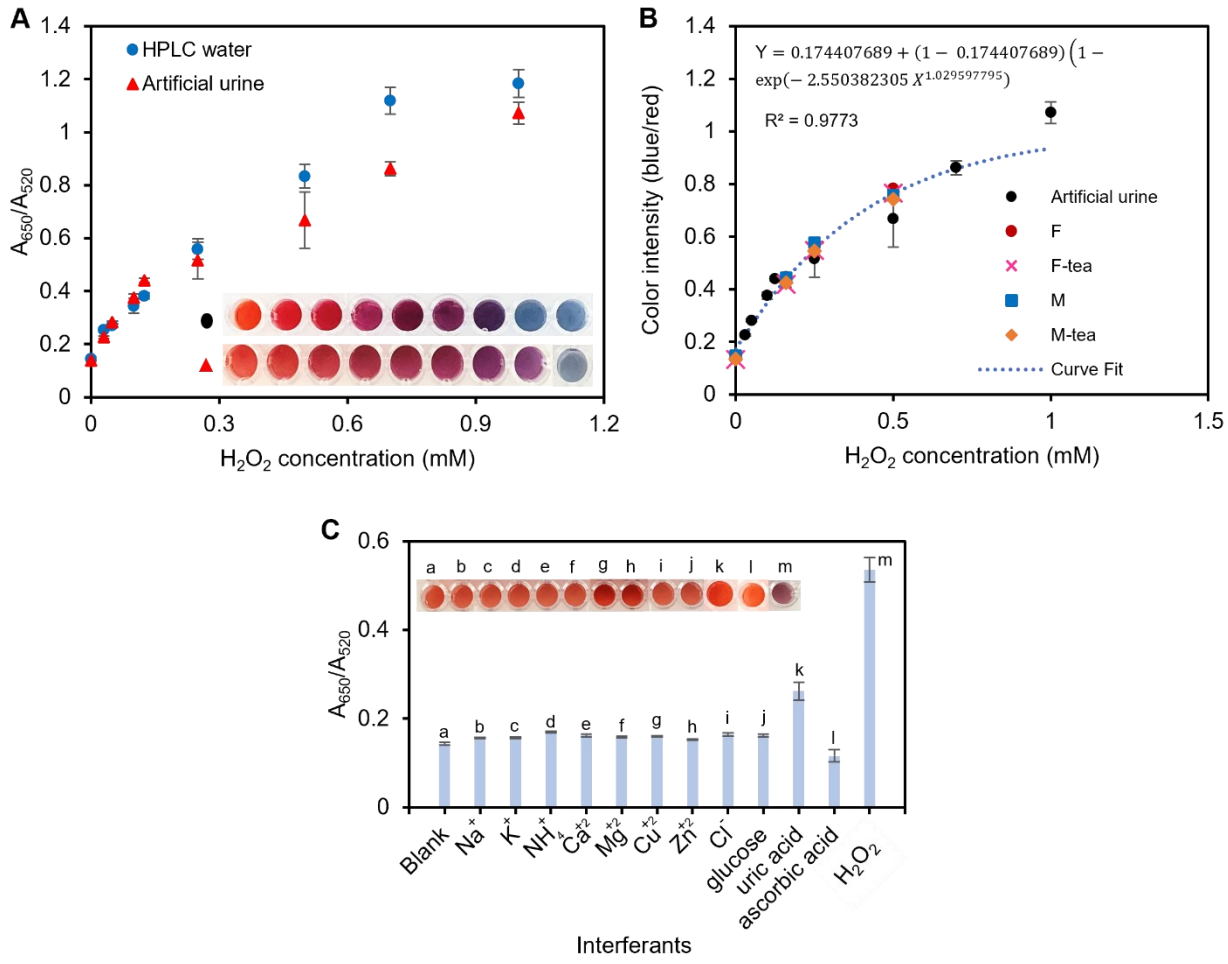


Figure 5S9 Plasmonic tablet sensor for $H_2O_2$ detection using UV-vis spectrophotometer. A) Calibration curve; B) Spiking analysis; C) Selectivity study.

Table 5S1 The spiking recovery analysis of proposed $H_2O_2$ assay before and after green tea consumption

| Samples | Amount added (mM) | Tablet sensor | | | Swab sensor | | |
|---|---|---|---|---|---|---|---|
| | | Amount found (mM) | %R | %RSD | Amount found (mM) | %R | %RSD |
| F | 0 | 0.03-0.04 | - | 4.53 | 0.01-0.04 | - | 1.27 |
| | 0.16 | 0.16-0.17 | 106-108 | 0.46 | 0.18-0.19 | 116-120 | 0.25 |
| | 0.25 | 0.22-0.27 | 91-110 | 4.37 | 0.28-0.29 | 115-118 | 0.29 |
| | 0.5 | 0.53-0.55 | 111-108 | 1.17 | 0.52-0.54 | 105-108 | 0.38 |
| F-tea | 0 | 0.00-0.01 | - | 1.79 | 0.00-0.03 | - | 1.51 |
| | 0.16 | 0.13-0.16 | 84-100 | 3.19 | 0.14-0.17 | 90-111 | 1.30 |
| | 0.25 | 0.22-0.25 | 91-103 | 2.74 | 0.25-0.27 | 101-109 | 0.77 |
| | 0.5 | 0.48-0.52 | 97-105 | 2.94 | 0.48-0.52 | 96-105 | 1.38 |
| M | 0 | 0.01-0.02 | - | 3.23 | 0.02-0.04 | - | 1.28 |
| | 0.16 | 0.16-0.17 | 104-109 | 0.96 | 0.14-0.18 | 92-112 | 1.22 |
| | 0.25 | 0.27-0.28 | 108-113 | 1.17 | 0.26-0.28 | 110-114 | 0.87 |
| | 5 | 0.53-0.59 | 107-118 | 3.22 | 0.50-0.59 | 101-119 | 3.07 |
| M-tea | 0 | 0.00-0.01 | - | 2.50 | 0.01-0.03 | - | 0.96 |
| | 0.16 | 0.15-0.16 | 95-100 | 0.84 | 0.13-0.14 | 84-92 | 0.47 |
| | 0.25 | 0.24-0.26 | 97-107 | 2.55 | 0.20-0.25 | 81-103 | 2.08 |
| | 0.5 | 0.42-0.47 | 85-95 | 3.74 | 0.40-0.50 | 80-100 | 3.13 |

Table 5S2 Comparison of recently reported methods for optical detection of hydrogen peroxide

| Sensing probe | Method | Response time (min) | LoD | Real samples | Note | Ref. |
|---|---|---|---|---|---|---|
| CuO nanoflakes | peroxidase activity/colorimetry | 15 | 0.96 μM | - | multistep preparation | [727] |
| Cysteine-AuNPs | catalytic activity/colorimetry | 20 | 0.5 μM | human sweat | Multiple steps with longer incubation time | [728] |
| DNA-gold nanoparticles | Fenton reaction/colorimetry | 10 | 1 μM | - | labor-intensive steps to prepare the probe | [729] |
| Gold nanoclusters (AuNCs) | peroxidase activity/colorimetry | 20 | 7 μM | - | multistep preparation | [730] |
| Phosphor-based film of $Li^{+}$ co-doped $CaWO_4:Tb^{3+}$/PVA-AgNPs | fluorescent probe and colorimetric detection | ≤ 5 s | 12.8/20 μM | human blood serum | complicated synthesis procedures | [731] |
| MXene/Gold nanoparticles heterostructure | catalase mimic/colorimetry | 40 | 7.51 nM | - | multistep preparation | [732] |
| Mustard seed-carbon quantum dots | catalytic activity/fluorescence | 15 | 15 μM | different fresh fruits | requires a light source for data interpretation | [733] |
| Dextran-gold nanoparticles tablet/swab | Fenton reaction/colorimetry | 10 | 50/100 μM | human urine | easy to synthesize and equipment-free data reading | This work |

**Supporting Information for Chapter 6**

## Chemicals and instruments

All the chemicals were of analytical grade and used as received. Tetrachloroauric acid (30 wt.% in dil. HCl), trisodium citrate, sodium hydroxide, dextran (100 kDa), uric acid, sodium chloride, urea, thiourea, ascorbic acid, hydrogen peroxide (30 wt.%), glucose, glucose oxidase (GOx) from *Aspergillus niger,* 3,3′,5,5′- tetramethylbenzidine, maltose, lactose, fructose and sulfuric acid were purchased from Sigma-Aldrich. Dimethyl sulfoxide was obtained from Fisher Scientific, Toronto, ON, Canada. Phosphate buffer (100 mM, 7.4 pH) was prepared using monosodium phosphate monohydrate (20.26 mM) and disodium phosphate heptahydrate (79.74 mM). Citrate-phosphate buffer (50 mM, 4.0 pH) was prepared using citric acid monohydrate (100 mM) and disodium phosphate heptahydrate (200 mM). The pH adjustment was performed using HCl and NaOH solutions. The TMB stock solution was prepared by dissolving 1 mg/mL in DMSO followed by preparing a working solution by diluting 1 mL of the DMSO stock with 9 mL phosphate citrate buffer of pH 4.0. The GOx solution (180 U/mL) was prepared in tris buffer (100 mM, 7.4 pH). Artificial urine was purchased from Biochemazone, Leduc, AB, Canada. Real urine samples were obtained from healthy volunteers and analyzed in this study according to the agreement of Concordia University's Institutional Review Board with the approval number SC5823 and the BioPermit number B-SJA-22–01. The UV−vis spectrophotometer (BioTek, Cytation 5, imaging reader), particle size analyzer (model Litesizer 500, Anton-Paar, Austria), and transmission electron microscopy (Talos L120C, 20−120 kV) are used for characterization of dAuNPs solution. For AFM image analysis (Anton Paar Tosca 400, Austria), a solid direct tablet was fixed to the sample stage onto with the tapping mode in air. An aluminum reflex coated cantilever (thickness: 30 nm, resonance frequency: 285 kHz, curvature height 10-15 μm; radius: <10 nm) was used, and the 600 × 600 pixel images were collected at a line rate of 0.3 lines/s. Image analysis was done using *Gwyddion* (free, open-source software, version 2.67).

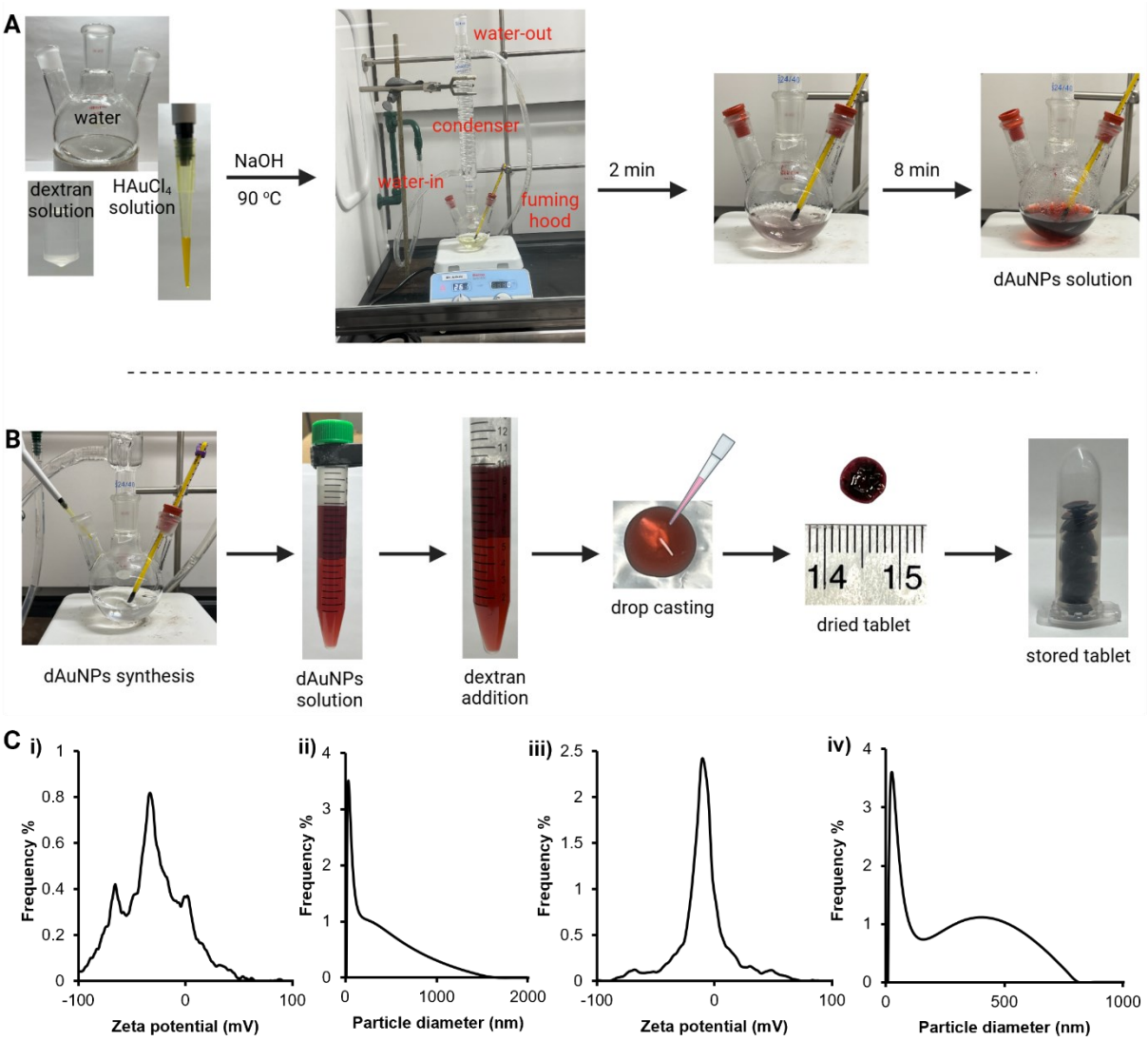


Figure 6S1 Synthesis of dAuNPs solution and tablet formation.
A) The chemical reduction method is used to produce colloidal dAuNPs; B) Indirect tablets are produced from dAuNPs solution after post-synthetic dextran addition; C) i) Zeta potential, and ii) hydrodynamic size of dAuNPs colloidal solution, iii) zeta potential, and iv) hydrodynamic size of the indirect tablet.

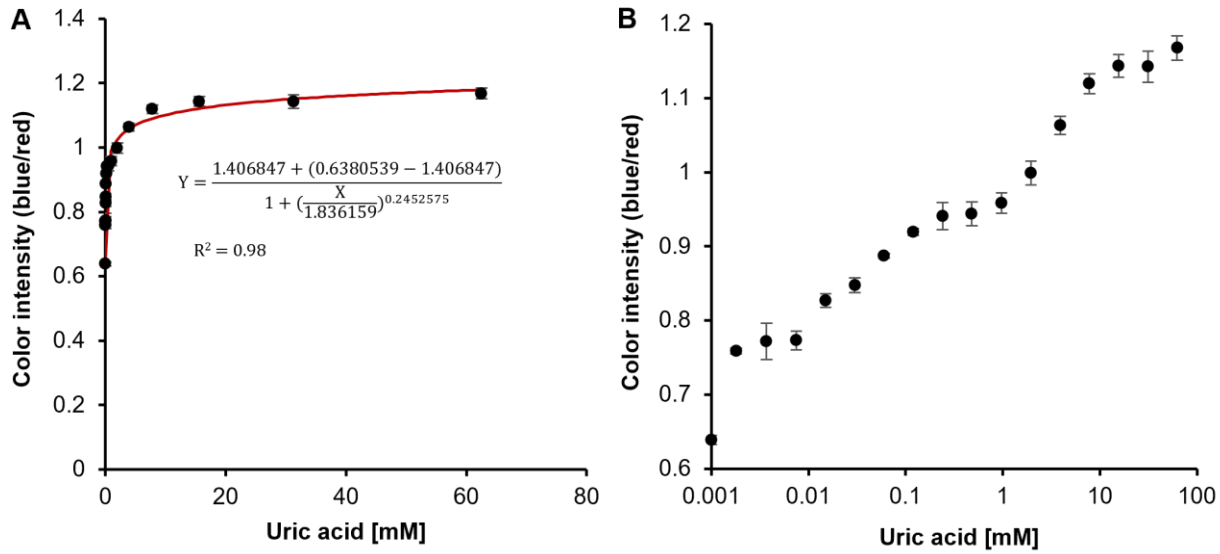


Figure 6S2 *ImageJ*-based quantification of uric acid with the direct tablet.
A) A calibration graph showing a sigmoidal curve; B) A calibration plot in log scale showing a gradual change in color intensity.

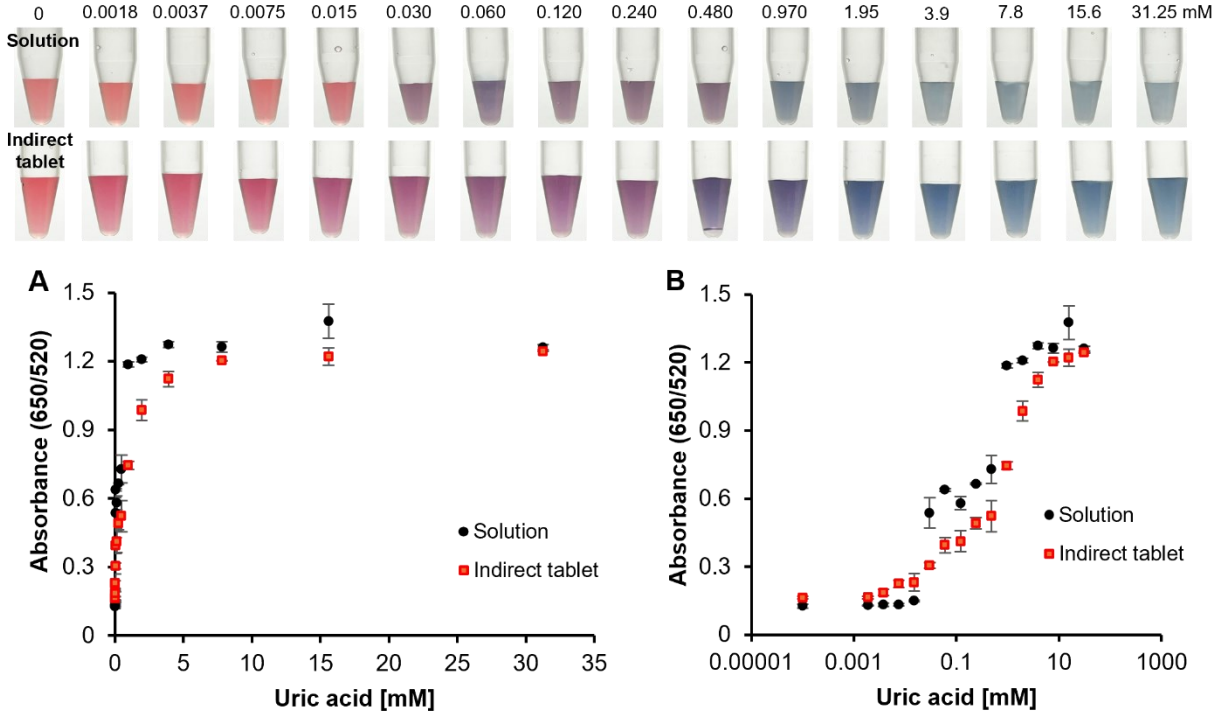


Figure 6S3 Calibration curve for the detection of uric acid using indirect tablet and solution.
A) The response curve showing a broader working range (0.0075 - 15.6 mM) with an indirect tablet as compared to the solution (0.03 - 1.95 mM); B) A calibration plot in log scale.

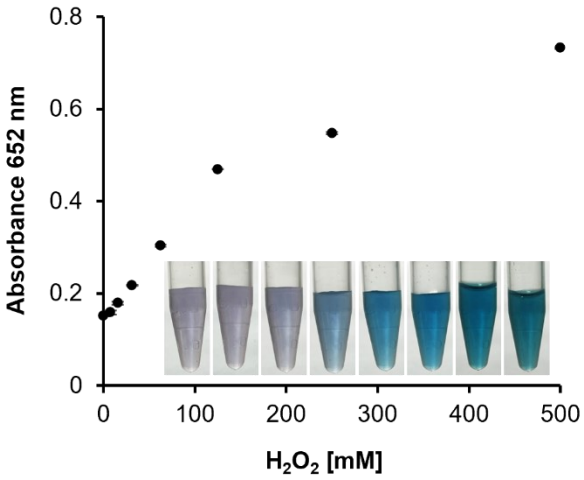


Figure 6S4 Calibration curve for the detection of $H_2O_2$ using a direct tablet.

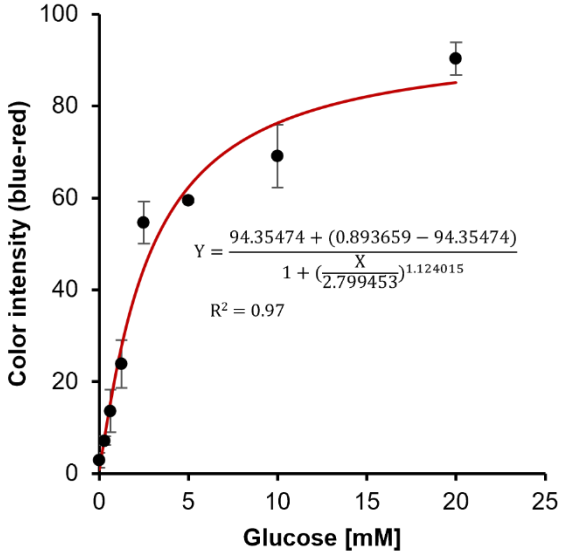


Figure 6S5 *ImageJ*-based quantification of glucose with the direct tablet.

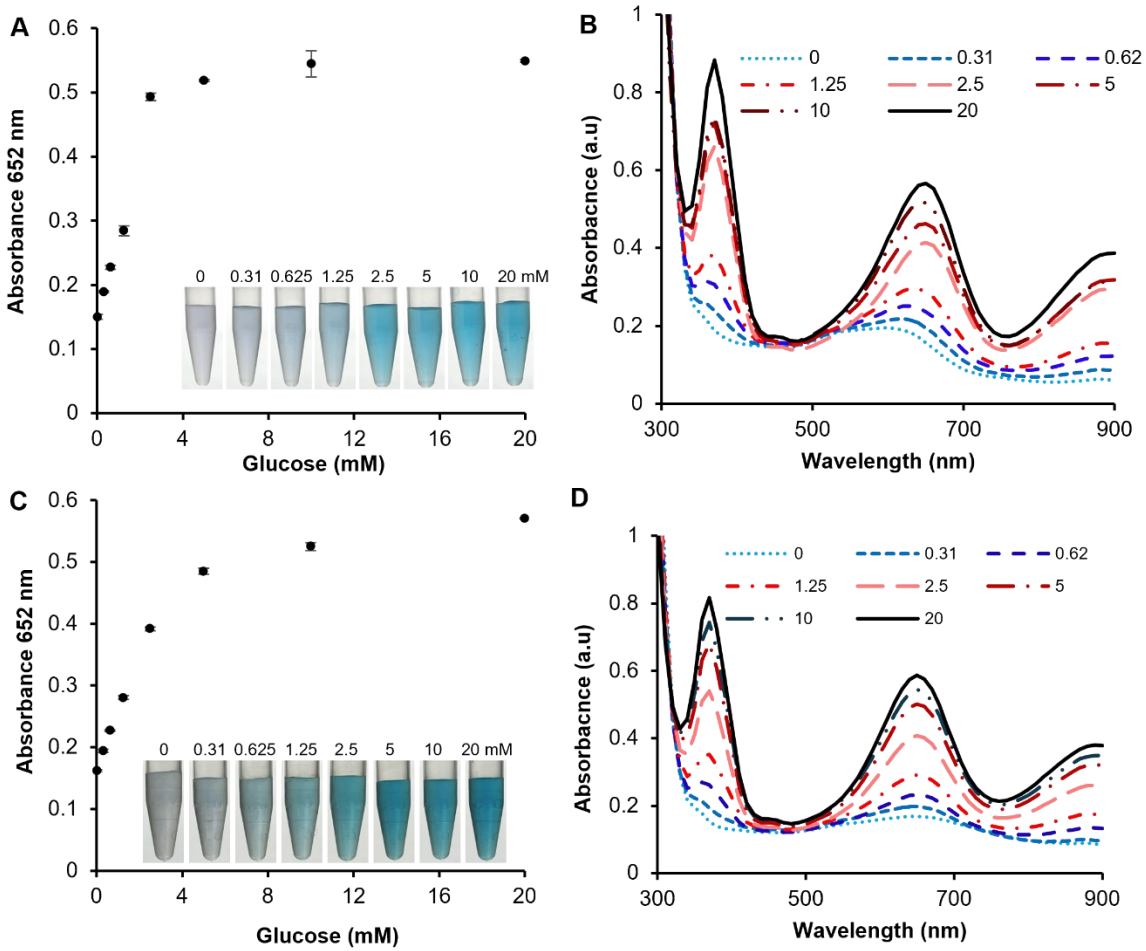


Figure 6S6 Calibration curve for the detection of glucose using indirect tablet and solution.

Table 6S1 Uric acid and glucose levels in different biological fluids

| **Analytes** | **Biological fluid** | **Normal/healthy range (mM)** | **Ref.** |
|---|---|---|---|
| Uric acid | Urine | 1.4 – 4.44 | [628] |
| | blood (serum) | 0.120 – 0.400 | [734] |
| | Saliva | 0.172 – 0.226 | [734] |
| | Sweat | 0.020 – 0.025 | [621] |
| | Tear | 0.025 – 0.150 | [735] |
| Glucose | Urine | 0 - 2.8 | [629] |
| | blood (serum) | 4.0 – 8.0 | [736] |
| | Saliva | 0.039 – 0.122 | [737] |
| | Sweat | 0.28 – 1.11 | [736] |
| | Tear | 0.1 – 0.6 | [738] |

Table 6S2 Distinguished features of direct and indirect tablets

| Aspect | Features | Direct Tablet | Indirect Tablet |
|---|---|---|---|
| Synthesis/ Preparation | Heat | room temperature (20 °C) | reflux temperature (100 °C) |
| | Time | 10 min | 60 min |
| | $HAuCl_4$ (for 25 mL colloidal solution) | 1 mM | 1 mM |
| | Dextran concentration | 2% (all at once during synthesis) | 2% (0.01% during synthesis + 1.99% after synthesis) |
| | NaOH | 1 M, 375 µL | 1 M, 50 µL |
| | Procedure | one-step: directly from solution to tablet | two-steps: an extra step of post-synthetic dextran addition involves |
| | Stability | >1 year (till to-date) | >4 years (till to-date) |
| | Storage | room temperature | room temperature |
| Detection | Particle size | 5 nm | 13 nm |
| | Zeta potential | -11.18 mV | -10.80 mV |
| | Hydrodynamic size | 276 nm | 292 nm |
| | Function | suitable for plasmonic and nanozyme sensor fabrication | suitable for plasmonic sensor fabrication |
| | Dual-functionality | excellent | good |

Table 6S3 Comparison of reported methods for the detection of uric acid and glucose in urine

| Analyte | Sensing probe | Method | Linear range | LoD | Ref. |
|---|---|---|---|---|---|
| Uric acid | nanoporous gold | electrochemical | 10 – 750 µM | 0.06 µM | [628] |
| | Cobalt tetroxide | colorimetric | 1-10 µM, 10-600 µM | 0.33 µM | [739] |
| | snowflake-like Ce-BTC@$MoS_2$ | electrochemical | 0.5-4.4 mM | 5 µM | [740] |
| | Carbon nanotubes with GdS-Gd2O3 nanoplates | electrochemical | 0.5-30 µM, 30-2000 µM | 0.380 µM | [741] |
| | graphene oxide (reduced) | electrochemical | 0.200 22.0 µM | 0.037 µM | [742] |
| | dextran-gold nanoparticles dual functional tablet (direct) | colorimetric | 1.87 -7800 µM | 3.7 µM | This work |
| Glucose | glucose oxidase + horseradish peroxidase dextran tablet | colorimetric | 0-1 mM | 0.013 mM | [626] |
| | polylactic acid and polyethylene glycol mat | electrochemical | 3.4 – 5.5 mM | 0.197 mM | [627] |
| | molecularly imprinted polymers | electrochemical | 1.37–330 µM, 14.38–330 µM | 1.37 uM, 14.38 µM | [743] |
| | hydrogel microspheres | SERS | 0-25 mM | 10 µM | [744] |
| | polymer nanogels – $TiO_2$ nanoparticles | colorimetric | 1-7 mM | 0.96 mM | [745] |
| | dextran-gold nanoparticles dual functional tablet (direct) | colorimetric | 0.625 – 10 mM | 0.625 mM | This work |